INSIGHTS INTO THE MOLECULAR MECHANISM OF THE MITOCHONDRIAL INTERMEMBRANE SPACE SULPHYDRYL OXIDASE ERV1

A thesis submitted to The University of Manchester for the degree of Ph.D.
In the Faculty of Life Sciences

2014

Efraín Herberto Ceh Pavía

LIST OF CONTENT

Word count: 33 756

LIST OF FIGURES

LIST OF TABLES

ABSTRACT

Mitochondria are involved in numerous cellular processes such as respiration, ATP production, calcium signalling and apoptosis. About 99% of mitochondrial proteins are nuclear-encoded and need to be imported into mitochondria for their function. The MIA pathway is used by many cysteine-containing proteins for their import into the mitochondrial intermembrane space (IMS). The pathway comprises two essential proteins: the disulphide carrier and import receptor Mia40, and the FAD-dependent sulphydryl oxidase Erv1. Together these proteins form a disulphide relay system inside the IMS. Initially, substrate proteins are imported in their cysteine-reduced form, which is oxidised by Mia40 in the IMS. Then, the now reduced Mia40 is in turn re-oxidised by Erv1. Finally, reduced Erv1 can transfer the electrons to oxygen directly, or via cyt *c*, to the respiratory chain. The overall aim of this study is to understand the structural and functional mechanisms of Erv1, from the effect of single mutations (R182H) to its quaternary structure and thermodynamic properties. The results are described in three chapters. First, biophysical techniques were used to evaluate the oligomerisation state of Erv1. Contrary to general belief, the results show that Erv1 adopts a tetramer conformation in solution. Tetramerisation provides Erv1 with a higher thermal stability, though it does not affect its oxidase activity. The second result chapter focuses on understanding the effects of a medically relevant mutant, Erv1 R182H, on the structure and function of the protein. The results show that at the physiological temperature of 37°C the mutant is less stable and becomes completely inactive after a few enzymatic cycles. The activity defect is linked to a weaker binding of the FAD cofactor in the mutant. Lastly, the third result chapter looks at the electron transfer within Erv1 from a thermodynamic perspective. Standard reduction potentials were determined for two of the three redox centres in Erv1. The results differ from those previously published, but are consistent with the current model of electron transfer in Erv1. Taken together, the results presented here offer an insightful perspective into the molecular mechanisms regulating Erv1.

DECLARATION

No portion of the work referred to in the thesis has been submitted in support of an application for another degree or qualification of this or any other university or other institute of learning.

COPYRIGHT STATEMENT

i. The author of this thesis (including any appendices and/or schedules to this thesis) owns certain copyright or related rights in it (the "Copyright") and s/he has given The University of Manchester certain rights to use such Copyright, including for administrative purposes.

ii. Copies of this thesis, either in full or in extracts and whether in hard or electronic copy, may be made only in accordance with the Copyright, Designs and Patents Act 1988 (as amended) and regulations issued under it or, where appropriate, in accordance with licensing agreements which the University has from time to time. This page must form part of any such copies made.

iii. The ownership of certain Copyright, patents, designs, trade marks and other intellectual property (the "Intellectual Property") and any reproductions of copyright works in the thesis, for example graphs and tables ("Reproductions"), which may be described in this thesis, may not be owned by the author and may be owned by third parties. Such Intellectual Property and Reproductions cannot and must not be made available for use without the prior written permission of the owner(s) of the relevant Intellectual Property and/or Reproductions.

iv. Further information on the conditions under which disclosure, publication and commercialisation of this thesis, the Copyright and any Intellectual Property and/or Reproductions described in it may take place is available in the University IP Policy (see http://www.campus.manchester.ac.uk/medialibrary/policies/intellectual-property.pdf), in any relevant Thesis restriction declarations deposited in the University Library, The University Library's regulations (see http://www.manchester.ac.uk/library/aboutus/regulations) and in The University's policy on presentation of Theses.

A BIT OF WISDOM

I hope to do it better in time. I myself am very far from satisfied with this but, well, getting better must come through doing it and through trying.

Vincent van Gogh

To doubt everything, or, to believe everything, are two equally convenient solutions; both dispense with the necessity of reflection.

Henri Poincaré

People learn something everyday, and a lot of times it's that what they learned the day before was wrong.

Bill Vaughan

IN NO PARTICULAR ORDER

My most heartfelt thanks go…

To my flatmates, for hearing me rant about my project.
To my labmates, for chipping in on the science.
To Supersónicos, for making life cheerful outside the lab.
To my mother and father, for their unconditional support and encouragement throughout the years.
To my grandparents, whose memory is still a source of motivation.
To M.J., who soothed me during trying nights.
To Darrel Lewis, for the late-night discussions and trusting me with the secrets of the MIB.
To Dr. Derren Heyes, for his comments on my work and all the help with the glove box.
To Dr. Karl Fisher, for his advice, guidance and helping me remain motivated when I was down.
To the people in Grant's, Ley's, Munro's, Swanton's and Scrutton's lab, they always lent me their equipment and had comments to share.
To those who came before me, their cells, plasmids and protocols made my work much easier.
To CONACyT, for providing the funding necessary to complete this work.
To my supervisor, Dr. Hui Lu, who had more faith in me than I. Thanks for all the discussions, comments, encouragements, disagreements, and simply outright support throughout these four years. You taught me a lot, sometimes without me realising it.

LIST OF ABBREVIATIONS

AMS	4-acetamido-4’-maleimidylstilbene-2,2’-disulfonic acid
ATP	Adenosine triphosphate
BA	Buffer A
BAE	Buffer AE
CD	Circular dichroism
DTT	Dithiothreitol
EPR	Electron paramagnetic resonance
ER	Endoplasmic reticulum
FAD	Flavin adenine dinucleotide
FMN	Flavin mononucleotide
GSH	Glutathione (γ-L-glutamyl-L-cysteinyl-glycine)
GSSG	Glutathione disulphide
HPLC	High-pressure liquid chromatography
IM	Inner membrane
IMS	Intermembrane space
IEC	Ion exchange chromatography
IPTG	Isopropyl β-D-1 thiogalactopyranoside
ITS	Intermembrane space-targeting signal
LB	Luria-Broth
mBBr	Monobromobimane
MIA	Mitochondrial IMS import and assembly
MISS	Mitochondria intermembrane space sorting signal
MALLS	Multiangle laser light scattering
OM	Outer membrane
PAM	Presequence translocase-associated motor
PDI	Protein disulfide isomerase

RPC	Reverse-phase chromatography
SAM	Sorting and assembly of mitochondria
SDS-PAGE	Sodium dodecyl sulfate polyacrylamide gel electrophoresis
SEC	Size exclusion chromatography
TCEP	Tris(2-carboxyethyl)phosphine
TFA	Trifluoroacetic acid
TIM	Translocase of the inner membrane
TOM	Translocase of the outer membrane
WT	Wild type
$\Delta\psi$	Membrane potential
E^{o}	Standard reduction potential

1. INTRODUCTION

Bioblasts, or what we now know as mitochondria, were first identified during the nineteen century by Richard Altmann and Carl Benda. Since then, they have been involved in numerous cellular processes such as respiration, adenosine triphosphate (ATP) production, calcium signalling, steroid biosynthesis and apoptosis (McBride et al., 2006). Furthermore, many diseases can be related to mitochondria, from neurodegenerative diseases like Alzheimer or Parkinson to premature aging, blindness and cancer (Wallace, 2005, Brandon et al., 2006, Bishop et al., 2010).

A typical eukaryotic cell harbours between a hundred and several thousand mitochondria, which fuse and divide to form a continuous dynamic network permeating the entire cell. The mitochondrion is separated from the cell's cytosol by a double membrane, a legacy of its bacterial origin. Hence, the mitochondrion is divided into four distinct compartments: matrix, inner membrane (IM), intermembrane space (IMS) and outer membrane (OM). However, the IM is highly folded and parts of it reach into the matrix forming tubular structures called cristae. This further divides the IMS into two sub-compartments that are separated by cristae junctions: the intracristal space and the luminal space found between the IM and the OM (Frey and Mannella, 2000, Mannella, 2006).

Mitochondria contain about 10% of the total cellular protein content, and yet, the mitochondrial genome is rather small counting only 8 and 13 proteins in yeast and humans, respectively. Most mitochondrial proteins are nuclear-encoded and need to be imported into mitochondria for their function (Chacinska et al., 2009, Stojanovski et al., 2012). In the following sections the various mitochondrial import pathways are briefly described, with emphasis on the mitochondrial IMS import and assembly (MIA) pathway. Next, a detailed explanation is given on the structure and function of sulphydryl oxidases, with emphasis on Erv1, the disulphide generator of the MIA pathway and the main focus of this study. Last, the current knowledge on the MIA pathway, including its substrate proteins and the pathway components, is reviewed in detail.

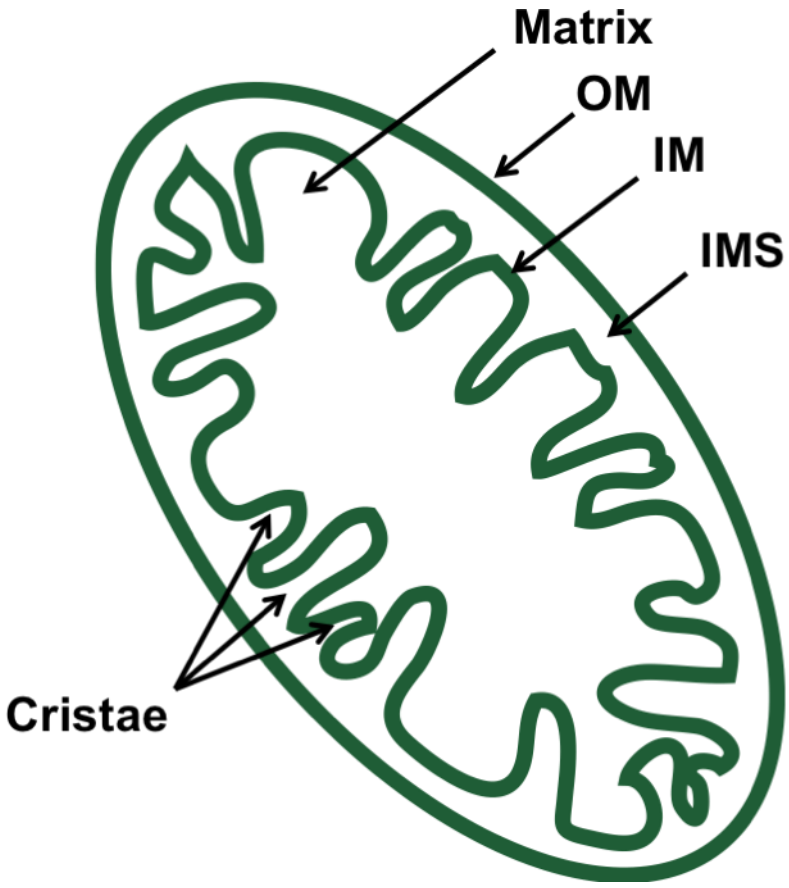

Figure 1.1 Mitochondrial compartments

Mitochondria can be divided into four compartments: matrix, outer membrane (OM), inner membrane (IM) and intermembrane space (IMS). The IM invaginations are called cristae.

1.1. Import and sorting into mitochondria

The past two decades have seen a boom in the understanding of mitochondrial protein biogenesis. Eukaryotic cells have developed several mechanisms for the import of the approximately 99% of mitochondrial proteins that are nuclear-encoded. Although there is still plenty to be elucidated at the mechanistic level, much is already known about the general import pathways. Mitochondrial precursor proteins are generally synthesised in the cytosol and stabilised by cytosolic chaperons before their post-translational import (Young et al., 2003, Chacinska et al., 2009, Zara et al., 2009). There are five major mitochondrial import pathways regulated by various protein complexes (Figure 1.2). These complexes are very dynamic with certain protein subunits being on and off a complex depending on the incoming precursor protein. Recent findings also suggest at least two of these complexes sometimes link to form a super-complex and expedite protein import (Chacinska et al., 2009, Stojanovski et al., 2012).

The final destination of precursor proteins depends on their mitochondria targeting signals, which can be divided into two major groups: 1) N-terminal positively charged amphipatic α-helices and, 2) internal targeting signals. The N-terminal targeting signals are the most ubiquitous and direct precursor proteins to either the IM or the matrix. Among the internal targeting signals three types have so far been identified: a) a β-signal in the last strand of β-barrel proteins sends them to the OM, b) a mitochondrial IMS sorting signal (MISS) directs proteins to the IMS, and c) some multiple internal targeting signals found in the hydrophobic transmembrane domains of certain IM proteins (Chacinska et al., 2009, Stojanovski et al., 2012). The current wealth of knowledge regarding the mitochondrial import pathways is summarised below.

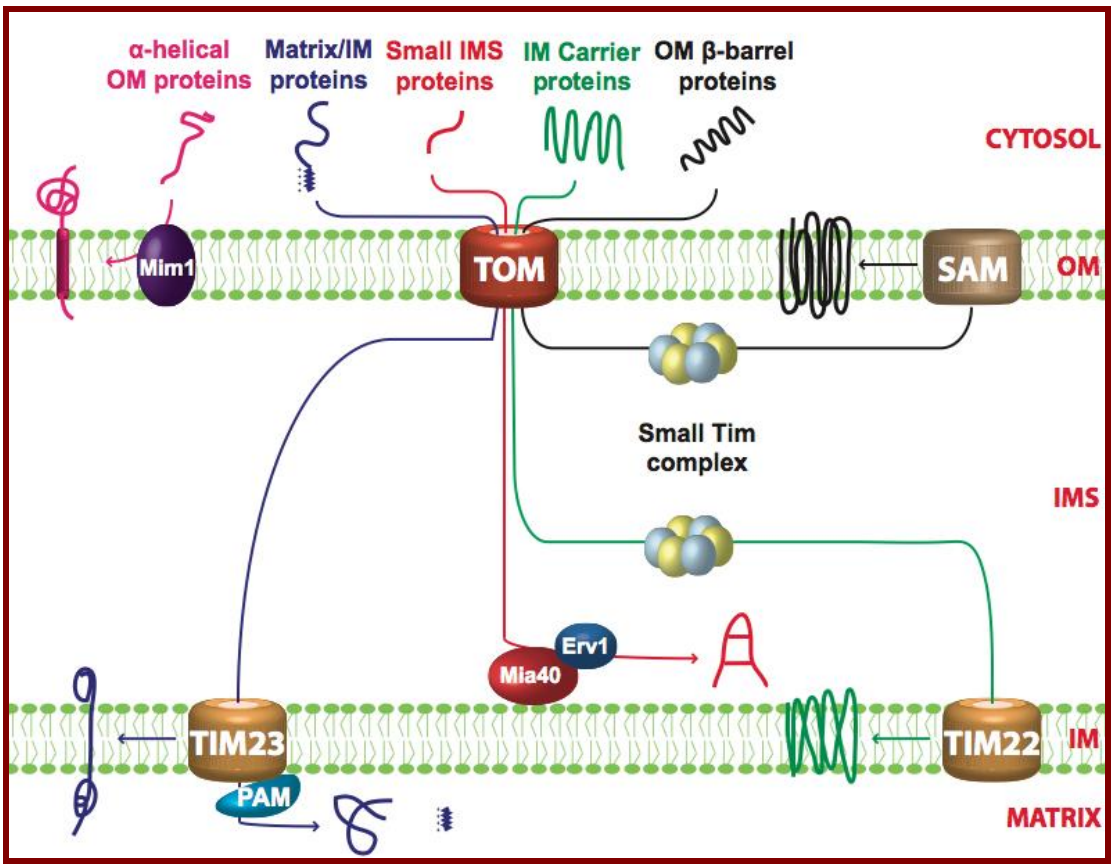

Figure 1.2 Overview of mitochondrial import and sorting pathways

Precursor proteins are imported post-translationally into mitochondria. Some α-helical proteins (pink) are inserted directly into the OM by Mim1. All other mitochondrial proteins must traverse the OM via the TOM complex before they are directed to downstream sorting pathways. Matrix and some IM proteins (blue) use the TIM23 pathway. The PAM complex is needed for the complete translocation of matrix proteins through the IM. IMS proteins (red) require both Mia40 and Erv1 for their import and oxidative folding. Multi-spanning IM carrier proteins (green) are chaperoned by the small Tim complexes to the TIM22 complex where they are inserted into the IM. Finally, OM β-barrel proteins (black) are also chaperoned by the small Tim complexes but are instead directed to the SAM complex for their insertion into the OM. TOM: translocase of the outer membrane, TIM: translocase of the inner membrane, PAM: presequence translocase-associated motor, SAM: sorting and assembly machinery, IM: inner membrane, IMS: intermembrane space, OM: outer membrane.

1.1.1. TOM – Entry gate into mitochondria

The translocase of the outer membrane (TOM) acts as the entry gate for nuclear-encoded mitochondrial proteins. Except for a few α-helical proteins of the OM, all other precursor proteins must first pass through the TOM complex before they are sorted to their respective mitochondrial compartments (Figure 1.1). The TOM complex is composed of seven proteins (Figure 1.3). Tom40 is a β-barrel protein that forms the pores through which precursor proteins are translocated (Hill et al., 1998). Tom20 and Tom70 recognise N-terminal and internal targeting signals, respectively (Brix et al., 1997, Wu and Sha, 2006). Tom22 mediates the transfer of precursor proteins from Tom20 to Tom40 (van Wilpe et al., 1999, Shiota et al., 2011). Finally, the three small proteins Tom5, Tom6 and Tom7 contribute to the biogenesis, stabilisation and dynamics of the TOM complex (Dekker et al., 1998, Model et al., 2001).

1.1.2. TOM/TIM22 – Insertion into the mitochondrial IM

The translocase of the inner membrane 22 (TIM22) facilitates the insertion of multi-spanning membrane proteins into the mitochondrial IM (Figure 1.3 A). The import through the TIM22 pathway is best described by the biogenesis of metabolite carrier proteins like the ATP/ADP carrier or the dicarboxylate transporter (Sirrenberg et al., 1996). Carrier precursor proteins contain an internal targeting signal that is recognised by Tom70 in the surface of mitochondria (Wiedemann et al., 2001). The precursor proteins then traverse the TOM complex in a loop-like conformation using energy derived from the ATP hydrolysis of cytosolic chaperons (Young et al., 2003, Wu and Sha, 2006, Zara et al., 2007). Next, the Tim 9/10 hexameric complex chaperones the precursor proteins through the aqueous IMS, keeping them from aggregation and delivering them to the TIM22 complex (Curran et al., 2002, Baker et al., 2009). The protein Tim12 binds the Tim 9/10 complex before the interaction with the TIM22 complex (Gebert et al., 2008). Four proteins form the TIM22 complex: Tim54, Tim22, Tim18 and Sdh3. Precursor proteins initially interact with Tim54, which supposedly provides a binding site for the Tim 9/10/12 complex. They are then inserted into the IM through the Tim22 protein (Rehling et al., 2003). The precise mechanism has yet to be unravelled but it requires the membrane potential and Tim22 dimerisation (Kovermann et al., 2002). Finally, Tim18 contributes to the assembly of the TIM22 comple

(Wagner et al., 2008). The function of Sdh3 is unknown but the protein was shown to interact with Tim18 (Gebert et al., 2011).

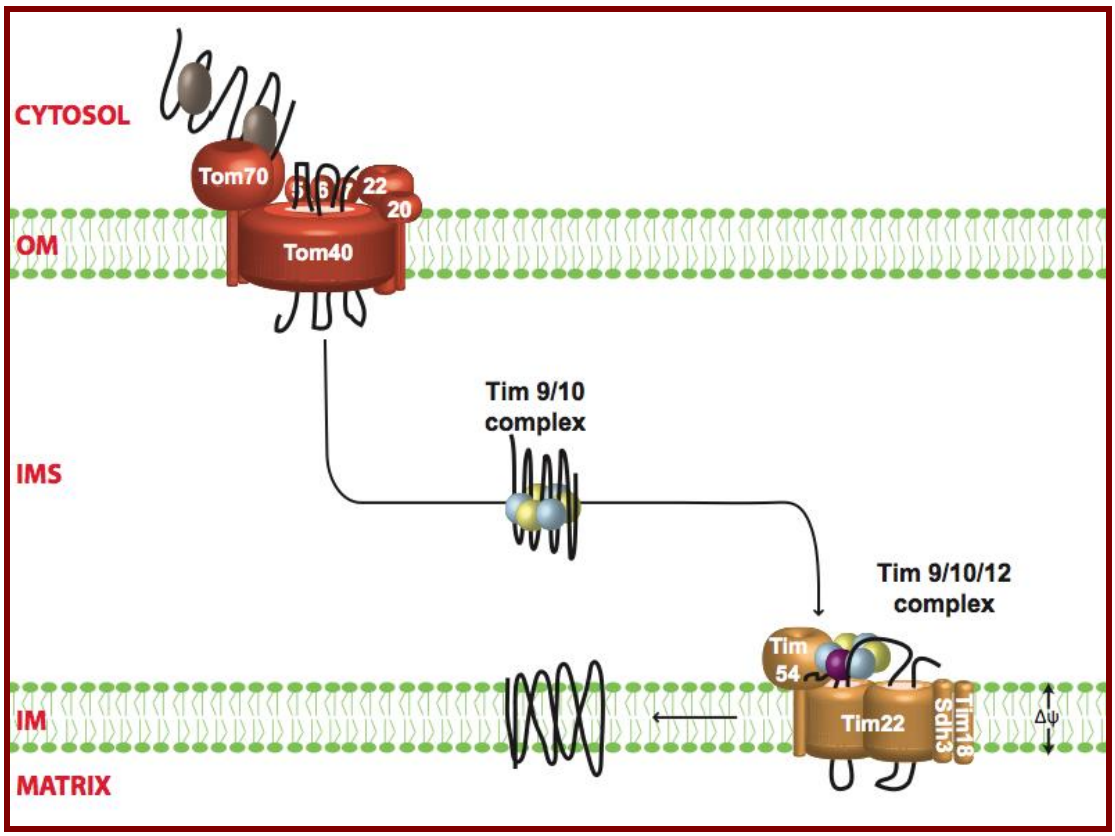

Figure 1.3 TOM/TIM22 pathway

Precursor proteins with hydrophobic internal targeting signals are delivered to Tom70 by cytosolic chaperones. Translocation through the TOM complex occurs in a loop conformation. The small Tim 9/10 complex then chaperones the precursor proteins through the IMS towards the TIM22 complex. Tim12 and Tim54 mediate the transfer from the small Tim 9/10 complex to the Tim22 channel. Finally, precursor proteins are folded and released into the IM in a process requiring the membrane potential ($\Delta\psi$). Tim18 and Sdh3 are required for the assembly and stability of the TIM22 complex. IM: inner membrane, IMS: intermembrane space, OM: outer membrane.

1.1.3. TOM/TIM23 – Import into the mitochondrial matrix and insertion into the IM

The translocase of the inner membrane 23 (TIM23) is in charge of translocating precursor proteins into the mitochondrial matrix and also of inserting single-spanning membrane proteins into the mitochondrial IM (Figure 1.4). The complex is composed of Tim23, Tim17 and Tim50. Another protein, Tim21, is found on and off the complex (Stojanovski et al., 2012). Tim21 directly connects the TIM23 complex to the TOM complex, thereby preventing precursor proteins to interact with the IMS (Chacinska et al., 2005). All precursor proteins of this pathway contain a canonical N-terminal targeting signal that is recognised by the cytosolic domain of Tom20 (Brix et al., 1997). After going through the TOM complex the precursor proteins immediately interact with the IMS domain of Tim50. Then, they simultaneously interact with Tim50 and Tim23 while their C-terminal is still inside the TOM complex (Dekker et al., 1997, Chacinska et al., 2003, Tamura et al., 2009, Gevorkyan-Airapetov et al., 2009). The insertion into Tim23 of the precursor proteins N-terminal depends on the membrane potential (van der Laan et al., 2007). It is at this stage that the pathway for matrix and IM proteins differs. Besides the N-terminal targeting signal, IM precursor proteins also include a hydrophobic stop-transfer signal. This signal is identified by the TIM23 complex, which then releases the precursor protein into the mitochondrial IM (Alder et al., 2008). Finally, to obtain the mature protein the matrix processing peptidase (MPP) cleaves the N-terminal targeting signal (Taylor et al., 2001). Interestingly, the TIM23 complex that promotes IM insertion is coupled to the respiratory chain complexes cytochrome *bc*1 (complex III) and cytochrome *c* oxidase (complex IV). Association with these two complexes appears to stimulate the insertion into the IM in a yet uncharacterised manner (Dienhart and Stuart, 2008).

For precursor proteins directed to the matrix, the energy from the membrane potential is not sufficient for their complete translocation through the TIM23 complex. The presequence translocase-associated motor (PAM) functions on the matrix side of the TIM23 complex and provides extra energy derived from the hydrolysis of ATP (Stojanovski et al., 2012). Its central component is the mitochondrial heat shock protein 70 (mt-hsp70) that converts the energy from ATP hydrolysis into the vectorial translocation of

precursor proteins. The PAM complex includes several other proteins whose function is to regulate mt-hsp70 activity and aid in its binding to the TIM23 complex (Neupert and Herrmann, 2007). Once inside the matrix, the N-terminal targeting signal is cleaved by MPP to obtain the mature protein (Taylor et al., 2001). Remarkably, in this last stage of the pathway the TIM23 complex has lost Tim21 and is therefore no longer bound to the TOM complex (Chacinska et al., 2003).

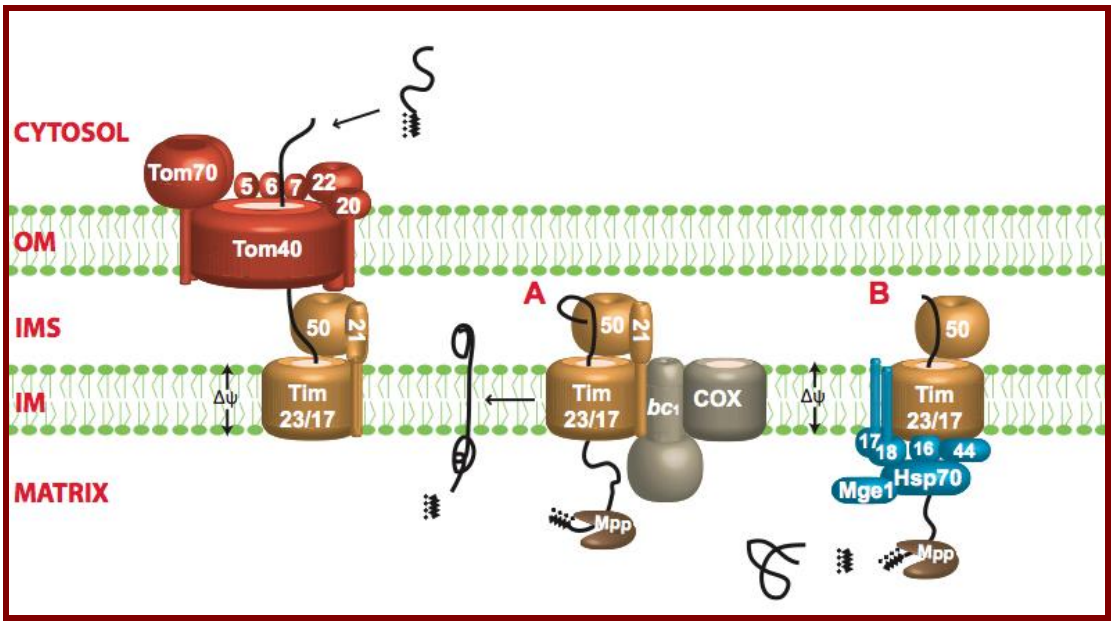

Figure 1.4 TOM/TIM23 pathway

Precursor proteins with an N-terminal targeting signal are preferentially recognised by Tom20 on the surface of mitochondria. The proteins traverse the OM through the TOM complex and are directed to the TIM23 complex by their interaction with Tim50. The TOM complex and the TIM23 complex are connected in a super-complex that prevents precursor proteins from interacting with the IMS. Entrance of the N-terminal sequence from precursor proteins into the TIM23 complex depends on the membrane potential ($\Delta\psi$). (A) Precursor proteins with a hydrophobic stop-transfer signal are released into the IM. The TIM23 complex is no longer linked to the TOM complex but is now bound to cytochrome bc_1 and cytochrome *c* oxidase (COX) of the respiratory chain. The mature protein is obtained by cleavage of the N-terminal targeting signal by MPP. (B) For their complete translocation, matrix proteins require the energy from both the $\Delta\psi$ and ATP hydrolysis by Hsp70. MPP cleaves the N-terminal targeting signal to obtain the mature protein. The TIM23 complex has lost Tim21 and is no longer bound to the TOM complex, but is now linked to the PAM complex. Pam16, Pam17, Pam18 and Pam44 help in the function of Hsp70 and in the binding of Hsp70 to TIM23. Mge1 contributes to the ATP hydrolysis activity of Hsp70. MPP: Mitochondrial processing peptidase, IM: inner membrane, IMS: intermembrane space, OM: outer membrane.

1.1.4. TOM/SAM – Insertion of β-barrel proteins into the mitochondrial OM

The sorting and assembly machinery (SAM) controls the insertion and folding of β-barrel proteins into the mitochondrial OM (Figure 1.5 A). Tom40 and porin are among the proteins that employ this pathway (Wiedemann et al., 2004). The SAM complex is composed of three membrane proteins: Sam50, Sam53 and Sam57. In this import pathway precursor proteins enter the IMS through the TOM complex and immediately interact with one of the small Tim hexameric complexes (Tim 9/10 or Tim8/13) (Wiedemann et al., 2004). Next, the precursor proteins are chaperoned to the SAM complex where their β-signal is recognised by Sam53. Complex formation between the β-signal, Sam53 and the pore-forming Sam50 initiates the insertion of the precursor protein into the SAM complex (Kutik et al., 2008). Lastly, the precursor proteins are folded and inserted into the mitochondrial OM by an unidentified mechanism occurring inside the SAM complex (Paschen et al., 2005, Kutik et al., 2008). The final release of the precursor proteins requires both Sam57 and the N-terminal of Sam50 (Chan and Lithgow, 2008).

1.1.5. Mim1 – Insertion of α-helical proteins into the mitochondrial OM

The insertion of α-helical proteins into the mitochondrial OM by Mim1 is the latest mitochondrial import pathway discovered (Figure 1.5 B). As such, it is also the least understood of all the pathways. The precursor proteins of this pathway are simply inserted into the OM without having to go through the TOM complex (Stojanovski et al., 2012). Single-spanning membrane proteins like Tom20 and Tom70 only require Mim1 for their insertion as (Becker et al., 2008, Hulett et al., 2008, Popov-Celeketic et al., 2008), while multi-spanning membrane proteins such as Ugo1 appear to need both Mim1 and the Tom70 receptor (Otera et al., 2007, Papic et al., 2011). The mechanisms of precursor protein recognition and further insertion into the OM have not been identified.

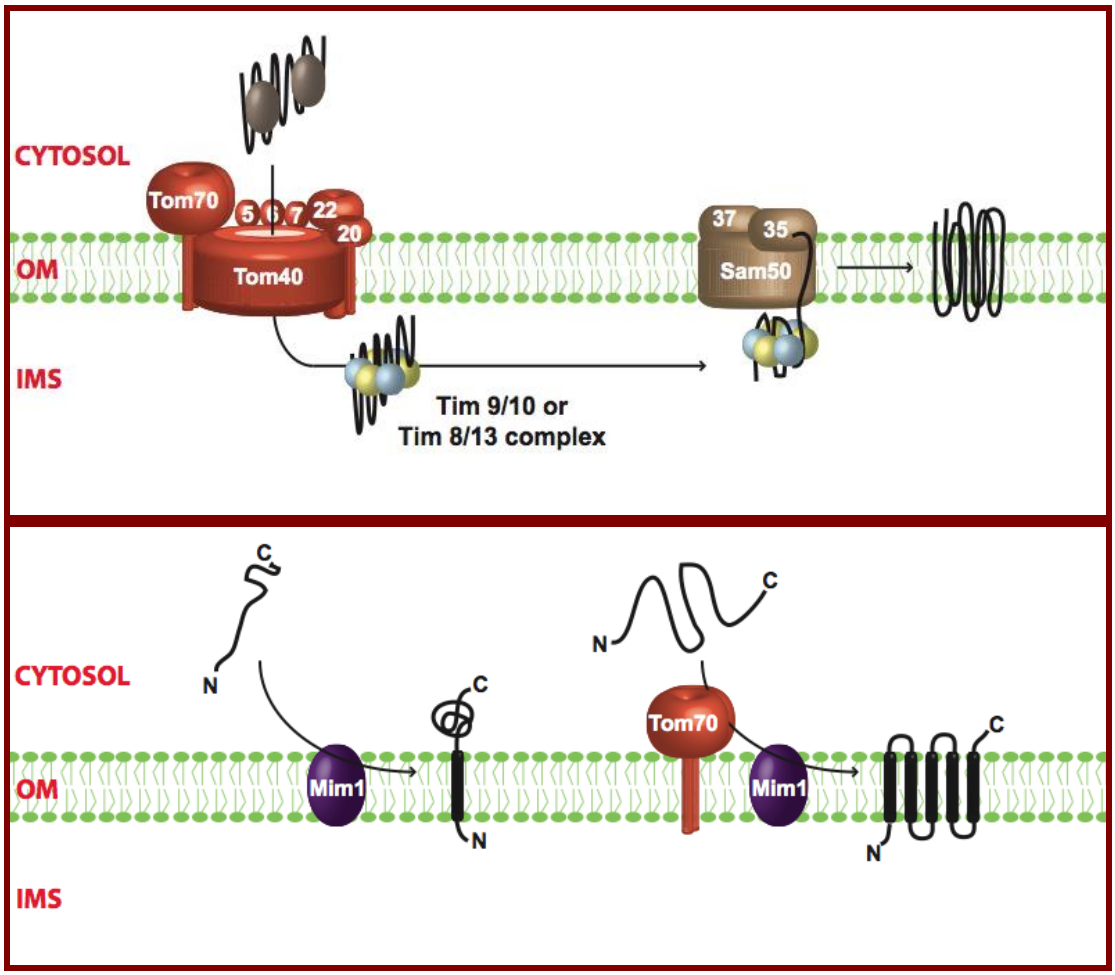

Figure 1.5 TOM/SAM and Mim1 pathways

A) Precursors of OM β-barrel proteins use cytosolic chaperones for their delivery to the TOM complex. The mechanism of translocation into the IMS is unknown but, on the IMS side of the TOM complex, the precursor proteins are bound by the small Tim complexes (Tim 9/10 or Tim 8/13). A β-signal is then recognised by Sam35, which promotes the interaction with the core protein Sam50. Finally, the precursor proteins are folded and inserted into the OM. The mechanism has not been elucidated but the final release into the OM requires Sam57. OM: outer membrane, IMS: intermembrane space.

B) Some OM α-helical proteins do not require the TOM complex for their mitochondrial import. Single-spanning transmembrane proteins employ Mim1 for their direct insertion into the OM, whereas multi-spanning transmembrane proteins require both Mim1 and Tom70 (but not the TOM complex) for their insertion. These two import pathways are still not well understood. OM: outer membrane, IMS: intermembrane space.

1.1.6. MIA pathway – Import into the mitochondrial IMS

The MIA pathway mediates the import of small, cysteine-containing IMS proteins that contain a MISS signal (Figure 1.6). The pathway employs two essential proteins, Mia40 and Erv1, each with redox-active disulphides. First, precursor proteins traverse the OM through the TOM complex and are tethered in the mitochondrial IMS by Mia40 (Naoe et al., 2004, Lutz et al., 2003). The interaction between Mia40 and precursor proteins is stabilised by formation of an intermolecular disulphide bond. The final result of this interaction is a precursor protein with a new disulphide bond and Mia40 with a reduced disulphide. Erv1 then reactivates Mia40 by oxidising the reduced disulphide (Mesecke et al., 2005). Finally, Erv1 itself is re-oxidised by reacting with either oxygen or cyt *c* (Bihlmaier et al., 2007, Bihlmaier et al., 2008), Interestingly, the latter reaction creates a link between the MIA pathway and the respiratory chain. The MIA pathway, and specifically Erv1, is reviewed in full in later sections.

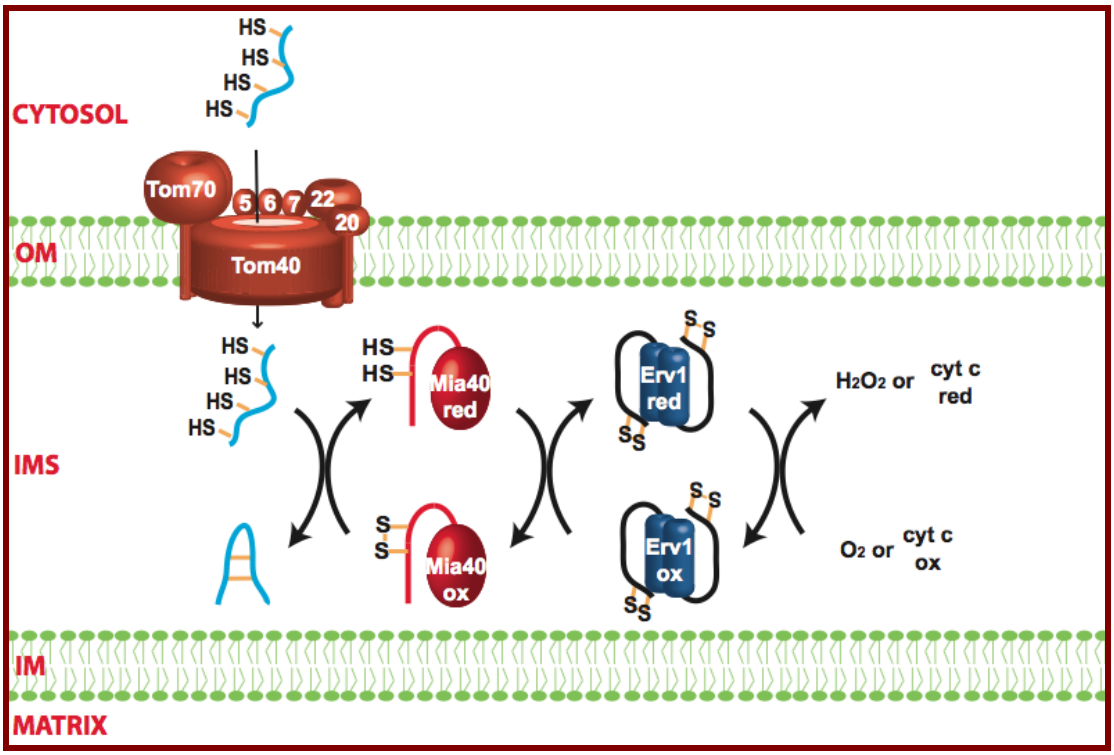

Figure 1.6 MIA pathway

Precursor proteins enter the IMS in a cysteine-reduced form. The proteins are first oxidised by the disulphide carrier Mia40. Next, Mia40 is re-oxidised by the sulphydryl oxidase Erv1, which in turn is re-oxidised by either oxygen or cyt *c*. IM: inner membrane, IMS: intermembrane space, OM: outer membrane.

1.2. Disulphide bond formation in the cell

Disulphide bonds are one of the most recurrent and important features in biological structures, where they most commonly play a role in stabilising the folding of proteins. However, disulphide bonds also participate in a wide variety of biological processes, from redox switches that regulate a protein's activity to being essential components in the active site of enzymes (Sevier and Kaiser, 2006, Wouters et al., 2010).

Proteins with disulphide bonds are mostly found in oxidative environments like the ER of eukaryotic cells and the periplasmic space of gram-negative and gram-positive bacteria (Table 1.1) (Inaba, 2010, Depuydt et al., 2011). Recently, however, a disulphide relay system was discovered inside the mitochondrial IMS that can insert disulphide bonds into a variety of substrate proteins (Herrmann and Riemer, 2012, Fischer and Riemer, 2013). Although the specific components of all these systems are different, they generally employ three factors: a disulphide carrier, a disulphide generator and an electron-accepting factor (Table 1.1). The disulphide carrier directly inserts disulphide bonds into unfolded or partially folded proteins, and usually has low substrate specificity. On the other hand, disulphide generators have narrower substrate specificity and only transfer their disulphide bonds to the disulphide carriers. This prevents the oxidising disulphide carriers from randomly inserting disulphide bonds into proteins and small molecules. Lastly, an electron-accepting factor is required that can take electrons from the reduced disulphide in the disulphide generator. These factors are generally protein cofactors like FAD and quinones that can use the electrons to reduce oxygen.

Table 1.1 Disulphide generating systems

Disulphide carrier	Disulphide generator	Electron-acceptor	Cellular localisation
DsbA	DsbB	Quinone	Periplasm of gram-negative bacteria
BdbD	BdbC	Quinone	Periplasm of gram-positive bacteria
Pdi1p/PDI	Ero1/ Ero1 a & B	FAD	ER of yeast/mammalian cells
Mia40	Erv1/ALR	FAD	IMS of yeast/mammalian cells
vvG4L	vvE10R + A2.5L	FAD	Viral proteins in bacterial cytosol

The disulphide generators are one of the most intriguing components of these pathways; they have solved the problem of disposing the electrons generated from introducing disulphide bonds during protein folding. Here, a detailed explanation is given on the sulphydryl oxidases, a blooming group of disulphide carriers that includes Erv1, as a prelude to the disulphide relay system of the mitochondrial IMS.

1.2.1. Sulphydryl oxidases: *De novo* formation of disulphide bonds

Sulphydryl oxidases are the net generators of disulphide bonds inside the cell. Whereas disulphide carriers simply exchange disulphide bonds between two proteins, sulphydryl oxidases catalyse the formation of new disulphide bonds by reducing oxygen to hydrogen peroxide. To do this, the proteins employ the FAD cofactor as a mediator to help transfer electrons from a reduced disulphide to oxygen (Kodali and Thorpe, 2010).

The electron transfer from a reduced disulphide to the isoalloxazine ring of FAD is believed to occur as depicted in Figure 1.7. Initially, rupture of the sulphydryl oxidase's disulphide bond (S_1-S_2) is achieved by the nucleophilic attack of a thiolate anion (S_3) from a substrate protein to the outermost sulphur of the disulphide bond (S_2). Computational analyses have suggested the optimal position of attack is for the incoming sulphur to be in line with both sulphur atoms of the protein disulphide (Bach et al., 2008). Once an intermolecular disulphide bond is formed between the attacking sulphur (S_3) and the outermost sulphur (S_2), the remaining sulphur (S_1) in the sulphydryl oxidase is free to form a charge-transfer complex with the isoalloxazine ring. Evidence for formation of this complex comes from both biophysical and structural approaches using wild-type or single cysteine mutants of various sulphydryl oxidases (Banci et al., 2012, Guo et al., 2012, Schaefer-Ramadan et al., 2013). The intermolecular disulphide bond (S_3-S_2) is next broken by the attack of a second thiolate anion (S_4) from the substrate protein, freeing the outermost sulphur (S_2) and producing a new disulphide bond (S_3-S_4) on the substrate protein. The negatively charged innermost sulphur (S_1) then attacks C4a of the isoalloxazine ring, covalently binding FAD. Next, an attack from the outermost sulphur (S_2) breaks the C4a adduct and reforms the initial disulphide bond (S_1-S_2) of the sulphydryl oxidase. In this step, both electrons

from the C4a adduct remain with the isoalloxazine ring, thereby reducing FAD (Kodali and Thorpe, 2010). Lastly, the transfer of electrons to oxygen regenerates the oxidised flavin and produces hydrogen peroxide. The steps controlling this last reaction are not well understood (Mattevi, 2006).

Sulphydryl oxidases are key components of the disulphide bond formation pathways mentioned earlier. As such, they are found in various parts of the cell like the ER, extracellular matrix and mitochondrial IMS (Kodali and Thorpe, 2010, Sevier, 2012). Sulphydryl oxidases can be divided into two different groups for their study: the ERV protein group and the Quiescin-sulphydryl oxidase (QSOX) protein group. The proteins in these groups all have an Erv fold (section 1.2.1.1), but otherwise differ in size, oligomerisation state, substrate specificity and the presence of other protein domains.

$$2RSH + O_2 \longrightarrow RS\text{-}SR + H_2O_2$$

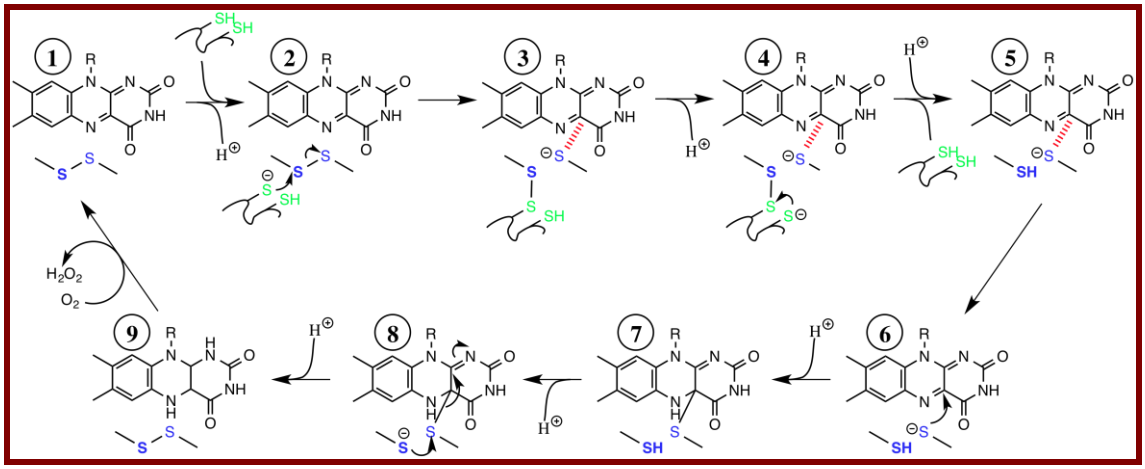

Figure 1.7 Model mechanism for the reaction of a sulphydryl oxidase

Proposed mechanism: The outermost sulphur of the disulphide bond in the protein (blue) is attacked by a thiolate substrate (green, 2) to form an intermolecular disulphide bond (3). A second thiolate from the substrate breaks the intermolecular disulphide bond (4) giving rise to a charge-transfer complex (5). The innermost sulphur attacks C4a of the isoalloxazine ring (6) forming an adduct (7). The outermost sulphur then breaks the adduct (8) to reform the original disulphide bond in the protein (9). In total, two electrons and two protons are transferred to the isoalloxazine ring. Finally, oxygen reacts with the reduced flavin to form hydrogen peroxide and oxidised flavin (1).

1.2.1.1. ERV protein family

The ERV family, also known as the ERV/ALR family, takes its name from a highly conserved Erv protein fold first recognised in Erv2 from *S. cerevisiae* (Gross et al., 2002). The acronym derives from Erv1, a homologue of Erv2, which was found to be essential for respiration and vegetative growth (Lee et al., 2000). In general, proteins in this family have molecular weights ranging from 15 to 30 kDa and contain a flexible and unstructured N- or C-terminal domain besides the Erv fold (Figure 1.8).

The Erv protein fold consists of about 100 amino acids and includes the essential CXXC redox-active disulphide, the $CX_{16}C$ structural disulphide and the FAD cofactor (Figure 1.9 A). The crystal structure of the Erv domain has been elucidated for five proteins in the family: *Arabidopsis thaliana* Erv1 (*At*ERv1), *S. cerevisiae* Erv1 (*Sc*Erv1), *S. cerevisiae (Sc*Erv2), *Rattus norvegicus* ALR (*Rn*ALR) and *Homo sapiens* ALR (*Hs*ALR) (Gross et al., 2002, Wu et al., 2003, Vitu et al., 2006, Daithankar et al., 2010, Guo et al., 2012). The Erv fold consisted of four tightly folded α-helices (H1 to H4) and a small fifth α-helix (H5) just outside the four-helix bundle (Figure 1.9 B). The crystal structures showed all proteins adopt a head-to-tail dimer conformation, with one subunit placed at a 55° angle with respect to the other (Figure 1.10 A). Helices H1 and H2 include conserved hydrophobic residues in their outer faces that form the dimer interface and are required to keep the protein in its dimer conformation (Figure 1.10 B) (Vitu et al., 2006, Fass, 2008, Guo et al., 2012)). The dimer is further stabilised by salt bridges and hydrogen bonds also between residues from H1 and H2 (Figure 1.10 C) (Guo et al., 2012). A single cysteine residue just outside the Erv fold of *Hs*ALR and *Rn*ALR was found to promote formation of inter-subunit disulphide bonds (Wu et al., 2003, Daithankar et al., 2010). However, this may be considered a particular case because this lonely cysteine is not found in any other protein of the ERV family.

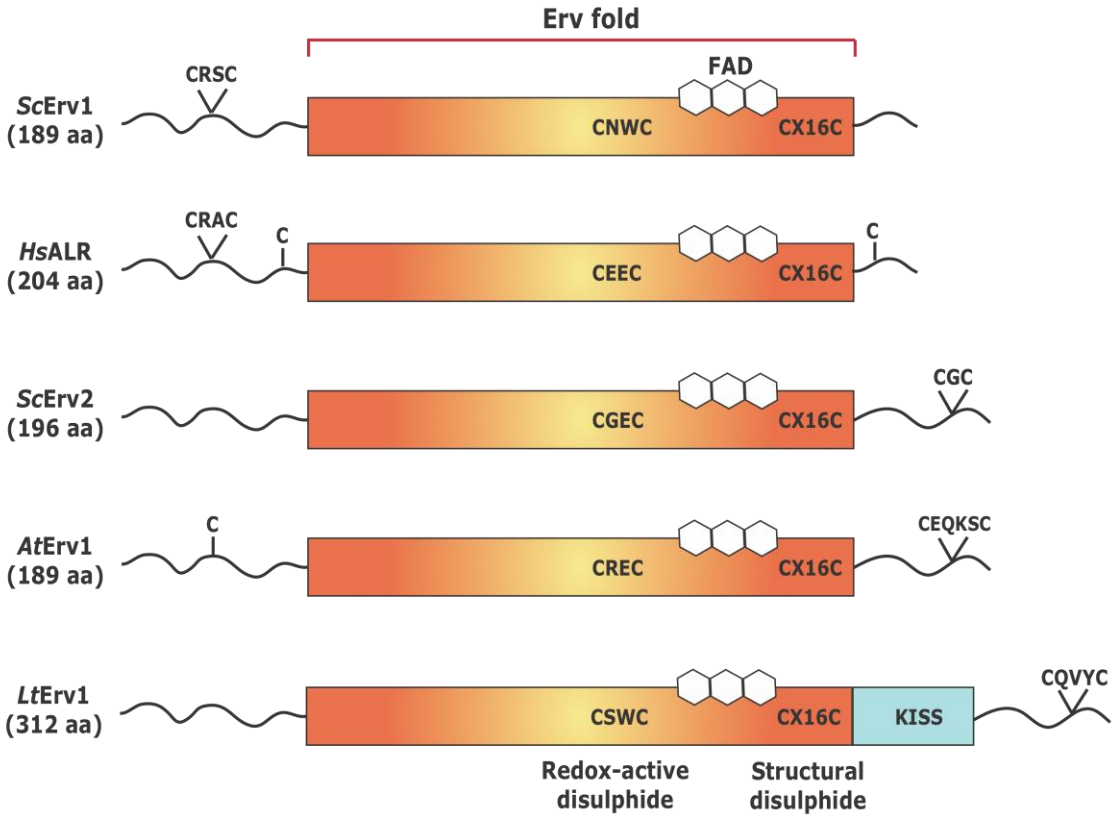

Figure 1.8 ERV family of proteins

Schematic construct, from N- to C-terminus, of proteins in the ERV family. The block (orange) represents the conserved Erv fold with the CXXC redox-active disulphide, the $CX_{16}C$ structural disulphide and the FAD cofactor. The CX_nC shuttle disulphide may be found at the N- or C-terminal in a flexible and unstructured polypeptide. Erv1 in *Leishmania tarentolae* also includes a Kinetoplastida-specifc second (KISS) domain. *Sc: Sacharomyces cerevisiae, Hs: Homo sapiens, At: Arabidopsis thaliana, Lt: Leishmania tarentolae.*

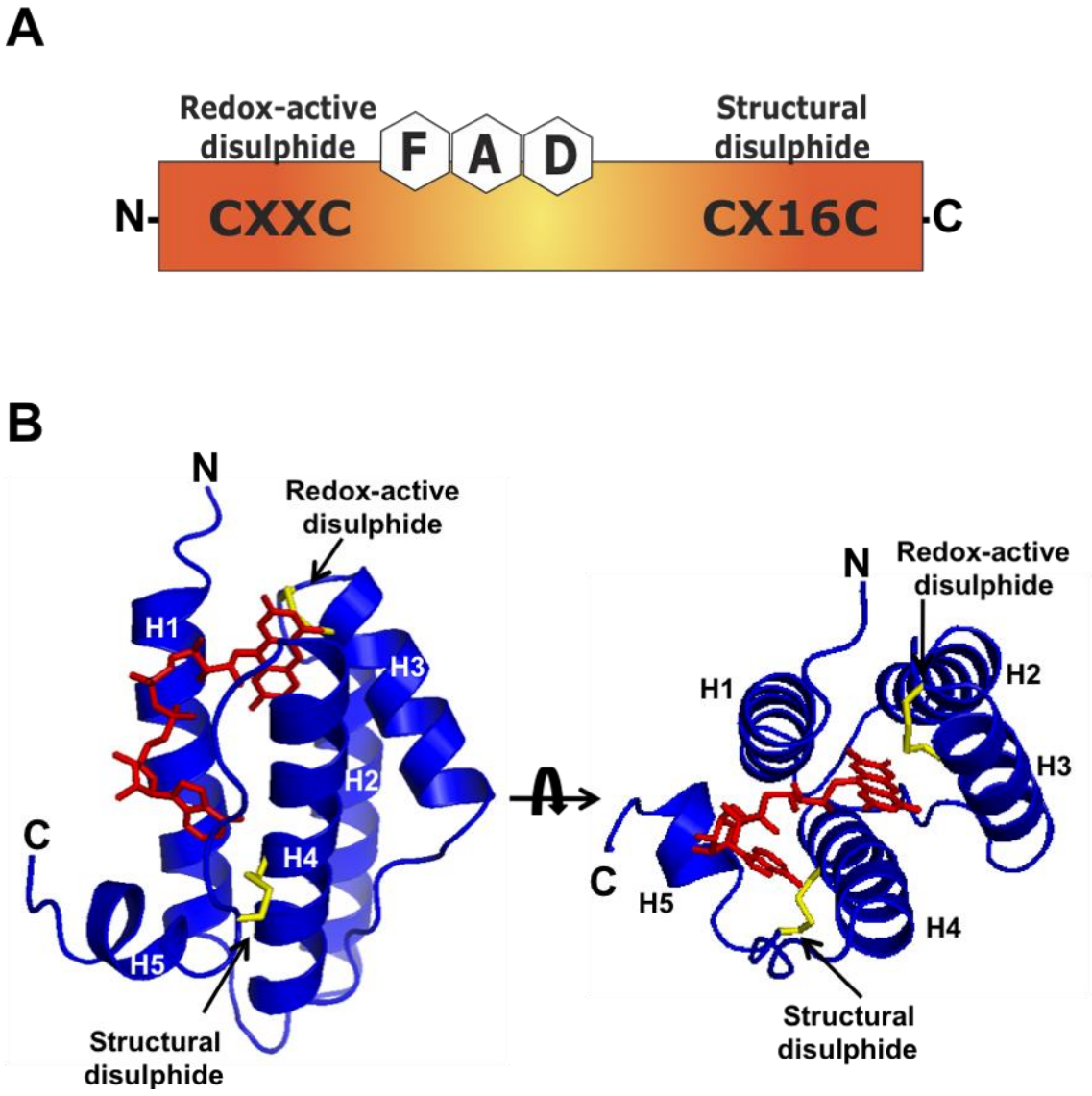

Figure 1.9 The Erv fold

A) Schematic construct, from N- to C-terminus, of the Erv fold.

B) Crystal structure of *Sc*Erv1 showing one subunit with the Erv fold. The structure is composed of a four-helix bundle (H1 to H4) and a small α-helix (H5). The isoalloxazine ring of FAD (red) is surrounded by H1 to H4, while the adenine moiety is enclosed by H1, H4 and H5. The CXXC redox-active disulphide is located at the N-terminus of H3. The $CX_{16}C$ structural disulphide connects H4 to H5. PDB: 4E0H.

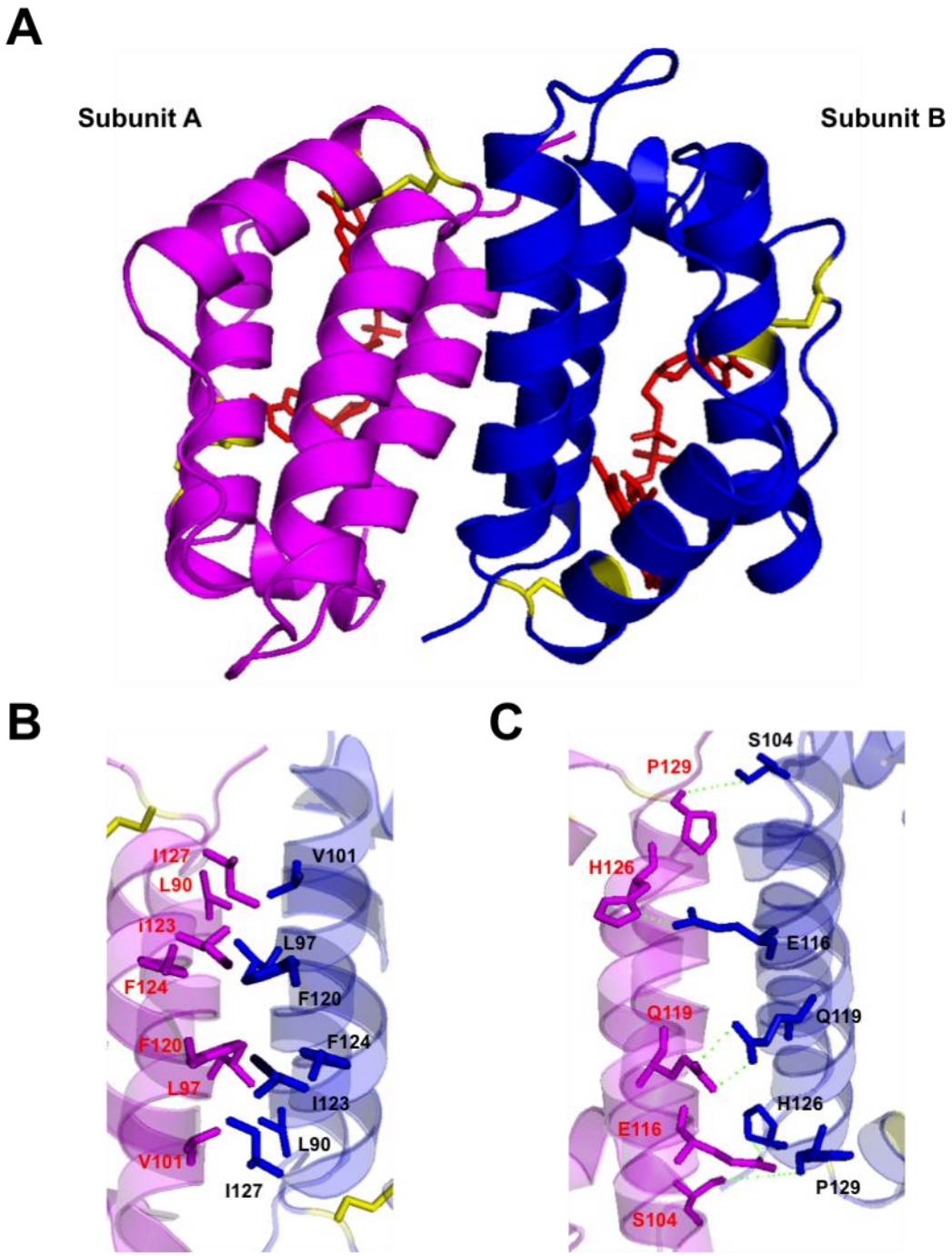

Figure 1.10 Dimer structure of the Erv domain

A) Crystal structure of *Sc*Erv1 showing the dimer conformation of the Erv domain with the FAD cofactor (red) and the disulphide bonds (yellow). The two dimer subunits (blue and magenta) are arranged in a head-to-tail dimer tilted at a 55°. PDB: 4E0H

B) Aromatic residues (blue and magenta sticks) forming the dimer interface of *Sc*Erv1. PDB: 4E0H

C) Residues (blue and magenta stick) forming hydrogen bonds (green) in the dimer interface of *Sc*Erv1. PDB: 4E0H

The Erv fold encloses the FAD cofactor. The isoalloxazine ring is buried in the four-helix bundle (H1 to H4) while the small fifth α-helix (H5) helps surround the adenine moiety (Figure 1.9 B). FAD adopts a peculiar conformation with the isoalloxazine and adenine moieties roughly parallel to one another, which so far has not been found in any other flavoproteins (Figure 1.11 A) (Fass, 2008). The two rings are about 10 Å apart at their closest point between the C8 methyl group of the isoalloxazine ring and the N7 nitrogen of the adenine moiety. This new conformation is partly stabilised by aromatic residues stacked successively above and below the FAD rings in a configuration reminiscent of that found in DNA (Fass, 2008). Additionally, polar amino acid residues also assist in the binding of FAD (Figure 1.11 C). For instance, the adenine moiety forms hydrogen bonds with a cysteine and two aspartate residues from H3. The phosphate groups of FAD are stabilised by hydrogen bonds with an arginine residue in H1, a histidine residue in H3 and a lysine residue found in the loop between H4 and H5. Finally, hydrogen bonds are also formed between the isoalloxazine ring and a tryptophan residue in H1 and either a histidine or an aspartate residue in H3. Most of these residues are highly conserved in the amino acid sequence of proteins in the ERV family, highlighting their importance for the binding of FAD (Figure 1.12). The only exception is the histidine/aspartate in H3 but either residue is still capable of forming a hydrogen bond.

There is one more residue, an arginine at the end of H5, which also links to the adenine moiety of FAD through a hydrogen bond in some of the proteins in the family (Figure 1.11 B). For example, it was found in *Sc*Erv1, *At*Erv1 and *Hs*ALR, but not in *Sc*Erv2 where the substituting glutamate did not form a hydrogen bond. Recent reports brought to attention the importance of this arginine for the FAD binding and overall function of proteins in the ERV family. Di Fonzo *et al.* (2009) showed that a histidine to arginine (R194H) mutation in *Hs*ALR was the cause of autosomal recessive myopathy in children. Furthermore, defects were also observed in the corresponding yeast *Sc*Erv1 R182H mutant strain (Di Fonzo et al., 2009). A complementary study then suggested that rupture of the arginine to FAD hydrogen bond in *Hs*ALR weakens the binding of FAD (Daithankar et al., 2010). Thus, although not strictly conserved, this arginine residue appears to be very important in stabilising FAD.

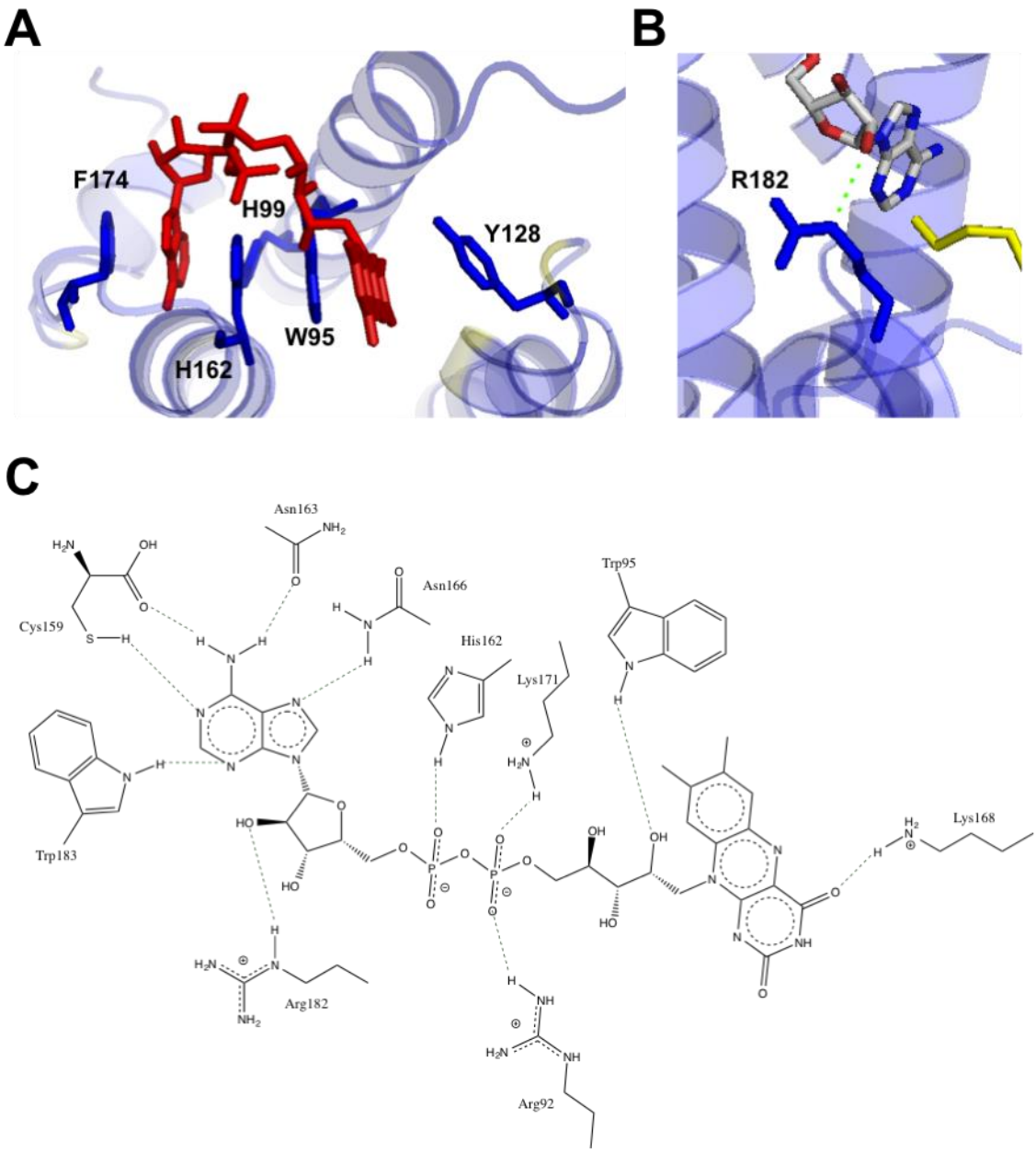

F

igure 1.11 Binding of FAD in the Erv fold

A) Crystal structure of *Sc*Erv1 showing the new conformation of FAD found in the ERV family. The adenine moiety and the isoalloxazine ring are almost parallel with a distance of ~10 Å between their closest atoms. In blue sticks are the conserved aromatic residues that form the DNA-like stacking conformation. PDB: 4E0H

B) Medically relevant arginine residue (R182) in *Sc*Erv1 that forms a non-conserved hydrogen bond (green) with the 2'-OH of the ribose moiety of FAD. PDB: 4E0H

C) Interactions stabilising the binding of FAD in the Erv fold of *Sc*Erv1. Several polar residues form hydrogen bonds (dashed lines) with FAD. Additionally,

some hydrophobic residues (green) further stabilise the binding. Most, but not all, of these interactions are conserved in other ERV proteins.

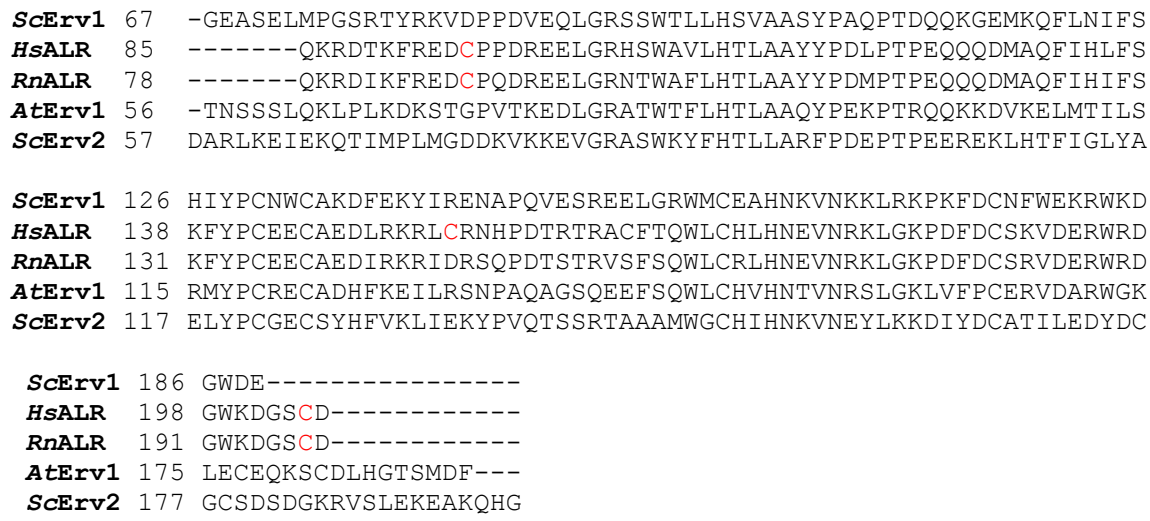

Figure 1.12 Sequence alignment of the Erv domain

Sequence alignment of the Erv domain for proteins in the ERV family. In yellow are the conserved cysteines forming the CXXC redox-active disulphide and the $CX_{16}C$ structural disulphide. In green are the semi-conserved hydrophobic residues that form the dimer interface. In magenta are the highly conserved residues that stabilise the DNA-like stacking conformation of FAD. In blue are the conserved residues that bind FAD through hydrogen bonds. *Sc: Sacharomyces cerevisiae, Hs: Homo sapiens, Rn: Rattus norvegicus, At: Arabidopsis thaliana.*

Another feature of the Erv fold is the highly conserved $CX_{16}C$ disulphide bond that links H4 with the N-terminus of H5 (Figure 1.9 B) (Gross et al., 2002, Fass, 2008). Although this disulphide bond does not participate in the electron transfer activity within the Erv fold, it does play a structural role in keeping the helix bundle more tightly folded (Ang and Lu, 2009).

Lastly, the Erv fold also includes the CXXC redox-active disulphide located at the N-terminus of H3 (Figure 1.9 B). This disulphide is almost perpendicular to the *re* side of the isoalloxazine ring with the second cysteine (C*) at ~3.5 Å of the C4a atom (Figure 1.13) (Gross et al., 2002, Fass, 2008). This configuration allows for the charge-transfer complex needed in the electron transfer between the CXXC redox-active disulphide and FAD (Banci et al., 2012, Guo et al., 2012, Schaefer-Ramadan et al., 2013). Despite the disulphide bond being solvent-accessible, the small crevice is only big enough to accept small reducing agents like DTT. Bulkier molecules such as TCEP or substrate proteins cannot reach the CXXC redox-active disulphide and thus cannot directly reduce the Erv fold (Ang and Lu, 2009).

To overcome the inaccessibility of the CXXC redox-active disulphide, proteins in the ERV family developed a CX_nC shuttle disulphide that transfers electrons from the substrate proteins to the Erv fold. Its precise location varies for proteins in the family, but is always found in a flexible, unstructured and very mobile polypeptide generally directly attached to the Erv fold (Figure 1.8). For instance, in *Sc*Erv2 and *At*Erv1, the shuttle disulphide is found in a C-terminal polypeptide (Sevier et al., 2001, Levitan et al., 2004); however, in *Sc*Erv1, *Rn*ALR and *Hs*ALR the polypeptide with the shuttle disulphide is located at the N-terminal (Hofhaus et al., 2003, Wu et al., 2003, Daithankar et al., 2009). Finally, the shuttle disulphide in Erv1 from *Leishmania tarentolae* (*Lt*Erv1) is also located at the N-terminal but, in this case, the protein also includes a Kinetoplastida-specific second (KISS) domain wedged between the Erv fold and the flexible polypeptide (Eckers et al., 2013).

The number (n) and identity of the amino acid residues between the two cysteines in the CX_nC shuttle disulphide is also not conserved among the proteins in the family (Figure 1.8). They go from just one residue (n=1), like in *Sc*Erv2, up to four residues (n=4) as in *Pf*Erv1 (Sevier et al., 2001, Basu et al., 2012). The only report that has addressed the relevance of these residues

observed that the CX_nC shuttle disulphide of *Sc*Erv2 can tolerate up to n=4 residues, but that n=0 is inactive (Vala et al., 2005). Interestingly, studies on small peptides showed that the oxidation and reduction of CX_nC disulphides are very slow for n=0 or n≥5 (Zhang and Snyder, 1989), adding further support to the findings on *Sc*Erv2.

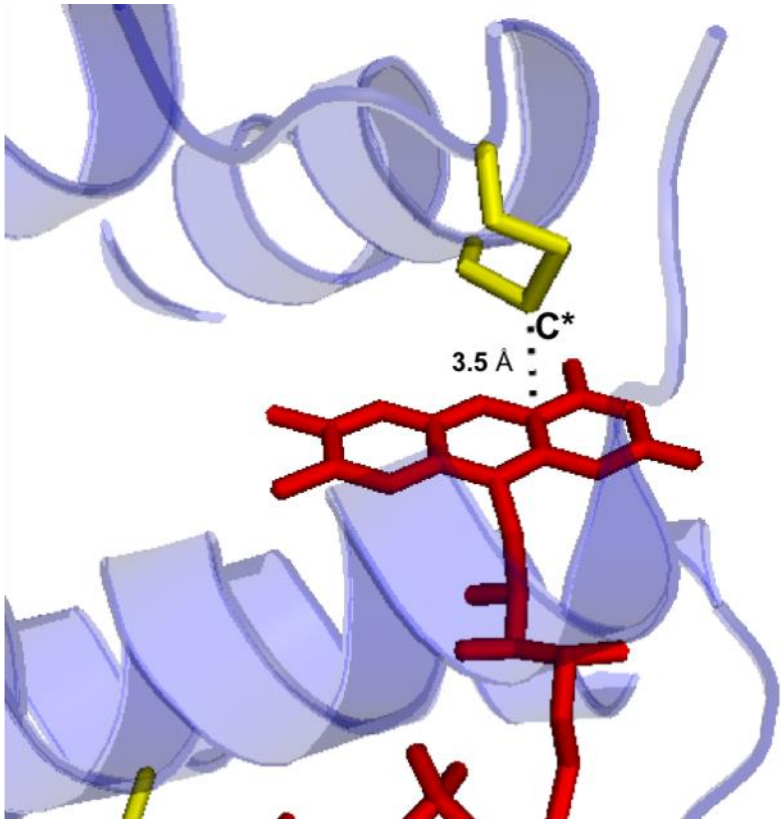

Figure 1.13 The CXXC redox-active disulphide bond in the Erv fold

The CXXC redox-active disulphide (yellow) is almost perpendicular to the *re* side of the isoalloxazine ring of FAD. The second cysteine (C*) is close enough (~3.5 Å) to rapidly interact with C4a. PDB: 4E0H

1.2.1.2. QSOX protein family

The main difference between QSOX and ERV proteins is in their number of structured protein domains; whereas ERV proteins only have one Erv domain, a generic QSOX protein comprises at least three domains (Figure 1.14): 1) a thioredoxin domain (Trx1) with a CXXC redox-active disulphide, 2) a helix-rich region (HRR) domain of unknown function and, 3) an Erv domain similar to those of the ERV family (Coppock and Thorpe, 2006, Heckler et al., 2008). Thus, proteins in the QSOX family are bigger and range in size from 50 to 80 kDa. Additionally, QSOX proteins in metozoans, but not in protozoans and plants, have a second thioredoxin domain (Trx2) that lacks the CXXC disulphide (Coppock and Thorpe, 2006, Kodali and Thorpe, 2010). Most QSOX proteins also have a C-terminal transmembrane sequence, although alternative soluble isoforms have also been found in certain species (Kodali and Thorpe, 2010, Sevier, 2012). The domains are ordered, from N- to C-terminal, in the sequence Trx1, Trx2, HRR and Erv (Kodali and Thorpe, 2010).

The proposed function of QSOX proteins is to aid in the oxidative folding of substrate proteins by inserting *de novo* disulphide bonds. Interestingly, unlike ERV proteins, QSOX proteins do not need to partner with a disulphide carrier for their function. The Trx1 domain contains a CXXC redox-active disulphide capable of directly interacting with substrate proteins. Next, the reduced disulphide of Trx1 shuttles the electrons to the CXXC redox-active disulphide of the Erv domain (Raje and Thorpe, 2003, Kodali and Thorpe, 2010). Studies with *Trypanosoma brucei* QSOX showed the disulphides of the Trx1 and Erv domains are at least 40 Å apart. However, the Trx1 domain can undergo a drastic rotation to bring the two CXXC disulphides within binding distance (Alon et al., 2012). Lastly, electrons are transferred to FAD and from there to oxygen (Hoober et al., 1996, Kodali and Thorpe, 2010). QSOX proteins have thus remarkably combined the functions of disulphide carriers and disulphide generators into one big protein.

Despite the oxidative power displayed by QSOX proteins, conclusive evidence is still lacking of which substrate proteins they interact with inside the cell (Sevier, 2012). Their intracellular location is surprisingly diverse, with QSOX proteins found in the ER, Golgi, secretory granules and even in the

nuclear membrane. They have also been found in secreted fluids such as egg white, semen, milk, tears and blood serum. Although absent in fungi, in humans there are several QSOX isoforms distributed mostly in the placenta, stomach, esophagus and lungs (Coppock and Thorpe, 2006, Kodali and Thorpe, 2010). Overall, the widespread locations of QSOX proteins suggest they play an important role in oxidative folding, but further research is still needed to identify their cellular protein substrates.

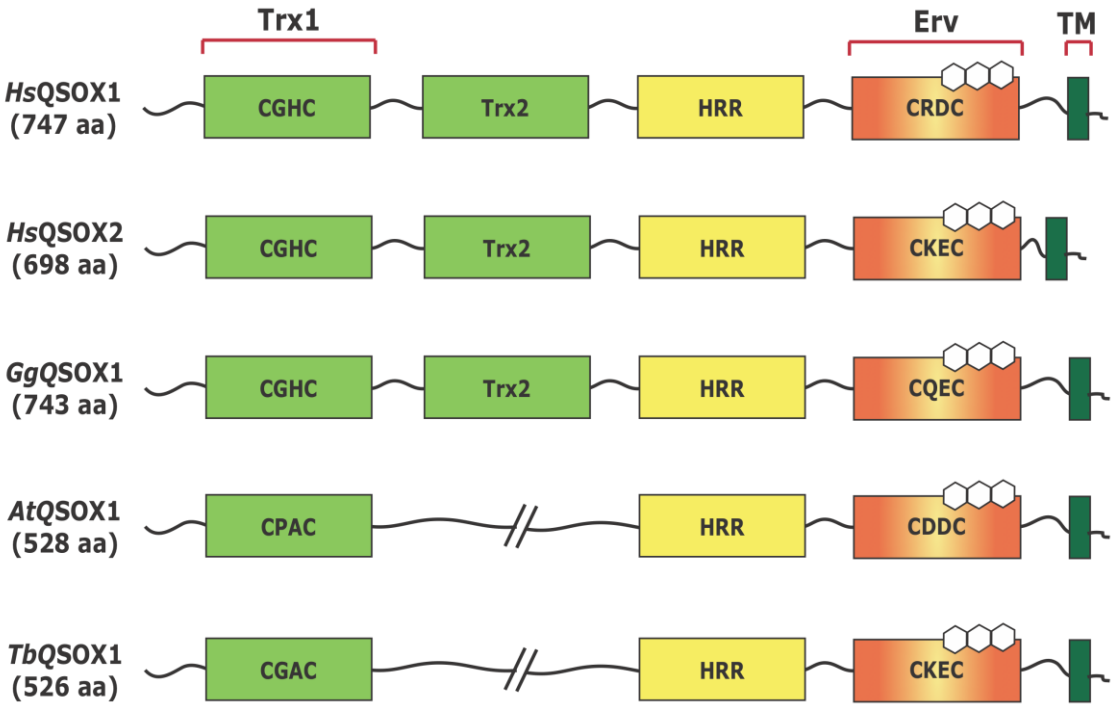

Figure 1.14 QSOX family of proteins.

Schematic construct, from N- to C-terminus, of proteins in the QSOX family. The QSOX proteins in metazoans (*Hs*QSOX 1 and 2, *Gg*QSOX1) have an additional inactive Trx2 domain. Trx1: thioredoxin domain with a CXXC redox-active disulphide, Trx2: thioredoxin domain lacking the CXXC disulphide, HRR: Helix-rich region, Erv: Erv domain, TM: Transmembrane domain, *Hs: Homo sapiens, Gg: Gallus gallus, At: Arabidopsis thaliana, Tb: Trypanosoma brucei.*

1.3. MIA pathway: Disulphide relay system of the mitochondrial IMS

The MIA pathway regulates the import and folding of cysteine-containing IMS proteins. Two essential proteins, Mia40 and Erv1, are at the core of the pathway and together form a disulphide relay system inside the mitochondrial IMS (Herrmann and Riemer, 2012, Fischer and Riemer, 2013).

1.3.1. Substrates of the MIA pathway

The proteins that employ the MIA pathway generally contain two or more cysteine residues and have a molecular weight beneath 30 kDa. For their study, they can be divided into three groups (Table 1.2): 1) classical substrates with either a twin CX_3C or twin CX_9C motif, 2) substrates with other CX_nC motifs, and 3) substrates with a canonical N-terminal mitochondria targeting signal (Fischer and Riemer, 2013). Proteins in this last group contain cysteine residues but do not require the MIA pathway for their import, only for their correct folding (Wrobel et al., 2013).

Although various proteins have been directly shown to be substrates of the MIA pathway, there are still dozens of potential substrates. If fact, a proteomic approaches have identified over 30 IMS proteins with CX_9C motifs (Longen et al., 2009, Cavallaro, 2010). Because these proteins lack an N-terminal mitochondrial targeting signal, it is very likely they employ the MIA pathway for their import. Thus, the actual count of MIA pathway substrates could be well past the current number of verified substrates.

Table 1.2 MIA pathway substrates

Twin CX_3C Twin CX_9C	**Other CX_nC**	**N-terminal targeting signal**
Tim8, Tim9, Tim10, Tim12, Tim13, Cox17, Cox19, Mdm1	Erv1, Sod1, Ccs1, Atp23	Mia40 Tim22

1.3.2. Mia40: Disulphide carrier and chaperone of the IMS

Mia40 is the initial point of contact for substrate proteins. It is a protein of 403 amino acids embedded in the mitochondrial IM, with a large part of it exposed to the IMS (Chacinska et al., 2004, Naoe et al., 2004, Terziyska et al., 2005). The protein can be thought of as two separate domains (Figure 1.15 A): the N-terminal domain (residues: 1-284) that includes the N-terminal mitochondria targeting signal and a transmembrane anchor, and the C-terminal domain (residues: 284-403) that contains the redox-active CPC motif essential for the disulphide carrier activity of Mia40.

In the MIA pathway, Mia40 transfers disulphide bonds from the disulphide generator Erv1 to the substrate proteins. Although originally considered to be involved only in the import of IMS proteins, recent reports have suggested Mia40 can also oxidise proteins already found in the IMS and whose mitochondrial import is independent of the MIA pathway. For example, Tim22 is a cysteine-containing IM protein that enters mitochondria through the TIM22 pathway (Kurz et al., 1999, Wagner et al., 2008). However, its final oxidative folding and assembly was shown to require Mia40 (Wrobel et al., 2013). Another role of Mia40 is that of a chaperone without the insertion of disulphide bonds into the substrate proteins. In this case the import of Atp23, with all its cysteine residues mutated to serines, still depended on Mia40 (Weckbecker et al., 2012). Lastly, in another MIA-pathway-independent role, the CPC motifs of two Mia40 proteins were found to coordinate a [2Fe-2S] cluster. The studies also showed Mia40 uptakes iron *in vivo*, suggesting Fe/S_Mia40 could have a still unidentified function inside the cell (Spiller et al., 2013).

Mia40 homologues can be found throughout the eukaryotic kingdom. Unlike Mia40 in fungi, where the protein is anchored to the IM, plants and animals have a soluble Mia40 consisting of only the C-terminal domain of their fungal counterparts (Hofmann et al., 2005, Terziyska et al., 2005, Chacinska et al., 2008). Prediction of mitochondrial-targeting signals for Mia40 homologues revealed that proteins in the fungi kingdom probably contain a mitochondrial-targeting signal (~90% probability), but those in plants and animals do not (Chacinska et al., 2008). The reason why fungal Mia40 has

retained, or developed, a mitochondrial-targeting signal is unknown since it is not required for its import and function in the IMS.

The activity of Mia40 resides entirely on its C-terminal domain. Studies with human Mia40, itself equivalent to only the C-terminal domain of *S. cerevisiae* Mia40, showed the protein can fully complement a yeast *ΔMIA40* deletion strain (Grumbt et al., 2007, Chacinska et al., 2008). Furthermore, a highly conserved ~70 amino acids core located in the C-terminal domain (Mia40c: residues 284-353) was demonstrated to be sufficient for yeast cell viability (Chacinska et al., 2008). Mia40c includes six invariant cysteine residues: C296, C298, C307, C317, C329 and C339 – hereafter called $C1^M$-$C6^M$, which are arranged in a CPC and two CX_9C motifs (Figure 1.15 A). Mass spectrometry analyses initially revealed the formation of three disulphide bonds: $C1^M$-$C2^M$, $C3^M$-$C6^M$ and $C4^M$-$C5^M$ (Grumbt et al., 2007). This finding was further confirmed by the crystal structure of Mia40c (Figure 1.15 B), which showed a rigid N-terminal loop followed by two anti-parallel α-helices ($H1^M$ and $H2^M$) in a helix-turn-helix conformation (Kawano et al., 2009). The $C3^M$-$C6^M$ and $C4^M$-$C5^M$ disulphide bonds link the two α-helices, while the $C1^M$-$C2^M$ disulphide bond is solvent-exposed and readily available for reduction (Grumbt et al., 2007, Kawano et al., 2009). *In vitro* and *in vivo* analyses using cysteine to serine mutants of Mia40 established that only $C1^M$-$C2^M$ and $C3^M$-$C6^M$ have an effect on protein activity. The $C1^M$-$C2^M$ disulphide bond participates in intermolecular disulphide bond formation with both MIA pathway substrate proteins and Erv1. However, only $C2^M$ is able to initiate the interaction with Erv1, whereas either $C1^M$ or $C2^M$ can form a disulphide bond with substrate proteins. The disulphide alternates between its oxidised and reduced state but does not influences the overall structure of Mia40 (Kawano et al., 2009, Terziyska et al., 2009). Contrarily, both the $C3^M$-$C6^M$ and the $C4^M$-$C5^M$ disulphide bonds play a role in keeping the tertiary structure of Mia40. The $C3^M$-$C6^M$ disulphide bond appears to be more important because its removal also strongly diminished the activity of Mia40 (Kawano et al., 2009, Terziyska et al., 2009).

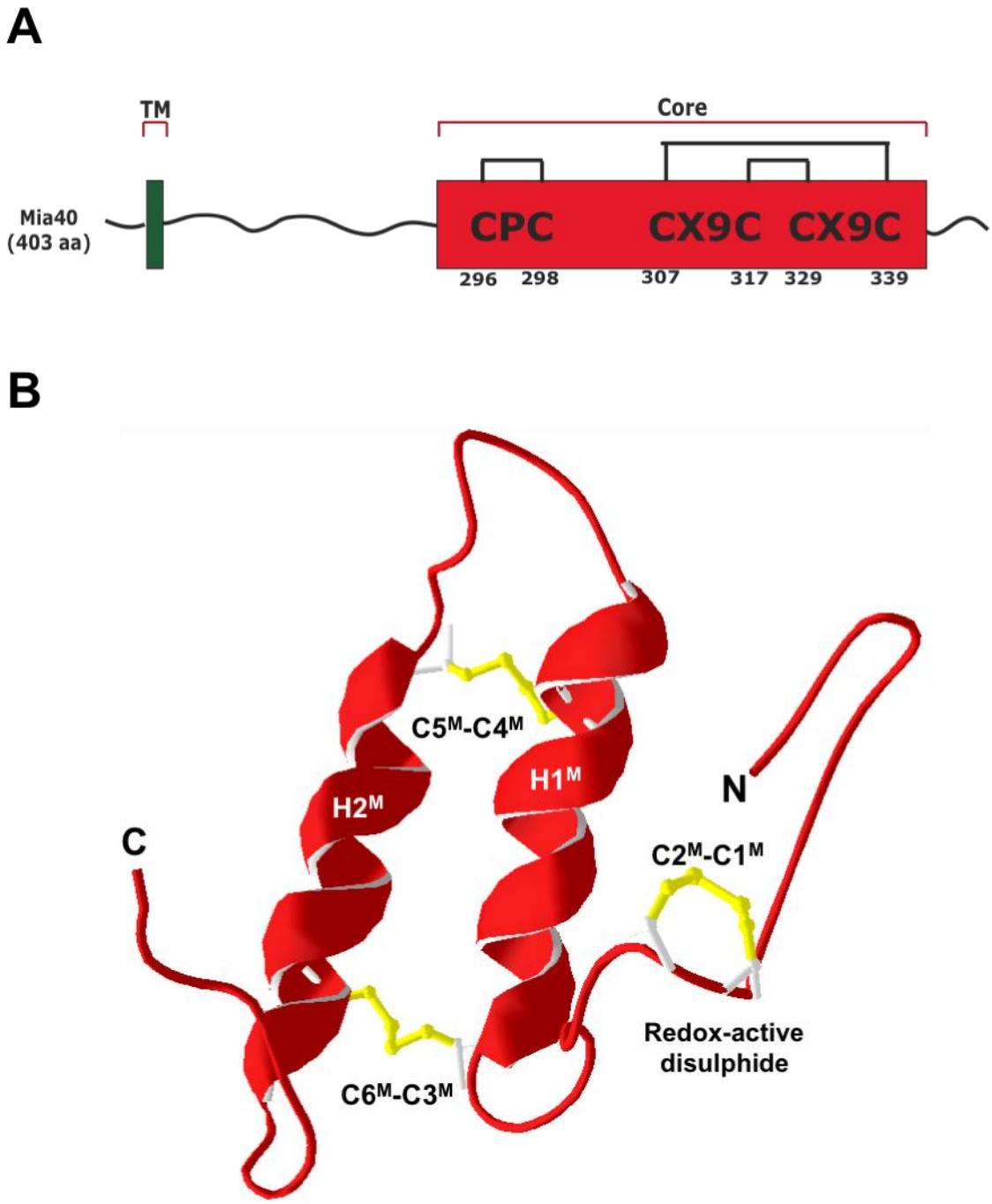

Figure 1.15 Mia40

A) Schematic construct, from N- to C-terminus, of *Sc*Mia40 showing the conserved Mia40 core (residues: 284-355) and the non-conserved N-terminal domain. TM: Transmembrane.

B) Crystal structure of fully oxidised *Sc*Mia40 core (residues: 284-355). The twin CX_9C motif forms two disulphide bonds ($C3^M$-$C6^M$ and $C4^M$-$C5^M$, in yellow) that connect the two anti-parallel α-helices ($H1^M$ and $H2^M$). The CPC redox-active disulphide ($C1^M$-$C2^M$) is located in a fixed loop at the N-terminal. PDB: 2ZXT

The crystal structure of Mia40c displayed a hydrophobic cleft positioned near the redox-active $C1^{M}$-$C2^{M}$ disulphide bond (Figure 1.16 A). Hydrophobic residues protruding from $H1^{M}$, $H2^{M}$ and the N-terminal loop contribute to the cleft and help maintain the loop in a rigid framework (Figure 1.16 B) (Kawano et al., 2009, Endo et al., 2010). This hydrophobic cleft is the point of anchor for substrate proteins. Mutation of four phenylalanine residues to glutamate resulted in either a lethal (F315E, F318E) or a temperature-sensitive (F311E, F334E) phenotype in the corresponding yeast strains. However, substitution of the phenylalanine residues for leucine or alanine did not cause any visible growth defect, suggesting it is the hydrophobicity of the residues that is important (Kawano et al., 2009). Interestingly, the Mia40 F311E and Mia40 F334E temperature-sensitive strains could be restored by overexpressing Erv1. This suggests these two residues do not only participate in substrate binding but also in the interaction of Mia40 with Erv1 (Kawano et al., 2009).

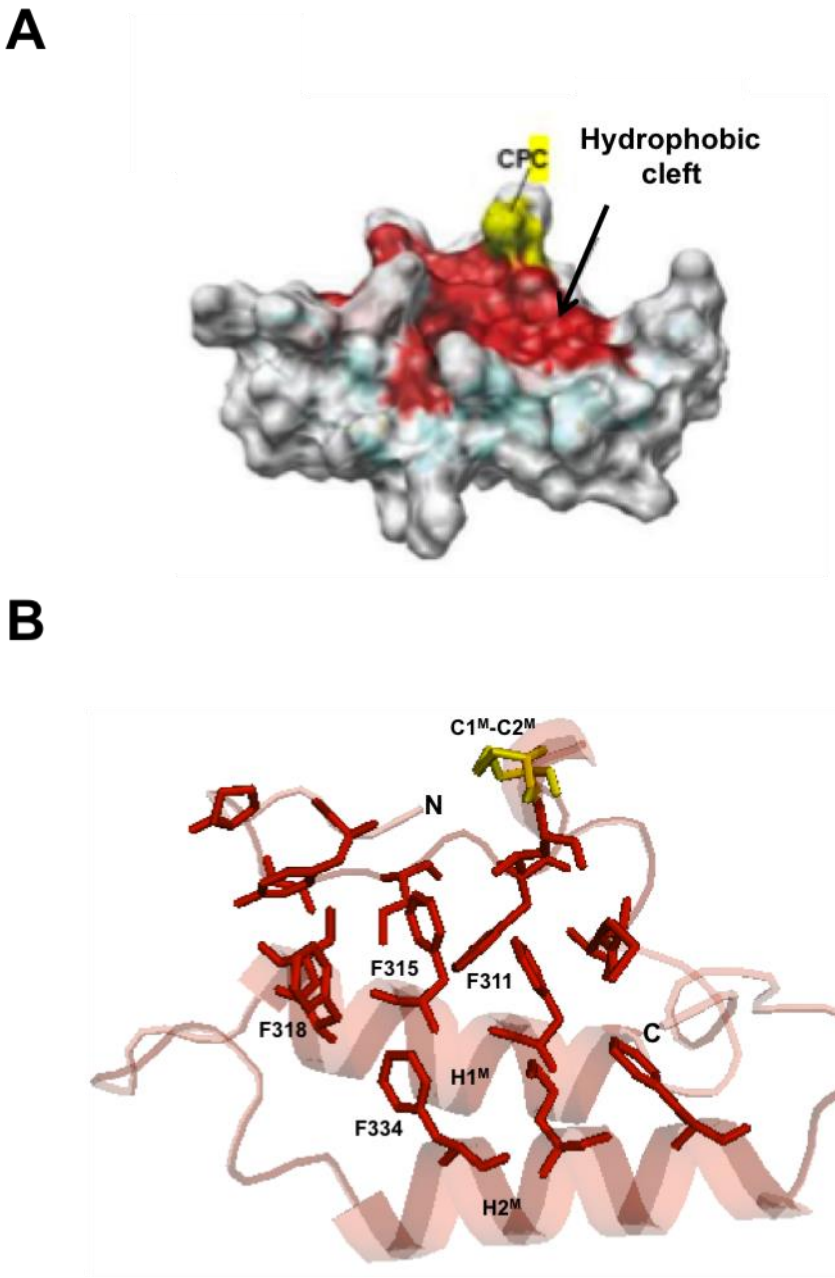

Figure 1.16 The hydrophobic cleft in Mia40

A) Molecular surface of Mia40 core (residues: 284-355) showing the hydrophobic cleft (red) that recognises both substrate proteins and the N-terminal domain of Erv1. $C2^M$ (yellow) of the CPC motif is looking towards the cleft. Adapted from Sideris *et al*. (2009)

B) Cyrstal structure of *Sc*Mia40 core (residues: 284-355) showing the hydrophobic residues (red sticks) from $H1^M$, $H2^M$ and the N-terminal loop that contribute to the hydrophobic cleft. Phenylalanine residues that have been shown to be important for substrate recognition are labelled. PDB: 2ZXT

1.3.3. Erv1: Sulphydryl oxidase of the mitochondrial IMS

The first mention of Erv1 came in studies of *S. cerevisiae petite* mutants where the protein was found to be essential for respiration and vegetative growth (Lisowsky, 1992). Erv1 is a sulphydryl oxidase of 189 amino acids belonging to the ERV protein family, with six cysteine residues arranged in three disulphide bonds: C30-C33, C130-C133 and C159-C176 – hereafter called C1-C2, C3-C4 and C5-C6 (Lee et al., 2000, Lange et al., 2001). The protein can be divided into a C-terminal domain (residues: 73-189) and a highly mobile N-terminal domain (residues: 1-72) (Figure 1.8). Neither the N-terminal domain nor the C-terminal domain are able to recover a *ΔERV1* yeast deletion strain. However, a combination of both does restore cell viability, indicating the two domains are required for the function of Erv1 *in vivo* (Bien et al., 2010).

The function of Erv1 in the MIA pathway is to act as a generator of new disulphide bonds. It re-oxidises the CPC motif of Mia40 and then transfers the electrons to either oxygen or cyt *c* (Ang and Lu, 2009, Bien et al., 2010). Although this function is well established, Erv1 has also been involved in the cell division cycle, the preservation of mitochondria morphology, the maintenance of mtDNA, the biogenesis of cytosolic Fe/S clusters and the maturation of the heme cofactor (Lisowsky, 1992, Lisowsky, 1994, Lange et al., 2001). However, because the main role of Erv1 is as part of a mitochondrial import pathway, it is difficult to assess whether its involvement is not due to an indirect defect in the import of other essential proteins. For example, a yeast strain with an arginine to histide (R182H) mutation displayed impaired complex IV activity, mtDNA instability, altered mitochondria morphology, lower cysteine-containing IMS protein content and slower growth at 37°C (Di Fonzo et al., 2009, Sztolsztener et al., 2013). Whether these defects are a direct or indirect cause of Erv1 malfunction is currently unknown.

The crystal structure of the Erv1 C-terminal domain showed the protein adopts an angled head-to-tail dimer conformation, similar to those observed for other proteins in the ERV family (Section 1.2.1.1) (Guo et al., 2012). Additionally, size exclusion chromatography experiments also indicated the C-terminal domain adopts a dimeric structure (Bien et al., 2010, Guo et al.,

2012). For Erv1, the dimer interface covers an area of 1830 $Å^2$ and is formed by the hydrophobic residues L90, L97, V101, F120, I123, F124 and I127. Polar residues S104, E116, G119, H126 and P129 also contribute to the dimer interface by forming hydrogen bonds (Guo et al., 2012).

The C-terminal domain includes the Erv fold. In it, C3-C4 is the redox-active disulphide and C5-C6 the structural disulphide. Mutation of one or both cysteines in C3-C4 completely abolished the oxidase activity of Erv1 against reducing agents like DTT or TCEP, indicating the C3-C4 disulphide is essential for Erv1 activity (Hofhaus et al., 2003, Ang and Lu, 2009). In fact, neither an Erv1 C3S mutant nor an Erv1 C4S mutant was capable of recovering a *ΔERV1* yeast deletion strain, suggesting that the C3-C4 redox-active disulphide is also required for the function of Erv1 inside the cell (Hofhaus et al., 2003, Bien et al., 2010). On the other hand, the C5-C6 disulphide plays a structural role in stabilising the Erv fold. Thermal denaturation analyses showed that deletion of either C3-C4 or C5-C6 influences the overall stability of Erv1, but the effect was stronger for C5-C6. The removal of C5-C6 lowered the melting temperature of Erv1 by 30°C, from 68°C for the wild-type to 38° for the C5,6S mutant. Furthermore, at the physiological temperature of 30°C about 20% of the C5,6S mutant appeared unfolded. Instead, deletion of C3-C4 exhibited a milder defect with a melting temperature of 52°C for Erv1 C3,4S (Ang and Lu, 2009).

The N-terminal domain of Erv1 includes the C1-C2 shuttle disulphide, which is thus called because its function is to transfer electrons between bulky reducing agents (e.g. TCEP, Mia40) and the C3-C4 redox-active disulphide. Mutation of one or both cysteines in C1-C2 resulted in the cell death of the yeast strain, indicating both cysteines are essential for Erv1 function in vivo (Hofhaus et al., 2003, Bien et al., 2010). *In vitro* assays then showed that removing the C1-C2 disulphide suppressed the activity of Erv1 against Mia40, but not against DTT (Hofhaus et al., 2003, Ang and Lu, 2009). Thus, the N-terminal domain, and more precisely the C1-C2 disulphide, is required for the interaction of Erv1 with the hydrophobic cleft of Mia40. In fact, in the case of *Hs*ALR, NMR experiments using confirmed its N-terminal domain interacts with the hydrophobic cleft of human Mia40 (Banci et al., 2011). These initial hydrophobic interactions are further stabilised by formation of an intermolecular disulphide bond between Erv1 and the CPC motif of Mia40.

So far no crystal structure of full-length Erv1 has been published, perhaps due to the high mobility of the N-terminal domain. However, the crystal structure of a full-length Erv1 C1,4S mutant allowed for the determination of a partial structure of the N-terminal domain (Figure 1.17 A) (Guo et al., 2012). This mutant has a C2-C3 inter-domain disulphide bond that restrained the motion of the N-terminal domain. Remarkably, formation of the C2-C3 disulphide bond promoted the folding of a small α-helix (H0) in the N-terminal domain from residues 36 to 47, which were followed by a defined loop from resides 14 to 35. However, the linker segment (48 to 83) from H0 to the C-terminal domain was not visible in the crystal structure, meaning the N-terminal could belong to either dimer subunit (Guo et al., 2012). Interestingly, the interaction between the N-terminal and the C-terminal domains goes beyond the formation of the C2-C3 inter-domain disulphide bond. Hydrogen bonds also help stabilised the interaction, from N-terminal to C-terminal domain (Figure 1.17 B): S32 and N34 to V87, L36 to D86, R31 to P84 and D24 to W132. Finally, hydrophobic contacts of two N-terminal domain patches (I21/I22 and T35) with their corresponding C-terminal domain patches (W132 and V87) also contribute to the interaction (Figure 1.17 C).

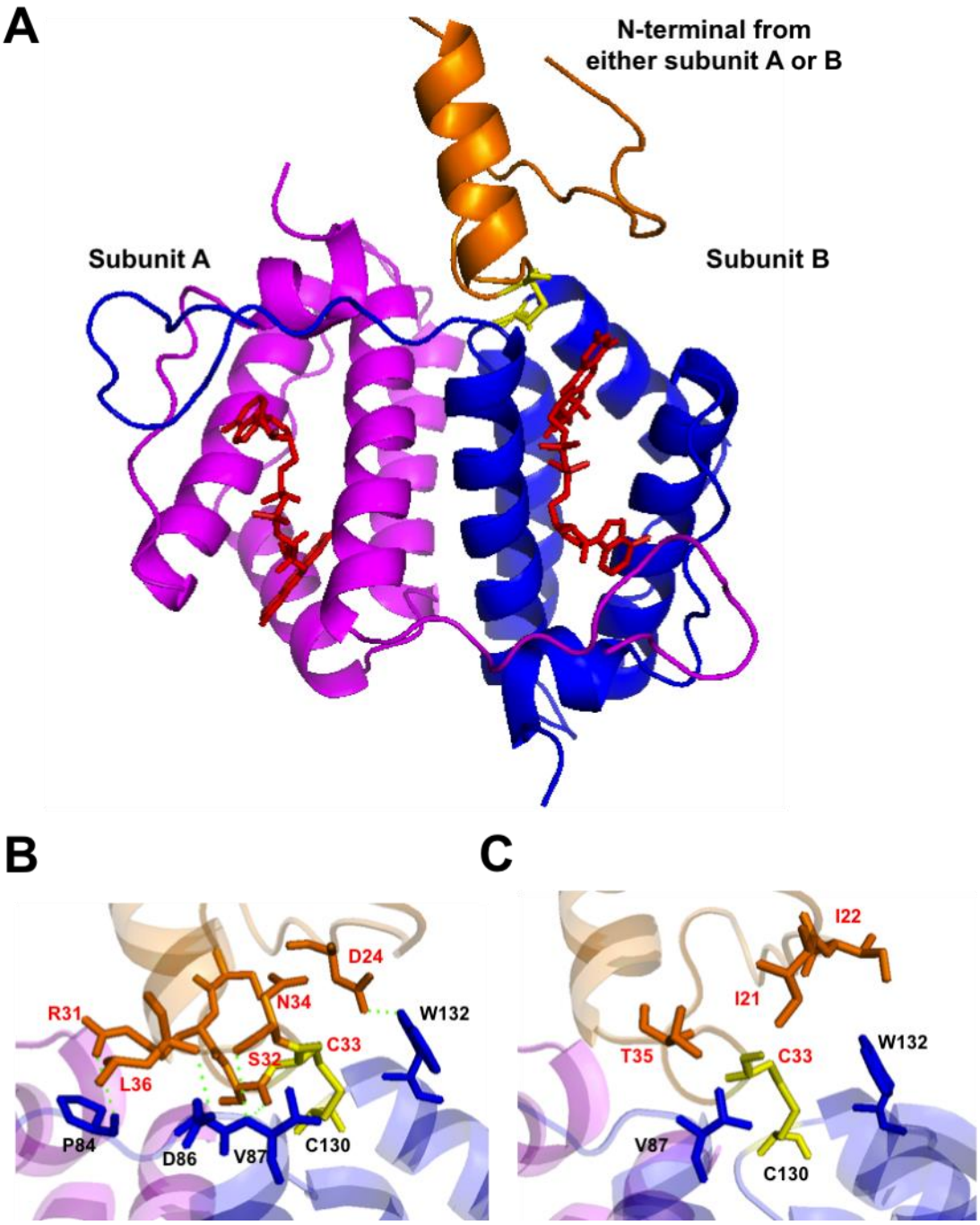

Figure 1.17 Crystal structure of ScErv1 C1,4S

A) Crystal structure of *Sc*Erv1 C1,4S showing subunit B (blue) connected to the partial structure of an N-terminal domain (orange) by a C2-C3 inter-domain disulphide bond (yellow). FAD is in red. The PDB: 3E0I

B) Crystal structure of *Sc*Erv1 C1,4S showing the residues that form hydrogen bonds (green) between the N-terminal (orange) and C-terminal (blue) domains. The C2-C3 inter-domain disulphide bond is in yellow. PDB: 3E0I

C) Crystal structure of *Sc*Erv1 C1,4S showing the hydrophobic residues that further stabilise the interaction between the N-terminal (orange) and C-terminal (blue) domains. The C2-C3 inter-domain disulphide bond is in yellow. PDB: 3E0I.

1.3.4. The MIA import pathway in detail

1.3.4.1. Substrate proteins in the cytosol

Most MIA pathway substrate proteins are imported post-translationally. A recent report using mammalian cells indicated substrate proteins remain in the cytosol for several minutes before their import, suggesting the same may occur with yeast proteins (Fischer et al., 2013). Only the cysteine-reduced and unfolded substrate proteins can enter mitochondria, both their fully and partially oxidised conformations are import-incompetent (Figure 1.18) (Lu and Woodburn, 2005, Morgan and Lu, 2008). Recently, the Trx and glutharedoxin (Grx) systems have been involved in keeping the substrate proteins reduced in the cytosol (Durigon et al., 2012, Banci et al., 2013a). First, deletion of the entire Trx system lowered the steady-state levels of Tim9 and Cox 19. Trx1 was then shown to enhance mitochondrial import of Tim9 and Cox19 *in organello*, presumably by keeping the proteins in their cysteine-reduced conformation. Finally, *in vitro* assays showed Trx1 is indeed able to reduce partially oxidised, one-disulphide bonded Tim9, but not its fully oxidised, two-disulphide bonded conformation (Durigon et al., 2012). On the other hand, mammalian Grx1, and to a lesser extent mammalian Trx1, were shown to keep human Mia40 in its reduced conformation when overexpressed in the cytoplasm of mammalian cells (Banci et al., 2013a). Thus, it appears both redoxin systems contribute to keeping the substrate proteins reduced and their relevance might be dictated by the species. Interestingly, earlier reports demonstrated that the binding of zinc by substrate proteins keeps them in their cysteine-reduced conformation even in the presence of GSSG (Morgan et al., 2009). However, no evidence has yet been available to indicate substrate proteins bind zinc inside the cell.

It is still unclear how MIA pathway substrate proteins are targeted to mitochondria. Studies have now identified a MISS (mitochondrial IMS sorting signal), also called ITS (IMS-targeting signal), in proteins with a twin CX_3C or twin CX_9C motif (Milenkovic et al., 2009, Sideris et al., 2009). This signal is sufficient to direct non-mitochondrial proteins to the IMS independently of its location in the protein (Sideris et al., 2009). However, no MISS/ITS recognition site has been identified in the surface of mitochondria and, moreover, other substrate proteins completely lack this signal. Curiously, the

only common denominator in all substrate proteins appears to be the presence of hydrophobic residues near the cysteine that first reacts with Mia40, but for this reaction to occur the substrate proteins must already be inside the IMS.

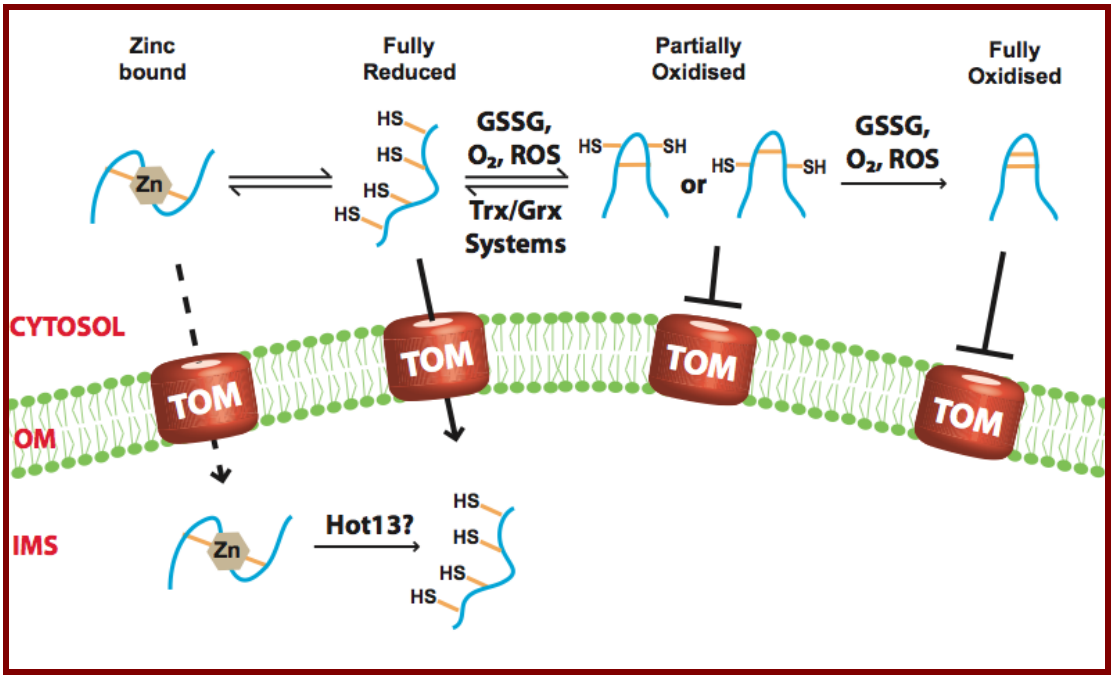

Figure 1.18 Keeping the substrate proteins reduced in the cytosol

The substrate proteins of the MIA pathway are kept reduced in the cytosol by the thioredoxin (Trx) and glutaredoxin (Grx) systems. Additionally, zinc binding may also play a role in keeping precursor proteins from oxidation. Only the fully cysteine-reduced substrate proteins can enter the mitochondrial IMS through the TOM complex. Partially oxidised and fully oxidised substrate proteins are import-incompetent. It is unknown if zinc-bound substrate proteins can enter mitochondria, but if so, then Hot13 could participate in sequestering zinc before oxidative folding.

1.3.4.2. Disulphide relay in the IMS

Substrate proteins enter the mitochondrial IMS through the TOM complex (Lutz et al., 2003). Inside the IMS Mia40 functions both as an import receptor and a disulphide carrier. The interaction between Mia40 and the substrate proteins is best understood for those with a twin CX_3C or twin CX_9C motif. These proteins have a MISS/ITS signal consisting of 9 amino acid residues, including the docking cysteine (the cysteine that first reacts with Mia40) (Figure 1.19 A). The location of the docking cysteine differs in each substrate protein; for example, in Tim9 and Tim10 (twin CX_3C) it appears to be the first cysteine (C_1), whereas for Cox 17 (twin CX_9C) it is the third cysteine (C_3) (Milenkovic et al., 2007, Sideris and Tokatlidis, 2007). Hydrophobic residues in positions ±3, ±4 and ±7 from the docking cysteine are also very important for recognition by Mia40. These three residues all face the same side of an α-helix in the substrate proteins, and are thus poised to interact with the hydrophobic cleft of Mia40 (Figure 1.19 A) (Milenkovic et al., 2009, Sideris et al., 2009). In fact, mutation of any of the first two residues (-3 or -4) inhibits the reaction between Mia40 and the twin CX_3C small Tim proteins. The remaining residues in the 9 amino acid sequence, although not essential, play a cooperative role and substitution of all of them strongly hinders protein import (Milenkovic et al., 2009, Sideris et al., 2009).

The oxidised conformation of twin CX_3C or twin CX_9C proteins has two disulphide bonds stabilising a helix-loop-helix structure (Figure 1.19 B) (Webb et al., 2006, Banci et al., 2008). The initial interaction with Mia40 yields a substrate protein with one disulphide bond. In the current mechanism, the docking cysteine attacks the CPC disulphide of Mia40 thereby forming an intermolecular disulphide bond with the substrate protein (Milenkovic et al., 2007, Sideris and Tokatlidis, 2007, Banci et al., 2010). During this process part of the substrate protein folds into the first α-helix. This folding is encouraged by the interaction between the hydrophobic cleft of Mia40 and the hydrophobic residues in the MISS/ITS (Figure 1.19 C) (Banci et al., 2010). Release from Mia40 is then achieved by the nucleophilic attack of another cysteine from the substrate protein, forming an intramolecular disulphide bond. In this last step the first α-helix of the substrate protein acts as a scaffold for the formation of the second α-helix, producing a protein with a

more native-like fold (Banci et al., 2010). Up to this point the mechanism is well understood. However, how the second disulphide bond is formed is currently under debate.

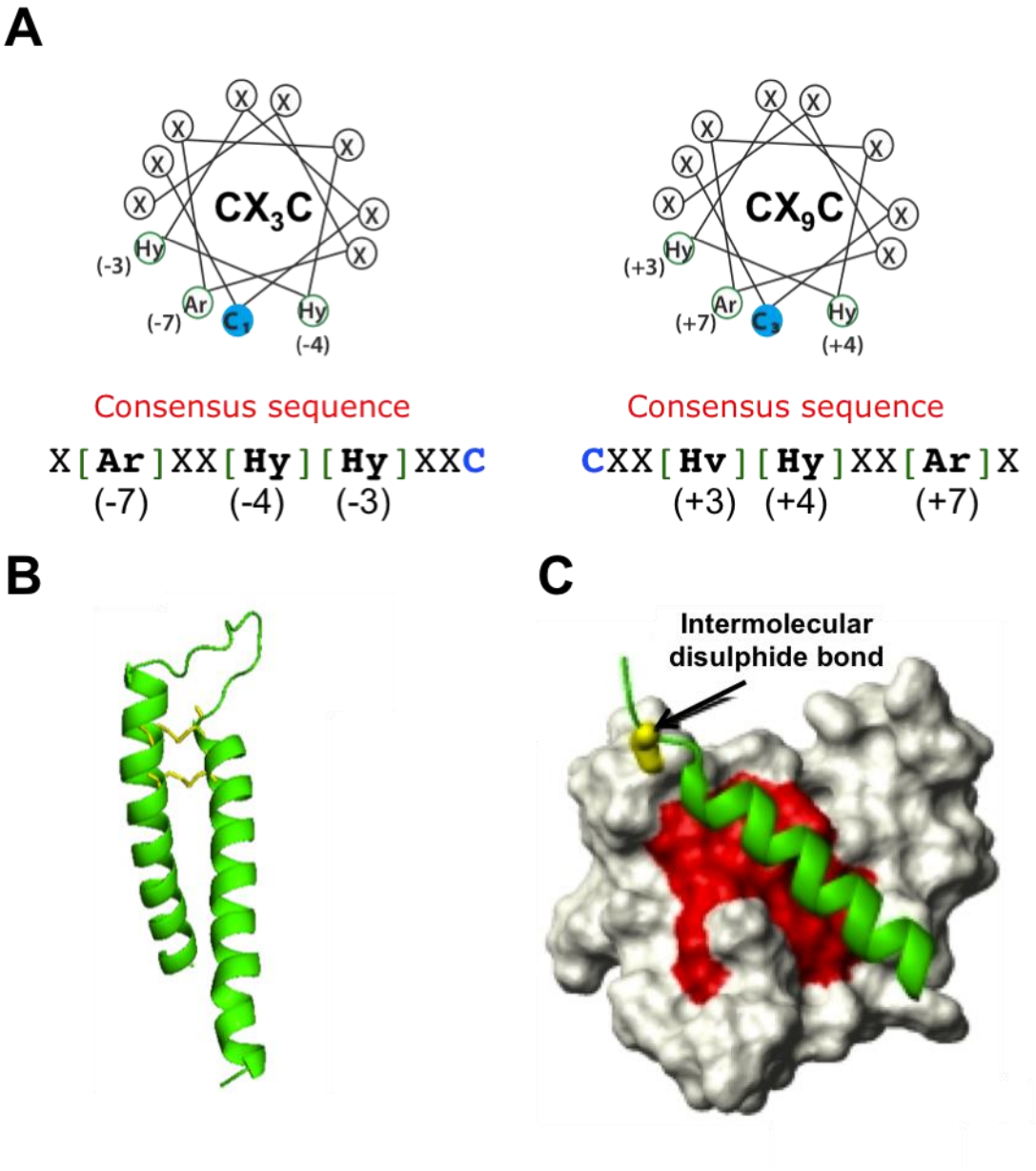

Figure 1.19 Mitochondrial IMS sorting signal

A) Consensus sequence for the mitochondrial IMS sorting signal (MISS) of twin CX_3C and twin CX_9C proteins. The docking cysteine (blue) is C_1 for twin CX_3C proteins and C_3 for twin CX_9C proteins. At positions ±3, ±4 and ±7 the residues are hydrophobic. These residues, as well as the docking cysteine, are facing the same side of the α-helix that interacts with the hydrophobic cleft of Mia40. Ar: aromatic, Hy: hydrophobic.

B) Crystal structure of fully oxidised Tim9 (twin CX_3C motif protein) showing the two anti-parallel α-helices connected by two disulphide bonds. PDB: 3DXR

C) Putative binding of Tim9 (green) to the hydrophobic cleft (red) of Mia40. The intermolecular disulphide bond is in yellow. Adapted from Banci *et al.* (2009).

One mechanism suggests substrate proteins go through several rounds of oxidation by Mia40 (Figure 1.20). In this case, the partially oxidised substrate protein would be recognised by a second Mia40 molecule, which would then insert a second disulphide bond ((Bien et al., 2010). The re-oxidation of Mia40 would be achieved by the subsequent interaction with Erv1. The evidence to support this hypothesis comes from *in vitro* studies where Mia40, when in large excess, was enough to completely oxidise twin CX_3C and twin CX_9C substrate proteins (Bien et al., 2010). Alternatively, under *in vitro* aerobic conditions oxygen has been shown to easily form the second disulphide bond on a partially folded protein (Banci et al., 2009). Finally, a second disulphide bond could also potentially be inserted by small molecules like GSSG.

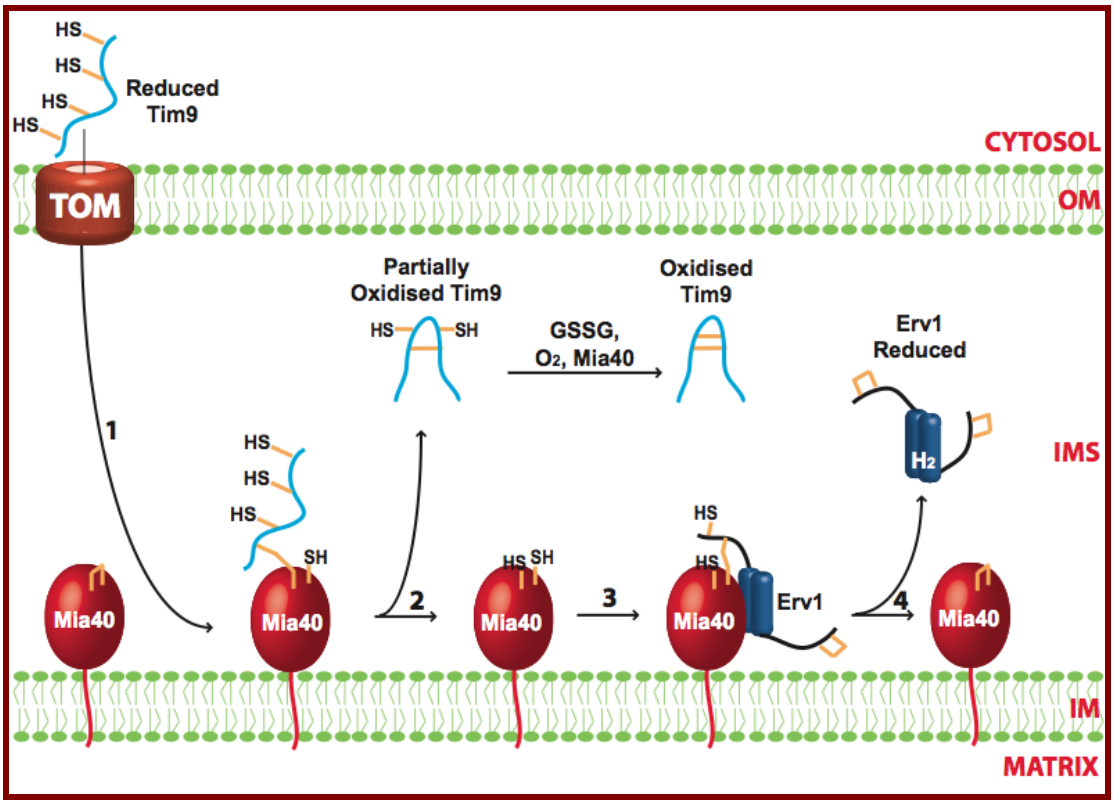

Figure 1.20 First model of substrate protein oxidation

In the first proposed model the substrate proteins (Tim9) traverse the OM through the TOM complex (1). Then, Mia40 recognises and inserts one disulphide bond into Tim9 (2). The second disulphide bond can be inserted by a second Mia40 molecule, oxygen or GSSG (3). Reduced Mia40 is re-oxidised by Erv1 (4) to re-start the pathway. IM: inner membrane, IMS: intermembrane space, OM: outer membrane.

Another mechanism proposed that substrate protein oxidation goes through a protein-Mia40-Erv1 ternary complex (Figure 1.21). The suggested steps in the mechanism are as follows: step 1) Mia40 transfers one disulphide bond to the substrate protein; step 2) Erv1 re-oxidises the CPC disulphide of Mia40; step 3) Mia40 can now insert a second disulphide bond to the substrate protein; step 4) Mia40 is re-oxidised by a second Erv1 molecule (Stojanovski et al., 2008). The evidence for this hypothesis comes from blue-native gel electrophoresis where a complex of Tim9, Mia40 and Erv1 was identified during the *in organello* mitochondrial import of radioactive Tim9. The ternary complex was resistant to DTT, indicating intermolecular disulphide bonds are not involved (Stojanovski et al., 2008). How this complex can be formed is a mystery because both Erv1 and the substrate proteins employ the same binding site in Mia40.

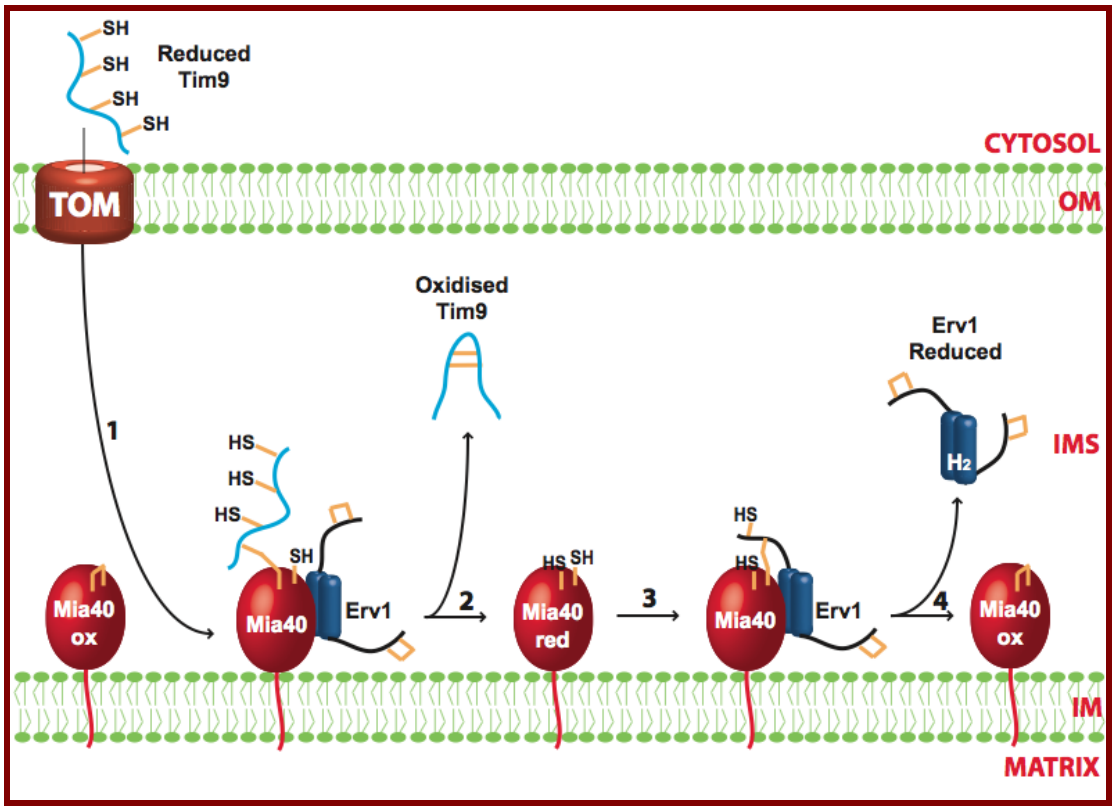

Figure 1.21 Second model of substrate protein oxidation.

In the second model substrate proteins (Tim9) enter the IMS through the TOM complex (1) and form a ternary complex with Mia40 and Erv1. Mia40 undergoes two reduction/oxidation cycles where Erv1 re-oxidises Mia40 allowing it to insert two disulphide bonds into Tim 9 before its release (2). The final products of this step are fully oxidised Tim9, reduced Mia40 and reduced Erv1. In the last step, reduced Mia40 is re-oxidised by a second Erv1 molecule (3) to produce oxidised Mia40 and reduced Erv1. IM: inner membrane, IMS: intermembrane space, OM: outer membrane.

For the disulphide relay to continue, reduced Erv1 must be re-oxidised (Figure 1.22). As a sulphydryl oxidase, Erv1 has been shown to readily transfer electrons to oxygen *in vitro* (Lee et al., 2000, Ang and Lu, 2009). However, cyt *c* has also emerged as a second electron acceptor of Erv1. Indirect evidence of cyt *c* involvement in the MIA pathway was obtained by following the steady-state percentage of oxidised Mia40 inside the cell. First, deletion of the cyt *c* genes in the Δ*cyc1*/Δ*cyc*7 yeast mutant strain decreased the percentage of oxidised Mia40. Inhibition of cyt *c* reductase activity also decreased the percentage of oxidised Mia40. However, inhibition of cyt *c* oxidase activity had the opposite effect (Bihlmaier et al., 2007). Because Erv1 has been shown to directly interact with cyt *c* in mitochondria (Dabir et al., 2007), these observations can best be explained by a diminished re-oxidation of Erv1 by cyt *c*. Furthermore, the shifts in the percentage of oxidised Mia40 were not observed in a Δ*cyc1*/Δ*cyc*7 yeast strain, confirming the requirement of cyt c ((Bihlmaier et al., 2007).

Dabir et *al.* (2007) proposed an alternative pathway that combines the use of both oxygen and cyt *c* as electron acceptors (Figure 1.22). After its reaction with reduced Erv1, cyt *c* can transfer the electrons to oxidised cytochrome *c* peroxidase (Ccp1). The now reduced Ccp1 can then remove the H_2O_2 previously produced during the reaction of Erv1 with oxygen. In this manner the final product of the Erv1 re-oxidation is H_2O, and not the harmful H_2O_2 (Dabir et al., 2007). However, these observations were obtained mostly *in vitro* and their relevance inside the mitochondrial IMS is still in question.

1.3.4.3. Other components of the MIA pathway

A third protein has also been implicated in the MIA pathway. The helper of Tim 13 (Hot13) is a non-essential IMS protein with a conserved zinc-finger, (Curran et al., 2004). The protein is not essential in yeast but a Δ*HOT13* deletion mutant showed a reduction of the steady-state levels of the small Tim proteins, a slight decrease in their import into mitochondria and, finally, a decrease in the steady-state percentage of oxidised Mia40 (Mesecke et al., 2008). Because the activity of Mia40 and Erv1 is inhibited by zinc ions (Morgan et al., 2009), Hot13 has been proposed to act as a zinc chelator that helps keep Mia40 and Erv1 in their active conformations (Mesecke et al., 2008). Still, because Hot13 is not essential for cell viability, its role as a

chelator in the MIA pathway may be considered a back up in case of fortuitous zinc binding by Mia40 or Erv1.

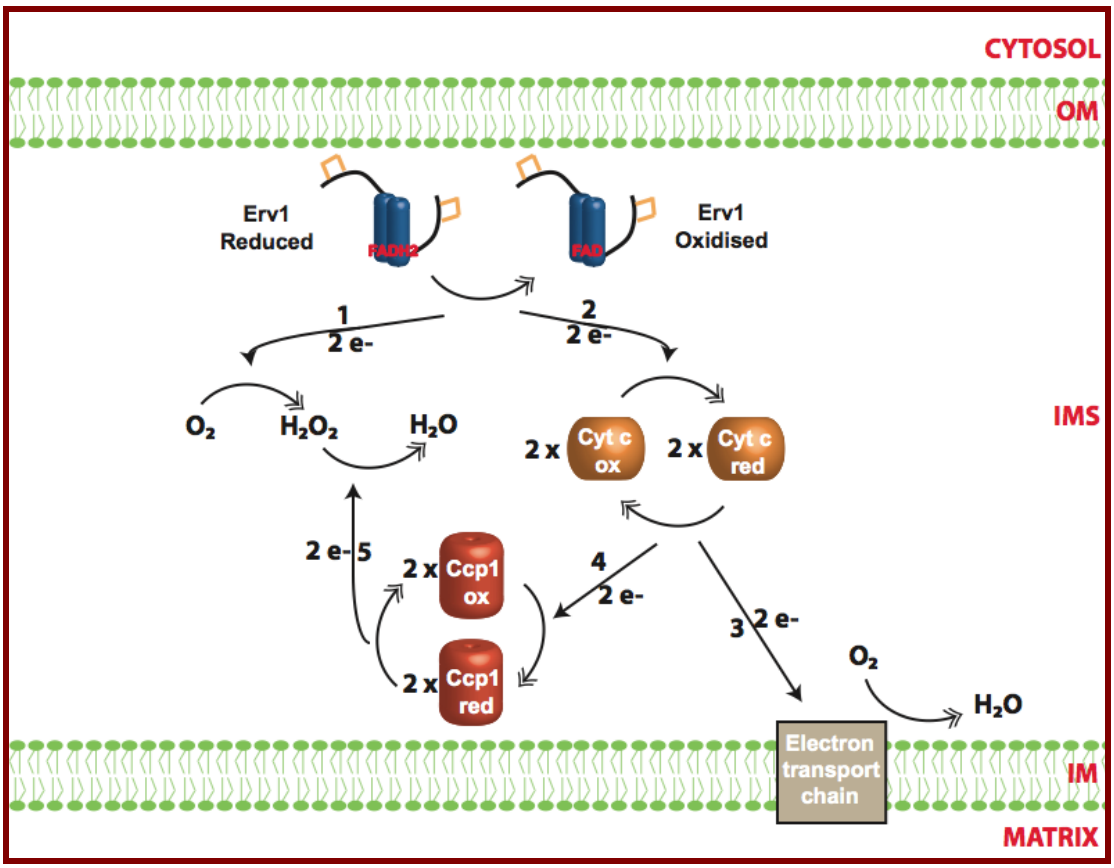

Figure 1.22 The re-oxidation pathways of Erv1

Reduced Erv1 can transfer electrons to either oxygen (1) or cyt *c* (2). From cyt *c*, the electrons can be delivered to the respiratory chain (3) or, alternatively, to cytochrome *c* peroxidase (Ccp1) (4). The now reduced Ccp1 can use the electrons to form H_2O (5) from the H_2O_2 first produced in the reaction of Erv1 with oxygen. IM: inner membrane, IMS: intermembrane space, OM: outer membrane.

2. AIM AND OBJECTIVES

The overall aim of this study is to understand, at the molecular level, the functional mechanism of the sulphydryl oxidase Erv1, a key component of the MIA pathway.

There were three major objectives:

1. Analysing the effect of oligomerisation on the stability and function of Erv1.

Hypothesis: Erv1 adopts a tetrameric quaternary structure in solution, which confers it with better folding and higher stability.

At the start of this project the oligomerisation state of Erv1 was unknown but assumed to be dimeric. Here, the oligomerisation state of Erv1 in solution was defined using MALLS. Furthermore, the impact of metal ions, FAD content and inter-subunit disulphide bonds on the stability of the tetramer was followed using SEC and UV-visible spectroscopy. Lastly, the folding, thermal stability and oxidase activity of the Erv1 tetramer was compared with that of a low-FAD-content Erv1 'dimer' using CD and oxygen consumption assays. In this way, it is expected to first decipher the oligomerisation state of Erv1 and then identify the factors that would affect it, as well as the advantages that Erv1 oligomerisation may provide.

2. Understanding the molecular basis behind autosomal recessive myopathy using the yeast protein Erv1 R182H.

At the start of this project nothing was known on the effect of the R182H mutation on the Erv1 protein, or of R194H on ALR. Thus, the objectives were to characterise the possible effects, if any, that the mutation may have on the folding, stability and activity of Erv1.

Initially, the effects on the structure were analysed using a combination of SEC, MALLS and CD. Next, both UV-visible and fluorescence spectroscopy were employed to study the binding of the FAD cofactor in the mutant protein. However, to study the activity of Erv1, the Mia40c purification protocol was

first optimised to increase the yield and remove the iron from Fe-Mia40c. Additionally, a protocol for the anaerobic reduction of cyt *c* was also established before the Erv1-cyt *c* activity assays could be carried out. Once this was achieved, both oxygen consumption assays and anaerobic cyt *c* reduction experiments were used to study the effect of the R182H mutation on the activity of Erv1. By comparing the results of Erv1 R182H with those of the wild-type protein, it is expected that any difference that appears in the folding, stability or activity of Erv1 may be linked with the phenotypes observed for the mutant inside the cell.

3. Elucidating the thermodynamics of the electron transfer mechanism in Erv1.

Hypothesis: The electron transfer within Erv1 is uphill.

How the electrons flow within Erv1, from one redox centre to the other, is already known. Here, to address whether the flow is thermodynamically favourable, an attempt was made to measure the standard reduction potentials of the 3 redox centres in Erv1. First, a protocol for the titration of FAD was established to measure the standard reduction potential of the cofactor under anaerobic conditions. Next, a second protocol also needed establishing to measure the midpoint of reduction of the C130-C133 active-site disulphide, also under anaerobic conditions. Additionally, the interaction between the redox centres was further analysed by doing anaerobic experiments on the wild-type and the Erv1 double-cysteine mutants. Lastly, the reduction intermediates of Erv1 were identified by EPR and spectroscopic techniques. Overall, by measuring the standard reduction potential of each redox centre in Erv1 we can determine whether the electron flow always goes from a more negative towards a more positive value (downhill) or vice versa (uphill).

3. MATERIALS AND METHODS

3.1. Solutions

Binding buffer:	40 mM imidazol, 50 mM Tris-HCl, 150 mM NaCl, pH 7.4
Washing buffer:	80 mM imidazol, 50 mM Tris-HCl, 150 mM NaCl, pH 7.4
Elution buffer:	500 mM imidazol, 50 mM Tris-HCl, 150 mM NaCl, pH 7.4
Dialysis buffer 1:	50 mM Tris-HCl, 150 mM NaCl, 350 mM EDTA, pH 8
Dialysis buffer 2:	50 mM Tris-HCl, 150 mM NaCl, 50 mM EDTA, pH 8
Dialysis buffer 3:	50 mM Tris-HCl, 10 mM NaCl, 1 mM EDTA, pH 8
Buffer A (BA):	50 mM Tris-HCl, 150 mM NaCl, pH 7.4
Buffer AE (BAE):	50 mM Tris-HCl, 150 mM NaCl, 1 mM EDTA, pH 7.4
Buffer B:	50 mM Tris-HCl, 10 mM NaCl, 0.3 mM EDTA, pH 8
Buffer C:	50 mM Tris-HCl, 1 M NaCl, 0.3 mM EDTA, pH 8
Urea solution:	8 M Urea, 50 mM Tris-HCl, 150 mM NaCl, 1 mM EDTA, pH 7.4

3.2. Site-directed mutagenesis

The ERV1 mutants were done using the QuickChange site-directed mutagenesis kit with Pfu DNA polymerase (Stratagene) and the primers listed in table 3.1. The plasmid pET-24a(+) (Novagen) containing the ERV1 WT gene was used as template for the polymerase chain reaction with the program shown in table 3.2. The constructs were verified by DNA sequencing.

The constructs pET-24a(+) ERV1 C30,33S and pET-24a ERV1 C130,133S were generated previously in the laboratory (Ang & Lu, 2009).

Table 3.1 Primers for site-directed mutagenesis

	Forward	Reverse
Erv1 R182H	5′-TAA TTT CTG GGA AAA ACA CTG GAA GGA CGG CTG GGA CGA-3′	5′-TCG TCC CAG CCG TCC TTC CAG TGT TTT TCC CAG AAA TTA-3′

Table 3.2 Site-directed mutagenesis program		
Step	**Temperature (°C)**	**Time (s)**
Initial denaturation	95	30
Denaturation	95	30
Annealing	55	60
Extension	68	840 (14 min)
Cycles: 18		

3.3. Sodium dodecyl sulfate polyacrylamide gel electrophoresis

Sodium dodecyl sulfate polyacrylamide gel electrophoresis (SDS-PAGE) gels were run using the Biorad mini-Protean III system (Bio-Rad). Typically, samples were mixed with an equal volume of 2X SDS- PAGE (4% (w/v) SDS, 8% (v/v) glycerol, 0.02% (w/v) bromophenol blue, 80mM Tris-HCl, pH 6.8) sample buffer, heated at 100°C for 5 minutes and spun on a bench-top centrifuge (20-25°C, 13 000 rpm, 10 min) before loading.

3.4. Protein purification

Erv1: The pET-24a(+) plasmid containing the ERV1 WT or mutant gene (R182H, R182A, W183F, C30,33S or C130,133S) was expressed in *E. coli* Rosetta-gamiTM 2 cells (Novagen). Cells containing the plasmid were grown in 6 liters of Luria-Broth (LB) (Formedium Ltd.) media with 50 µg/mL of kanamycin (Fisher Scientific) at 37°C until an OD600 of 0.3-0.4. Cells were then cooled down at 4°C for ~20 min. Expression of the Erv1-His6 tagged protein was induced overnight (no longer than 16 h) at 16°C by addition of isopropyl β-D-1 thiogalactopyranoside (IPTG) (ForMedium Ltd.) and FAD (Sigma) to final concentrations of 0.5 mM and 10 µM, respectively. Cells were harvested by centrifugation (4°C, 5000 rpm, 15 min) using an Avanti® J-26 XP centrifuge (Beckman Coulter) and then the pellet was resuspended in binding buffer (40 mM imidazol, 50 mM Tris-HCl, 150 mM NaCl, pH 7.4) to ~0.2 mg/mL. The resuspended cells were again complemented with 10 µM FAD unless otherwise stated in the results. Cells were disrupted by sonication (12/48 s ON/OFF, 35% amplitude, 60 min) in the presence of 3 EDTA-free protease inhibitor cocktail tablets (Roche) using a Bandelin sonicator

(SONOPLUS). The cell lysate was centrifuged (4°C, 17 000 rpm, 60 min) using an Avanti® J-E centrifuge (Beckman Coulter) and the protein was confirmed to be in the supernatant with a 12% SDS-PAGE gel.

The supernatant obtained from the 6 L was then added to a column with 5 mL of Ni-NTA His-Bind beads (Novagen) pre-equilibrated with binding buffer. The column was washed with at least 5X bed volumes (BV) of binding buffer, followed by 10X BV of washing buffer (80 mM imidazol, 50 mM Tris-HCl, 150 mM NaCl, pH 7.4). The bound Erv1-His_6 protein was eluted with 15-20 mL of elution buffer (500 mM imidazol, 50 mM Tris-HCl, 150 mM NaCl, pH 7.4) and an extra 10 µM FAD was added unless stated otherwise. All column steps were performed at 4°C. The proteins were divided into 500 µl aliquots, snap-frozen with liquid nitrogen and kept at -80°C until use.

Before their use the proteins were further purified by size exclusion chromatography (SEC) using an ÄKTA*design* (Pharmacia Biotech) and a Superdex 200 10/300 GL gel filtration column (GE Healthcare).

Mia40c (amino acids 284–403): The pGEX 4T-1 Vector (GE Healthcare) containing the MIA40c gene was expressed in *E. coli* BL21 (DE3) cells (Stratagene). Cells containing the plasmid were grown in 12 liters of LB media with 100 µg/mL of ampicillin (Fisher Scientific) at 37°C until an OD_{600} of 0.3-0.4. Expression of the GST-Mia40c tagged proteins was induced for 16-20 h at 16°C by addition of IPTG to a final concentration of 0.5 mM. Cells were harvested by centrifugation (4°C, 5000 rpm, 15 min) and then resuspended in buffer A (BA: 50 mM Tris-HCl, 150 mM NaCl, pH 7.4) to ~0.2 mg/mL. Cells were disrupted by sonication (12/48 s ON/OFF, 35% amplitude, 60 min) in the presence of 6 EDTA-free protease inhibitor cocktail tablets. The cell lysate was centrifuged (4°C, 17 000 rpm, 60 min) and the protein was confirmed to be in the supernatant with a 15% SDS-PAGE gel.

The supernatant was mixed with 20 mL of Glutathione Sepharose 4B beads (GE Healthcare) pre-equilibrated with BA and left swirling at 4°C for 16 h. The column was washed with 15X BV of BA and then thrombin was added to a 10-15 U/mL final concentration. After incubation for ~20 h at 4°C the cleaved protein was collected and the fractions containing Mia40c were pooled together. When necessary the protein was concentrated by centrifugation

(15°C, 4000 rpm) using a 20 mL, 5-kDa cutoff Vivaspin™ tube (GE Healthcare) and a Sigma 3-18 K centrifuge (SciQuip). The protein was kept at -80°C until use.

The affinity-purified protein includes an iron-bound form of Mia40c. The protein was therefore treated to 3 dialysis steps (4°C, 24 h each) in BA buffer with diminishing EDTA concentrations (350 mM, 50 mM and 1 mM) to remove most of the iron. Further purification was done by ion exchange chromatography (IEC) using a 5 mL HiTrap Q HP column (GE Healthcare), buffer B (50 mM Tris-HCl, 10 mM NaCl, 0.3 mM EDTA, pH 8) and increasing amounts of buffer C (50 mM Tris-HCl, 1 M NaCl, 0.3 mM EDTA, pH 8) according to the gradient in table 3.3. The Mia40c protein not containing iron was then collected, concentrated as before and divided into 500 µl samples. The protein was kept at -20°C until use.

Table 3.3 Ion exchange chromatography – Mia40c

Step	Gradient (%C)	Column volumes
Column wash	0	5
1	10	5
2	15	6
3	20	5
Wash	100	5
Equilibration	0	10

*Buffer B: 50 mM Tris-HCl, 10 mM NaCl, 0.3 mM EDTA, pH 8
*Buffer C: 50 mM Tris-HCl, 1 M NaCl, 0.3 mM EDTA, pH 8

3.5. Anaerobic assays

For all anaerobic experiments the assays were done within an anaerobic glove box (Belle Technology), with oxygen levels maintained below 2 ppm. Buffers were made anaerobic by extensive bubbling with oxygen-free nitrogen, prior to incubation inside the anaerobic glove box. Furthermore, the proteins were purified using either a Superdex 200 10/300 GL or a Superdex 75 10/300 GL column and an ÄKTA*purifier* system also within an anaerobic glove box.

3.5.1. Preparation of partially reduced Mia40c

Partially reduced Mia40c (pr-Mia40c) was made by incubating the IEC-purified protein with 8 mM Tris(2-carboxyethyl)phosphine (TCEP) (~pH 7) for 1 h at 25°C. Excess TCEP was removed using a Superdex 75 10/300 GL column and an ÄKTA*purifier* within an anaerobic glove box. pr-Mia40c was stable inside the glove box for several hours, or could alternatively be stored in liquid nitrogen overnight without any discernible oxidation. The protein concentration was measured using the extinction coefficient in table 3.4.

3.5.2. Preparation of cyt *c*

Cyt c: Solid cyt *c* (Sigma) from *S. cerevisiae* was first dissolved in buffer AE (BAE: 50 mM Tris-HCl, 150 mM NaCl, 1 mM EDTA, pH 7.4). Typically, the partially oxidised (~70%) protein was treated with 40 mM of potassium ferricyanide for 1 h at 25ºC to further oxidise it. Removal of excess potassium ferricyanide was done with a Superdex 75 10/300 GL column inside an anaerobic glove box. Only the peak representing the cyt *c* monomeric fraction was used for the experiments.

Cyt *c* protein concentration and oxidation state were measured using the extinction coefficients in table 3.4. The UV-visible spectra of SEC purified proteins were measured after treatment with potassium ferricyanide (fully oxidised) or sodium dithionite (fully reduced, Sigma). The oxidation state was calculated by interpolating the absorbance at 550 nm of untreated SEC purified cyt *c*.

3.5.3. FAD redox titrations

Electron potential measurements were conducted in BAE with protein concentrations (based on bound FAD) of 30-80 µM. Mediators for improved conductivity between the protein and electrode were added. Typically, these were (final concentrations): 2 µM phenazine methyl sulfate ($E_{1/2}$ 80 mV vs normal hydrogen electrode (NHE)), 7 µM 2-hydroxy-1,4-naphthoquinone ($E_{1/2}$ -145 mV vs NHE), 1 µM benzyl viologen ($E_{1/2}$ -311 mV vs NHE), and 0.3 µM methyl viologen ($E_{1/2}$ -430 mV vs NHE). Sodium dithionite solutions (in BAE) were made up fresh inside the glove box immediately before the experiment. Small volumes (0.5 – 5 µl) of the solution were gradually added to reduce the

protein (~5 mL). Adequate time (10-20 min) was allowed for electronic equilibration following each addition of reductant, and prior to the spectrum being recorded at a stabilised reduction potential. Spectra were recorded from 300 to 800 nm using a fiber optic probe (Varian) immersed in the protein solution and connected to a Cary 50 Bio UV-visible spectrophotometer. The electron potential was monitored using a SevenEasy pH meter (METTLER TOLEDO) with a Pt/Calomel electrode and a correction factor of +240 mV to adjust the electron potential. The protein was mixed slowly throughout the assay using an 8.5 mm magnetic flea on a magnetic stirrer. The experiments were done at 25ºC.

To calculate the standard redox potentials (E_0) the collected data were fitted to the Nernst equation (Section 6.3) with the measured electron potential (E) and the normalised FAD absorbance (Abs) as the independent and dependent variables, respectively. Briefly, the absorbance at either 460 or 453 nm (depending on the protein) was normalised (from 0 to 1) and the maximum (Abs=1) was set as the initial concentration of oxidised FAD. The amount of reduced FAD was then calculated by taking Red=1-Abs and these values were used to calculate the E_0 for each measurement. The number of electrons was always restricted to z=2. The standard redox potentials in this work represent the average of at least 2 independent experiments. All fittings were done using the Origin 8.5 software.

3.5.4. FAD electron titration

Electron titrations of the FAD cofactor in Erv1 were conducted in BAE using protein concentrations (based on bound FAD) ranging from 30 to 60 µM. A freshly made sodium dithionite solution was titrated using an anaerobic FAD solution of known concentration (ε_{450} = 11.3 mM^{-1} cm^{-1}). This titration was done before and after the Erv1 assays to obtain an average normality. Small known volumes (0.5-2 µl) of dithionite solution were then used to reduce the protein. The UV-visible spectrum was recorded from 250 to 700 nm after each addition (equilibration time of 10-15 min) using a Cary 50 Bio UV-visible spectrophotometer. The point at which the reduction of FAD was complete (no further decrease in absorbance at either 460 or 453 nm, depending on the protein) marked the number of electrons required for complete FAD reduction. The values presented here are the average of 2 independent experiments.

3.5.5. Alkylation assay

Thiol-disulphide redox state was followed using the agent 4-acetamido-4'-maleimidylstilbene-2,2'-disulphonic acid (AMS) assay. The thiol-modifier AMS (Molecular Probes) covalently links any free thiols resulting in an increase in the molecular weight of 0.5 kDa per thiol. In the assay, protein samples were taken along the FAD electron potential experiment and mixed with an equal volume of anaerobic 2X SDS-PAGE sample buffer containing 2 mM AMS. The positive control for complete oxidation of the Erv1 C3-C4 disulphide was made by mixing the protein with 1 mM dithiothreitol (DTT, Sigma), then adding 10 mM AMS and finally adding 2X SDS-PAGE sample buffer. The samples were run on a 15% SDS-PAGE gel.

3.5.6. Electron paramagnetic resonance

Aerobic proteins were concentrated using 3 kDa cutoff Amicon Ultra-0.5 mL centrifugal filters (Merck Millipore) and a bench top centrifuge at 14 000 rpm. Buffer exchange into anaerobic BAE was done using 1 mL of Bio-Gel P-6DG resin (Bio-Rad) in a crystal Pasteur pipette inside an anaerobic glove box. A sodium dithionite solution was slowly added to reduce the protein to the point of maximum semiquinone formation (maximum absorbance at λ = 585 nm). The protein was then transferred to an electron paramagnetic resonance (EPR) tube, sealed and snap-frozen with liquid nitrogen outside the glove box. Proteins were kept at ~4 K in liquid helium until the analysis. EPR spectra were recorded at X-band frequency using a Bruker ELEXSYS E500 spectrometer equipped with an ESR900 cryostat (Oxford Instruments). The sample temperature was 15 K. Spectra were recorded at non-saturating microwave power (50 μW), using 100 KHz modulation frequency and 0.2 mT modulation amplitude. 16 scans were co-added and an 'NMR gaussmeter' (teslameter) was used to determine g values.

3.5.7. Stopped flow

All anaerobic fast kinetic experiments were done using a stopped flow instrument (Applied Photophysics) inside an anaerobic glove box. The assays used the smaller 5 mm path-length stopped flow cell.

Figure 3.1 shows a diagram of a single mixing stopped flow instrument. Typically, each reacting species is placed inside one of two syringes (A and B). A driving piston then pushes both syringes simultaneously into the mixer. The applied force is sufficient for the mixture to enter a cell where either the fluorescence or the absorbance can be measured. In this study, two cells with different path-lengths (5 and 10 mm) were used depending on the assays, mainly to diminish the amount of protein required for each experiment.

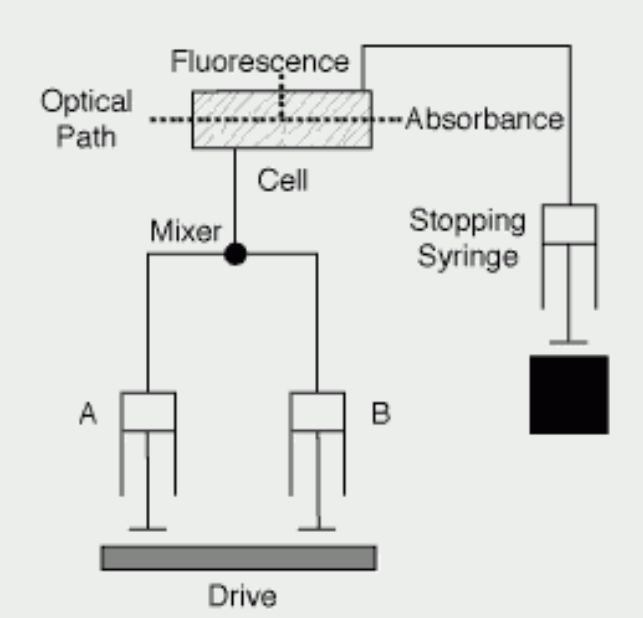

Figure 3.1 Single mixing stopped flow instrument.

Erv1-cyt c reaction: The effect of the Erv1 R182H mutation on the Erv1 interaction with cyt *c* was studied by following cyt *c* reduction. In the experiment, partially reduced Mia40 (syringe A, 60 μM) was rapidly mixed with a cyt *c*/Erv1 wt (or R182H) solution (syringe B, 80 μM cyt *c*) where the Erv1 concentration was as stated in the text (either 0.2 or 3 μM inside the cell). The proteins were temperature equilibrated for 30 min before the start. The reduction of cyt *c* was followed by its change in absorbance at 550 nm.

The plots shown in this work represent the average of 4 repeats done on the same day. The low yield of the Mia40c purification and the large quantities required in doing these assays (despite the use of a smaller cuvette) made it unfeasible to perform independent experiments. Instead, for comparison, both Erv1 wt and Erv1 R182H were tested jointly using the same pr-Mia40c and cyt *c* protein preparations.

3.6. Aerobic assays

3.6.1. Fluorescence

Fluorescence measurements were recorded using a Cary Eclipse fluorescence spectrophotometer (Varian Ltd.) in a 1 cm path-length quartz cuvette. Erv1 proteins were diluted in BAE and the FAD fluorescence emission was recorded from 400 to 650 nm after excitation at either 450 or 460 nm. The experiments were done at 25ºC.

FAD release: The release of FAD from Erv1 during its reaction with pr-Mia40c was followed by the increase in fluorescence at 530 nm (Em. slit: 10). For each assay, 140 µM of pr-Mia40c at 37°C were placed in the cuvette and the reaction was started by addition of Erv1 to a 1.5 µM concentration. Excitation of FAD was done at 455 nm (Ex. Slit: 20). The kinetic profiles represent the average of 4 independent experiments.

3.6.2. Multiangle laser light scattering

Multiangle laser light scattering analysis was done with purified protein applied to a Superdex 200 10/300 GL column running at a flow rate of 0.71 mL/min in BAE. Samples eluting from the column passed through an in-line DAWN HELEOS-II laser photometer (λ = 658 nm) and an Optilab rEX refractometer. Light scattering intensity and eluant refractive index were analyzed using ASTRA v5.3.4.13 software to give a weight-averaged molecular mass. The standard deviations represent the precision of a single measurement. The light scattering analyses are courtesy of Marjorie Howard from the Faculty's Biomolecular Core Facility at the University of Manchester, UK.

3.6.1. UV-visible

Absorption spectra of all SEC-purified proteins was recorded from 250 to 700 nm, at 1 nm intervals, in a 1 cm path-length quartz cuvette (Hellma Analytics) using a Cary 50 Bio UV-Visible spectrophotometer (Varian Ltd.).

Measurement of the FAD extinction coefficient for Erv1 was done by releasing FAD with 1% SDS. Free FAD concentration was then calculated using ε_{450} = 11.3 mM^{-1} cm^{-1} (Koziol, 1971). The proteins were in BAE and the experiments were done using 3 different protein dilutions. The extinction

coefficients are summarised in table 3.4. Unless otherwise stated all Erv1 concentrations indicate FAD concentration.

Table 3.4 Extinction coefficients

Protein	λ (nm)	ε (mM^{-1} cm^{-1})
Erv1 wt	460	12.3
Erv1 R182H	460	11.8
Erv1 R182A	460	---
Erv1 W183F	460	---
Erv1 C1,2S[a]	460	11.1
Erv1 C3,4S[a]	453	12.1
Cyt *c* reduced	550	29.5
Cyt *c* oxidised	550	8.4
apo-Erv1[b]	280	42.3
pr-Mia40c[b]	280	11.7

[a] Ang *et a*l. (2009). Buffer A
[b] Calculated using the ProtParam tool on the ExPASy server.

FAD content: To calculate the FAD/Erv1 ratio the FAD concentration was measured by releasing FAD as previously explained. The protein concentration of the same sample was then measured using the BCA assay according to the manufacturer's protocol. All percentages represent the average of at least 4 independent measurements.

FAD dissociation: An 8 M Urea solution (8 M Urea, 50 mM Tris-HCl, 150 mM NaCl, 1 mM EDTA, pH 7.4) was mixed with Erv1 to give a final concentration of 10 µM protein and 7 M Urea. FAD release was monitored by the change in absorbance at 496 nm. The experiments were done at 25ºC.

The exponential decay half-life (τ) was calculated by fitting the decrease in absorbance at 496 to equation 1 in section 5.3, using A496 and time as the dependent and independent variables, respectively. The profiles and half-lives presented in this work represent the average of 3 experiments done on the same day. All fittings were done using the Origin 8.5 software.

3.6.4. Circular dichroism

Circular dichroism was done using a Chirascan CD spectrometer Far-UV and near-UV spectra of Erv1 proteins were recorded with a 0.2 mm (far-UV) or a 5 mm (near-UV) path-length quartz cuvette (Hellma Analytics). Each spectrum represents an average of 4 independent experiments, and in each individual experiment the spectrum was measured 4 times from 200 to 260 nm (far-UV) or 250 to 320 nm (near-UV), at 1 nm intervals. All measurements were done in BAE buffer at 25°C.

Thermal denaturation: The temperature stability of Erv1 in BAE was measured at 222 nm (far-UV, 0.22 mg/ml) or 272 nm (near-UV, 0.5 mg/ml) in 1°C intervals from 10-90°C, with a temperature increase of 1 °C/min. The thermal denaturation profiles represent the average of 4 independent experiments. The melting temperature (T_M) was calculated by obtaining the first derivative of each profile and then finding the maximum. The melting temperatures reported here represent the average of 4 independent measurements.

3.6.5. Oxygen consumption assay

Oxygen consumption was monitored using a Clark-type oxygen electrode (Hansatech Instruments). Electrode calibration was done at each temperature according to the manufacturer instructions. The Erv1 proteins were always pre-incubated for 30 min to 2 hours at the reaction temperature (25 or 37°C) before being placed in the oxygen electrode chamber, and this did not affect the activity of the proteins. For measurements with TCEP as electron donor, 495 µl of Erv1 were placed in the oxygen electrode chamber and the reaction was started by addition of 5 µl of TCEP to a 5 mM final concentration. The experiments were done in BAE in the presence or absence of 80 units of Superoxide dismutase (Sigma). The profiles and relative initial rates represent the average of 3 assays done on the same day for Erv1 wt and Erv1 R182H.

For measurements with pr-Mia40c (section 3.5.1) as electron donor, the reaction was initiated by addition of Erv1 (typically 5-10 µl) to a pr-Mia40c solution in BAE. Erv1 and pr-Mia40 concentrations are as stated in the text. The profiles and relative initial rates represent the average of 3 assays done on the same day. The low yield of the Mia40c purification and the large quantities needed to do the assays (at least 3 repeats for reliable profiles)

made it difficult to perform independent experiments on different days. Instead, for comparison, both Erv1 wt and Erv1 R182H were tested together with the same calibration of the oxygen electrode and using the same pr-Mia40c preparation.

3.6.6. Stopped flow

FAD association: Erv1 apo-proteins were prepared by treating the SEC-purified proteins with 8 M Urea in BA buffer while bound to a 1 mL HisTrap HP column (GE Healthcare). FAD release was followed by the absorbance at 280 nm using an ÄKTA*prime* and deemed finished after the baseline was achieved. Apo-proteins were then washed considerably (~30 BV) with BA prior to their elution with elution buffer. Buffer exchange into BAE was done using a Superdex 200 10/300 GL column and the apo-protein concentration was measured using the extinction coefficient in table 3.4.

For the experiments, equimolar amounts of apo-protein (syringe A, 40 µM) and FAD (syringe B, 40 µM) were rapidly mixed using a stopped flow instrument (Applied Photophysics). FAD binding was followed at 496 nm. The experiments were done at 25ºC.

3.6.7. Reverse-phase chromatography

Reverse-phase chromatography was done using an Ultimate 3000 standard high-pressure liquid chromatography (HPLC) system (Dionex) and an Aeris widepore 3.6 µm, XB-C18, 150 x 4.6 mm HPLC column (Phenomenex). Solvents acetonitrile (ANC, Fisher Scientific) and water (Sigma-Aldrich) were both HPLC grade. Trifluoroacetic acid (TFA, Sigma-Aldrich) was used as ion-pairing agent. Typically, 20-40 µg of total protein was injected in volumes of 50 µl and run with the gradient: 27.5 to 39.5% ACN, 0.2% TFA, 1 mL/min, 80 min.

Reduced proteins were made by incubating either Mia40c or Erv1 C3,4S with 1 mM DTT for 20 min at 25°C. TFA was then added to stop the reaction prior to injection.

4. RESULTS AND DISCUSSION I: CHARACTERISATION OF THE OLIGOMERISATION STATE OF ERV1.

4.1. Introduction

Oligomerisation is defined as the transient or permanent association of two or more polypeptide chains. A survey indicated that at least 35% of proteins form homo- or hetero-oligomers inside the cell (Goodsell and Olson, 2000). Furthermore, from an evolutionary standpoint, protein oligomerisation presents various advantages including higher thermal stability, the possibility for more complex functions and the capacity for allosteric control (Nooren and Thornton, 2003, Ali and Imperiali, 2005)

Proteins of the ERV family are believed to adopt a dimer conformation. This idea is supported by crystallisation studies where the core domain of various ERV proteins displayed dimeric quaternary structures (Gross et al., 2002, Wu et al., 2003, Levitan et al., 2004, Daithankar et al., 2010, Guo et al., 2012). Furthermore, purified full-length recombinant proteins formed disulphide-bonded dimers visible in non-reducing SDS-PAGE, adding to the conclusion that the proteins indeed form dimers (Lee et al., 2000, Daithankar et al., 2010, Guo et al., 2012). However, previous research in our laboratory appeared to contradict the idea that Erv1 is a dimer. Whereas the core domain of Erv1 definitely adopted a dimer quaternary structure, SEC analyses suggested full-length Erv1 may exist in higher oligomeric conformations (Ang, 2010). At the time of this study no report had so far addressed the oligomerisation state of the full-length proteins under non-denaturing conditions.

Here, a direct approach using MALLS was employed to first determine the oligomerisation state of Erv1. Experiments were then designed to investigate the stability of the oligomerisation state and discover possible advantages offered by the oligomerisation of Erv1.

4.1. Purification of Erv1 wt

The purification of Erv1 wt is a well-established protocol in our laboratory and, as such, the protein was successfully purified from *E. coli* Rosetta-gami™ 2 cells (Section 3.4). Figure 4.1 shows a reducing SDS-PAGE of an Erv1 purification procedure. Briefly, the protein was properly overexpressed (Figure 4.1, lane 2) and found to be soluble (Figure 4.1, lane 4). After binding to Ni-NTA His-Bind beads, the Erv1-$(H)_6$ tagged protein was eluted using 500 mM imidazol (Figure 4.1, lane 7). The protein used for the assays presented in this work was further purified by SEC using a Superdex 200 and shown to be over 90% pure (Figure 5.1, lane 8). This result is similar to those previously obtained for the wild-type Erv1 purification (Ang, 2010). Furthermore, although no additional assays were employed to confirm the integrity of the protein, thus purified Erv1 has been previously shown to be intact by mass spectrometry in our laboratory.

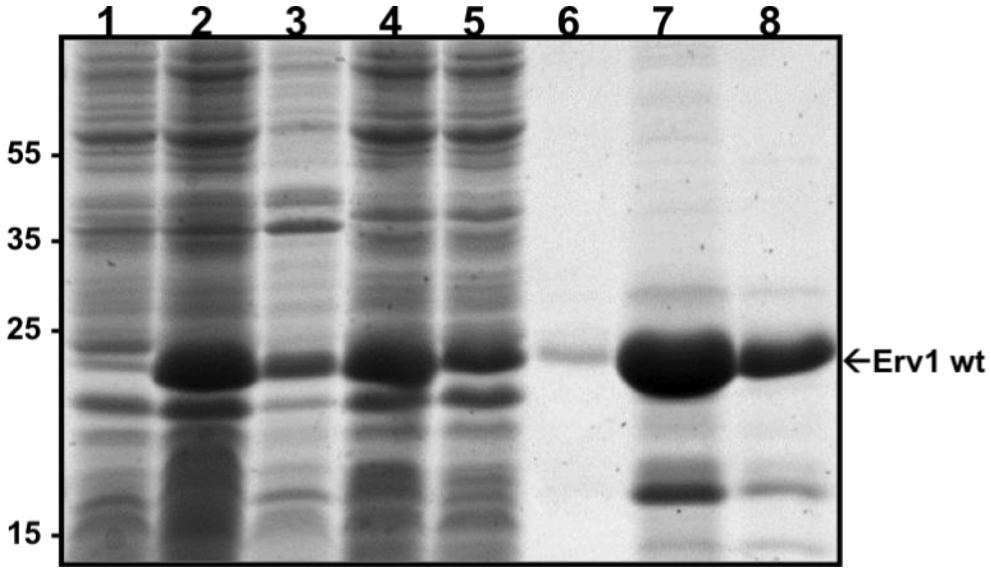

Figure 4.1 SDS-PAGE of a purification of Erv1 wt

Reducing SDS-PAGE of an Erv1 wt affinity purification visualised using coomassie-blue staining. Lanes: 1) cells grown to log phase, 2) overnight induction at 16°C, 3) sonication pellet, 4) sonication supernatant, 5) flowtrough from Ni-NTA His-Bind beads, 6) wash with 80 mM imidazol, 7) elution with 500 mM imidazol, 8) after SEC.

4.3. Determination of the oligomerisation state of Erv1

The initial step in this study was to determine the oligomerisation state of full-length recombinant Erv1. The protein was purified with a C-terminal His_6-tag linked by a leucine and glutamate residue. First, Erv1 was run through a Superdex 200 SEC column using BA buffer, as in the earlier protocol. A SEC column is tightly packed with small agarose beads, each of which has zigzag-shaped conduits through their middle. Proteins can either pass through the conduct or go around the beads. The smaller the protein the more it tends to pass through the conduct and, therefore, takes longer to elute. Figure 4.2 shows Erv1 eluted at ~12.5 mL with a shoulder at ~10.5 mL. The peak was quite broad starting at ~9.5 mL and ending at ~14.5 mL. The smaller peak at ~8.5 mL represents soluble aggregates of molecular weights higher than 200 kDa for they eluted at the same position as the void volume (V_0) of the column. Because Erv1 eluted before the biggest molecular weight marker (albumin: 67 kDa), the only conclusion that can be drawn from this observation is that the molecular weight of Erv1 is likely to be greater than 67 kDa.

One explanation for the high molecular weight considers the fortuitous presence of metal ions, namely zinc. Coordination of zinc by cysteine and histidine residues is a common feature of proteins with zinc finger motifs (Brayer et al., 2008). In the case of Erv1, zinc has been shown to inhibit its oxidase activity, probably by binding to its disulphide bonds while in their reduced state (Morgan et al., 2009). Thus, two Erv1 molecules could potentially be united with their disulphide bonds separately coordinating zinc, thereby increasing the apparent molecular weight of Erv1. To check this hypothesis 1 mM EDTA was added to the BA buffer and the protein was run again through the same SEC column (Figure 4.2). Erv1 eluted at a similar position (~12.7 mL) as in the absence of EDTA, but in this case the peak was much narrower (from ~12.0 to ~14.5 mL). The shoulder at ~10.5 mL was greatly decreased suggesting protein in this position shifted to the main peak at ~12.7 mL. Overall, this result indicates peak broadening is mainly due to Erv1 forming high oligomers by coordinating metal ions. However, the high oligomeric species found at ~12.7 mL does not require metal ions for its formation.

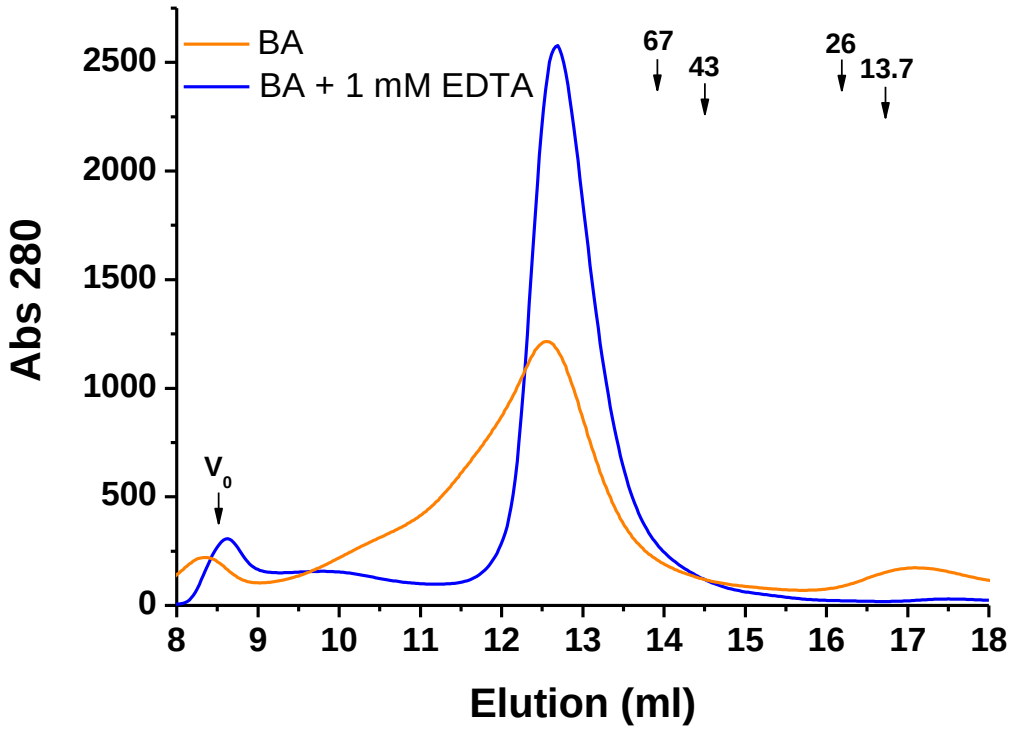

Figure 4.2 Size exclusion chromatography of Erv1 in the presence of EDTA

Size exclusion chromatography of full-length recombinant Erv1 on a Superdex 200 10/300 GL column run using either BA buffer (orange) or BA + 1 mM EDTA (blue). Proteins were assayed directly after affinity purification. Molecular weight markers: albumin (67 kDa), ovalbumin (43 kDa), chymotrpsin (26 kDa) and ribonuclease A (13.7 kDa). Void volume V_0 = 8.5 mL.

SEC is a technique that separates proteins based both on their molecular weight and their shape. Measured apparent molecular weights are generally inaccurate for proteins that do not have a molten-globule shape. Therefore, to obtain a more accurate molecular weight, Erv1 was analysed by MALLS coupled to the same Superdex 200 column (Figure 4.3). This technique determines the molecular weight based on the intensity of scattered light at various angles independently of protein shape (Wyatt, 1993). The experiment showed Erv1 has a molecular weight of 88 ± 2 kDa. Because the Erv1 monomer has a molecular weight of 22 kDa (Lee et al., 2000), the data is consistent with Erv1 forming a tetramer. Furthermore, the even molecular weight distribution throughout the peak indicates that only one oligomeric species is present.

These results demonstrate the full-length recombinant Erv1 used in the laboratory adopts a tetramer conformation. The stability of the quaternary structure does not depend on the presence of metal ions. During the course of this study a report indicated full-length Erv1 adopts a dimer conformation. Their conclusion was based on SEC experiments where Erv1 eluted between the molecular weights markers of 67 and 43 kDa (Bien et al., 2010). Both this and their approach used the exact same protein construct. Hence, further studies were performed with Erv1 to determine if different conditions could affect its oligomerisation state.

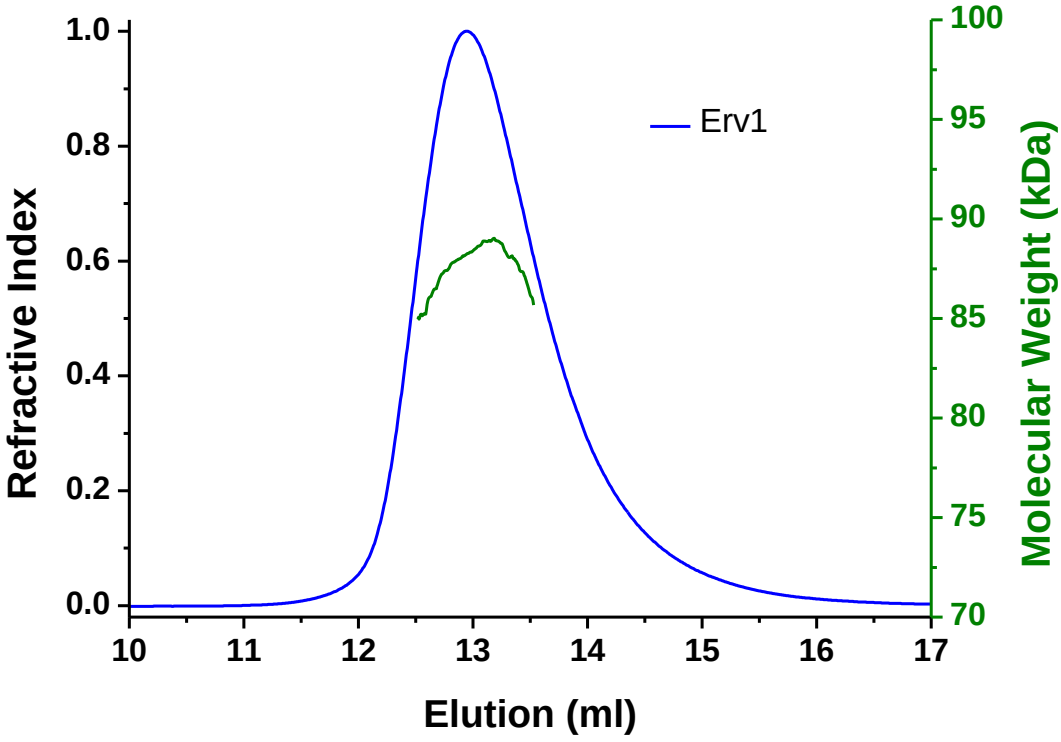

Figure 4.3 Multiangle laser light scattering of Erv1

Multiangle laser light scattering of full-length recombinant Erv1 (blue). Only the main peak (~12.7 mL) from a previous size exclusion experiment was used for the assay. The measured molecular weight (olive green) is 88 ± 2 kDa, indicating the protein adopts a tetramer conformation.

4.4. Determination of the effects of FAD binding on the oligomerisation state of Erv1

Purification of recombinant Erv1 includes addition of FAD during protein induction (10 μM), cell lysis (50 μM) and after affinity purification (50 μM). All of these FAD supplements were shown to increase the final percentage of bound FAD (100x[FAD]/[Protein]) in the purification of *S. cerevisiae* Erv2 (Gross et al., 2002). Figure 4.4 A shows a typical SEC profile of Erv1 when purified without the last two FAD supplements ($Erv1^{-FAD}$). The protein eluted as two peaks at ~12.2 and ~13.5 mL. This result suggests peak 1 (P1) could be attributed to a tetramer and peak 2 (P2) to a lower oligomerisation state of Erv1. To check whether the lower oligomerisation state of P2 was related to a change in the FAD binding percentage of Erv1, the fraction of this peak was incubated with 10-fold excess FAD (1 h, 25°C) and then re-analysed using the same size exclusion column (Figure 4.4 B). The results show incubation with FAD restored the tetramer conformation of Erv1, as compared with Erv1 purified with all three FAD supplements ($Erv1^{+FAD}$). This suggests a link exists in Erv1 between oligomerisation state and FAD binding.

The previous results imply P2 has a lower percentage of FAD bound to Erv1. Indeed, comparison of the UV-visible spectra of P2 with that of $Erv1^{+FAD}$ shows decreased absorptions at 275, 380 and 460 nm for P2 (Figure 4.5). This could be explained by a lower amount of FAD present in the sample. Because protein concentrations are the same in both samples the result also suggests a lower FAD to protein ratio for P2. To conform this, FAD binding percentages were calculated by independently measuring protein concentration using the BCA assay and FAD concentration after its release from Erv1 by 1% SDS (free FAD $\varepsilon_{FAD} = 11.3\ mM^{-1}\ cm^{-1}$) (Koziol, 1971). $Erv1^{+FAD}$ gave a FAD binding percentage of 96 ± 6%. However, P2 of $Erv1^{-FAD}$ gave a FAD binding percentage of 20 ± 1%. Hence, these results demonstrate that a lower FAD to protein ratio can shift the quaternary structure of Erv1 towards lower oligomerisation states.

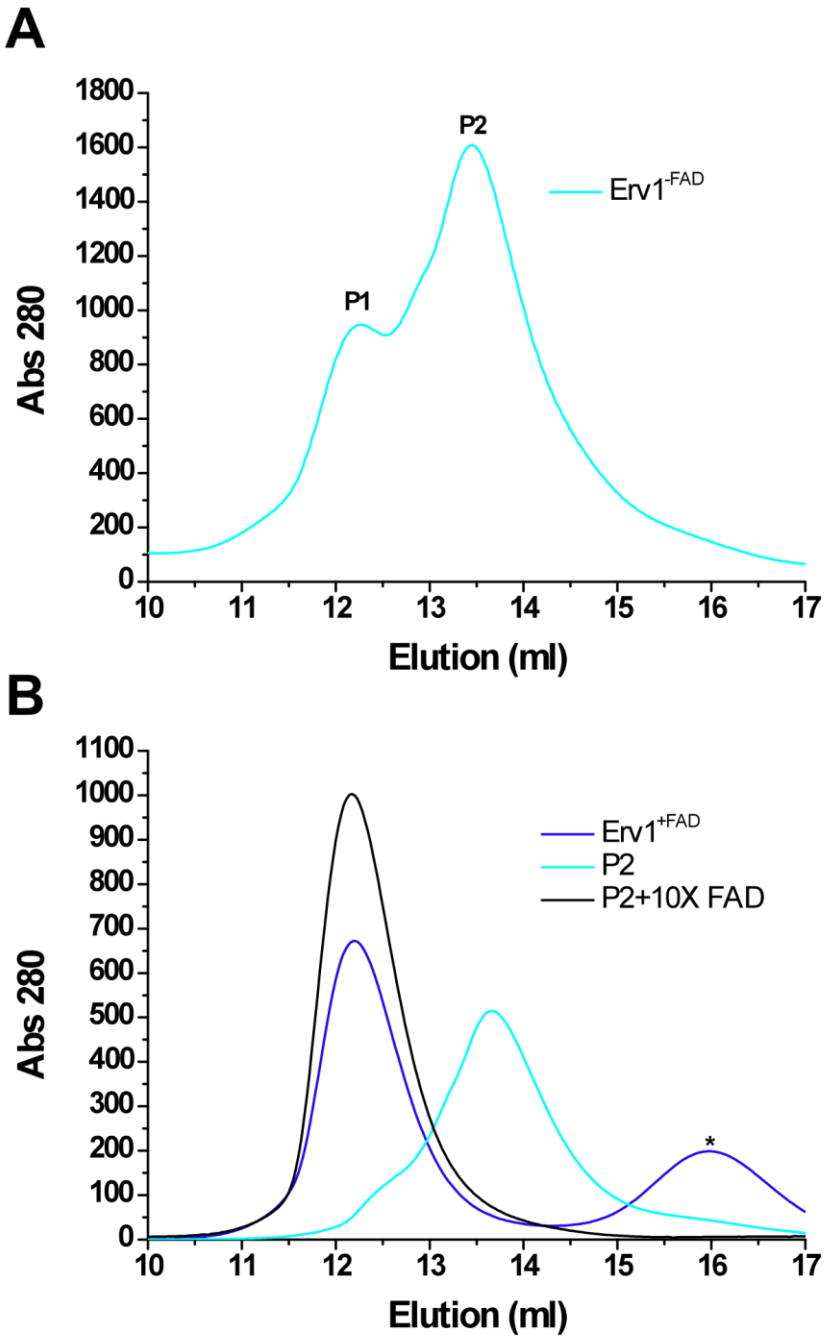

Figure 4.4 Size exclusion chromatography of Erv1 purified with or without FAD supplement

A) Size exclusion chromatography of Erv1 without FAD supplemented during cell lysis and after affinity purification ($Erv1^{-FAD}$). The protein was run on a Superdex 200 10/300 GL column in BAE buffer. P1: Peak 1, P2: Peak 2.

B) Size exclusion chromatography of $Erv1^{+FAD}$ (blue, 0.5 mg/mL), P2 of A (cyan, 0.5 mg/mL) and P2 of A pre-incubated with 10 fold FAD (black, 0.5 mg/mL). *Unknown peak.

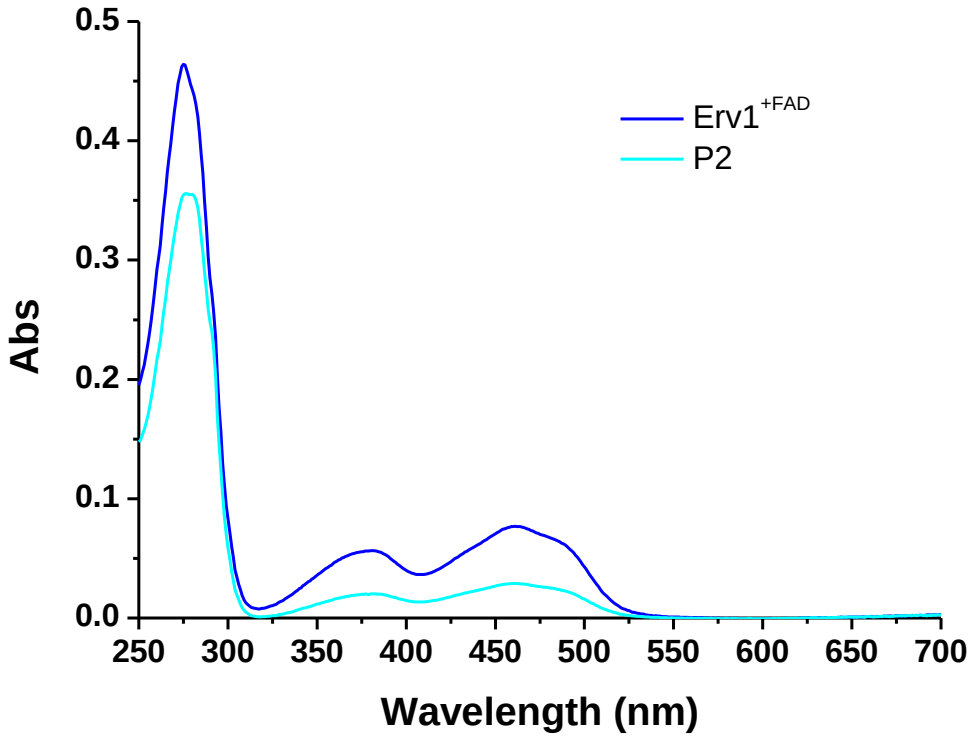

Figure 4.5 UV-visible spectra of different oligomerisation states of Erv1

UV-visible spectra of Erv1^{+FAD} (blue) and P2 of Erv1^{-FAD} (cyan) taken after SEC (Figure 4.3 B). The spectra were normalised to the same protein concentration as measured by Bradford assay.

Next, MALLS was used to determine the oligomerisation state of each peak in Erv1^{-FAD} (Figure 4.6 A). Initially, the results show P1 has a molecular weight ranging from 85 to 115 kDa, whereas P2 has a molecular weight between 35 and 50 kDa. In MALLS, when a peak displays a molecular weight line descending from high to low without oscillating around a specific value, it generally indicates the presence of a mixture of oligomerisation states. Furthermore, in this assay the molecular weights were overestimated because the light scattering baseline was not properly achieved due to the presence of protein aggregates. A run of P1 alone gave lower molecular weights between 73 and 96 kD, but there was still no horizontal line designating a fixed molecular weight (Figure 4.6 B). This may be explained by a small contribution from P2 that could affect the measurements. Thus, a fair assumption would be that P1 indeed contains tetrameric Erv1.

However, P2 of Erv1^{-FAD} gave two discernible overlapping peaks (P3 and P4) when reloaded on the column by itself: one with molecular weights from 45 to 48 kDa and one with molecular weights from 28 to 37 kDa (Figure 4.6 C). Therefore, P3 corresponds to dimeric Erv1, while P4 may be attributed to monomeric Erv1. These results show P2 of Erv1^{-FAD} actually represents a mixture of dimer and monomer that could not be separated. At this point, it is still unknown if the mixture represents separate dimers and monomers indistinguishable by SEC or an equilibrium between the two. Nevertheless, it is clear that a lower percentage of bound FAD not only disrupts tetramer formation but also opens the possibility of forming Erv1 monomers.

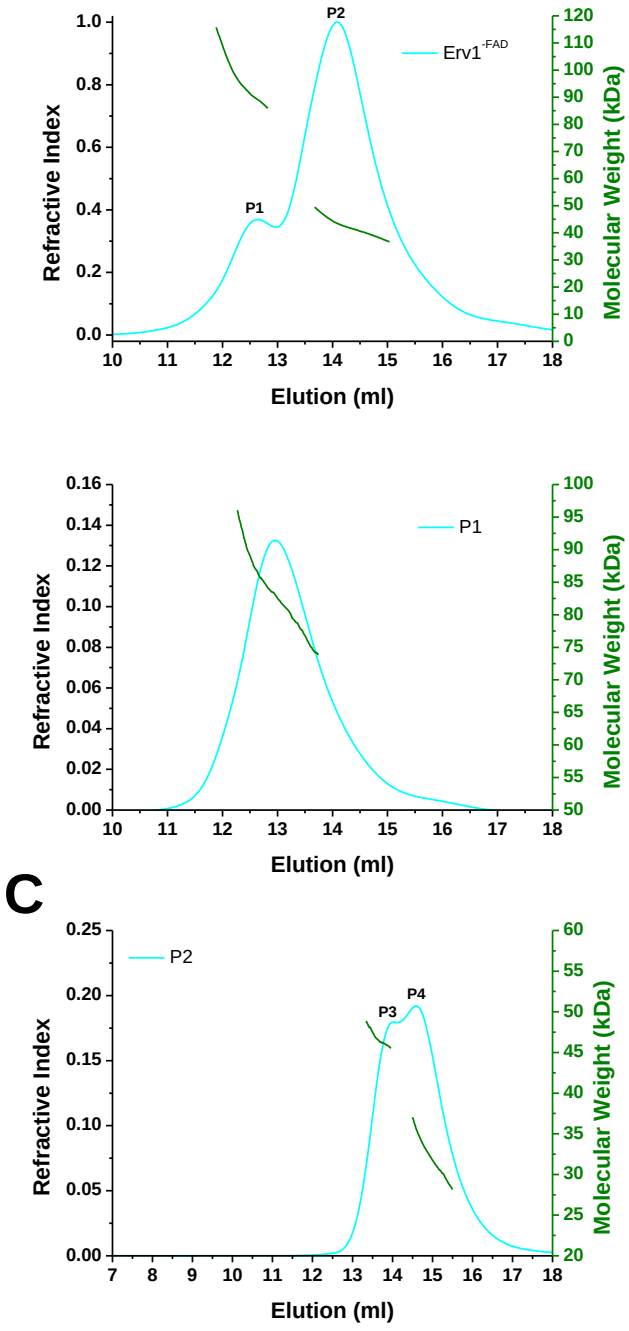

Figure 4.6 Multiangle laser light scattering of Erv1 purified without FAD supplement

A) Multiangle laser light scattering of Erv1 without FAD supplemented during cell lysis and after affinity purification ($Erv1^{-FAD}$). Molecular weight of: P1= 85 to 115 kDa, P2 = 35 to 50 kDa. The molecular weights are overestimated because the light scattering did not reach a proper baseline.

B) Multiangle laser light scattering of P1 from A. Only one peak is observed with the molecular weight going from 73 to 96 kDa.

C) Multiangle laser light scattering of P2 from A. Two peaks can be distinguished. Molecular weight of: P3 = 45 to 48 kDa, P4 = 29 to 37 kDa.

4.5. Effect of the oligomerisation state on the folding and thermal stability of Erv1

Modification of the quaternary structure is sometimes accompanied by a change in the secondary structure of the protein. The next step was therefore to compare the secondary structure of $Erv1^{+FAD}$ and P2 using circular dichroism (CD). In the far-UV region (wavelengths 180 to 260 nm), the chromophore under study is the peptide backbone giving a weak and broad $n \rightarrow \pi^*$ signal centred at around 220 nm and an intense $\pi \rightarrow \pi^*$ signal at around 190 nm. Hence, CD data collected in this region provides information regarding the folding of secondary structures. Figure 4.7 A shows the far-UV CD spectra of $Erv1^{+FAD}$ and P2. Peaks at 208 and 220 nm are characteristic of α-helical proteins (Martin and Schilstra, 2008), indicating the secondary structure of both oligomerisation states is mostly α-helical. This observation agrees with the published crystal structure of core domain Erv1 (Guo et al., 2012). However, P2 displayed an overall decrease in its CD intensity (~30%) compared to $Erv1^{+FAD}$. This can be interpreted as a percentage of protein in P2 being either misfolded or unfolded. Furthermore, subtraction of the P2 spectrum from that of $Erv1^{+FAD}$ produced a bell-shaped peak centred at 230 nm (Figure 4.7 A, inset). Positive peaks in this wavelength range are characteristic of a strong interaction between two or more aromatic residues in the protein structure (Martin and Schilstra, 2008). The data therefore reveals that the structure of $Erv1^{+FAD}$ includes close contacts between two or more aromatic residues that strongly interact with each other. However, in P2, although new aromatic-aromatic interactions could potentially be formed, the overall result due to the lower secondary folding is the loss of this type of interactions, which resulted in the weaker CD signal at 230 nm for P2. Collectively, this analysis indicates the tetramer conformation of $Erv1^{+FAD}$ is better folded than the conformation of P2. The results also highlight that some aromatic interactions may be important or only found in the tetramer, perhaps even form part of an unknown inter-subunit interface.

Next, CD was also used to examine the thermal stability of the different oligomerisation states of Erv1. Because Erv1 is mostly α-helical, the signal at 222 nm was chosen to follow its secondary structure in a temperature-

dependent manner (Figure 4.7 B). The results show Erv1^{+FAD} remained fully folded up to temperatures of 40-45°C, then it gradually unfolded until it became completely unfolded at temperatures of ~75°C. P2, however, remained folded only up to ~30°C and was completely unfolded at temperatures of ~70°C. The melting temperatures (T_M) of Erv1^{+FAD} and P2 are 68.3 ± 4.8°C and 58.0 ± 1.4°C, respectively, indicating tetramerisation conferred Erv1 with higher thermal stability.

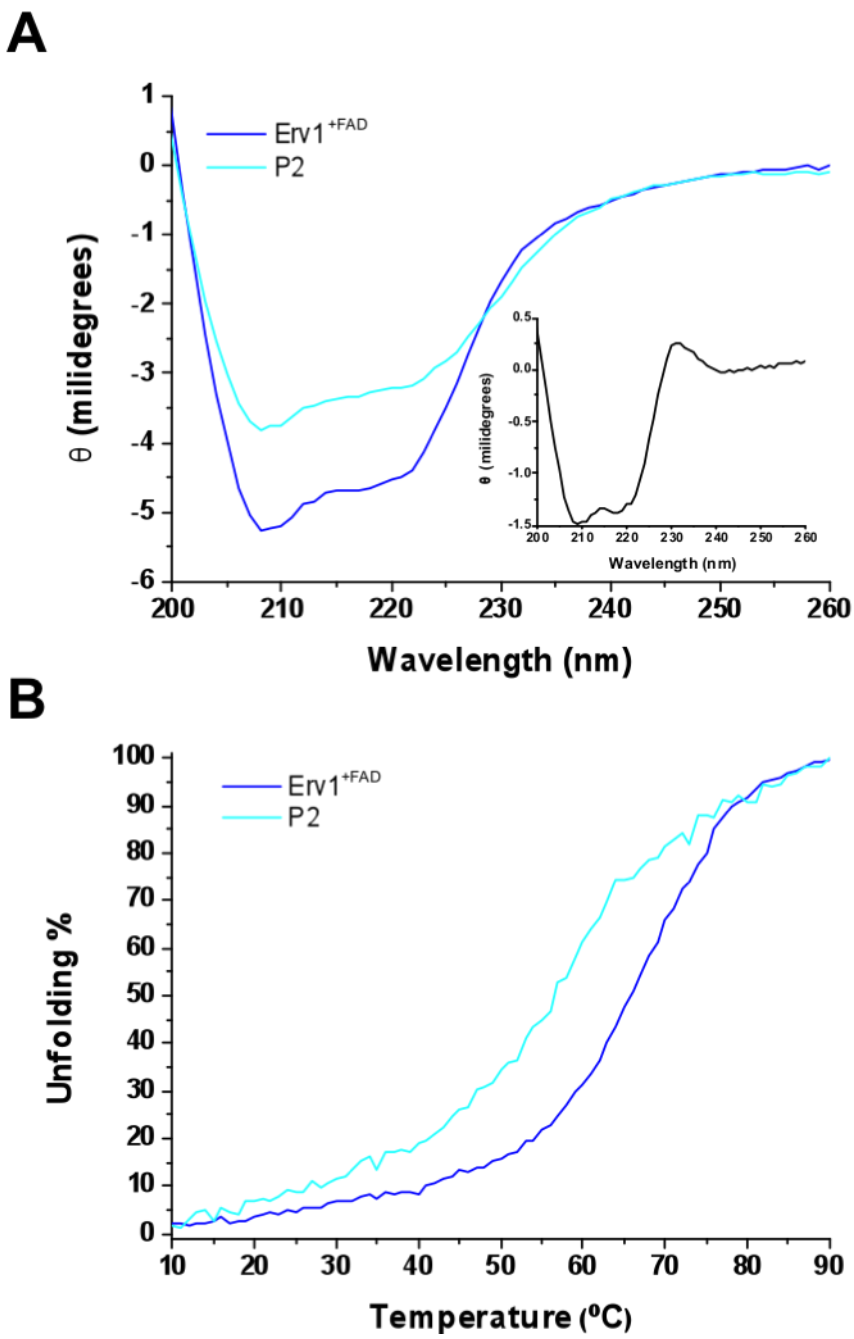

Figure 4.7 Secondary structure and thermal stability of different oligomerisation states of Erv1

A) Far-UV circular dichroism spectra of Erv1^{+FAD} (blue, 0.22 mg/ml) and P2 (cyan, 0.22 mg/ml) in BAE buffer at 25°C. The spectra represent the average of 4 independent experiments. Inset: subtraction of the P2 spectrum from that of the Erv1^{+FAD}. The peak centred at 230 nm is characteristic of aromatic-aromatic interactions.

B) Thermal denaturation of Erv1^{+FAD} (blue) and P2 (cyan) in BAE buffer. Protein unfolding was followed by far-UV circular dichroism at 222 nm (0.22 mg/ml). Temperature increase: 1 ºC/min, 10-90ºC. The curves represent the average of 4 independent experiments.

4.6. Effect of the oligomerisation state on the oxidase activity of Erv1

Changes in quaternary structure are often coupled with changes in protein function or activity. Sulphydryl oxidases such as Erv1 employ oxygen as an electron acceptor and, as such, their activity can be easily followed using an oxygen consumption assay. Hence, the effect of the oligomerisation state on the activity of Erv1 was studied using an oxygen electrode where the oxygen concentration decreases upon mixing of Erv1 with a disulphide reducing agent (e.g. DTT, TCEP). The disulphide reducing agent TCEP was used as electron donor in the experiments. TCEP is a bulkier molecule than the more generally employed reducing agent DTT and cannot interact directly with the C3-C4 redox-active disulphide of Erv1 (Ang and Lu, 2009). As a result, TCEP best mimics the physiological Mia40-Erv1 interaction.

It has also been shown that in the absence of superoxide dismutase (SOD) an unwanted superoxide/TCEP-catalysed oxygen consumption may overshadow the Erv1-mediated reaction (Daithankar et al., 2012). Reactions were therefore conducted by adding 5 mM TCEP to 1 μM Erv1 in the presence of 80 U/mL SOD (Figure 4.8). The results show that, upon addition of TCEP, P2 consumes oxygen slightly faster than $Erv1^{+FAD}$. The calculated relative initial rates are 0.910 ± 0.018 and 1.054 ± 0.051 μM/s for $Erv1^{+FAD}$ and P2, respectively. Thus, despite its different oligomerisation state and higher level of unfolding, P2 displayed no reduction in the oxidase activity. It follows that enhancement of the oxidase activity of Erv1 is unlikely to be the reason behind tetramerisation.

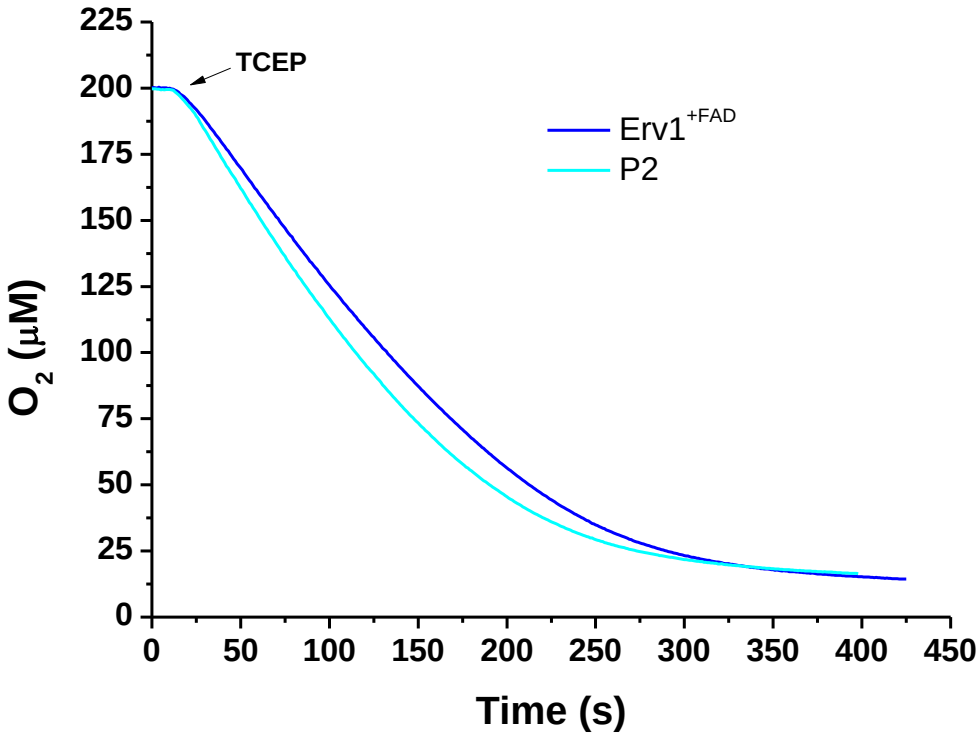

Figure 4.8 Oxidase activity of different oligomerisation states of Erv1

Oxygen consumption of $Erv1^{+FAD}$ (blue, 1 µM) and P2 (cyan, 1 µM) in the presence of 80 U/mL of superoxide dismutase. Reactions were done in BAE buffer and started by addition of 5 mM TCEP. The Erv1 concentrations are based on FAD content. The profiles represent the average of at least 2 assays on the same day.

4.7. Effect of reducing agents on the oligomerisation state of Erv1

The previous section demonstrated that tetramerisation does not improve the oxidase activity of Erv1. One possible explanation is that the functionally "active conformation" of Erv1 is the dimer. To check this theory, an oxidase reaction was conducted inside a size exclusion column using $Erv1^{+FAD}$. The column was first equilibrated with BAE buffer plus 5 mM TCEP and 80 U/mL SOD. Then, $Erv1^{+FAD}$ was injected and its oligomerisation state determined based on its elution position (Figure 4.9 A). The results show $Erv1^{+FAD}$ remained a tetramer as it eluted at the same position as when ran in BAE buffer without TCEP. Therefore, under the reaction conditions of ~250 μM O_2, 5 mM TCEP and 80 U/mL SOD the protein still reacts as a tetramer.

A closer look at figure 4.9 A shows Erv1 is still mostly oxidised during the assay (the absorbance at 460 nm indicates the FAD cofactor is not fully reduced in BAE + TCEP). Thus, an assay was devised to study the oligomerisation state of Erv1 while in a fully reduced state (reduced C1-C2 and C3-C4 disulphides as well as FAD). To achieve this, $Erv1^{+FAD}$ was run through a size exclusion column using anaerobic BAE buffer ± 1 mM TCEP inside an anaerobic glove box (Figure 4.9 B). The lack of oxygen helps to maintain Erv1 in its reduced state. Despite addition of 1 mM TCEP the majority of the protein still eluted as a tetramer. A small fraction of the protein eluted at ~13.9 mL, a position attributed to the dimer conformation. However, this small peak may represent a fraction of Erv1 that has lost FAD (Section 4.4). Therefore, even in its fully reduced state Erv1 remains a tetramer.

Overall, these results indicate a strong reducing environment does not affect the quaternary structure of Erv1. Even though Erv1 forms disulphide-bonded dimers (Ang, 2010), the results imply these inter-subunit disulphides are not needed for tetramerisation. It is still possible that the micromolar concentrations (> 20 μM) required for the assays are too high to visualise Erv1 in a complete dimer conformation. Nevertheless, it does appear Erv1 functions as a tetramer during its oxidase activity.

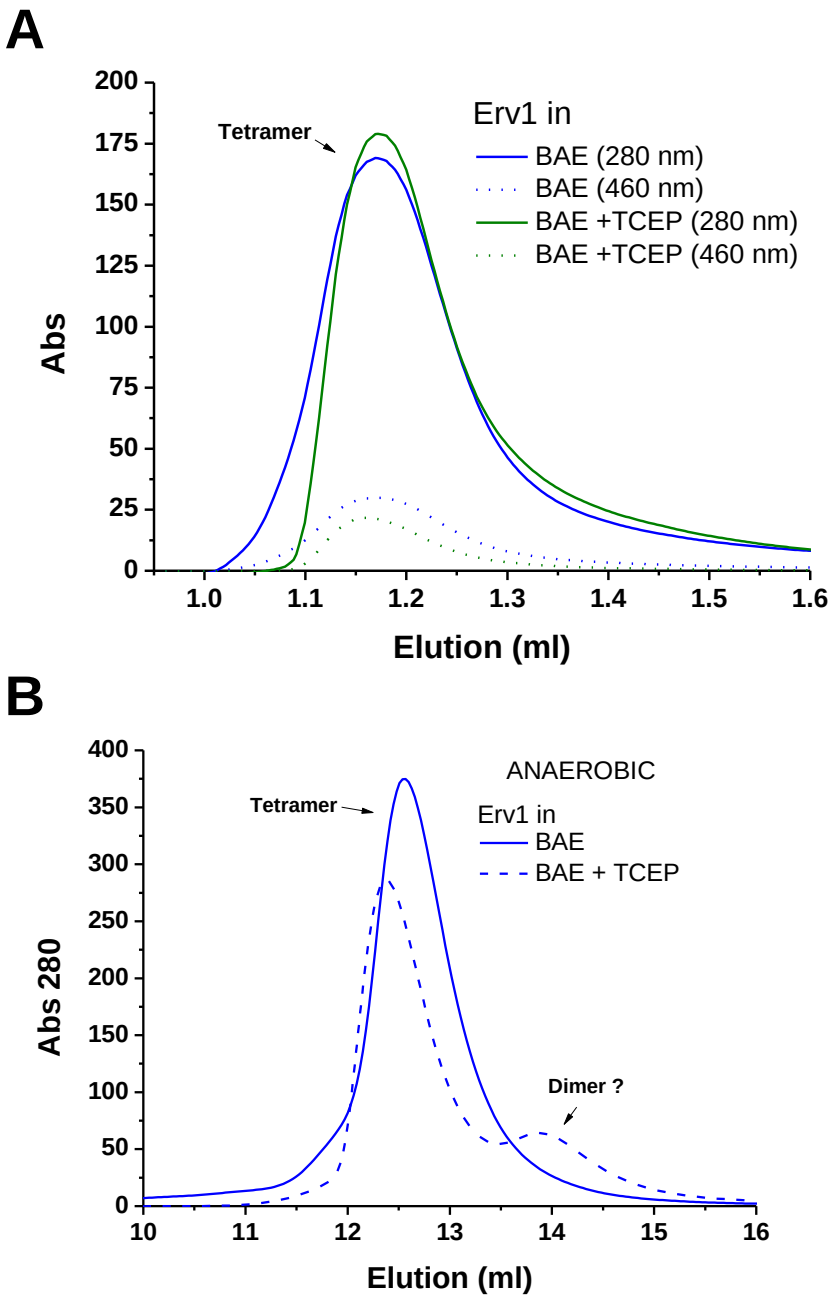

Figure 4.9 Size exclusion chromatography of Erv1 in the presence of the reducing agent TCEP.

A) Size exclusion chromatography of Erv1 using either BAE buffer (blue) or BAE + 5 mM TCEP, 80 U/mL SOD (olive green). The proteins were run on a Superdex 200 PC 3.2/30 column at room temperature. Under the reaction conditions of ~250 µM O_2, 5 mM TCEP and 80 U/mL SOD the protein still reacts as a tetramer.

B) Size exclusion chromatography of Erv1 (0.5 mg) using either anaerobic BAE buffer (blue) or anaerobic BAE + 1 mM TCEP (blue, dashed). The proteins were run on a Superdex 200 10/300 GL column at 20°C inside an anaerobic glove box. Even when fully reduced Erv1 remains a tetramer.

4.8. Discussion

The crystal structure of the core domain of proteins in the ERV family showed them to adopt a homodimer conformation (Gross et al., 2002, Wu et al., 2003, Levitan et al., 2004, Daithankar et al., 2012, Guo et al., 2012). The Erv fold consists of five α-helices, four of which are used to surround the FAD cofactor while the short fifth helix remains just outside the bundle (Section 1.2.1.1, Figure 1.9). The dimer interface is formed by hydrophobic residues on helix 1 (H1) and helix 2 (H2) of each fold, with the two subunits poised at a 55° angle with respect to one another (Fass, 2008). Recently, the crystal structure of the core domain of Erv1, which includes the Erv fold, demonstrated the protein also forms homodimers (Guo et al., 2012). The results presented in this chapter looked instead at the quaternary structure of full-length Erv1. Unlike the construct used for crystallisation, the protein employed in this study also includes the flexible N-terminal domain (residues: 1-82).

During the course of this study one report directly addressed the oligomerisation state of full-length Erv1 and suggested the protein adopts a dimeric quaternary structure (Bien et al., 2010). Initially, an experiment using mitochondria with co-expressed Erv1-His and Erv1-HA tagged proteins showed that, when Erv1-His was pulled down using His-specific beads, Erv1-HA was also purified. This result thus indicated that the protein oligomerises inside mitochondria. A second result using protein crosslinkers and SDS-PAGE then showed the protein could form dimers. However, the crosslinking was not complete for there was still a strong band representing the monomer and, additionally, the upper part of the gel was not published. Hence, the possibility of a higher oligomerisation state for Erv1 should not be discarded. The last result showed the purified protein eluted between the molecular weight markers of 67 and 43 kDa in a SEC experiment, which lead to the protein being considered a dimer (Bien et al., 2010). However, the MALLS experiments presented here showed that, when Erv1 elutes between the 67 and 43 kDa markers, the peak actually represents a mixture of dimer and monomer that could not be separated. A link was identified between the oligomerisation state of Erv1 and the FAD binding percentage of Erv1. When Erv1 exhibited a low FAD content (~20%) the protein eluted below the 67 kDa marker in SEC. On the other hand, if Erv1 had a high percentage of protein-

bound FAD (~95%) then it eluted above the 67 kDa marker. Thus, it is conceivable the dimer conformation reported for full-length Erv1 actually corresponds to a protein with a low percentage of FAD bound to it.

In support of a tetramer Erv1 the MALLS analysis determined a molecular weight of 88 kDa for full-length Erv1. Considering the monomer has a molecular weight of 22 kDa (Lee et al., 2000), the data indicates that Erv1 adopts a tetramer conformation in solution. Furthermore, oligomerisation can be useful for a protein to improve or control its function and folding stability (Nooren and Thornton, 2003). Here, CD studies showed the Erv1 'dimer' is about 30% less folded than the Erv1 tetramer, suggesting tetramerisation is coupled to a higher folding in Erv1. Additionally, tetramerisation conferred on Erv1 a higher resistance to temperature, with a difference in T_M of ~10°C between Erv1 'dimer' and Erv1 tetramer, and was either a cause or a pre-requisite of a high FAD content. On the other hand, the oxidase activity of Erv1 was not affected suggesting tetramerisation does not offer an advantage in the activity. However, a fault in these assays is that they were done using different concentrations (~20 μM for SEC, 1 μM for oxygen consumption) without a previous knowledge of the Erv1 dissociation constant (K_d). Thus, it is possible that, upon dilution, the tetramer dissociates into dimers or even monomers thus giving the impression of having the same activity as Erv1 'dimer'. Generally, it is highly important to know the K_d of a protein to be certain that the same oligomerisation state is present on each assay. Lastly, more experiments are required to ascertain the oligomerisation state of Erv1, starting by analytical ultracentrifugation (AUC) that could be employed to confirm the formation of a tetramer and obtain the K_d of Erv1. Another important point that needs to be addressed is the removal of the his-tag to ensure that tetramer formation is not due to its presence.

4.9. Conclusion

Collectively, the results presented here indicate full-length Erv1 forms a tetramer under the conditions tested here, which increased its secondary structure folding and thermal stability. Tetramer formation was independent of intermolecular disulphide bonds but tightly linked to FAD binding in Erv1. However, it remains to be seen if Erv1 remains a tetramer at low sub-micromolar concentrations and also whether it forms tetramers *in vivo*.

5. RESULTS AND DISCUSSION II: CHARACTERISATION OF THE ERV1 R182H MUTATION

5.1. Introduction

Enzymes are highly evolved catalysts in charge of conducting a variety of reactions. They come in all types, from big and complex structures capable of catalysing very specific reactions to small proteins often not even substrate specific. A common trait, however, is that mutations in the active site of an enzyme generally leads to changes in its function.

ALR, the human counterpart of Erv1, works as an enzyme in the mammalian MIA pathway (Lisowsky et al., 2001, Farrell and Thorpe, 2005). Recently, a single arginine to histidine substitution (R194H) in the C-terminal end of ALR was identified as the cause of autosomal recessive myopathy (Di Fonzo et al., 2009). Two copies of a defective *ALR* gene were found in three children from healthy parents. The children were affected by congenital cataract, progressive muscular hypotonia, sensorineural hearing loss and developmental delay (Di Fonzo et al., 2009). At a cellular level the effects included a lower cysteine-containing protein content, abnormal mitochondrial morphology, reduction of respiratory-chain activity and increased accumulation of mitochondrial DNA (mtDNA) deletions (Di Fonzo et al., 2009). The mutant equivalent Erv1 R182H in *S. cerevisiae* also showed reduced respiratory-chain activity, higher level of mtDNA mutability, altered mitochondrial morphology and a thermosensitive phenotype with delayed cell growth in solid medium at 37°C (Di Fonzo et al., 2009). Further experiments then showed a lower mitochondrial content of MIA pathway substrates and mislocalisation of Mia40 to the cytosol (Sztolsztener et al., 2013). These defects are however not a cause of Erv1 degradation for it was shown the Erv1 R182H mutant is expressed and localised similarly to the wild-type (Sztolsztener et al., 2013).

Here, the purified Erv1 R182H mutant was studied *in vitro* using a range of biophysical techniques. First, the effects of the mutation on the folding and stability of Erv1 were characterised. Then, the activity of Erv1 R182H was compared with that of Erv1 wt at different temperatures. Lastly, the link between Erv1 activity and the stability of FAD binding was also investigated.

5.2. Purification of the Erv1 R182H mutant

The Erv1 R182H mutant was successfully purified from *E. coli* Rosetta-gami™ 2 cells (Section 3.4). Reducing SDS-PAGE showed the protein was properly overexpressed (Figure 5.1, lane 2) and found mostly in the supernatant (Figure 5.1, lane 4). The final protein after affinity purification was yellowish in colour and mostly pure with only a few extra bands below 15 kDa (Figure 5.1, lane 7). Further purification by SEC using a Superdex 200 indicated the main peak represents Erv1 R182H at approximately 90% pure (Figure 5.1, lane 8). In this study both Erv1 wt and Erv1 R182H were purified on average at 8 mg of protein per gram of *E. coli* cells.

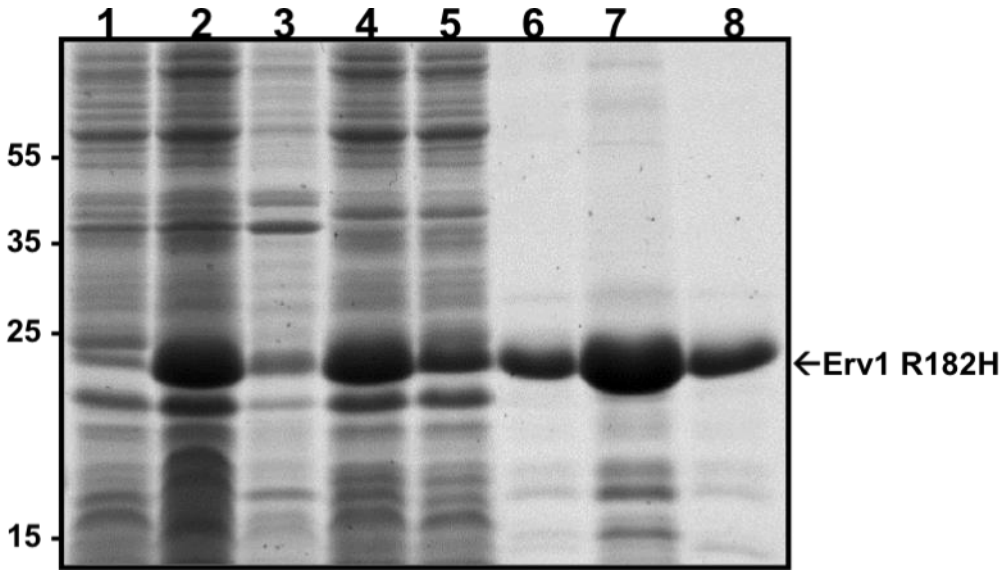

Figure 5.2 SDS-PAGE of a purification of Erv1 R182H

Reducing SDS-PAGE of an Erv1 R182H affinity purification visualised using coomassie-blue staining. Lanes: 1) cells grown to log phase, 2) overnight induction at 16°C, 3) sonication pellet, 4) sonication supernatant, 5) flowtrough from Ni-NTA His-Bind beads, 6) wash with 80 mM imidazol, 7) elution with 500 mM imidazol, 8) after SEC.

5.3. Effect of the R182H mutation on the oligomerisation state of Erv1

The initial step in the characterisation of the Erv1 R182H mutant was to determine its oligomerisation state. To that end, the protein was first run through a Superdex 200 SEC column in BAE buffer (Figure 5.2 A). Erv1 R182H eluted in two peaks, a small peak at ~12.7 mL and a large peak at ~14 mL. This indicates a small proportion of Erv1 R182H forms a tetramer but the majority of it has a lower molecular weight than that of Erv1 wt (section 4.1). By comparing its elution with that of the protein markers, an apparent molecular weight of ~67 kDa was estimated, suggesting a trimer conformation (Erv1 monomer = 22 kDa).

As mentioned earlier, SEC does not offer an accurate measurement of the molecular weight for proteins that do not have a molten-globule shape. To obtain a more accurate weight the Erv1 R182H mutant was next analysed by MALLS (Figure 5.2 B). The result shows the main peak of Erv1 R182H has a molecular weight of 44 ± 1 kDa, revealing the mutant protein to be a dimer. Thus, although the mutation is not located at the dimer interface identified in the crystal structure of Erv1 (Fass, 2008, Guo et al., 2012), the single amino acid substitution clearly changes its oligomerisation state. It is possible that the R182H mutation is instead localised in a yet unidentified oligomerisation interface important for tetramer formation.

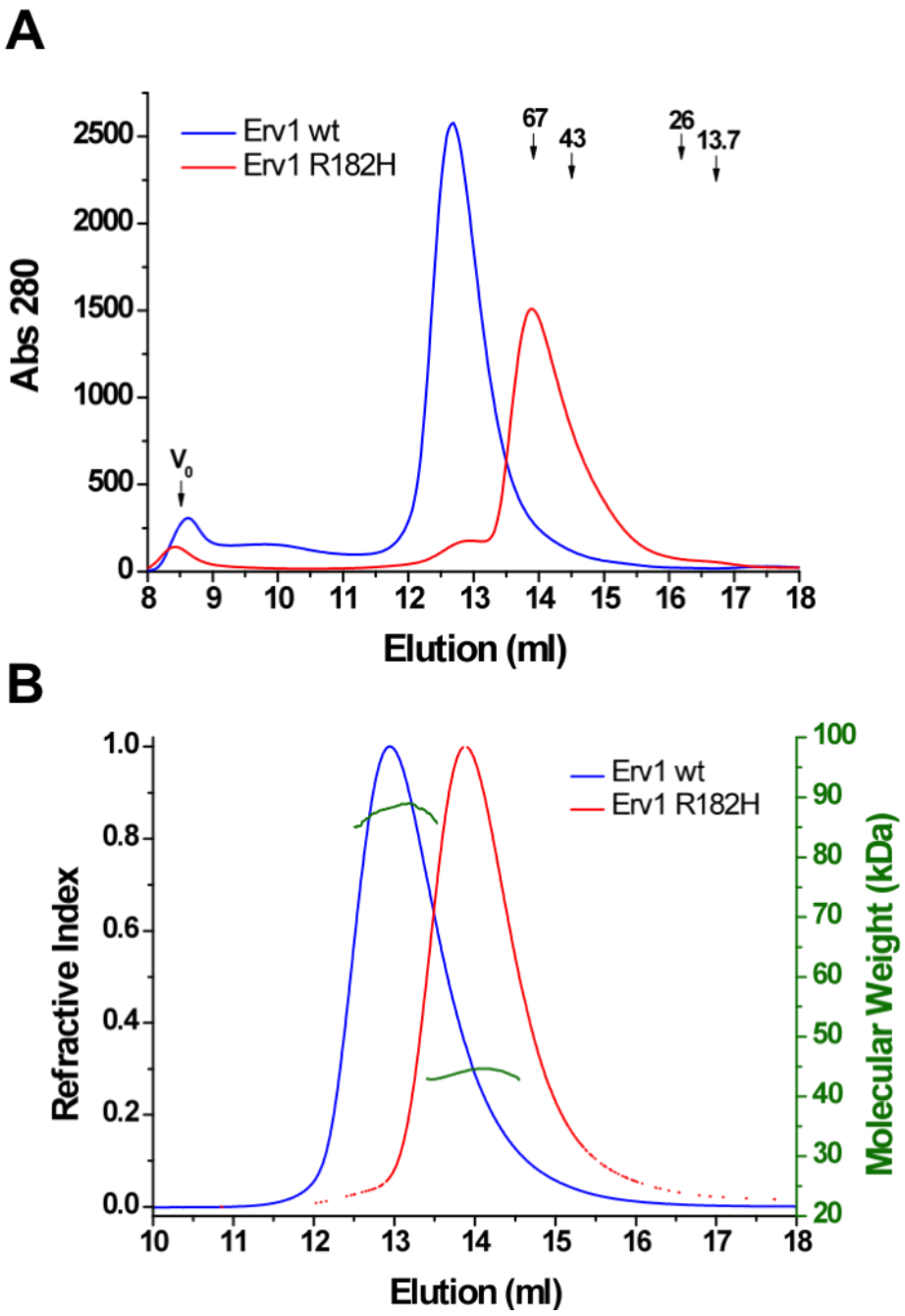

Figure 5.3 Oligomerisation state of Erv1 wt and Erv1 R182H

A) Size exclusion chromatography of Erv1 R182H (red) on a Superdex 200 10/300 GL column run in BAE buffer. The protein was assayed directly after affinity purification. Molecular weight markers: albumin (67 kDa), ovalbumin (43 kDa), chymotrpsin (26 kDa) and ribonuclease A (13.7 kDa). Void volume V_0 = 8.5 mL. For comparison, Erv1 wt is in light blue.

B) Multiangle laser light scattering of Erv1 R182H (red). The fraction corresponding to the main peak from a previous size exclusion experiment was used for the assay. The molecular weight (olive green) of Erv1 R182H is 44 ± 1 kDa, indicating the mutant adopts a dimer conformation.

5.4. Effect of the R182H mutation on the FAD binding of Erv1

Enzymes occasionally use cofactors to help them in their function. Often, a mutation near the cofactor can affect the enzymes ability to bind them. Thus, the next step in the characterisation looked at the binding of FAD by Erv1 using various spectroscopic techniques. First, the UV-visible spectra of both Erv1 wt and Erv1 R182H were clearly superimposed (Figure 5.3 A). A slight but reproducible difference in the FAD maximum absorption wavelength (λ_{max}^{FAD}) was observed in the spectra; whereas Erv1 wt gave a λ_{max}^{FAD} of 460 nm, the Erv1 R182H mutant gave a λ_{max}^{FAD} of 459 nm. Still, superimposition of the spectra does not necessarily mean both proteins bind FAD with the same FAD to protein ratio. The FAD binding percentage was therefore calculated using the BCA assay for protein concentration and treatment with 1% SDS to measure the FAD concentration. The percentages were similar for Erv1 wt and Erv1 R182H with values of 96 ± 6 and 93 ± 6%, respectively. The results are summarized in Table 5.1.

Another characteristic of FAD that could be affected by the mutation is its standard reduction potential (E^o). A change in the E^o would signify a difference in the reactivity of the mutant. Thus, measurements of the E^o of FAD were taken using the same techniques later described in section 6.1. A E^o of -152 ± 12 mV (z=2) was obtained for the Erv1 R182H mutant, which is similar to the one measured for Erv1 wt (Table 5.1; Section 6.2).

Next, the effect of the R182H mutation on FAD fluorescence was analysed. Figure 5.3 B shows a ~5 fold increase in the FAD fluorescence emission intensity (530 nm) of Erv1 R182H over that of Erv1 wt. This finding suggests a stronger quenching of FAD fluorescence in Erv1 wt compared to that in the Erv1 R182H mutant. Flavoenzymes quench the fluorescence of their flavin cofactor (FMN, FAD) by stacking aromatic residues around it, which can interact with the excited isoalloxazine ring (Munro and Noble, 1999). Hence, a stronger quenching can be taken as a signal of a tighter FAD binding in Erv1 wt.

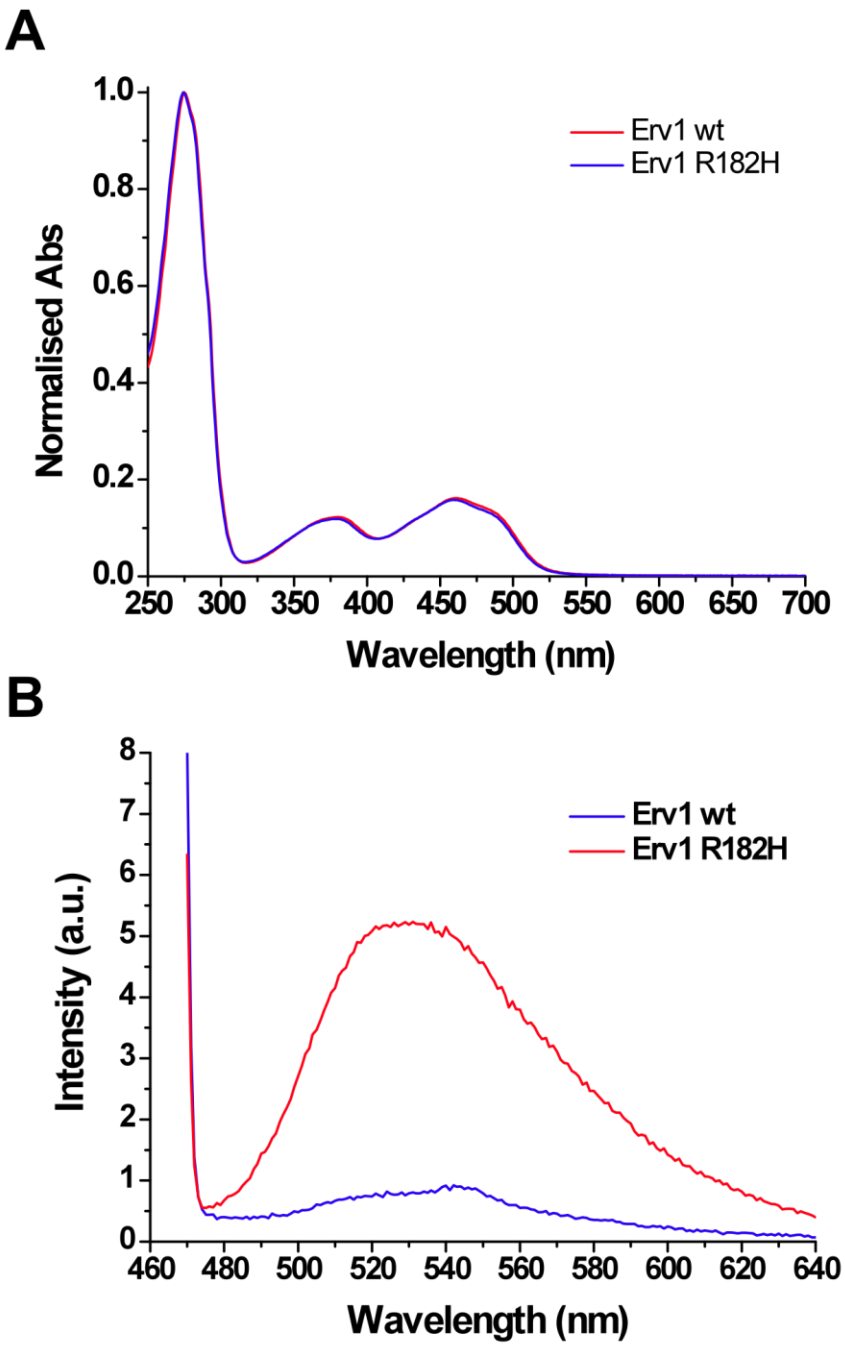

Figure 5.4 FAD spectra of Erv1 wt and Erv1 R182H

A) UV-visible spectra of Erv1 wt (blue) and Erv1 R182H (red) normalised at 275 nm.

B) FAD fluorescence of Erv1 wt (blue, 10 μM) and Erv1 R182H (red, 10 μM). The Erv1 R182H mutant shows less quenching of the emission intensity. Excitation = 460 nm. Protein concentrations based on FAD content.

Table 5.1 FAD binding of Erv1				
Protein	**λ_{max}(nm)**	**ε (mM^{-1} cm^{-1})**	**%FAD**	**E^{o}(mV)**
Erv1 wt	460	12.3	96±6	-157±7
Erv1 R182H	459	11.8	93±6	-152±12

Further evidence of a weaker FAD binding in the mutant arose when the chemical stability of Erv1 was evaluated by treating the proteins with urea. Initially, Erv1 was bound to a 1 mL HisTrap HP column. Then, a urea gradient (0→8 M) was applied while the release of FAD was followed at 460 nm (Figure 5.4 A). Erv1 wt required 8 M urea to completely unbind its FAD, whereas Erv1 R182H only needed 4.5 M urea. This pointed to weaker binding of FAD in the Erv1 R182H mutant. The conclusion was further supported by kinetic studies where the wild-type and mutant proteins were treated with 7 M urea and the release of FAD from Erv1 was followed by the decrease in absorbance at 496 nm (Figure 5.4 B). In the assays, fitting of the absorbance at 496 nm to an exponential decay (equation 1, section 3.6.3) gave relative half-lives (τ) of 1.82 ± 0.17 and 0.30 ± 0.05 min for Erv1 wt and Erv1 R182H, respectively, indicating FAD was released ~6 times more quickly from the mutant protein than from the wild-type.

$$A = A_0\left(\tfrac{1}{2}\right)^{t/\tau} \qquad (1)$$

A = Absorbance
A_0 = Initial absorbance
t = time
τ = half-life of decaying quantity

In spite of these differences, when equimolar amounts of FAD and either apo-Erv1 wt or apo-Erv1 R182H were mixed, both proteins bound FAD with similar kinetics (Figure 5.4 C). The result indicates the on-rate constant (k_{on}) for the binding of FAD by apo-Erv1 is the same for both proteins. Therefore, considering the faster release of FAD shown before (Figure 5.4 A and B), it follows that the weaker FAD binding in Erv1 R182H most likely relates to a different off-rate constant (k_{off}).

$$\text{FAD} + \text{apo-Erv1} \underset{k_{\text{off}}}{\overset{k_{\text{on}}}{\rightleftharpoons}} [\text{Erv1-FAD}]$$

Collectively, these results agree with previous findings using the ALR R194H mutant (Daithankar et al., 2010). In both cases the mutant proteins exhibited a weaker FAD binding, with different off-rate constants compared to the wild-types.

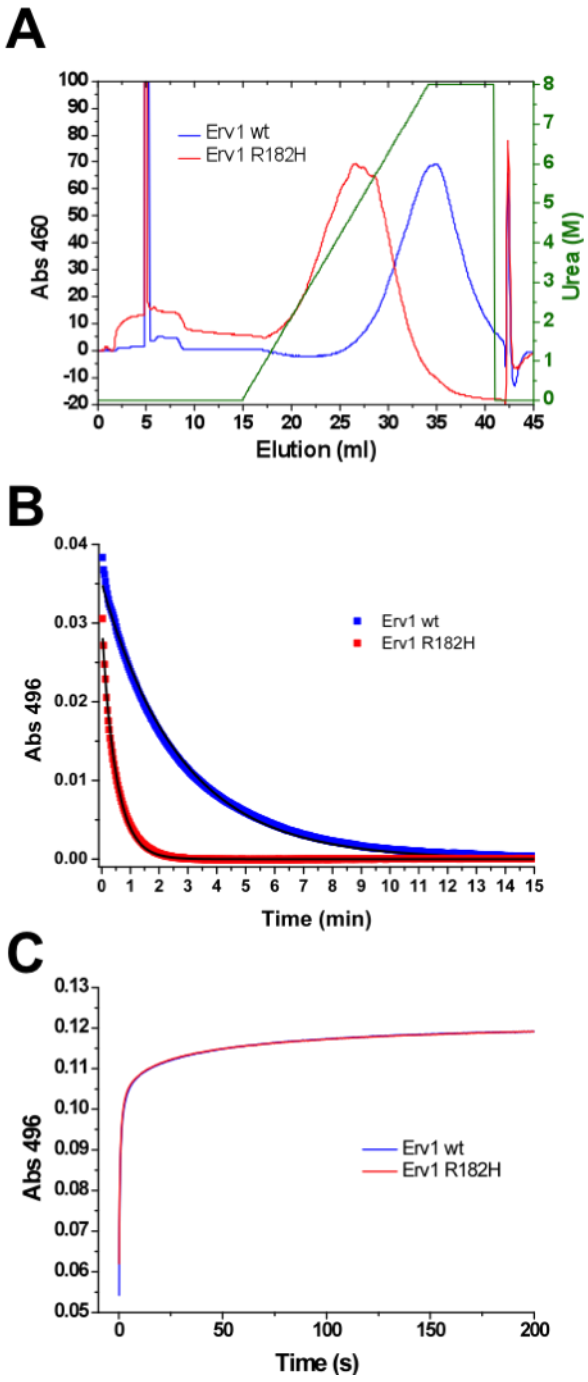

Figure 5.5 Stability of FAD binding in Erv1 wt and Erv1 R182H

A) FAD release from Erv1 wt (blue, 2 mg) and Erv1 R182H (red, 2 mg). Proteins were bound to a 1 ml HisTrap HP column and then treated with a 0 to 8 M urea gradient. The release of FAD was followed by its absorbance at 460 nm.

B) Kinetics of FAD release followed at 496 nm after addition of 7 M Urea to 10 µM Erv1 wt (blue) and Erv1 R182H (red). Fitting to an exponential decay gave relative half-lives of 1.87 ± 0.17 and 0.30 ± 0.05 for Erv1 wt and Erv1 R182H, respectively. Values represent the average of 3 assays on the same day.

C) FAD uptake by apo-Erv1 wt (blue) and apo-Erv1 R182H (red). Equimolar amounts (20 µM inside the cell) of FAD and apo-Erv1 were used. Binding was followed at 496 nm using a stopped-flow instrument.

5.5. Effect of the R182H mutation on the folding of Erv1

The R182H mutation changes the oligomerisation state of Erv1 and its ability to bind FAD. A plausible explanation for these two alterations is a modification of the secondary structure folding of Erv1. Thus, further characterisation of Erv1 R182H was done by circular dichroism (CD). The CD signal on the far-UV region is generally employed for the study of secondary structures (Section 4.4) and here both Erv1 wt and Erv1 R182H were analysed under identical conditions (Figure 5.5 A). The results show peaks at 195, 208 and 220 nm characteristic of α-helical proteins (Martin and Schilstra, 2008). However, as in the case of P2 (section 4.5), the change in the oligomerisation state in the Erv1 R182H mutant was accompanied by a lower level of secondary folding (~20% less) than that of the wild-type. Furthermore, when the spectrum of Erv1 R182H was subtracted from that of Erv1 wt a peak centred at 230 nm was again generated (Figure 5.4 A, inset), suggesting that the same strong aromatic-aromatic interactions that were lost in the Erv1 wt 'dimer' (P2 in section 4.5) are also absent in Erv1 R182H.

Near-UV CD is commonly used to study tertiary structure pockets where phenylalanine, tyrosine and tryptophan residues are the absorbing chromophores. As such, the technique was employed to test whether there is also a difference in tertiary structure between Erv1 wt and Erv1 R182H. The near-UV CD spectra of both proteins are presented in figure 5.4 B. The signal around 272 nm represents absorption by tyrosine residues, whereas signals at 285 and 292 nm represent absorption by tryptophan residues (Martin and Schilstra, 2008). However, not all aromatic residues contribute to the spectra. In general, immobilised aromatic residues or those that closely interact with other neighbouring aromatic residues produce the strongest signals (Martin and Schilstra, 2008). This means the weaker signals at 285 and 292 nm of the Erv1 R182H spectrum can best be interpreted as coming from lost interactions between aromatic residues.

Jointly, both far and near UV CD results show the R182H mutation modifies the overall conformation of Erv1, decreasing its secondary folding by about 20% and causing some changes on its tertiary structure. The data also adds further evidence to support the observation that strong interactions between two or more aromatic residues are important for tetramerisation.

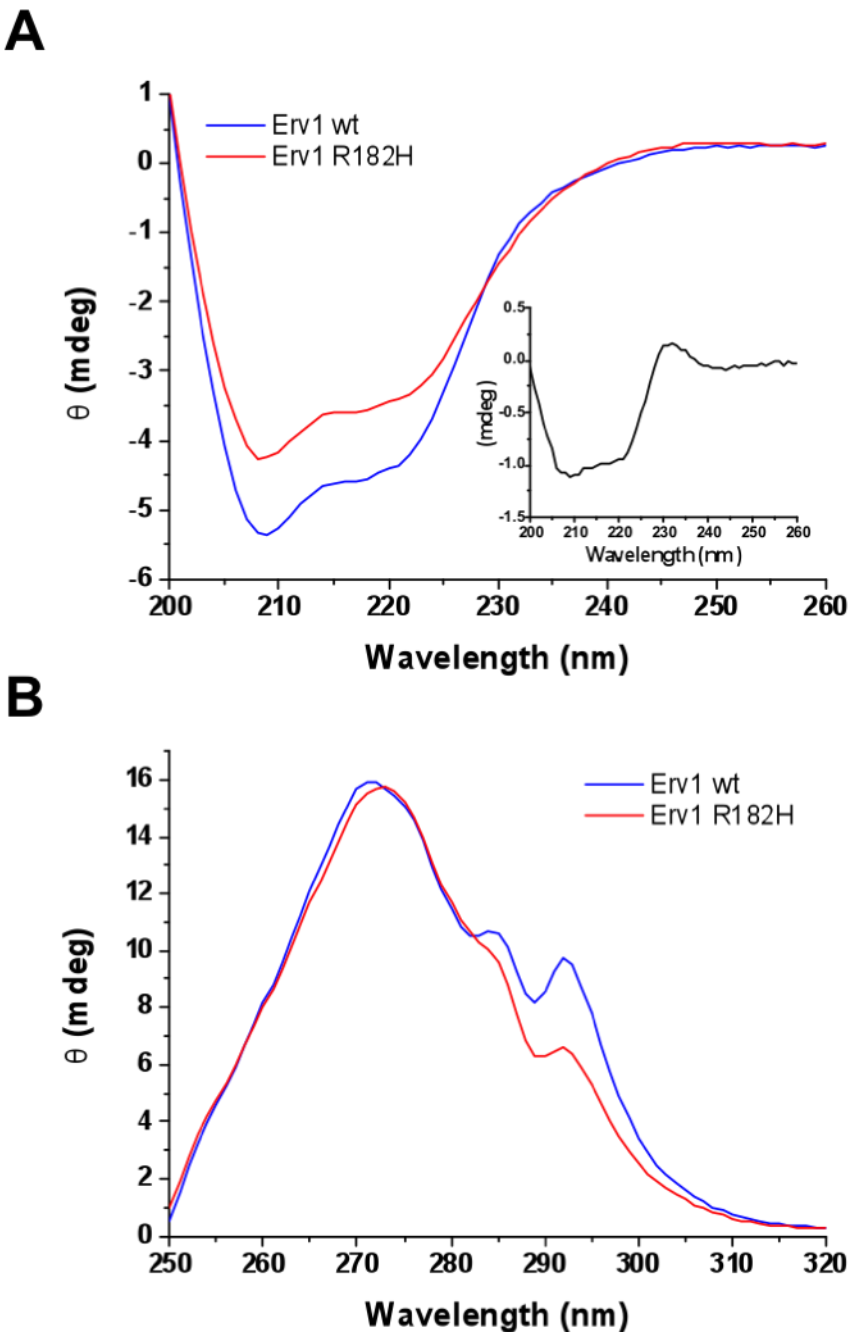

Figure 5.6 Circular dichroism spectra of Erv1 wt and Erv1 R182H

A) Far-UV circular dichroism spectra of Erv1 wt (blue, 0.22 mg/ml) and Erv1 R182H (red, 0.22 μM) in BAE buffer at 25°C. The spectra represent the average of 4 independent experiments. Inset: subtraction of the Erv1 R182H spectrum from that of Erv1 wt. The peak centred at 230 nm is characteristic of aromatic-aromatic interactions.

B) Near-UV circular dichroism of Erv1 wt (blue, 0.5 mg/ml) and Erv1 R182H (red, 0.5 mg/ml) in BAE buffer at 25°C. Signal at 272 nm represents tyrosine residues. Signal at 285 and 292 nm represent tryptophan residues. The spectra represent the average of 4 independent experiments.

5.5. Effect of the R182H mutation on the oxidase activity of Erv1

5.5.1. At 25°C

One function of Erv1 is to catalyse the transfer of electrons from partially reduced Mia40 (pr-Mia40) to oxygen (Lee et al., 2000, Mesecke et al., 2005, Ang and Lu, 2009, Tienson et al., 2009). Thus, the oxidase activity of Erv1 wt and Erv1 R182H was studied using an oxygen consumption assay. First, TCEP was used as the reducing agent to best imitate the electron transfer from Mia40 to Erv1 (Ang and Lu, 2009). Reactions were started by addition of 5 mM TCEP to 3 µM Erv1 in the presence of 80 U/mL SOD. Figure 5.6 A presents oxygen consumptions profiles for Erv1 wt and Erv1 R182H at 25°C. Clearly, both proteins consumed oxygen with similar kinetics when TCEP was used as electron donor at 25°C (Table 5.2).

Next, the physiological substrate Mia40 core (Mia40c) was employed (Figure 5.6 B). Exchange of full-length Mia40 for Mia40c inside *S. cerevisiae* displayed no phenotype (Terziyska et al., 2009), but Mia40c is easier to purify and was thus employed in these assays. Partially reduced Mia40c (pr-Mia40c) consists of Mia40c with a reduced CPC motif and was made by treating Mia40c with TCEP. The excess reducing agent was then removed by SEC and the protein was immediately used. When 35 µM of pr-Mia40c were used as electron donor the reaction again proceeded with similar kinetics for both Erv1 wt and Erv1 R182H (Table 5.2). This indicates the mutation does not affect the reaction of Erv1 with Mia40.

Taken together, these results suggest the electron transfer from Mia40 to Erv1, and from there to O_2, is not affected in the Erv1 R182H mutant when the reactions are done at 25°C. Again, the results agree with those reported for ALR where the R194H mutation did not affect its oxidase activity at 25°C (Daithankar et al., 2010).

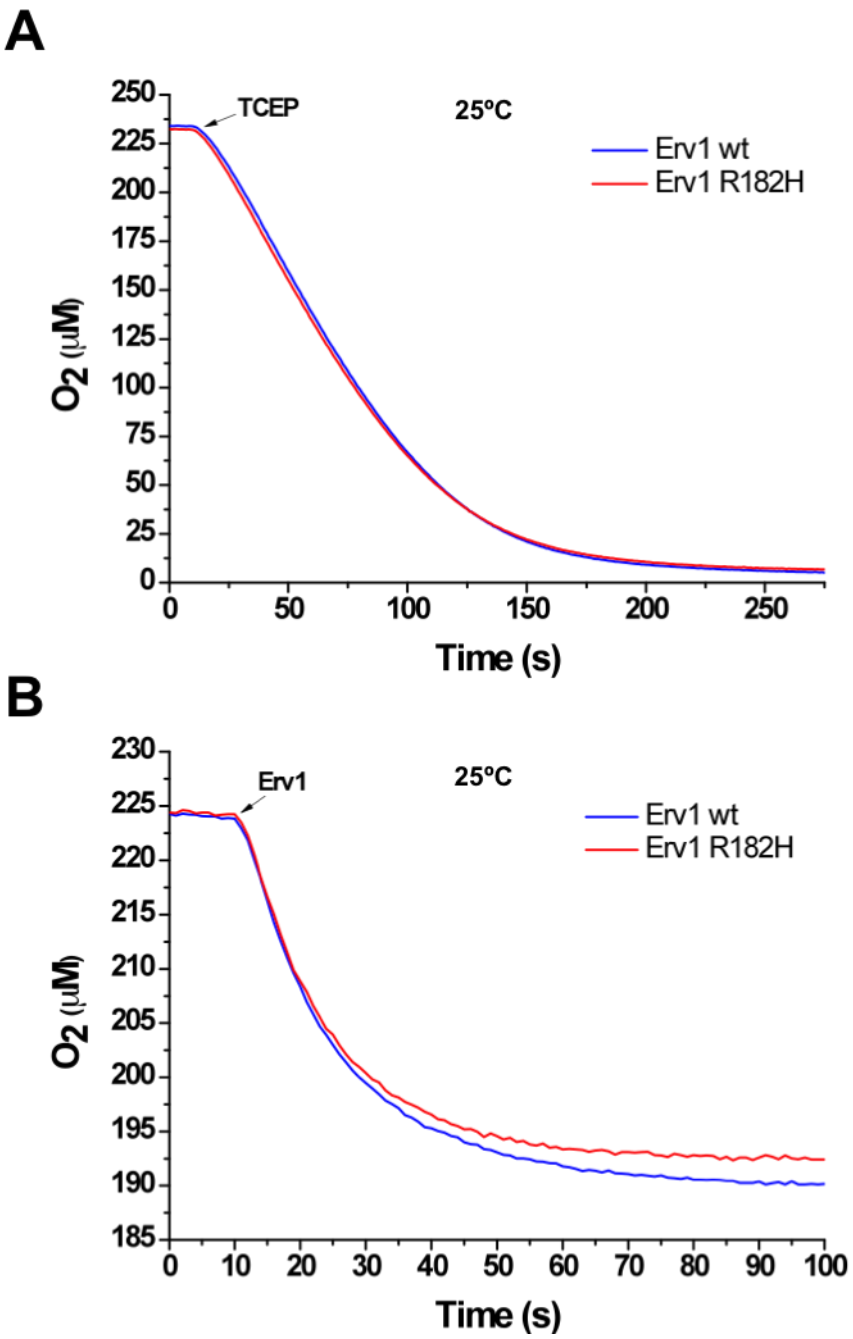

Figure 5.7 Oxidase activity of Erv1 wt and Erv1 R182H at 25°C

A) TCEP as electron donor: Oxygen consumption of Erv1 wt (blue, 3 µM) and Erv1 R182H (red, 3 µM) at 25ºC in the presence of 80 U/ml of superoxide dismutase. Reactions were done in BAE buffer and started by addition of 5 mM TCEP. The profiles represent the average of 3 assays on the same day.

B) Mia40 as electron donor: Oxygen consumption of Erv1 wt (blue, 3 µM) and Erv1 R182H (red, 3 µM) at 25°C using 35 µM pr-Mia40c as electron donor. Reactions were done in BAE buffer. The profiles represent the average of 3 assays on the same day.

5.5.2. At 37°C

The first report on the Erv1 R182H mutation showed a growth defect in yeast at 37°C (Di Fonzo et al., 2009). It therefore stands to reason the activity of Erv1 R182H might only be destabilised at temperatures near 37°C. To start, an oxygen consumption assay was performed at 37°C using 5 mM TCEP as electron donor in the presence of SOD (Figure 5.7 A). When an Erv1 concentration of 3 µM was used, Erv1 wt consumed oxygen slightly faster than Erv1 R182H but the mutant was still capable of reacting with the TCEP/O_2 couple (Table 5.2).

In order to be thorough, various Erv1 concentrations were checked for defects in their reaction with TCEP. Interestingly, when the Erv1 concentration was lowered to 0.2 µM the oxidase activity of Erv1 R182H stopped after a few enzymatic cycles (Figure 5.7 B); whereas Erv1 wt continued to steadily consume oxygen even after 300 s, Erv1 R182H completely stopped reacting after about 150 s. The mutant consumed in total ~5 µM of oxygen giving a protein turnover ([O_2]/[Erv1]) of ~25 before the reaction came to a halt. To confirm these results, increasing concentrations of Erv1 wt and Erv1 R182H were checked for their final oxygen consumption (Figure 5.7 C). The total amount of oxygen consumed before Erv1 R182H broke down increased with protein concentration, suggesting the mutant undergoes a certain number of turnovers before it stops. More importantly, in the assay, at Erv1 concentrations of 3 µM or more the Erv1 R182H mutant consumed the same amount of oxygen as Erv1 wt, thus hiding the activity defect.

The results showing Erv1 R182H concentrations of 3 µM conceal the activity defect question the significance of the oxidase activity studies done at 25°C. When similar experiments were conducted using 0.2 µM Erv1 and 5 mM TCEP, the results now exhibited an activity defect for the Erv1 R182H mutant (Figure 5.7 D). However, the effect was not as strong as at 37°C. The mutant still reacted with similar kinetics as Erv1 wt up to ~200 s, then it started to slow down but was still viable after ~600 s. Overall, the data points towards an oxidase activity defect in Erv1 R182H that is otherwise hidden unless the right set of conditions are used. Furthermore, the defect is stronger at temperatures of 37°C.

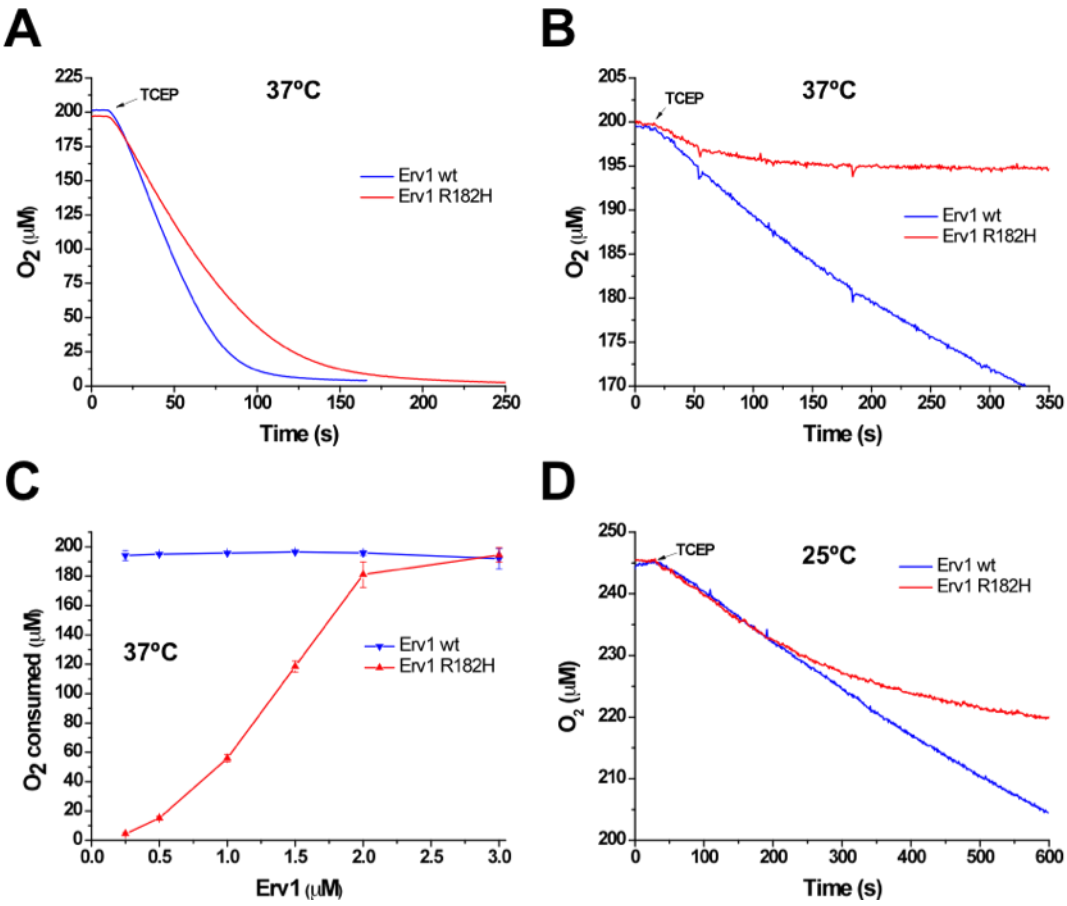

Figure 5.8 TCEP as electron donor: Oxidase activity of Erv1 wt and Erv1 R182H at 37°C

A) Oxygen consumption of Erv1 wt (blue, 3 µM) and Erv1 R182H (red, 3 µM) at 37ºC in the presence of 80 U/ml of superoxide dismutase. Reactions were done in BAE buffer and started by addition of 5 mM TCEP. The profiles represent the average of 3 assays on the same day.

B) As in A only the Erv1 concentration was 0.2 µM.

C) Final oxygen consumed by increasing concentrations of Erv1 wt (blue) and Erv1 R182H (red) at 37ºC. Reaction started by addition of 5 mM TCEP in the presence of 80 U/ml of SOD. Values represent the average of 2 measurements on the same day.

D) As in A only the Erv1 concentration was 0.2 µM and the temperature 25ºC.

The next step was to check whether the fault in the Erv1 R182H mutant was due only to a specific interaction with TCEP, or whether it was also present during the reaction with Erv1's physiological substrate Mia40. In figure 5.8 a similar behaviour to that observed with TCEP can also be seen when pr-Mia40c was used as electron donor. Despite the temperature of 37°C, if Erv1 concentrations of 3 μM are used then both Erv1 wt and Erv1 R182H react with similar kinetics when mixed with 35 μM of pr-Mia40c (Figure 5.8 A, Table 5.2). On the other hand, if the Erv1 concentration is set to 0.2 μM then Erv1 R182H breaks down after consuming ~12 μM of pr-Mia40c, giving a protein turnover of ~60 (Figure 5.8 B). Thus, the activity defect is not unique to the interaction of Erv1 with TCEP.

Table 5.2 Relative initial rates of Erv1

[C]	Protein	TCEP (μM/min)		pr-Mia40c (μM/min)[a]	
		25°C	37°C	25°C	37°C
3 μM	Erv1 wt	126.5±0.5	173.1±9.1	103.9±8.5	149.3±32.2
	Erv1 R182H	124.9±8.5	124.5±3.1	102.9±6.6	134.2±6.3
0.2 μM	Erv1 wt	4.2±0.2	7.7±1.5	17.0±1.5	31.3±1.8
	Erv1 R182H	3.8±1.3	3.7±0.2	11.8±0.4	13.5±0.4

All rates represent an average of at least 2 measurements done on the same day, with Erv1 wt and Erv1 R182H done together.

[a] For the assays with 3 μM Erv1, 35 μM of pr-Mia40c were used; whereas 60 μM of pr-Mia40c were used with 0.2 μM Erv1.

The data presented demonstrates that, at the restrictive temperature of 37°C, the R182H mutation halts the oxidase activity of Erv1. However, Erv1 R182H is capable of fully reacting with pr-Mia40c when high enough concentrations of Erv1 are used. This particular result suggests that the Mia40-Erv1 interaction is not specifically affected in the mutant, but that any failed interaction more likely represents a breakdown of Erv1 itself. Because the dissociation constant (K_d) of Erv1 R182H is not known, it is possible that at low concentrations the mutant becomes a monomer thereby releasing FAD. However, simple dilution of the protein was not sufficient to render the mutant inactive and cause the release of FAD as explained in section 5.8. Thus, a possible change in oligomerisation state, although not ruled out, it could not be directly behind the observed activity defect. Lastly, at similar Erv1 concentrations, different protein turnovers were obtained for TCEP and pr-

Mia40c as electron donors suggesting that the reaction intermediates may play a role in the activity defects. Additional explanation on this difference is given in the discussion.

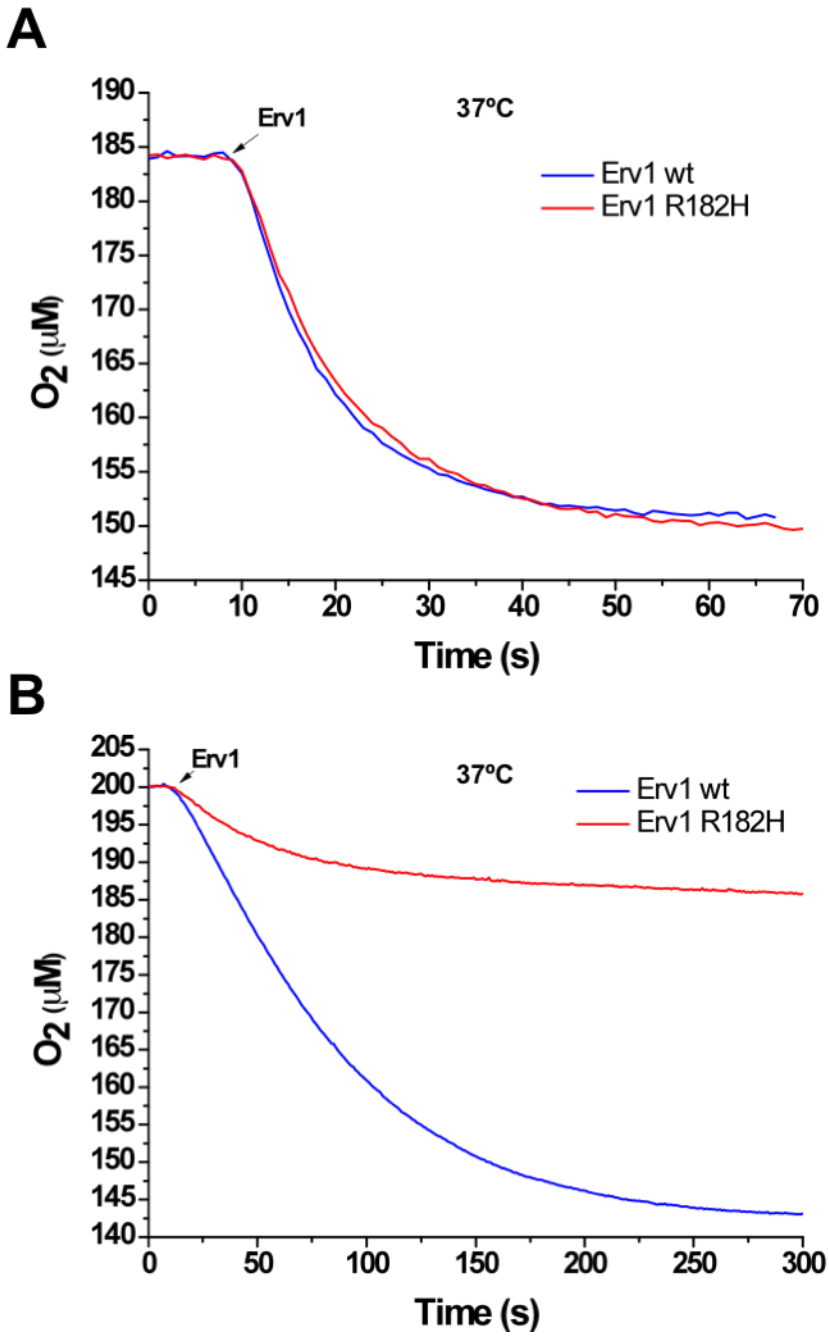

Figure 5.9 Mia40 as electron donor: Oxidase activity of Erv1 wt and Erv1 R182H at 37°C

A) Oxygen consumption of 3 µM Erv1 wt (blue) and Erv1 R182H (red) at 37ºC using 35 µM pr-Mia40c as electron donor. Reactions were done in BAE buffer. The profiles represent the average of 3 assays on the same day.

B) Oxygen consumption of 0.2 µM Erv1 wt (blue) and Erv1 R182H (red) at 37ºC using 60 µM pr-Mia40c as electron donor. Reactions were done in BAE buffer. The profiles represent the average of 3 assays on the same day.

5.6. Effect of the R182H mutation on the reduction of cyt *c*

The previous section showed that the R182H mutation causes a defect on the oxidase activity of Erv1. The defect is present independently of whether TCEP or pr-Mia40c is used as electron donor. Therefore, one possibility is that the defect is specific to the interaction of Erv1 with oxygen. Earlier reports have demonstrated cyt *c* also works as an electron acceptor of Erv1 both *in vitro* and *in vivo* (Allen et al., 2005, Dabir et al., 2007, Bihlmaier et al., 2008). This allows cyt *c* to be used as an alternative to oxygen to study the activity of Erv1. To that end, an assay was established to check whether the Erv1-cyt *c* reaction was also affected in the Erv1 R182H mutant.

Reduction of the heme cofactor in cyt *c* can be followed by its change in absorbance at 550 nm. To avoid any oxygen interference the oxygen was removed from all solutions by bubbling nitrogen through them. Additionally, the experiments were done inside an anaerobic glove box where the oxygen concentration is kept below 2 ppm. In the experiments cyt *c* reduction was followed after rapidly mixing a solution of Erv1 + cyt *c* (syringe A) with pr-Mia40c (syringe B) using a stopped flow instrument.

First, final concentrations after mixing of 3 μM Erv1, 40 μM cyt *c* and 30 μM pr-Mia40c were used (Figure 5.9 A). At 25°C, both Erv1 wt and Erv1 R182H displayed the same kinetic curves indicating the two proteins reduced cyt *c* with similar rates. When the assay was repeated at 37°C the Erv1 R182H mutant reduced cyt *c* somewhat faster than Erv1 wt. These results suggest that, even at the restrictive temperature of 37°C, the reaction between Erv1 R182H and cyt *c* is not affected.

Previous assays established Erv1 concentrations of 3 μM could hide the oxidase activity defect of Erv1 R182H. Hence, the cyt *c* reduction assays at 37°C were repeated using only 0.2 μM Erv1. Figure 5.9 B shows the Erv1 R182H mutant fails to reduce cyt *c* after a few catalytic cycles. However, an accurate measurement of the protein turnover was difficult because of background reduction of cyt *c* by pr-Mia40c. Still, the results do indicate the Erv1-cyt *c* reaction is also slowed down by the R182H mutation. Furthermore,

the activity defect of Erv1 R182H is not specific for the reaction with oxygen or with cyt *c*.

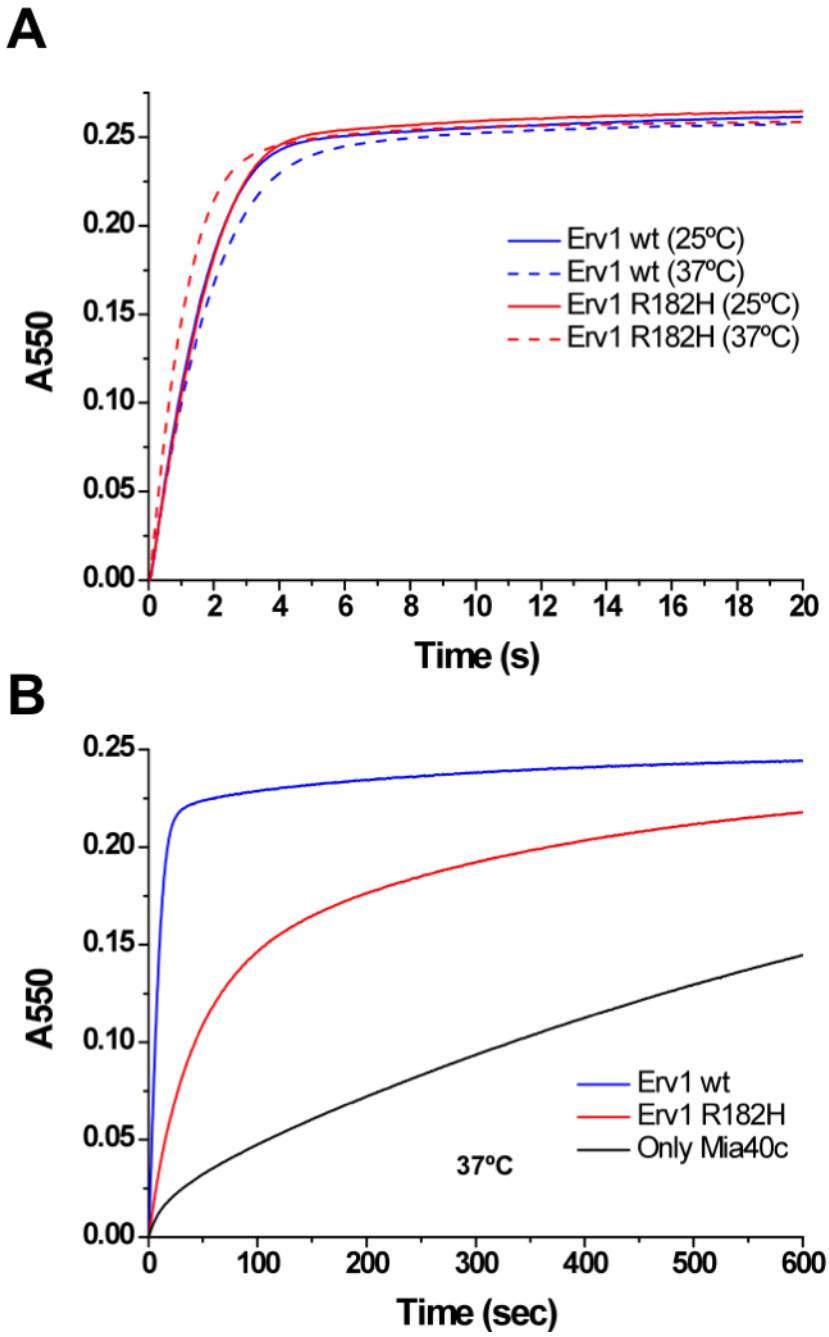

Figure 5.10 Reduction of cyt *c* by Erv1 wt and Erv1 R182H

A) Cyt *c* reduction by 3 µM Erv1 wt (red) and Erv1 R182H (blue) followed at 550 nm. Concentrations inside the cell: 3 µM Erv1, 30 µM pr-Mia40c and 40 µM cyt *c*. Reactions were done in BAE buffer using an anaerobic stopped flow. The profiles represent the average of 4 repeats on the same day.

B) As in A only the Erv1 concentration inside the cell was 0.2 µM. The temperature was 37°C. The black line represents background reduction of cyt *c* by pr-Mia40c. The profiles represent the average of 4 repeats on the same day.

5.7. Effect of the R182H mutation on the thermal stability of Erv1

The activity of an enzyme generally increases with temperature until it reaches a critical point. Any further rise in temperature then causes the enzyme to unfold or aggregate, thereby decreasing or completely losing its activity. A likely explanation for the loss of activity in Erv1 R182H is therefore that the protein may not be properly folded at temperatures nearing 37°C. To check this, circular dichroism was selected, as it is a proven technique used to follow protein unfolding. Initially, the far-UV CD signal at 222 nm was used to follow the secondary structure of Erv1 R182H as the temperature increased. Figure 5.10 shows Erv1 R182H is still folded up to temperatures of 30-35°C. Then it unfolded with a steep slope until it reached a temperature of ~70°C, at which point the protein was completely unfolded. The T_M for Erv1 R182H was 59.5 ± 3.5°C. When compared with Erv1 wt (T_M = 68.3 ± 4.8°C, section 4.3), the Erv1 R182H mutant is, on the whole, less thermally stable. In fact, its thermal behaviour is reminiscent of that of Erv1 'dimer' (section 4.3). This suggests the lower thermal stability of Erv1 R182H is a consequence of the protein adopting a dimer conformation, as opposed of a tetramer for Erv1 wt. Nevertheless, the protein appeared mostly folded (~90%) at 37°C suggesting that large-scale protein unfolding is not the cause behind the Erv1 R182H activity defect.

To further study the effect of temperature on the structure of Erv1, thermal denaturation coupled with near-UV CD was used to look at the unfolding of the tertiary structure. In some cases, the technique proves more sensitive to small, localised changes in structure than far-UV CD. Figure 5.10 also shows the unfolding of Erv1 wt and Erv1 R182H when followed by near-UV CD at 272 nm. Again, the T_M decreased from 69.4 ± 1.4°C for Erv1 wt to 58.6 ± 1.4°C for Erv1 R182H. Furthermore, the curves did not vary when different wavelengths (285 and 292 nm) were selected to follow protein unfolding. Both proteins also showed no considerable disruption in structure at 37°C. Thus, although near-UV CD only looks at certain pockets of tertiary structure (those containing phenylalanine, tyrosine and tryptophan), this result suggests no great change occurs in the vicinity of aromatic residues in Erv1 at temperatures near 37°C.

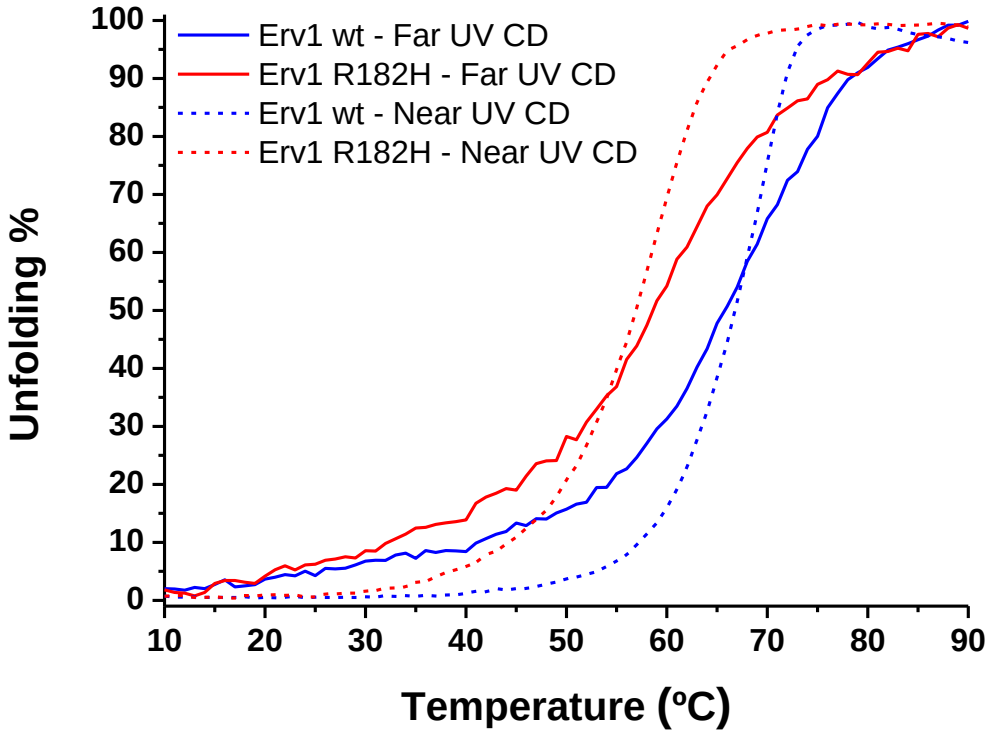

Figure 5.11 Thermal stability of Erv1 wt and Erv1 R182H

Thermal denaturation of Erv1 wt (blue) and Erv1 R182H (red). Protein unfolding was followed by far-UV CD at 222 nm (0.22 mg/ml, BAE) and near-UV CD at 272 nm (0.5 mg/ml, BAE). Temperature increase: 1 ºC/min, 10-90ºC. The curves represent the average of 4 independent experiments.

5.8. Effect of the R182H mutation on FAD binding during the enzymatic cycle of Erv1

The experiments in section 5.4 showed FAD is more weakly bound in Erv1 R182H than in Erv1 wt. Accordingly, previous reports using the human analogue ALR also showed a weaker FAD binding in the corresponding ALR R194H mutant (Daithankar et al., 2010) . However, it is unknown whether a connection exists between this weaker FAD binding and the activity defect of Erv1 R182H. One possibility is that during the enzymatic activity of the mutant FAD is somehow destabilised or released. To test this hypothesis, the binding of Erv1 to FAD after its enzymatic reaction was analysed by both UV-visible and fluorescence spectroscopy (Figure 5.11 A). To this end, 1.5 µM of Erv1 wt or Erv1 R182H was mixed with 140 µM of pr-Mia40c and the reaction was conducted for 25 min at 37°C. As a control, 1.5 µM of each protein was also incubated for 25 min at 37°C but without pr-Mia40c.

The UV-visible spectra showed that the position of the FAD maximum absorption wavelength (λ_{max}^{FAD}) was the same for Erv1 wt regardless of whether pr-Mia40c was added (+pr-Mia40c) or not (-pr-Mia40c), with $\lambda_{max}^{wt\_FAD} = 460$ nm. However, the λ_{max}^{FAD} of Erv1 R182H shifted from 459 nm to 450 nm when the protein underwent a reaction (Figure 5.11 A). A λ_{max}^{FAD} of 450 nm is typical of free FAD (Koziol, 1971) indicating the cofactor is no longer bound to Erv1 R182H. Because the λ_{max}^{FAD} did not change for the control of Erv1 R182H (-pr-Mia40c), the data suggests the release of FAD resulted from the reaction with pr-Mia40c.

To further validate the hypothesis, FAD release from Erv1 R182H was also followed using FAD fluorescence. The same samples used in the UV-visible assays were checked for their FAD fluorescence when excited at 450 nm. Figure 5.11 A shows the FAD fluorescence spectra of Erv1 wt does not change despite reacting with pr-Mia40c. However, in the case of Erv1 R182H, a ~2.2 fold increase in fluorescence intensity at 525 nm was evident when the protein reacted with pr-Mia40c. As mentioned before, Erv1 quenches the fluorescence of FAD by means of the aromatic residues surrounding the cofactor (Munro and Noble, 1999). Hence, the increase in fluorescence intensity most likely indicates the discharge of FAD into the solution. Lastly, to

corroborate that FAD is only released upon reaction with pr-Mia40c, and not by mere dilution of the protein, the FAD fluorescence was followed over time as the reaction proceeded. Figure 5.11 B shows that the FAD fluorescence in Erv1 R182H stays the same despite the low concentration (1.5 μM) and the temperature of 37°C, indicating FAD remained bound to the mutant under these conditions. However, in the presence of pr-Mia40c, the FAD fluorescence increased over time suggesting FAD was released from Erv1 R182H as the reaction occurred. Taken together, these results show FAD is released because and during the enzymatic reaction of Erv1 R182H.

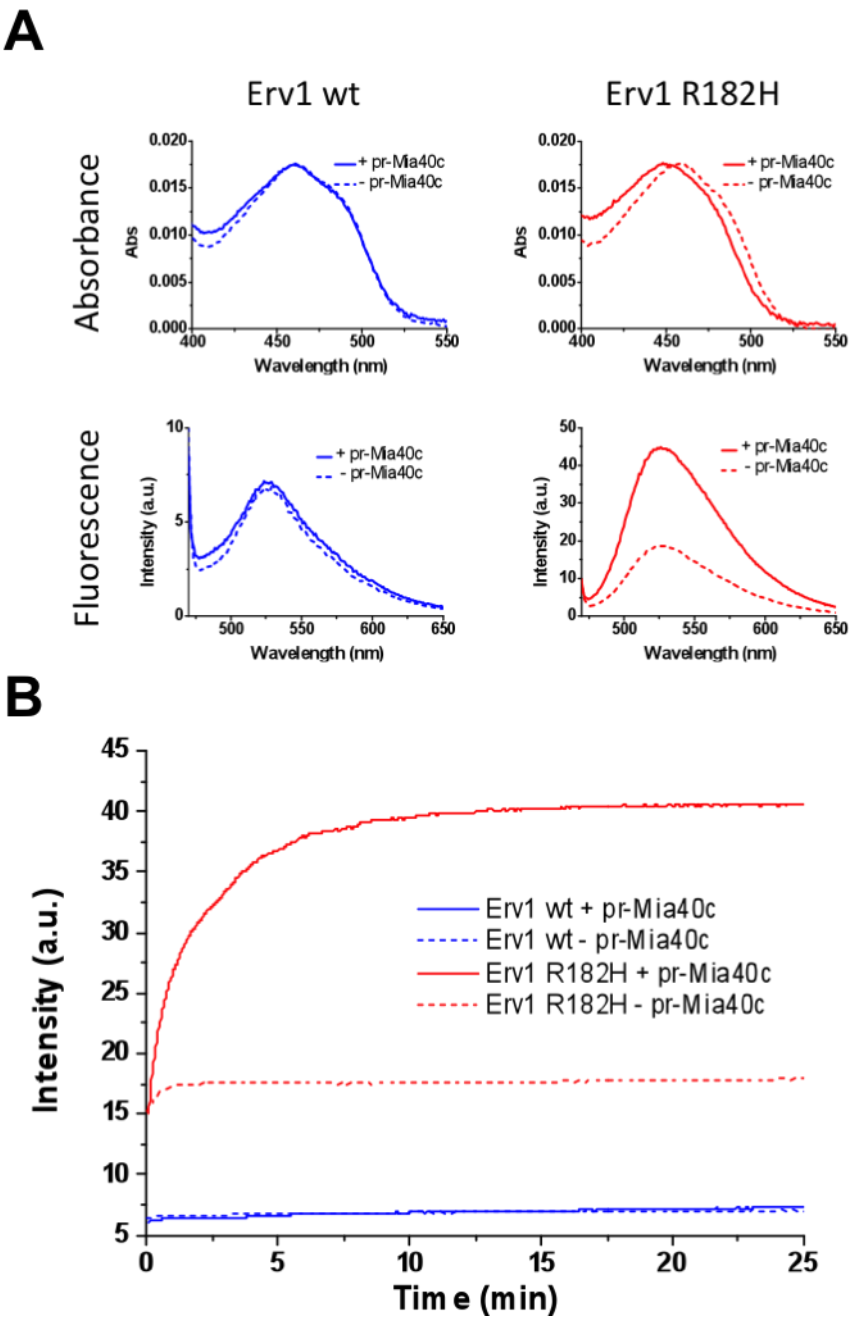

Figure 5.12 FAD binding of Erv1 wt and Erv1 R182H with or without addition of pr-Mia40c

A) UV-visible spectra and FAD fluorescence (Ex: 450 nm) of Erv1 wt (blue, 1.5 µM) and Erv1 R182H (red, 1.5 µM) with (–) or without (--) having undergone a reaction with 140 µM pr-Mia40c. The reaction was conducted at 37ºC for 25 min in BAE buffer.

B) Kinetics of FAD release followed by the increase in FAD fluorescence of 1.5 µM Erv1 wt (blue) and Erv1 R182H (red) with (–) or without (--) having undergone a reaction with 140 µM pr-Mia40c at 37°C in BAE buffer. The curves represent the average of 4 independent experiments.

5.9. Discussion

Enzymes are well-tuned machines that catalyse a variety of specialised reactions. As such, small changes in their amino acid coding sequence can often lead to a complete disruption of their activity. Recently, Di Fonzo *et al.* (2009) reported the first disease-causing mutation directly related to the MIA pathway. A single amino acid substitution in human ALR, where the arginine at position 194 was exchanged for a histidine, was pinpointed as the cause behind autosomal recessive myopathy (Di Fonzo et al., 2009). When this project began little was known regarding the effects of the corresponding Erv1 R182H mutant on yeast *S. cerevisiae* and no reports had addressed how the mutation affected the protein. In this broad study evidence is presented that shows the R182H mutation affects Erv1 in four ways: 1) it lowers the secondary structure folding and changes its oligomerisation state, 2) it weakens its binding of FAD, 3) it lowers its thermal stability and, 4) the binding of FAD is further impaired in Erv1 R182H during its catalytic reaction, which disrupts its activity. Thus, this work serves as a first approach towards understanding autosomal recessive myopathy from a molecular mechanism standpoint.

5.9.1. The R182H mutation affects the folding of Erv1

The initial results in this chapter demonstrated the R182H mutation changes the quaternary structure of Erv1: whereas Erv1 wt forms a tetramer of 88 kDa, Erv1 R182H formed a dimer of 44 kDa. However, the mutated arginine (R182) is far from the dimer interface identified on the crystal structure of the C-terminal domain Erv1 (Guo et al., 2012), so its importance on the oligomerisation state must be explained otherwise. One possibility requires R182 to be part of another inter-subunit interface not visible on the crystal structures. Because the core domains of proteins in the ERV family all crystallised as dimers (Fass, 2008), it is conceivable the second interface that would produce the tetramer conformation was not apparent in the structures. If such were the case, far- and near-UV CD experiments suggested this second interface would probably involve aromatic residues on both sides.

A second possibility links the weaker FAD binding in Erv1 R182H with its change in oligomerisation state. There is precedence in the relationship

between cofactor binding and oligomerisation state in flavoproteins: both dihydrolipoamide dehydrogenase and vanillyl-alcohol oxidase form a higher oligomer upon correctly binding their FAD cofactor (Lindsay et al., 2000, Tahallah et al., 2002). Moreover, in the case of Erv1, mutations of certain residues in the vicinity of FAD have been shown to alter its oligomerisation state. The mutants Erv1 W183F, Erv1 C3S and Erv1 C4S all form dimers (unpublished results) and closely interact with FAD (Guo et al., 2012). It follows that alteration in the binding of FAD by Erv1 R182H could potentially cause the protein to dimerise.

5.9.2. The R182H mutation weakens the stability of FAD binding in Erv1

The next part of this chapter explored the difference in FAD binding between Erv1 wt and Erv1 R182H. Both proteins exhibited a similar FAD content of approximately 96%. During the course of this study a report addressed the effect of the R194H mutant on human ALR and showed the mutant contained 20% less FAD than ALR wt (Daithankar et al., 2010). Such difference may be explained by two reasons: 1) a specifically stronger effect on ALR R194H compared to Erv1 R182H or, 2) the faster protein induction of ALR at 30°C compared with our slower induction of Erv1 at 16°C during protein purification perhaps affected the mutants more so than the wlld-type.

Regardless of the similar FAD content in Erv1 wt and Erv1 R182H, additional data showed the mutation does indeed affect the binding of FAD. The FAD fluorescence was more strongly quenched in Erv1 wt than in Erv1 R182H. This difference could be explained by changes in the microenvironment surrounding FAD. Flavoproteins normally quench their cofactor fluorescence by stacking aromatic residues that interact with the excited isoalloxazine ring (Munro and Noble, 1999, Lakowicz, 2006). In the case of Erv1, highly conserved tyrosine (Y128) and tryptophan (W95) residues are parallel to the isoalloxazine ring of FAD (Guo et al., 2012). The lower quenching of FAD fluorescence in Erv1 R182H therefore suggests a looser stacking of aromatic residues, which translates into a higher mobility or shifting of the isoalloxazine ring and thus weaker FAD binding.

Further evidence for the weaker binding of FAD in Erv1 R182H came from urea denaturation experiments. When Erv1 wt and Erv1 R182H were treated

with 7 M urea the mutant released its FAD much faster than the wt. In fact, at this urea concentration, the release of FAD from Erv1 R182H was ~6 times faster than from Erv1 wt. Conversely, FAD uptake by apo-Erv1 wt and apo-Erv1 R182H proceeded with similar kinetics. Thus, in combination the results indicate the on-rate constant for the binding of FAD by Erv1 is the same for both proteins. However, the off-rate constant is bigger for Erv1 R182H, which leads to a larger dissociation rate constant and weaker FAD binding. A previous report also showed a quicker FAD release for ALR R194H when treated with 6 M guanidine-hydrochloride. Furthermore, both ALR wt and ALR R194H displayed the same on-rate constant thus confirming the validity of our results (Daithankar et al., 2010).

5.9.3. The loss of enzymatic activity is due to impaired FAD binding in Erv1 R182H

The results presented here indicate the R182H mutation affects the activity of Erv1. The activity defect was stronger at temperatures of 37°C and occurred regardless of whether TCEP or pr-Mia40c was used as electron donor, and was also present when both oxygen or cyt *c* was used as electron acceptor. This suggests the problem lies in Erv1 R182H itself and not on its interaction with other proteins/molecules.

Interestingly, the defect was dependent upon the initial concentration of Erv1 and was more readily visible as the concentration decreased. Thus, one possibility is that, upon dilution, the protein dissociates into monomers that are inactive or unstable. In this regard the dissociation constant (K_d) would need to be established for the mutant, or at least verify that at the concentrations employed the oligomerisation state of the protein has not changed. However, a couple of observations indicate that a potential change in oligomerisation state is not the direct cause behind the activity defects. First, in the oxygen consumption assays with TCEP as substrate Erv1 was generally diluted first and then incubated at this low concentration. Regardless of the incubation period (5-15 min) the defect was consistently the same. A similar behaviour was also observed in the cyt *c* reduction experiments where Erv1 was diluted to 0.4 µM, a concentration known to produce a defect, and incubated for 1 hour before doing the reaction. Taken together, because the defect is not dependent upon the incubation period, these observations

suggest mere dilution of the mutant protein is not sufficient to impair its binding of FAD. Instead, UV-visible and FAD fluorescence experiments showed that the binding of FAD in Erv1 R182H becomes increasingly impaired only during its enzymatic reaction. When the mutant protein was incubated with pr-Mia40c the fluorescence of FAD increased, indicating either it was released from the protein or a weaker quenching. That was not the case when Erv1 R182H was simply diluted. As a control it was shown that the FAD fluorescence in Erv1 wt remains the same in both cases. In conclusion, an impaired binding of its FAD cofactor causes the defect in the activity of Erv1 during its catalytic reaction, which likely perturbs the flow of electrons inside the protein. Furthermore, the effect appears stronger as the concentration is lowered because it causes Erv1 to go through more catalytic cycles, thereby inactivating it faster.

In a previous report, Daithankar *et al.* (2010) found no clear defect on the activity of ALR R194H at 25°C when assayed using DTT or human Mia40 as electron donors (Daithankar et al., 2010). With DTT as the disulphide reducing agent, ALR R194H was ~60% more efficient than ALR wt as compared by their k_{cat}/K_m values. With human Mia40, a lower rate constant k_{cat} for ALR R194H was compensated by an equally lower K_m, thus making the mutant as efficient as the wt (Daithankar et al., 2010). Furthermore, the catalytic efficiency k_{cat}/K_m of both ALR wt and ALR R194H was the same when the human Mia40/cyt *c* couple was used at 25°C (Daithankar et al., 2010). Here, the initial oxygen consumption experiments also exposed no difference in the oxidase activity of Erv1 wt and Erv1 R182H when done at 25°C and high protein concentrations. Thus, it would be interesting to check whether the activity of human ALR R194H is actually affected at the restrictive temperature of 37°C.

5.9.4. The Big Picture

The *S. cerevisiae* Erv1 R182H mutant strain exhibited genetic instability of mtDNA, mitochondrial morphological changes, lower complex IV activity, lower levels of IMS proteins that require the MIA pathway and mislocalisation of Mia40 to the cytosol (Daithankar et al., 2010, Sztolsztener et al., 2013). Some of these effects could be explained by a breakdown of Erv1 R182H that

subsequently causes the mitochondrial import pathways to fail. Erv1 is part of the MIA pathway and, as such, is responsible for the import of a variety of proteins (Herrmann and Riemer, 2012, Fischer and Riemer, 2013). Among these are Cox19 and Cox 17, both of which are required for complex IV assembly (Rigby et al., 2007) and have decreased levels in the yeast Erv1 R182H strain (Sztolsztener et al., 2013). Cox19 is a metallochaperone whose function is to deliver copper directly to complex IV. Cox17 instead transfer its copper to Sco1 and Cox11 who then deliver it to complex IV (Rigby et al., 2007). In this case, a disruption of the MIA pathway would lower the import level of Cox 19 and Cox17 that in turn would result in decreased complex IV assembly and activity. Additionally, other proteins like the small Tims also require the MIA pathway for their import. These proteins function as chaperons in other mitochondrial protein import pathways that coordinate entrance of a wide number of proteins (Section 1.1 and Appendix C). Hence, when their mitochondrial levels are lowered, as is the case in yeast Erv1 R182H, the import of several other essential proteins (AAC carrier, Tim23) is also affected. Generally speaking, a basic disruption of the MIA pathway could create a plethora of side effects as those seeing in the yeast Erv1 R182H mutant strain.

5.10. Conclusion

Overall, the data showed the mutation lowered the secondary structure folding, changed the oligomerisation state and decreased the thermal stability of Erv1 by approximately 10°C. Furthermore, the binding of FAD was also affected in the Erv1 R182H mutant. Conversely, unlike the results reported for ALR R194H, the activity of Erv1 was in this case affected by the mutation due to a stronger impaired binding of FAD during the enzymatic reaction. Thus, this chapter provides an initial appraisal of the effects of the R182H mutation on Erv1 while complementing the findings on ALR R194H

6. RESULTS AND DISCUSSION III: REDOX CHARACTERISATION OF ERV1

6.1. Introduction

Oxidation-reduction (redox) reactions are concerned with the transfer of electrons between two species. The standard reduction potential (E^o) of a species expresses its affinity for electrons; in other words, the likelihood that a species is reduced during a redox reaction. Thus, in a reaction between two or more redox centres, the difference in E^o indicates the thermodynamically favourable direction of electron flow from the more negative redox centre towards the more positive one.

There are three known redox centres in Erv1 (Figure 6.1 A): the C1-C2 shuttle disulphide, the C3-C4 redox-active disulphide, and the FAD cofactor. All these centres are required for electrons to flow through Erv1 under physiological conditions. (Lee et al., 2000, Hofhaus et al., 2003, Dabir et al., 2007, Ang and Lu, 2009). The current model of electron flow within Erv1 (Figure 6.1 B) indicates electrons first reach it through the interaction between its C1-C2 shuttle disulphide and Mia40. Next, electrons are quickly passed to the C3-C4 redox-active disulphide. The proximity of C3-C4 to FAD facilitates electrons being then transferred to FAD. Finally, electrons are released unto oxygen or cyt *c* (Ang and Lu, 2009, Bien et al., 2010). Recently, Dabir *et al.* (2007) measured the standard reduction potentials of the three redox centres in Erv1. They reported a E^o of -320 mV for the C1-C2 shuttle disulphide, -150 mV for the C3-C4 redox-active disulphide and -215 mV for FAD (Dabir et al., 2007). Based on these values the flow of electrons from C3-C4 to FAD in Erv1 is not favoured thermodynamically.

A second discrepancy arises when the E^o of the C1-C2 shuttle disulphide is placed in the context of the MIA pathway. Standard reduction potentials have been determined for each redox centre involved in the pathway (Figure 6.1 C). Substrate proteins like Tim9, Tim10 or Cox17 have standard reduction potentials ranging from -310 to -340 mV. These values represent a four-electron transfer where two disulphide bonds are simultaneously introduced into the proteins (Lu and Woodburn, 2005, Voronova et al., 2007, Morgan and

Lu, 2008). Mia40, the link between substrates and Erv1, has a E^o of -290 mV for the two-electron reduction of its CPC disulphide bond (Tienson et al., 2009). Thus, the more positive E^o indicates the electron transfer from substrates to Mia40 is thermodynamically favourable. However, the E^o of the C1-C2 shuttle disulphide of Erv1 (-310 mV) is more negative than that of Mia40. This means electrons preferentially flow from Erv1 to Mia40, and not the other way around.

Finally, the E^o of the mitochondrial IMS (E^o_{IMS}) was recently measured at -306 mV. This value was shown to be directly linked with the E^o of the cytosol but independent of that of the mitochondrial matrix (Kojer et al., 2012). Furthermore, the same report also suggested that a correlation exists between the E^o_{IMS} and the concentration of Erv1. Indeed, the E^o_{IMS} shifted towards more positive and oxidising values when the Erv1 concentration was increased (Kojer et al., 2012). This broad understanding of the Erv1 redox behaviour, particularly with respect to the standard reduction potentials of its three redox centres, is the first step in elucidating the connection between Erv1 and the E^o_{IMS}

In this chapter, the standard reduction potentials of the redox centres in Erv1 were measured. Initially, standard reduction potentials were obtained for FAD in Erv1 wt and the double cysteine mutants Erv1 C1,2S and Erv1 C3,4S. The number of electrons required to completely reduce the FAD in Erv1 was then determined for all three proteins. A E^o for the C3-C4 redox-active disulphide was also obtained using a thiol-alkylation assay couple with SDS-PAGE. Lastly, an attempt was made to measure the E^o of the C1-C2 shuttle disulphide.

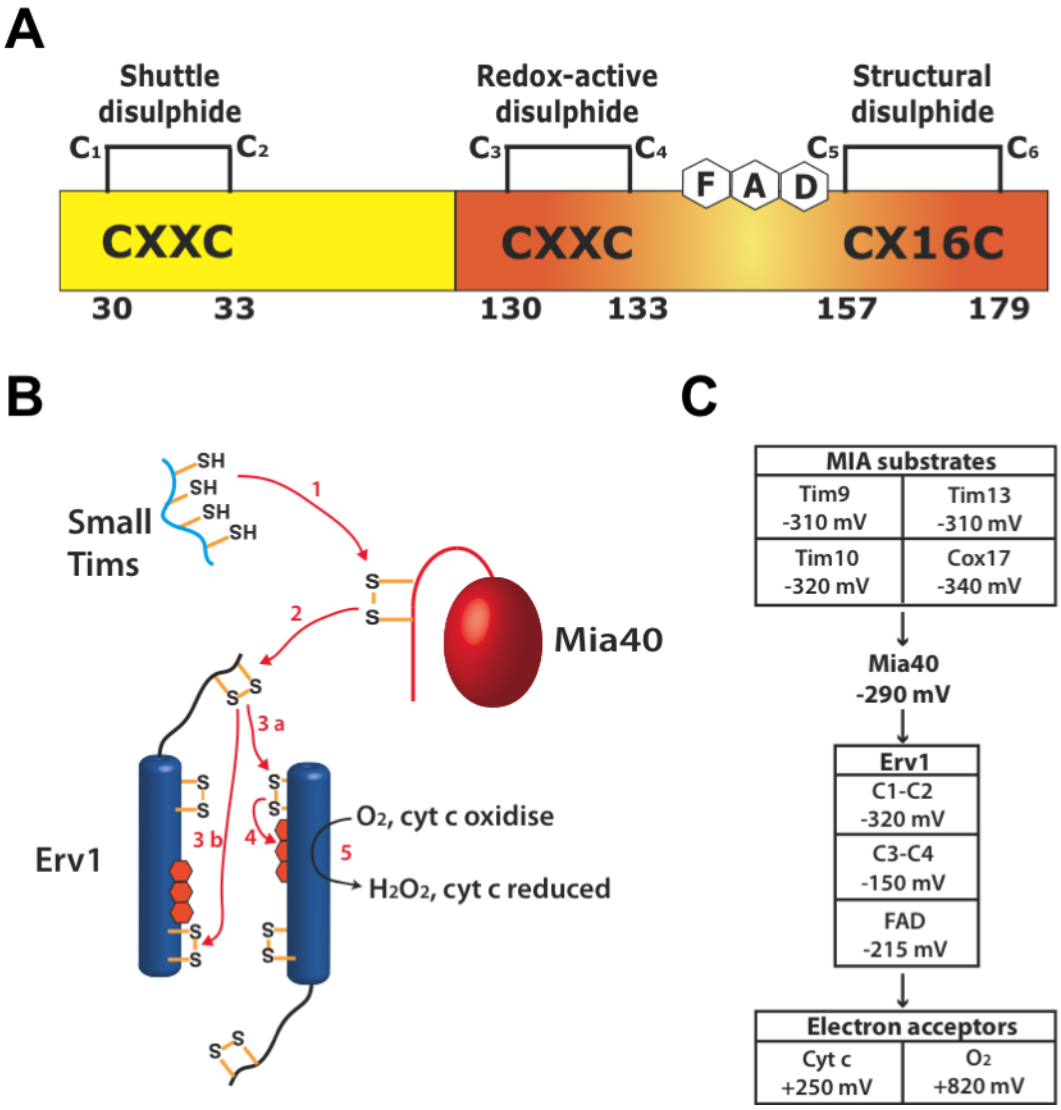

Figure 6.1 Standard reduction potentials of the MIA pathway

A) Schematic representation of Erv1. The three redox centres are: the C1-C2 shuttle disulphide, the C3-C4 redox-active disulphide and FAD. In yellow is the flexible N-terminal domain. In orange is the C-terminal domain with the Erv fold.

B) Electron flow in the MIA pathway. Electrons are transferred from the small Tims to Mia40 (1), and then to the Erv1 C1-C2 shuttle disulphide (2). Electrons can then go to the C3-C4 redox-active disulphide of the same (3b) or alternate subunit (3a). Next, electrons move from Erv1 C3-C4 to FAD (4). The final electron acceptor is either oxygen or cyt *c* (5).

C) Standard reduction potentials of the different components involved in the MIA pathway. The number of electrons exchanged in each redox reaction is 4 (Tim9, Tim10, Tim13, Cox17), 2 (Mia40, Erv1, O_2) and 1 (cyt *c*).

6.2. Purification of the Erv1 C1,2S and Erv1 C3,4S mutants

The Erv1 C1,2S and Erv1 C3,4S double cysteine mutants were successfully purified from *E. coli* Rosetta-gami™ 2 cells (Section 3.4) as previously shown (Ang, 2010). Briefly, both mutants were properly overexpressed (Figure 6.2 top and bottom, lanes 2) and found mostly in the supernatant (Figure 6.2, lanes 4). Final protein purity after SEC was over 90% for both proteins (Figure 6.2, lanes 8).

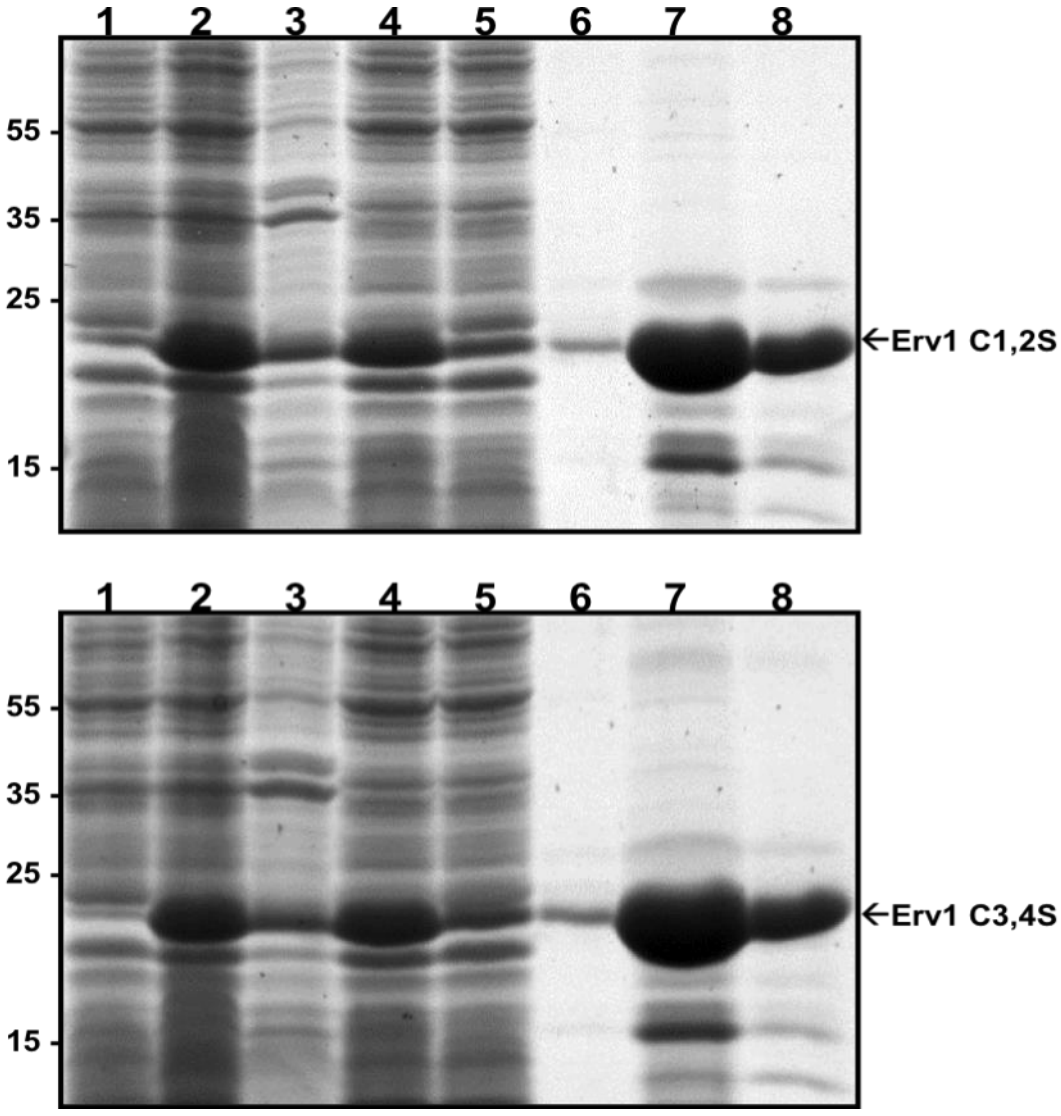

Figure 6.2 SDS-PAGE of a purification of Erv1 C1,2S and Erv1 C3,4S.

Reducing SDS-PAGE of an Erv1 C1,2S and an Erv1 C3,4S affinity purification visualised using coomassie-blue staining. Lanes: 1) cells grown to log phase, 2) overnight induction at 16°C, 3) sonication pellet, 4) sonication supernatant, 5) flowtrough from Ni-NTA His-Bind beads, 6) wash with 80 mM imidazol, 7) elution with 500 mM imidazol, 8) after SEC.

6.3. Determination of the standard reduction potential of FAD in Erv1 wt

In the accepted model of electron flow within Erv1 the FAD cofactor functions as the last electron acceptor. Unlike disulphide bonds, FAD can participate in both one- and two-electron transfers, thereby making it an ideal candidate to react with both oxygen (z=2) and cyt *c* (z=1). Yet, the reported value for the E^{o} of FAD in Erv1 (-215 mV) is more negative than that of the C3-C4 redox-active disulphide (-150 mV) (Dabir et al., 2007). This suggests that either FAD is not the last electron acceptor in Erv1 or the electron transfer from C3-C4 to FAD is thermodynamically unfavourable. Alternatively, the E^{o} may not have been accurately determined. Therefore, the redox behaviour of Erv1 was initially studied by checking the value for the E^{o} of FAD.

Reduction of FAD by stepwise addition of sodium dithionite inside an anaerobic glove box allows us to calculate its E^{o} by fitting the captured data to the Nernst equation (2). Various mediators (section 3.5.4) are used to bridge the reduction of FAD with the measured electron potential of the solution. Figure 6.3 A shows the UV-visible spectra recorded during a typical FAD redox titration of Erv1 wt at pH 7.4. Initially, fully oxidised FAD exhibited peaks at 380 and 460 nm characteristic of protein-bound flavin (Massey, 2000). Then, addition of sodium dithionite shifted the electron potential of the solution towards more negative values and decreased the absorbance of both FAD peaks. In addition, a new shoulder arose beyond 530 nm suggesting the formation of a semiquinone intermediate (section 6.7). Finally, further addition of sodium dithionite completely reduced FAD and made the shoulder disappear from the spectra.

The peak at 460 nm was chosen to follow the reduction of FAD during the redox titration. Thus, the absorbance at 460 nm was plotted *versus* the electron potential and the resulting data fitted to the Nernst equation (Figure 6.3 B). This equation relates the measured electron potential (E) with the temperature, concentration of oxidised and reduced FAD, number of electrons transferred (z) and the E^{o} of the species under study. Reduction of FAD from fully oxidised to fully reduced is a two electron process and, as such, the fitting for z=2 gave a E^{o} of -157 ± 7 mV. This places the E^{o} of FAD in Erv1 at a far more positive value (by ~60 mV) than the one previously reported by

Dabir *et al*. (2007). Furthermore, this E^{o} is also closer in value to that of FAD in the short form human ALR (E^{o} =-178 mV, Table 6.2) (Farrell and Thorpe, 2005).

$$E = E^{o} - \frac{RT}{zF} \ln\left(\frac{[\text{Reduced}]\, a_{red}}{[\text{Oxidised}]\, a_{ox}}\right) \qquad (1)$$

$R = \text{Gas constant } 8.314\ (J\ K^{-1} mol^{-1})$
$T = \text{Temperature } (K)$
$F = \text{Faraday constant } 9.648\text{x}10^{4}\ C mol^{-1}$
$z = \text{Number of electrons transferred}$
$a = \text{Activity} = 1$

A closer examination of the plot in figure 6.2 B exposed an unusual FAD reduction from electron potentials -180 to -280 mV. Reduction of FAD in this region occurred with a considerably gentler slope compared to the expected behaviour dictated by the Nernst equation (Figure 6.3 B, red line). One possible explanation for this deviation involves the reduction of a second Erv1 redox centre. Therefore, the next step in this study measured the number of electron equivalents required for complete FAD reduction in Erv1.

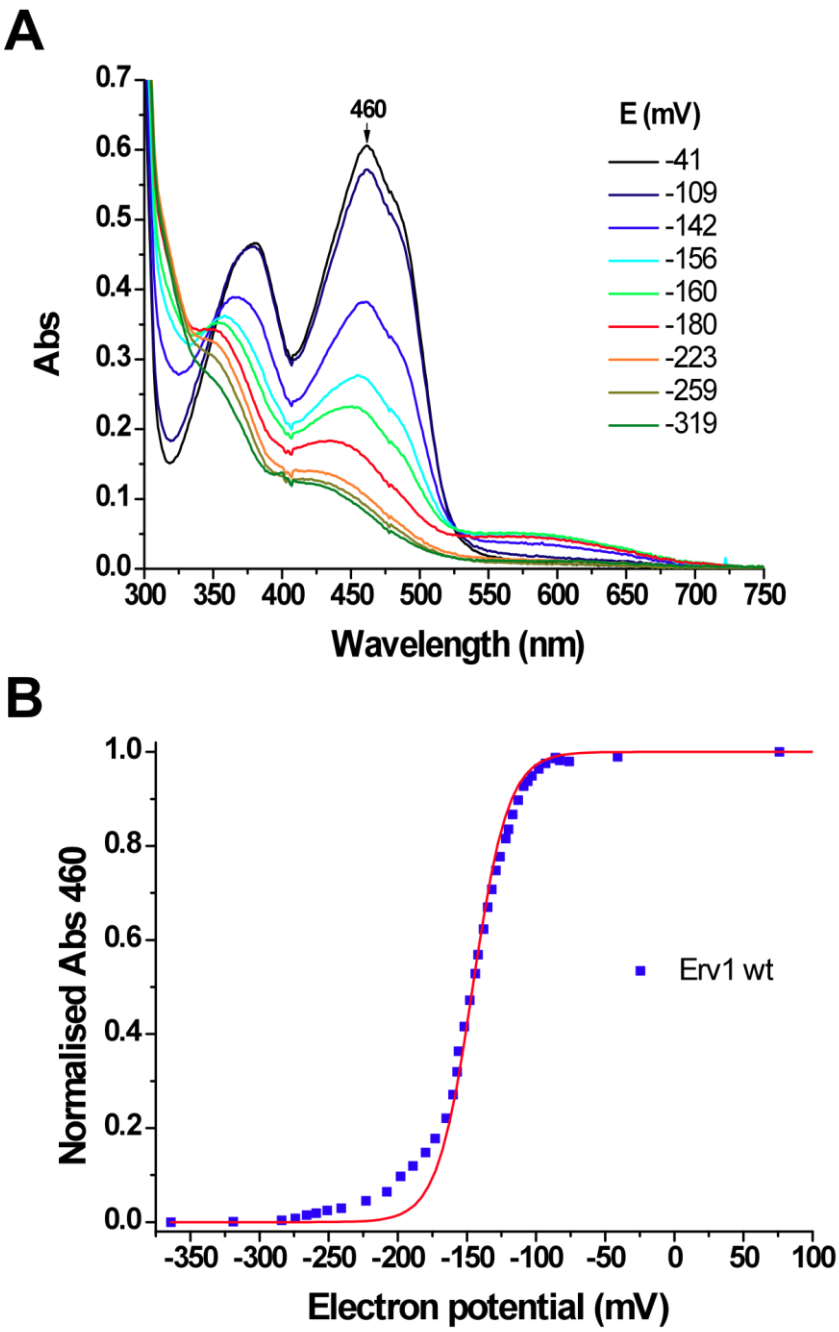

Figure 6.3 FAD redox titration of Erv1 wt

A) Representative UV-visible spectra of Erv1 wt (64 μM in BAE) recorded at various electron potentials during an anaerobic reduction of FAD by increasing amounts of sodium dithionite. FAD goes from fully oxidised (black line) to fully reduced (olive green line). Peaks at 380 and 460 nm are characteristic of protein-bound flavin. The shoulder beyond 530 nm marks the formation of a semiquinone intermediate (section 6.7).

B) Plot of normalised absorbance at 460 nm *versus* electron potential for the experiment in A. The data was fitted using the Nernst equation for z = 2 and T = 298 K (red line). The average of 2 independent experiments gave a standard reduction potential of -157 ± 7 mV.

6.4. Determination of the number of electrons required for complete FAD reduction in Erv1

Erv1 has three known redox centres: two disulphide bonds and the FAD cofactor (Lee et al., 2000, Dabir et al., 2007). Both the reduction of a disulphide bond and that of FAD require two electrons. Hence, six electrons in total could potentially be needed to completely reduce FAD if a redox equilibrium was established between all three redox centres.

An electron titration using a sodium dithionite solution of known concentration was used to calculate the electrons needed to completely reduce FAD in Erv1 wt. Figure 6.4 A shows the UV-visible spectra of Erv1 wt after the addition of an increasing number of electron equivalents (electrons/FAD) of sodium dithionite. Again, the absorbance at 460 nm decreased upon reduction and a shoulder appeared beyond 530 nm representative of a semiquinone intermediate. Addition of 2 electron equivalents did not however yield the spectrum of fully reduced FAD, and the semiquinone intermediate was still present at this stage. When FAD reduction was followed using the absorbance at 460 nm the data showed only about 85% of FAD was reduced after the initial addition of 2 electron equivalents (Figure 6.4 B). An extra supplement of ~2 more electron equivalents then completely reduced FAD. Therefore, the results indicate a total of 3.7 ± 0.2 electrons are needed to achieve full reduction of FAD in Erv1 wt.

The requirement of approximately 4 electron equivalents implies two redox centres were reduced during the electron titration, one of which was FAD. Furthermore, it also suggests the E^{o} of this redox centre and that of FAD are close enough in value to share electrons. To determine which of the two disulphide bonds was being reduced alongside FAD, the Erv1 C1,2S and Erv1 C3,4S double cysteine mutants were analysed for their electron equivalents requirement.

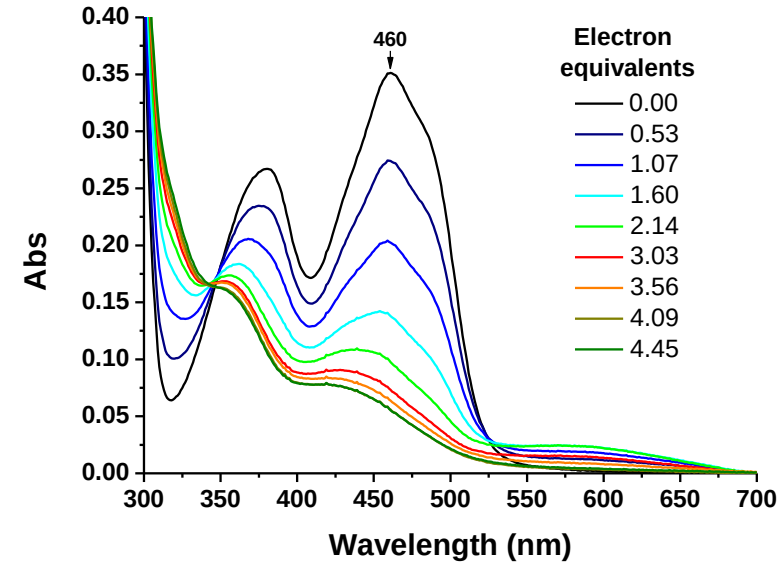

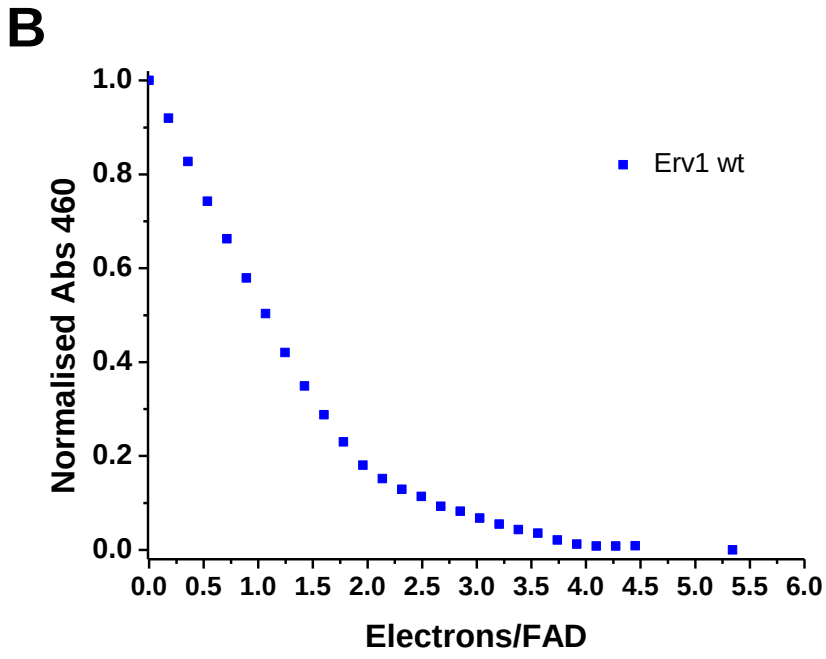

Figure 6.4 Electron titration of FAD in Erv1 wt

A) UV-visible spectra of Erv1 wt (28 µM in BAE) recorded after addition of 0.00, 0.53, 1.07, 1.60, 2.14, 3.03, 3.56, 4.09 and 4.45 electron equivalents (electrons/FAD) of sodium dithionite inside an anaerobic glove box. FAD goes from fully oxidised (black) to fully reduced (olive green).

B) Plot of normalised absorbance at 460 nm *versus* electron equivalents for the assay in A. Addition of 2 electron equivalents only reduced ~85% of FAD, whereas 3.7 ± 0.2 electron equivalents were needed to reduce FAD completely. The value represents the average of 2 independent experiments.

6.5. Determination of the number of electron equivalents and standard reduction potential of FAD in the double cysteine mutants Erv1 C1,2S and Erv1 C3,4S

The results obtained for Erv1 wt indicated that a second redox centre was simultaneously reduced with FAD. The two other redox centres in Erv1 are the C1-C2 shuttle disulphide and the C3-C4 redox-active disulphide. Thus, to identify which disulphide bond was reduced, electron titration experiments were conducted using the double cysteine mutants Erv1 C1,2S and Erv1 C3,4S. As shown in figure 6.5 A, the UV-visible spectrum of Erv1 C1,2S exhibited peaks at 380 and 460 nm, similar to those of Erv1 wt and in accordance with earlier reports (Ang and Lu, 2009). Addition of sodium dithionite decreased the absorbance of these two peaks but, interestingly, in this case the shoulder beyond 530 nm was not reliably visible. Moreover, addition of 2 electron equivalents did not yield the spectrum of fully reduced FAD. Analysis of the data showed only about 95% of FAD was reduced after addition of 2 electron equivalents, and a total of 4.2 ± 0.4 electron equivalents were needed to completely reduce the FAD in Erv1 C1,2S (Figure 6.5 B). It therefore follows that the C1-C2 shuttle disulphide is unlikely to be the other redox centre being reduced during the electron titration of FAD in Erv1 wt.

Next, the electron requirement of Erv1 C3,4S was investigated (Figure 6.5). Its UV-visible spectrum exhibited peaks at 377 and 453 nm, reflecting its close proximity to FAD and in full agreement with published literature (Ang et al., 2009, Guo et al., 2012). Again, addition of sodium dithionite decreased the absorbance of both these peaks and there was no evidence of a shoulder beyond 530 nm (Figure 6.6 A). In this case, however, reduction of the FAD cofactor occurred more rapidly. The spectrum for fully reduced FAD was obtained after adding just 2.22 electron equivalents. Indeed, data analysis showed removal of C3-C4 lowered the electron requirement for complete FAD reduction to just 2.3 ± 0.2 electron equivalents (Figure 6.6 B). The result is consistent with the fact that C4 was shown to be near enough (~3 Å) to interact with the FAD cofactor in the structure of Erv1 (Guo et al., 2012). In combination, these two results suggest reduction of C3-C4 is required to completely reduce FAD in Erv1 wt. Hence, electrons added during an Erv1 wt

electron titration are distributed between the FAD cofactor and the C3-C4 redox-active disulphide.

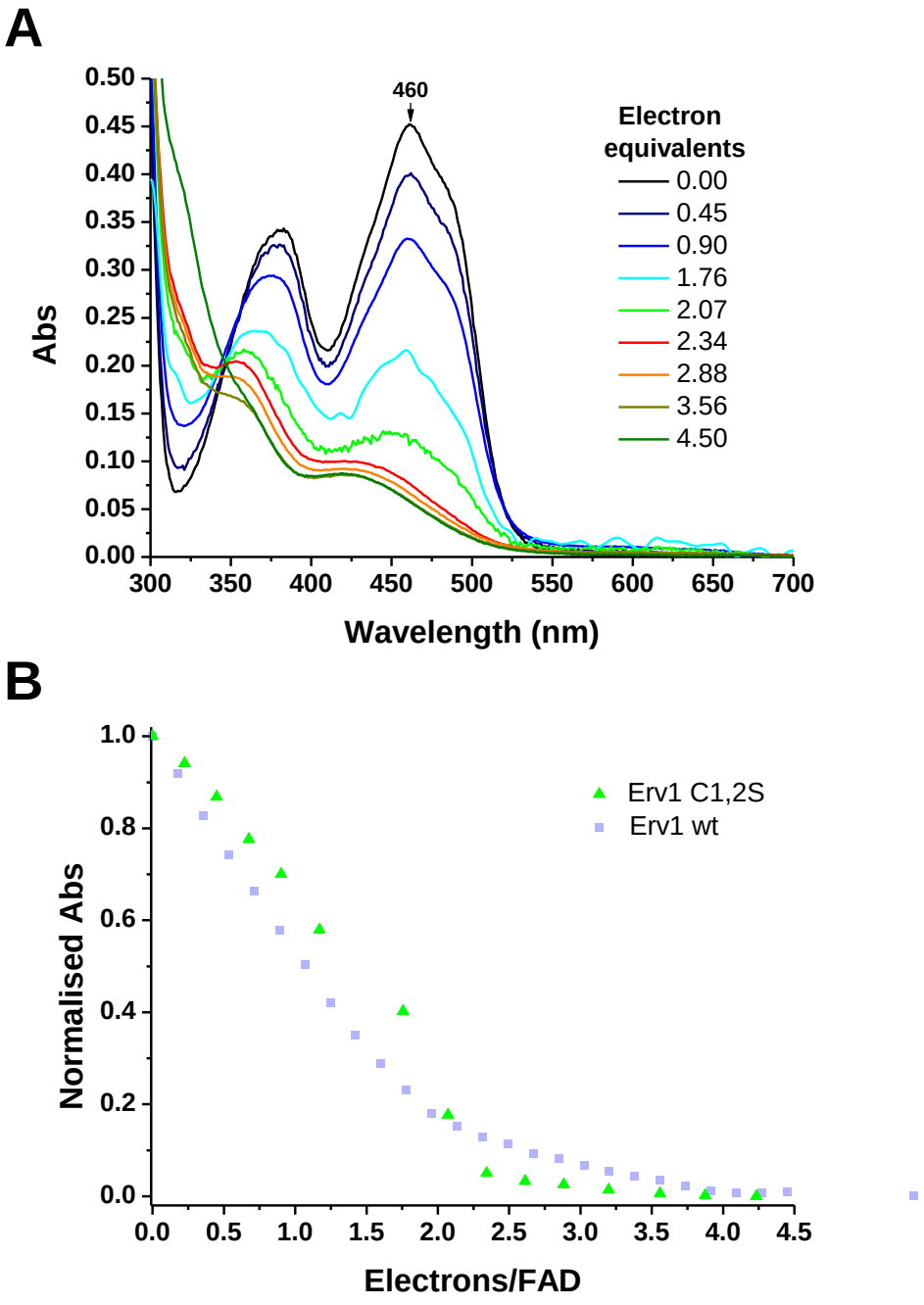

Figure 6.5 Electron titration of FAD in Erv1 C1,2S

A) UV-visible spectra of Erv1 C1,2S (41.5 μM in BAE) recorded after addition of 0.00, 0.45, 0.90, 1.76, 2.07, 2.34, 2.88, 3.56 and 4.50 electron equivalents of sodium dithionite inside an anaerobic glove box. Fully oxidised Erv1 C1,2S (black) exhibited peaks at 380 and 460 nm. FAD goes from fully oxidised to fully reduced (olive green).

B) Plot of normalised absorbance at 460 nm *versus* electron equivalents for the assay in A. Addition of 2 electron equivalents to Erv1 C1,2S (green) only reduced ~95% of FAD, whereas 4.2 ± 0.4 electron equivalents were needed to

reduce FAD completely. The value represents the average of 2 independent experiments. For comparison, Erv1 wt is in light blue.

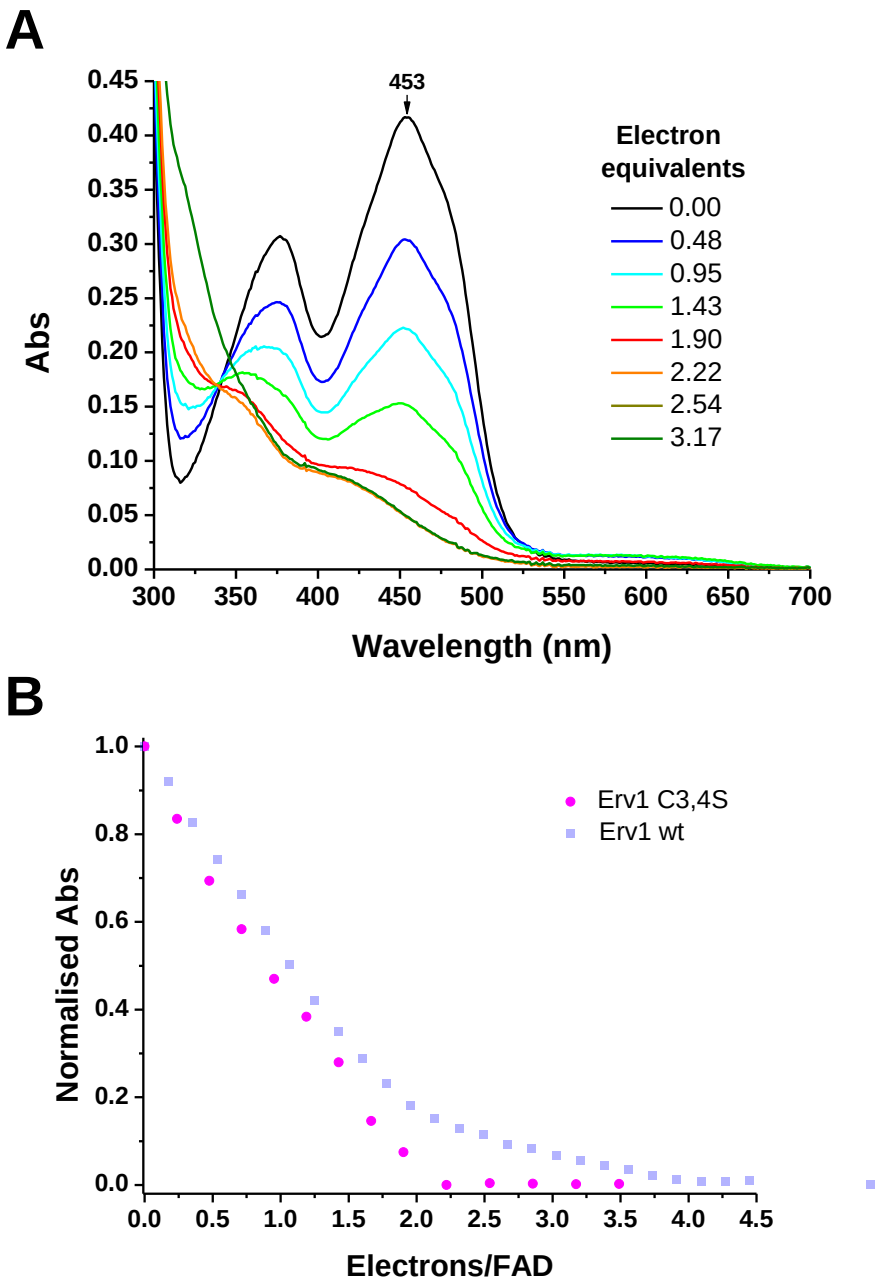

Figure 6.6 Electron titration of FAD in Erv1 C3,4S

A) UV-visible spectra of Erv1 C3,4S (34 μM in BAE) recorded after addition of 0.00, 0.48, 0.95, 1.43, 1.90, 2.22, 2.54 and 3.17 electron equivalents of sodium dithionite inside an anaerobic glove box. Fully oxidised Erv1 C3,4S (black) exhibited peaks at 377 and 453 nm. FAD goes from fully oxidised to fully reduced (olive green).

B) Plot of normalised absorbance at 453 nm *versus* electron equivalents for the assay in A. Only 2.3 ± 0.2 electron equivalents were needed to completely reduce FAD in Erv1 C3,4S (magenta). The value represents the average of 2 independent experiments. For comparison, Erv1 wt is in light blue.

The effect of each disulphide bond on the Erv1 redox behaviour was further studied by measuring the E^o of FAD in Erv1 C1,2S and Erv1 C3,4S. To that end, FAD redox titration experiments as described in section 6.3 were conducted for each mutant and are shown in figures 6.7 A and B. Next, in the case of Erv1 C1,2S, fitting of the absorbance at 460 to the Nernst equation gave a E^o of -145 ± 1 mV for z=2 (Figure 6.7 C). This value is close to the E^o of FAD measured in this study for Erv1 wt (Table 6.1). Moreover, the more gradual FAD reduction between electron potentials -180 and -280 mV was also displayed in this mutant. This result indicates that the mutation of the C1-C2 shuttle disulphide does not alter the E^o of FAD in Erv1.

On the other hand, fitting of the absorbance at 453 nm for Erv1 C3,4S displayed an excellent fit to the Nernst equation (Figure 6.7 C). The E^o of FAD in Erv1 C3,4S was measured at -198 ± 5 mV for z=2, displaying a shift in E^o towards more negative and reducing values. This change in E^o may be explained by the proximity of C3-C4 to FAD in Erv1. Disulphide bonds are generally willing acceptors of electrons and, consequently, can pull the electron cloud away from the FAD cofactor. Hence, when in the vicinity of a disulphide, FAD is less negative and thus more capable of accepting electrons (more positive E^o).

Taken together the results suggest it is the electron distribution between C3-C4 and FAD that causes the slower FAD reduction in Erv1 wt. Furthermore, 2 electron equivalents are needed to reduce FAD and another 2 to reduce C3-C4, giving the total of 4 electron equivalents calculated for Erv1 wt. The results support the C3-C4 redox-active disulphide as the second redox centre reduced simultaneously with FAD. The standard reduction potentials and electron equivalents requirements for Erv1 wt, Erv1 C1,2S and Erv1 C3,4S are summarised in Table 6.1.

Table 6.1 Redox behaviour of FAD in Erv1

Protein	E° (mV)	Electrons/FAD
Erv1 wt	-157 ± 7	3.7 ± 0.2
Erv1 C1,2S	-145 ± 1	4.2 ± 0.4
Erv1 C3,4S	-198 ± 5	2.3 ± 0.2

All values represent an average of at least 2 independent experiments.

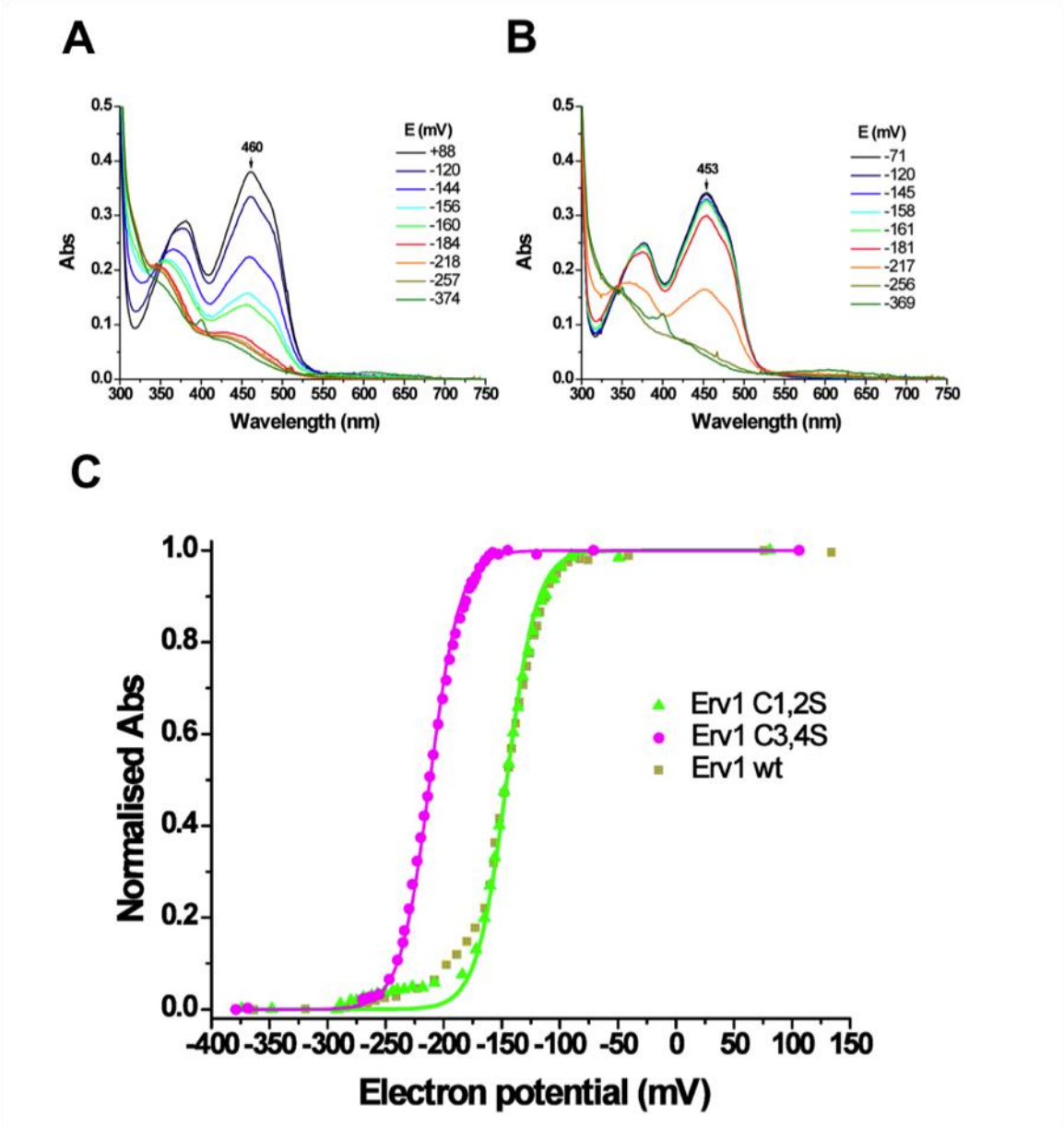

Figure 6.7 FAD redox titration of Erv1 C1,2S and Erv1 C3,4S

A) Representative UV-visible spectra of Erv1 C1,2S (56 µM in BAE) recorded at various electron potentials during an anaerobic reduction of FAD by increasing amounts of sodium dithionite. FAD goes from fully oxidised (black) to fully reduced (olive green).

B) As in A but for Erv1 C3,4S (30 µM in BAE).

C) Plot of normalised absorbance *versus* electron potential for Erv1 C1,2S (460 nm, green) and Erv1 C3,4S (453 nm, magenta). The data were fitted (solid lines) using the Nernst equation for z = 2 and T = 298 K. The average of at least 2 independent experiments gave a standard reduction potential of -145 ± 1 mV for Erv1 C1,2S and -198 ± 5 mV for Erv1 C3,4S. For comparison, Erv1 wt is in light blue.

6.6. Determination of the standard reduction potential of the C3-C4 redox-active disulphide of Erv1

As described in the previous section, the gentle reduction of FAD between electron potentials -180 and -280 mV represents an electron distribution with the C3-C4 disulphide. Therefore, a thiol modification assay was used to confirm the interaction between C3-C4 and FAD, and determine the E^{o} of C3-C4. To do this, the AMS reagent covalently binds any accessible free thiols and shifts a protein's molecular weight by 0.5 kDa per free thiol. Proteins with oxidised or reduced disulphide bonds thus run at different speeds on SDS-PAGE depending on their number of free thiols.

To start, samples were taken along an FAD redox titration of Erv1 C1,2S and were immediately mixed with anaerobic SDS-PAGE sample buffer containing 1 mM AMS. The Erv1 C1,2S mutant was used to avoid any possible interference from the C1-C2 shuttle disulphide; the sample buffer was used to completely unfold the protein thus exposing the cysteines of the C3-C4 redox-active disulphide. The results (Figure 6.8 A) show that, at an electron potential of -112 mV, there was only one band of ~22 kDa corresponding to Erv1 C1,2S with C3 and C4 forming a disulphide bond (Ox). Then, as the electron potential shifted towards more negative and reducing values, an additional band appeared (~23 kDa) indicating two AMS molecules were bound to Erv1 C1,2S. This new band represents Erv1 C1,2S with a reduced C3-C4 disulphide (Red). Finally, at an electron potential of -348 mV, all the Erv1 C1,2S had the C3-C4 disulphide in its reduced conformation. It follows that, from -140 to -300 mV, there is a correlation between the amount of reduced C3-C4 disulphide and the electron potential measured during an FAD redox titration. This directly confirms the change in slope in FAD redox titrations of Erv1 wt is due to reduction of the C3-C4 redox-active disulphide. What is more, somewhere between electron potentials -257 and -275 mV, 50% of the C3-C4 disulphides are reduced. Hence, it can be estimated that the midpoint electron potential of the C3-C4 redox-active disulphide is about -266 ± 9 mV.

The AMS assay confirmed a redox equilibrium exists in Erv1 between its C3-C4 redox-active disulphide and the FAD cofactor. Thus, provided enough time is allowed for the equilibrium to be reached, a plot of FAD absorbance

versus electron potential can be used as an indirect measurement of the C3-C4 redox-active disulphide midpoint electron potential. Figure 6.8 B shows two independent FAD redox titration experiments for Erv1 C1,2S where extra points were taken from electron potentials -140 to -300 mV. Although an attempt to fit the data to the Nernst equation was unsuccessful, still a midpoint electron potential was estimated from the assays. If the absorbance at -190 mV is taken as C3 and C4 forming mostly a disulphide bond, and the absorbance at -300 mV as C3 and C4 being completely reduced, the electron potential at which the initial absorbance (at -190 mV) is halved represents the reduction of 50% of the C3-C4 disulphide bonds. In this manner a midpoint electron potential of -245 mV was obtained for the C3-C4 redox-active disulphide of Erv1.

Based on these two different measurements the midpoint electron potential of the Erv1 C3-C4 redox-active disulphide is around -256 ± 11 mV at pH 7.4.

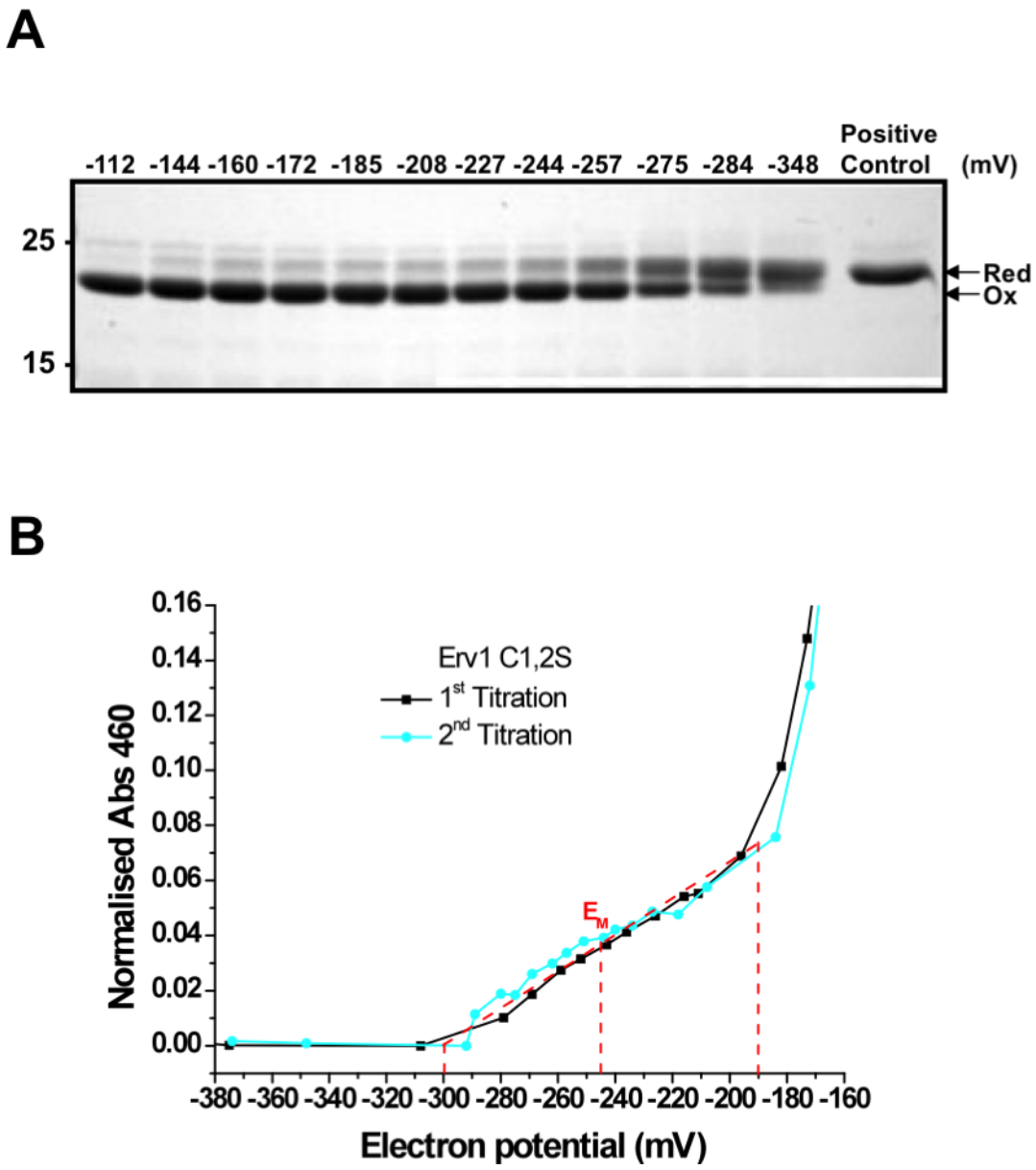

Figure 6.8 Midpoint electron potential of the C3-C4 redox-active disulphide

A) SDS-PAGE showing an AMS assay of samples taken at different points along a FAD redox titration of Erv1 C1,2S. The C3-C4 redox-active disulphide is increasingly reduced as the electron potential moves towards more negative values. Ox: Erv1 C1,2S with intact C3-C4 disulphide. Red: Erv1 C1,2S with two AMS molecules bound to reduced C3 and C4. AMS = 0.5 kDa. Positive control: Erv1 C1,2S first treated with 1 mM DTT and then 10 mM AMS. A midpoint electron potential of -266 ± 9 mV was estimated from the data.

B) Zoom in of a plot of normalised absorbance at 460 nm *versus* electron potential for two different FAD redox titrations of Erv1 C1,2S. This region represents the redox equilibrium between FAD and the C3-C4 redox-active disulphide of Erv1. A midpoint electron potential of -245 mV was estimated from the data.

6.7. Determination of the standard reduction potential of the C1-C2 shuttle disulphide in Erv1

Both Erv1 and Mia40 form the central backbone of the MIA pathway, within which, the function of Erv1 is to reoxidise pr-Mia40 by means of its C1-C2 shuttle disulphide (Herrmann and Riemer, 2012). However, the reported E^o of C1-C2 is -320 mV, making it more reducing than that of the CPC disulphide in Mia40 (E^o = -290 mV) (Dabir et al., 2007, Tienson et al., 2009). To complete the study on the redox behaviour of Erv1 several attempts were made to measure the E^o of its C1-C2 shuttle disulphide.

The E^o of a disulphide bond can be determined by first establishing a redox equilibrium between a species of known E^o and the protein of interest. Typically used species, such as the GSH/GSSG couple, can sometimes form GSH-protein adducts that may shift the redox equilibrium and affect the measurements (Aslund et al., 1997). To avoid this, pr-Mia40c was instead selected as the species to establish a redox equilibrium with Erv1 C3,4S. The Erv1 C3,4S double cysteine mutant was chosen to disrupt the electron transfer from the C1-C2 shuttle disulphide to FAD. This methodology of using direct protein-protein redox equilibrium has been successfully employed for proteins like glutaredoxin 1 and 3 from *E. coli* (Aslund et al., 1997). After establishment of the redox equilibrium, the oxidised and reduced protein conformations need to be separated and quantified. In these experiments, reverse-phase chromatography (RPC) was used to separate proteins based on their distinct hydrophobicities.

Initially, a mixture of oxidised Mia40c and oxidised Erv1 C3,4S was run on an XB-C18 HPLC column using a water to acetonitrile gradient (Figure 6.8 A). The two oxidised proteins were easily separated, with oxidised Mia40c eluting as two peaks at 13.4 and 15.9 min and oxidised Erv1 C3,4S eluting as one peak at 51.0 min. The identity of the peaks was then confirmed by analysing the individual proteins. Next, a mixture of pr-Mia40c and reduced Erv1 C3,4S was run under the same experimental conditions as the oxidised proteins (Figure 6.9 B). The results show pr-Mia40c eluted as only one peak at 18.2 min, whereas reduced Erv1 C3,4S eluted at 51.4 min. Superimposition of the two chromatography profiles (Figures 6.9 C and D) shows sufficient separation between the oxidised and reduced conformations of Mia40c.

However, the two peaks of Erv1 C3,4S clearly overlapped, suggesting their current separation is not enough to accurately quantify each individual conformation.

The experiments shown here represent the best results obtained so far. Mixtures of Mia40c and Erv1 C3,4S were successfully separated using RPC. Furthermore, the oxidised and reduced conformations of Mia40c were also successfully separated. However, a good separation was not achieved for the oxidised and reduced conformations of Erv1 C3,4S. Various other conditions than the one shown here were also tried for their ability to separate these two conformations. Among these, exchanging negatively-charged ion-pairing agent TFA for positively-charged tetraethylammonium sharpened the Erv1 C3,4S peak but considerably broadened the Mia40c peak. Moreover, neither extending the gradient nor narrowing the acetonitrile concentrations improved the resolution. Alternative methods to determine the E^{o} of the C1-C2 shuttle disulphide are given in the discussion.

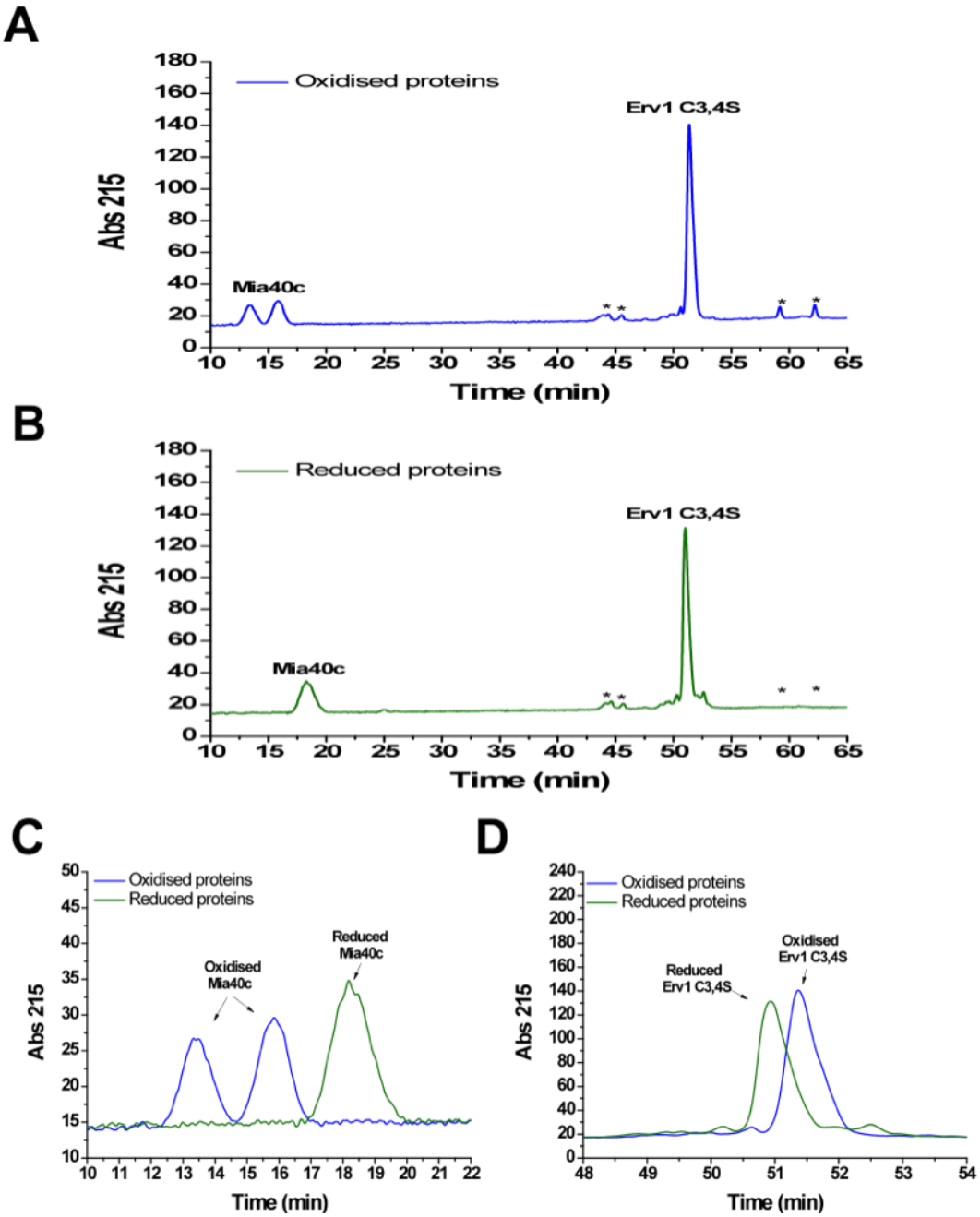

Figure 6.9 Reverse-phase chromatography of Mia40c and Erv1 C3,4S

A) Reverse-phase chromatography of oxidised Mia40c and oxidised Erv1 C3,4S run on an Aeris widepore XB-C18, 150 x 4.6 mm HPLC column. *Unknown species.

B) Reverse-phase chromatography of pr-Mia40c and reduced Erv1 C3,4S run on an Aeris widepore XB-C18, 150 x 4.6 mm HPLC column. *Unknown species.

C) Zoom in of A and B superimposed around the Mia40c region. Oxidised Mia40c (blue) appears as two peaks with retention times of 13.7 and 15.9 min. pr-Mia40c (olive green) eluted as just one peak with a retention time of 18.5 min.

D) Zoom in of A and B superimposed around the Erv1 C3,4S region. Oxidised Erv1 C3,4S (blue) eluted with a retention time of 51.4 min. Reduced Erv1 C3,4S (olive green) eluted with a retention time of 51.0 min.

6.8. Identification of the redox intermediate in Erv1

The FAD redox titration experiments presented in section 6.3 exposed the formation of a redox intermediate as Erv1 wt became increasingly reduced. The isoalloxazine ring of FAD can exist in three different oxidation states (Figure 6.10): fully oxidised, semiquinone and fully reduced (Massey, 2000). While in its semiquinone state, isoalloxazine can also be found as two different types (neutral or anionic) distinguishable by their UV-visible spectrum and electron paramagnetic resonance (EPR) profile. Figure 6.11 A shows the UV-visible spectrum of fully oxidised and partially reduced Erv1 wt. Partially reduced Erv1 wt was obtained by adding 1.4 electron equivalents of sodium dithionite inside an anaerobic glove box. Untreated Erv1 wt exhibited peaks at 380 and 460 nm characteristic of fully oxidised FAD. However, upon reduction, the absorbance of the peaks decreased and their position shifted to 360 and 450 nm with a new shoulder appearing beyond 530 nm. These red shifts and the shoulder beyond 530 nm are typical features of a blue neutral semiquinone (Massey and Palmer, 1966, Massey, 2000). This semiquinone state results from the addition of one electron and one proton (H^+) to the oxidised state of FAD (Figure 6.10).

To confirm this result, the same sample used in the UV-visible assay was further analysed by EPR. Figure 6.11 B shows a first-derivative X-band EPR spectrum with a signal centred at $g = 2.0038$ and a line-width of 18 G. This G-value, along with the broad line-width, indicates the flavin radical is a blue neutral semiquinone. Furthermore, a semiquinone concentration of ~11 μM was determined by comparing the area of the peaks with that of a known standard. This indicates about 7 % of the total FAD present (153.8 μM) was in a blue semiquinone state.

Overall, based on both UV-visible and EPR experiments, the redox intermediate was identified as a blue neutral semiquinone. No evidence was found for the presence of a red anionic semiquinone at the conditions tested.

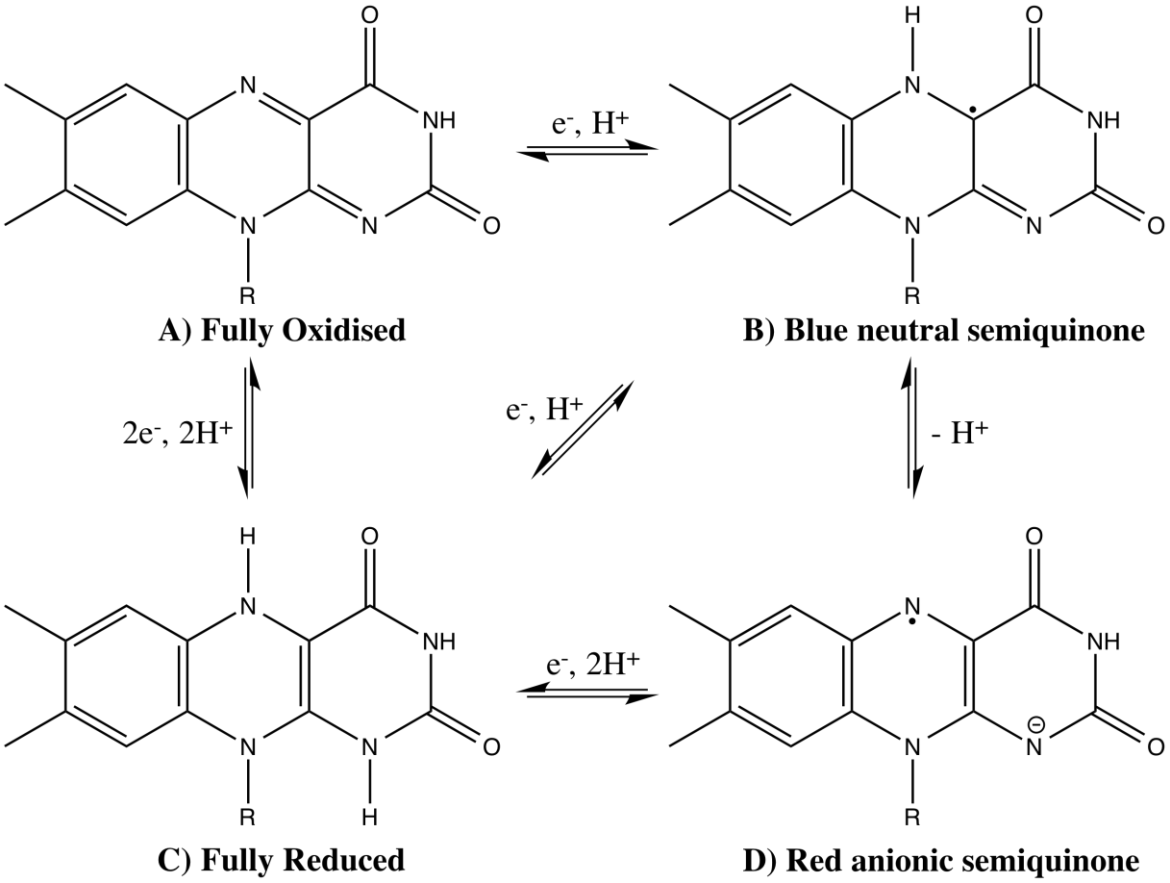

Figure 6.10 Isoalloxazine redox states

The isoalloxazine ring of FAD can adopt three redox states: Fully oxidised (A), semiquinone (B and C) and fully reduced (D). In its semiquinone state isoalloxazine can form a blue neutral semiquinone (B) or a red anionic semiquinone (C). Conversion from fully oxidised to the semiquinone state requires a one-electron reduction; whether the semiquinone is neutral or anionic generally depends on pH. Alternatively, fully oxidised FAD can be transformed into fully reduced FAD by a two-electron reduction plus addition of two protons (H^+).

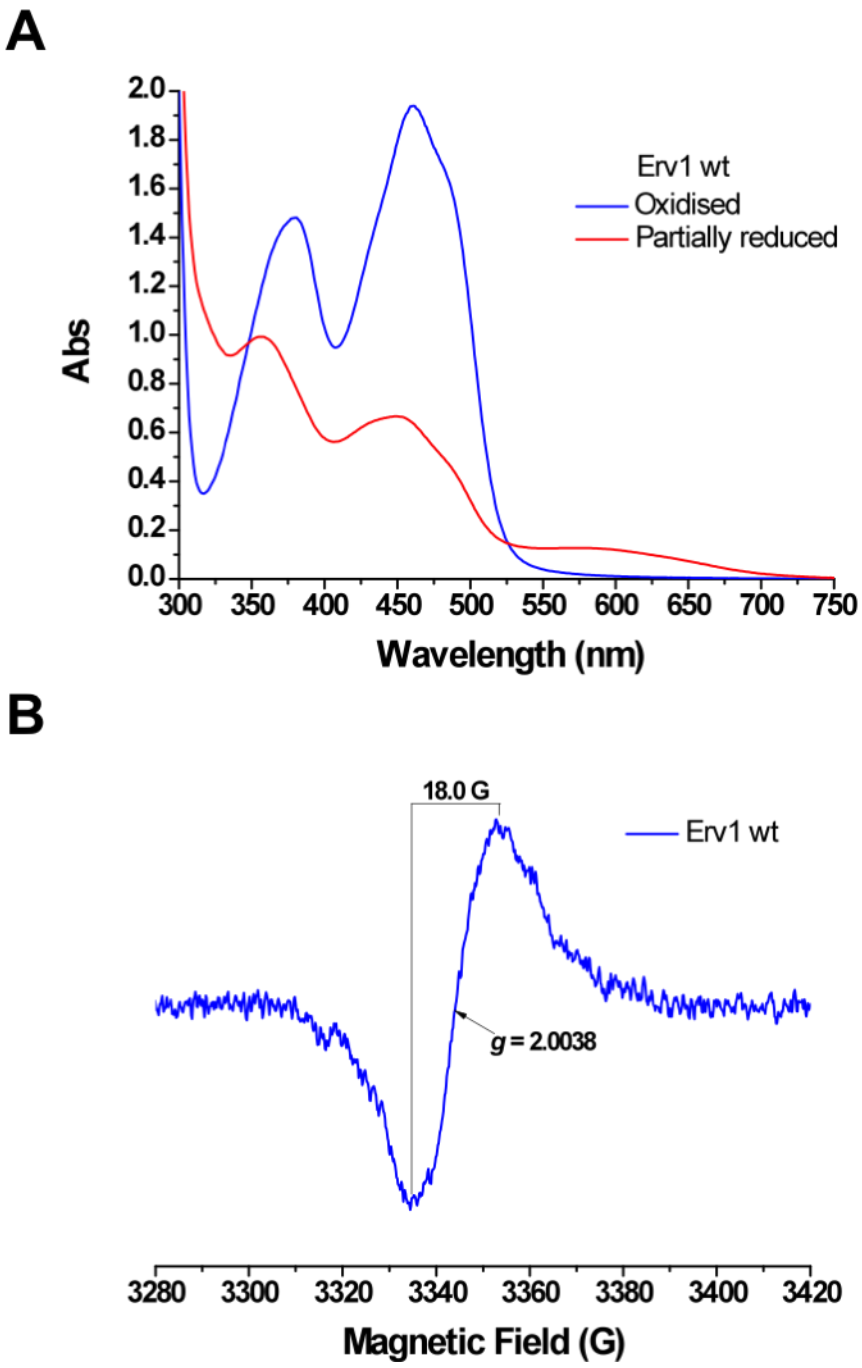

Figure 6.2 Semiquinone formation in Erv1

A) UV-visible spectra of 153.8 μM fully oxidised (blue) or partially reduced (red) Erv1 wt. Partially reduced Erv1 wt was obtained by adding 1.4 electron equivalents (electrons/FAD) of sodium dithionite inside an anaerobic glove box. The spectrum of partially reduced Erv1 wt displays the characteristic traits (a shoulder beyond 530 nm) of a blue neutral semiquinone. BAE buffer, pH 7.4.

B) First-derivative X-band electron paramagnetic resonance spectra of the partially reduced Erv1 wt from A. The signal is centred at g = 2.0038 with a line width of 18.0 G. These values indicate the presence of a blue neutral semiquinone.

6.9. Discussion

The electron transfer between two redox centres can be uphill (from a more positive to a more negative E^o) or downhill (from a more negative to a more positive E^o). However, reactions do not always follow the direction of electron flow dictated by the standard reduction potentials. In the case of Erv1 the current model suggests the initial electron transfer is downhill from C1-C2 ($E^o = -320$ mV) to C3-C4 ($E^o = -150$ mV), followed by an uphill transfer to FAD ($E^o = -215$ mV). In this model the highly positive standard reduction potentials of oxygen (+820 mV) and cyt *c* (+250) create an electron sink that drives the reaction forwards (Dabir et al., 2007). This chapter presented alternative values for the standard reduction potentials that allow us to offer a second model where the electron transfer from FAD to C3-C4 is downhill.

6.6.1. The E^o of FAD is more reducing than previously reported.

The first part of this study focused on the E^o of the FAD redox centre in Erv1. The results determined a E^o of -157 ± 7 mV for FAD; however, Dabir *et al.* (2007) reported a E^o of -215 mV, which is different from the value obtained here (Dabir et al., 2007). The reduction of FAD requires the uptake of two protons at pH values below the p*Ka* of reduced FAD, making all measured standard reduction potentials dependent upon pH. Thus, the pH must be taken into account when comparing the standard reduction potentials measured in two different experiments. Using an adjustment of -59 mV per pH unit increase the reported E^o of -215 mV at pH 7.0 becomes -238.6 mV at pH 7.4. It follows that the E^o presented here is about 80 mV more positive than the one previously published. When comparing both methodologies, Dabir *et al.* (2007) employed a slightly similar technique to the one used here but measured fewer titration points (9 compared to >25 for this assay). Their experiments used lower Erv1 concentrations (10 μM) and higher amounts of mediators (3 mediators at 10 μM each), which masked the UV-visible spectra of FAD: there was no visible FAD peak at ~460 nm but instead there was a peak at ~520 nm. Furthermore, there were no isosbestic points during the titration due to shifts in the UV-visible baseline (Dabir et al., 2007). Overall, although it is difficult to pinpoint a specific mistake in the measurements done by Dabir *et al.* (2007), the data they presented raised some doubts.

6.6.2. A downhill electron flow from C3-C4 to FAD

Two methodologies, AMS assay and FAD titration, were used in this study to estimate a midpoint electron potential of -256 ± 11 mV for the C3-C4 redox-active disulphide. This value is more negative than the E^{o} of FAD measured here, which indicates a downhill flow of electrons from C3-C4 to FAD. A closer examination of the FAD electron titration experiments provided additional support for this conclusion. In the assays, FAD in Erv1 wt required ~4 electrons equivalents to be fully reduced, indicating a redox equilibrium was established between FAD and C3-C4. More importantly, FAD was always the redox centre to take up most of the electrons at the start, with about 85% of FAD being reduced after the addition of 2 electron equivalents. This indicates that, between FAD and C3-C4, it is FAD the redox centre more willing to take electrons and, accordingly, it must have the more positive E^{o}.

The discrepancies between the two models may just represent a difference in the assigning of the measured standard reduction potentials to the redox centres in Erv1. In the previous assays the measurement of the E^{o} of C3-C4 was done by monobromobimane (mBBr) fluorescence (Dabir et al., 2007). First, an equilibrium was established between Erv1 and various redox buffers. The excess redox buffer was then removed and mBBr was added to Erv1. The binding of mBBr to protein thiols formed a fluorescent adduct and, therefore, the reduction of disulphide bonds was followed by the increase in mBBr fluorescence. The data presented by Dabir *et al.* (2007) displayed two transitions in the mBBr fluorescence intensity: one large transition (80% intensity increase) at -330 mV and one small transition (20% intensity increase) at -150 mV (Dabir et al., 2007). From this data the conclusion was that two disulphide bonds were being reduced: C1-C2 and C3-C4. However, in theory, if two thiols were exposed with each transition then both transitions should have displayed a similar increase in fluorescence, which was not the case. Furthermore, only the large transition at -330 mV could be verified by tryptophan fluorescence despite a tryptophan (W132) being located between C3 and C4 (Guo et al., 2012). Thus, another possible explanation for the transition at -150 mV, and one that agrees with our reported E^{o} of FAD, is that the small increase in fluorescence represents a minor amount of reduced C3-C4 that was found in redox equilibrium with reduced FAD.

6.6.3. Redox behaviour of other ERV proteins

The redox behaviour of Erv1 can be placed in context with the other two proteins of the ERV family that have been studied so far: *Sc*Erv2 and short form *Hs*ALR (sf-*Hs*ALR). In the case of sfALR only 2 electron equivalents were needed to completely reduce FAD, even in the presence of the C3-C4 redox-active disulphide (Table 6.2) (Farrell and Thorpe, 2005). Therefore, the difference between the standard reduction potentials of FAD and C3-C4 in sf-*Hs*ALR is big enough that the redox equilibrium is totally shifted towards reduced FAD. However, both Erv1 and Erv2 required 4 electron equivalents to completely reduce their FAD cofactor (Table 6.2). But, unlike Erv1, addition of 2 electron equivalents to Erv2 only reduced ~50% FAD suggesting the standard reduction potentials of the FAD and C3-C4 redox centres are closer in value in Erv2 than in Erv1 (Wang et al., 2007). Finally, the E^{o} of FAD in Erv1 is more positive than those reported for Erv2 (-200 mV) and sf-*Hs*ALR (-178 mV, Table 6.2) (Farrell and Thorpe, 2005, Wang et al., 2007). Thus, when compared with other proteins of the ERV family, the redox behaviour of Erv1 is somewhere between that of *Sc*Erv2 and sf-*Hs*ALR. However, in all three cases the E^{o} of FAD is more or as positive as that of the C3-C4 redox-active disulphide, suggesting the electron transfer from C3-C4 to FAD is downhill.

Table 6.2 FAD redox behaviour of proteins in the ERV family

Protein	E°(mV)	Electrons/FAD	
Erv1 wt[a]	-157	4	This report
Erv1 wt[b]	-215	---	Dabir *et a*l. (2007)
Short form ALR[a]	-178	2	Farrel *et al.* (2005)
Erv2[a]	-200	4	Wang *et al.* (2007)

[a] Done at pH 7.4-7.5
[b] Done at pH 7.0

6.6.4 The E^{o} of the C1-C2 shuttle disulphide

The final piece of the puzzle was concerned with the E^{o} of the C1-C2 shuttle disulphide. Unfortunately, all attempts to measure it proved unsuccessful. Although the oxidised and reduced conformation of Mia40c were easily separated by RPC, that was not the case for Erv1 C3,4S. The C1-C2 shuttle

disulphide is located in the flexible and unstructured N-terminal domain of Erv1 (Banci et al., 2013b). Therefore, it is not unexpected that the reduction of the C1-C2 disulphide does not lead to the exposure of hydrophobic residues.

Two solutions have been considered in order to improve the separation of the oxidised and reduced conformations of Erv1 C3,4S. The first one involves adding a thiol-binding agent, such as AMS, that upon binding to the reduced conformation would greatly increase the hydrophobicity of Erv1 C3,4S. The oxidised and reduced conformations can then be separated by RPC. A second possible solution involves the use of mass spectrometry to separate and quantify the two conformations. After a redox equilibrium is reached between Erv1 C3,4S and Mia40c, the samples are treated with iodoacetate to trap the reduced cysteines. Next, DTT is used to break the disulphide bond of the oxidised state and the samples are now treated with (1,2, ^{13}C) bromoacetate. Following trypsin, treatment the samples are finally run through a mass spectrometer. In this case the oxidised and reduced conformation of each protein are separated based on the 4 Da difference in mass created by the heavy carbons of the acetate. This approach has been successfully employed before to measure the E^{o} of the active site disulphides of human protein disulphide isomerase (PDI) (Chambers et al., 2010).

6.8. Conclusion

The E^{o} of FAD in Erv1 wt and the double cysteine mutants Erv1 C1,2S and Erv1 C3,4S was measured in this study. The results showed the E^{o} of FAD is strongly influenced by the presence of the C3-C4 redox-active disulphide. The close proximity of C3-C4 to FAD allows for an electron distribution between the two redox centres, with 4 electron equivalents being needed to fully reduce the FAD in Erv1. The midpoint electron potential of the C3-C4 redox-active disulphide was also measured and shown to be more negative than that of FAD. Based on these results an alternative model for the electron transfer within Erv1 was proposed where the electron flow from C3-C4 to FAD is downhill. More experiments are required to calculate the standard reduction potential of C1-C2 and complete the electron pathway.

7. OVERALL CONCLUSIONS AND OUTLOOK

The overall aim of this study was to investigate the molecular mechanisms regulating the structure and function of the mitochondrial sulphydryl oxidase Erv1.

The first part of this study looked at the stability of the quaternary structure of Erv1 using various biophysical techniques. The results showed Erv1 forms a tetramer under the conditions tested, offering an alternative model for the oligomerisation state of Erv1. Tetramer formation conferred Erv1 with more secondary folding, higher FAD binding and increased thermal stability. However, the oligomerisation state needs also be addressed after removal of the His tag from Erv1 to ensure that tetramerisation is not caused by the exogenous tag. More importantly, at this point it is unknown whether Erv1 adopts a tetramer or a dimer conformation *in vivo* and this point should be clarified. If Erv1 does in fact form a tetramer, then its dissociation constant needs to be measured to verify that the same oligomerisation state is present in all the experiments. This is of particular importance in the activity assays because we do not know if the dimer and tetramer conformations of Erv1 have the same or different activity. Overall, the conclusions drawn for the oligomerisation state of Erv1, both *in vitro* and *in vivo*, remain speculative and experiments such as AUC and blue-native electrophoresis need to be carried out to complement them.

Many other questions still need to be addressed to know whether the tetramer conformation is physiologically relevant. At this point it is unknown how the tetramer is formed and which residues are important for oligomerisation. Furthermore, the question remains why Erv1 forms tetramers when other proteins in the ERV family form dimers? What advantage does oligomerisation provide to Erv1?

The second part of this study represents the first report addressing the Erv1 R182H mutant from a protein standpoint. In terms of structure the Erv1 R182H mutant formed dimers in solution, had a lower thermal stability, and displayed a weaker binding of the FAD cofactor. Furthermore, both the oxidase and cyt *c* reduction activity of Erv1 R182H were also affected, defects

which were apparently not shared by the corresponding ALR R194H mutant (Diathankar et al., 2010). However, because the conditions under which the experiments were performed are not the same, it would be interesting to check whether the Erv1 R182H activity defect could be now reproduced in the mammalian protein. This would be a major step towards understanding why the R194H mutation has such devastating effects on mammalian cells.

Another important finding presented here offers an alternative explanation for the reported *in vivo* results that suggest both the Mia40-Erv1 and the Erv1-cyt *c* interactions are directly affected by the R182H mutation (Di Fonzo et al., 2009; Sztolsztener et al. 2013). Our results showed that an impaired binding of the FAD cofactor causes the failure in the activity of Erv1 R182H during its catalytic reaction. Because the results indicate the enzyme itself is inactivated, this would indirectly affect the interaction with Mia40 and cyt *c* giving the impression that the mutation directly disrupts these interactions. However, the question arises of why is the enzyme only inactivated during the enzymatic reaction? Stability assays suggested FAD remains bound to the oxidised state of the mutant even after 24 h at 37°C and low (1.5 μM) protein concentrations (unpublished results), but loss its activity at different time points of a catalytic reaction depending on the electron donor that was used. These observations suggest the unstable conformation of Erv1 R182H, the one with impaired FAD binding, might best be represented by an intermediate of its catalytic reaction (e.g. Erv1-$FADH_2$). Thus, the next question that would need to be addressed is which of the Erv1 reactions intermediates is the one that inactivates the protein?

Finally, although the results presented in this study discovered a defect in the activity of Erv1 R182H, it remains to be seen if this defect indeed translates into a disrupted MIA pathway. Failure of the MIA pathway components could potentially affect the import and oxidative folding of proteins going to the IMS, IM or matrix. Because MIA pathway substrates are involved in a diversity of mitochondrial functions, this would offer a likely explanation for the various phenotypes observed in the Erv1 R182H yeast strain. Therefore, *in vitro* import assays into mitochondria from a Erv1 R182H yeast strain would help elucidate if the mutation affects protein import, specially if the assays are done at the restrictive temperature of 37°C. Furthermore, measuring the steady-state levels of matrix and IM proteins in

this yeast strain would offer support that the mutation disrupts protein import into mitochondria.

The third part of this study focused on the redox behaviour of Erv1. The redox potentials of the FAD and the C130-C133 redox centres were determined to be -157 and -255 mV, respectively. These new values denote a downhill electron flow from C130-C133 to FAD. The results disagree with a previous report where FAD appeared to be more reducing than C130-C133. Instead, a downhill electron flow was further supported by electron titration experiments that showed the FAD redox centre is reduced before the C3-C4 redox centre, indicating FAD has the most oxidising redox potential of the two. However, the standard reduction potential of the C1-C2 shuttle disulphide is still lacking, and will need to be measured to complete our understanding of the electron transfer within Erv1.

Recently, the redox potential of the mitochondrial IMS (E^{o}_{IMS}) was determined to be -306 mV and was shown to be regulated by the redox potential of the cytosol (Kojer et al., 2012). Interestingly, the redox state of Mia40 depended on the E^{o}_{IMS}, but the opposite was not valid because upregulation of Mia40 did not change the E^{o}_{IMS}. On the other hand, the upregulation of Erv1 did shift the E^{o}_{IMS} towards more oxidising values, a phenotype also obtained by the upregulation of cytosolic glutathione reductase (Kojer et al., 2012). Therefore, it is possible that Erv1 plays a role in regulating the E^{o}_{IMS}. Because Mia40 did not display a similar effect as Erv1, it suggests the function of Erv1 on the E^{o}_{IMS} is independent of the MIA pathway. However, neither is it a direct interaction of Erv1 with the GSH/GSSG redox buffer because GSH is not a substrate of Erv1. Thus, now that new E^{o} for the redox centres in Erv1 have been measured, the question remains of if and how Erv1 regulates the E^{o}_{IMS}?

REFERENCES

ALDER, N. N., SUTHERLAND, J., BUHRING, A. I., JENSEN, R. E. & JOHNSON, A. E. (2008) Quaternary structure of the mitochondrial TIM23 complex reveals dynamic association between Tim23p and other subunits. *Mol Biol Cell,* 19**,** 159-70.

ALI, M. H. & IMPERIALI, B. (2005) Protein oligomerization: how and why. *Bioorg Med Chem,* 13**,** 5013-20.

ALLEN, S., BALABANIDOU, V., SIDERIS, D. P., LISOWSKY, T. & TOKATLIDIS, K. (2005) Erv1 mediates the Mia40-dependent protein import pathway and provides a functional link to the respiratory chain by shuttling electrons to cytochrome c. *J Mol Biol,* 353**,** 937-44.

ALON, A., GROSSMAN, I., GAT, Y., KODALI, V. K., DIMAIO, F., MEHLMAN, T., HARAN, G., BAKER, D., THORPE, C. & FASS, D. (2012) The dynamic disulphide relay of quiescin sulphydryl oxidase. *Nature,* 488**,** 414-8.

ANG, S. K. (2010) Characterisation of the sulphydryl oxidoreductase system of the mitochondrial intermembrane space. University of Manchester.

ANG, S. K. & LU, H. (2009) Deciphering structural and functional roles of individual disulfide bonds of the mitochondrial sulfhydryl oxidase Erv1p. *J Biol Chem,* 284**,** 28754-61.

ASLUND, F., BERNDT, K. D. & HOLMGREN, A. (1997) Redox potentials of glutaredoxins and other thiol-disulfide oxidoreductases of the thioredoxin superfamily determined by direct protein-protein redox equilibria. *J Biol Chem,* 272**,** 30780-6.

BACH, R. D., DMITRENKO, O. & THORPE, C. (2008) Mechanism of thiolate-disulfide interchange reactions in biochemistry. *J Org Chem,* 73**,** 12-21.

BAKER, M. J., WEBB, C. T., STROUD, D. A., PALMER, C. S., FRAZIER, A. E., GUIARD, B., CHACINSKA, A., GULBIS, J. M. & RYAN, M. T. (2009) Structural and functional requirements for activity of the Tim9-Tim10 complex in mitochondrial protein import. *Mol Biol Cell,* 20**,** 769-79.

BANCI, L., BARBIERI, L., LUCHINAT, E. & SECCI, E. (2013a) Visualization of redox-controlled protein fold in living cells. *Chem Biol,* 20**,** 747-52.

BANCI, L., BERTINI, I., CALDERONE, V., CEFARO, C., CIOFI-BAFFONI, S., GALLO, A., KALLERGI, E., LIONAKI, E., POZIDIS, C. & TOKATLIDIS, K. (2011) Molecular recognition and substrate mimicry drive the electron-

transfer process between MIA40 and ALR. *Proc Natl Acad Sci U S A,* 108**,** 4811-6.

BANCI, L., BERTINI, I., CALDERONE, V., CEFARO, C., CIOFI-BAFFONI, S., GALLO, A. & TOKATLIDIS, K. (2012) An electron-transfer path through an extended disulfide relay system: the case of the redox protein ALR. *J Am Chem Soc,* 134**,** 1442-5.

BANCI, L., BERTINI, I., CEFARO, C., CENACCHI, L., CIOFI-BAFFONI, S., FELLI, I. C., GALLO, A., GONNELLI, L., LUCHINAT, E., SIDERIS, D. & TOKATLIDIS, K. (2010) Molecular chaperone function of Mia40 triggers consecutive induced folding steps of the substrate in mitochondrial protein import. *Proc Natl Acad Sci U S A,* 107**,** 20190-5.

BANCI, L., BERTINI, I., CEFARO, C., CIOFI-BAFFONI, S., GAJDA, K., FELLI, I. C., GALLO, A., PAVELKOVA, A., KALLERGI, E., ANDREADAKI, M., KATRAKILI, N., POZIDIS, C. & TOKATLIDIS, K. (2013b) An intrinsically disordered domain has a dual function coupled to compartment-dependent redox control. *J Mol Biol,* 425**,** 594-608.

BANCI, L., BERTINI, I., CEFARO, C., CIOFI-BAFFONI, S., GALLO, A., MARTINELLI, M., SIDERIS, D. P., KATRAKILI, N. & TOKATLIDIS, K. (2009) MIA40 is an oxidoreductase that catalyzes oxidative protein folding in mitochondria. *Nat Struct Mol Biol,* 16**,** 198-206.

BANCI, L., BERTINI, I., CIOFI-BAFFONI, S., JANICKA, A., MARTINELLI, M., KOZLOWSKI, H. & PALUMAA, P. (2008) A structural-dynamical characterization of human Cox17. *J Biol Chem,* 283**,** 7912-20.

BASU, S., LEONARD, J. C., DESAI, N., MAVRIDOU, D. A., TANG, K. H., GODDARD, A. D., GINGER, M. L., LUKES, J. & ALLEN, J. W. (2012) Divergence of Erv1-associated mitochondrial import and export pathways in trypanosomes and anaerobic protists. *Eukaryot Cell,* 12**,** 343-55.

BECKER, T., PFANNSCHMIDT, S., GUIARD, B., STOJANOVSKI, D., MILENKOVIC, D., KUTIK, S., PFANNER, N., MEISINGER, C. & WIEDEMANN, N. (2008) Biogenesis of the mitochondrial TOM complex: Mim1 promotes insertion and assembly of signal-anchored receptors. *J Biol Chem,* 283**,** 120-7.

BIEN, M., LONGEN, S., WAGENER, N., CHWALLA, I., HERRMANN, J. M. & RIEMER, J. (2010) Mitochondrial disulfide bond formation is driven by inter-subunit electron transfer in Erv1 and proofread by glutathione. *Mol Cell,* 37**,** 516-28.

BIHLMAIER, K., MESECKE, N., KLOEPPEL, C. & HERRMANN, J. M. (2008) The disulfide relay of the intermembrane space of mitochondria: an oxygen-sensing system? *Ann N Y Acad Sci,* 1147**,** 293-302.

BIHLMAIER, K., MESECKE, N., TERZIYSKA, N., BIEN, M., HELL, K. & HERRMANN, J. M. (2007) The disulfide relay system of mitochondria is connected to the respiratory chain. *J Cell Biol,* 179**,** 389-95.

BISHOP, N. A., LU, T. & YANKNER, B. A. (2010) Neural mechanisms of ageing and cognitive decline. *Nature,* 464**,** 529-35.

BRANDON, M., BALDI, P. & WALLACE, D. C. (2006) Mitochondrial mutations in cancer. *Oncogene,* 25**,** 4647-62.

BRAYER, K. J., KULSHRESHTHA, S. & SEGAL, D. J. (2008) The protein-binding potential of C2H2 zinc finger domains. *Cell Biochem Biophys,* 51**,** 9-19.

BRIX, J., DIETMEIER, K. & PFANNER, N. (1997) Differential recognition of preproteins by the purified cytosolic domains of the mitochondrial import receptors Tom20, Tom22, and Tom70. *J Biol Chem,* 272**,** 20730-5.

CAVALLARO, G. (2010) Genome-wide analysis of eukaryotic twin CX9C proteins. *Mol Biosyst,* 6**,** 2459-70.

CHACINSKA, A., GUIARD, B., MULLER, J. M., SCHULZE-SPECKING, A., GABRIEL, K., KUTIK, S. & PFANNER, N. (2008) Mitochondrial biogenesis, switching the sorting pathway of the intermembrane space receptor Mia40. *J Biol Chem,* 283**,** 29723-9.

CHACINSKA, A., KOEHLER, C. M., MILENKOVIC, D., LITHGOW, T. & PFANNER, N. (2009) Importing mitochondrial proteins: machineries and mechanisms. *Cell,* 138**,** 628-44.

CHACINSKA, A., LIND, M., FRAZIER, A. E., DUDEK, J., MEISINGER, C., GEISSLER, A., SICKMANN, A., MEYER, H. E., TRUSCOTT, K. N., GUIARD, B., PFANNER, N. & REHLING, P. (2005) Mitochondrial presequence translocase: switching between TOM tethering and motor recruitment involves Tim21 and Tim17. *Cell,* 120**,** 817-29.

CHACINSKA, A., PFANNSCHMIDT, S., WIEDEMANN, N., KOZJAK, V., SANJUAN SZKLARZ, L. K., SCHULZE-SPECKING, A., TRUSCOTT, K. N., GUIARD, B., MEISINGER, C. & PFANNER, N. (2004) Essential role of Mia40 in import and assembly of mitochondrial intermembrane space proteins. *EMBO J,* 23**,** 3735-46.

CHACINSKA, A., REHLING, P., GUIARD, B., FRAZIER, A. E., SCHULZE-SPECKING, A., PFANNER, N., VOOS, W. & MEISINGER, C. (2003)

Mitochondrial translocation contact sites: separation of dynamic and stabilizing elements in formation of a TOM-TIM-preprotein supercomplex. *EMBO J,* 22**,** 5370-81.

CHAMBERS, J. E., TAVENDER, T. J., OKA, O. B., WARWOOD, S., KNIGHT, D. & BULLEID, N. J. (2010) The reduction potential of the active site disulfides of human protein disulfide isomerase limits oxidation of the enzyme by Ero1alpha. *J Biol Chem,* 285**,** 29200-7.

CHAN, N. C. & LITHGOW, T. (2008) The peripheral membrane subunits of the SAM complex function codependently in mitochondrial outer membrane biogenesis. *Mol Biol Cell,* 19**,** 126-36.

COPPOCK, D. L. & THORPE, C. (2006) Multidomain flavin-dependent sulfhydryl oxidases. *Antioxid Redox Signal,* 8**,** 300-11.

CURRAN, S. P., LEUENBERGER, D., LEVERICH, E. P., HWANG, D. K., BEVERLY, K. N. & KOEHLER, C. M. (2004) The role of Hot13p and redox chemistry in the mitochondrial TIM22 import pathway. *J Biol Chem,* 279**,** 43744-51.

CURRAN, S. P., LEUENBERGER, D., OPPLIGER, W. & KOEHLER, C. M. (2002) The Tim9p-Tim10p complex binds to the transmembrane domains of the ADP/ATP carrier. *EMBO J,* 21**,** 942-53.

DABIR, D. V., LEVERICH, E. P., KIM, S. K., TSAI, F. D., HIRASAWA, M., KNAFF, D. B. & KOEHLER, C. M. (2007) A role for cytochrome c and cytochrome c peroxidase in electron shuttling from Erv1. *EMBO J,* 26**,** 4801-11.

DAITHANKAR, V. N., FARRELL, S. R. & THORPE, C. (2009) Augmenter of liver regeneration: substrate specificity of a flavin-dependent oxidoreductase from the mitochondrial intermembrane space. *Biochemistry,* 48**,** 4828-37.

DAITHANKAR, V. N., SCHAEFER, S. A., DONG, M., BAHNSON, B. J. & THORPE, C. (2010) Structure of the human sulfhydryl oxidase augmenter of liver regeneration and characterization of a human mutation causing an autosomal recessive myopathy. *Biochemistry,* 49**,** 6737-45.

DAITHANKAR, V. N., WANG, W., TRUJILLO, J. R. & THORPE, C. (2012) Flavin-linked Erv-family sulfhydryl oxidases release superoxide anion during catalytic turnover. *Biochemistry,* 51**,** 265-72.

DEKKER, P. J., MARTIN, F., MAARSE, A. C., BOMER, U., MULLER, H., GUIARD, B., MEIJER, M., RASSOW, J. & PFANNER, N. (1997) The Tim core complex defines the number of mitochondrial translocation contact sites

and can hold arrested preproteins in the absence of matrix Hsp70-Tim44. *EMBO J,* 16**,** 5408-19.

DEKKER, P. J., RYAN, M. T., BRIX, J., MULLER, H., HONLINGER, A. & PFANNER, N. (1998) Preprotein translocase of the outer mitochondrial membrane: molecular dissection and assembly of the general import pore complex. *Mol Cell Biol,* 18**,** 6515-24.

DEPUYDT, M., MESSENS, J. & COLLET, J. F. (2011) How proteins form disulfide bonds. *Antioxid Redox Signal,* 15**,** 49-66.

DI FONZO, A., RONCHI, D., LODI, T., FASSONE, E., TIGANO, M., LAMPERTI, C., CORTI, S., BORDONI, A., FORTUNATO, F., NIZZARDO, M., NAPOLI, L., DONADONI, C., SALANI, S., SALADINO, F., MOGGIO, M., BRESOLIN, N., FERRERO, I. & COMI, G. P. (2009) The mitochondrial disulfide relay system protein GFER is mutated in autosomal-recessive myopathy with cataract and combined respiratory-chain deficiency. *Am J Hum Genet,* 84**,** 594-604.

DIENHART, M. K. & STUART, R. A. (2008) The yeast Aac2 protein exists in physical association with the cytochrome bc1-COX supercomplex and the TIM23 machinery. *Mol Biol Cell,* 19**,** 3934-43.

DURIGON, R., WANG, Q., CEH PAVIA, E., GRANT, C. M. & LU, H. (2012) Cytosolic thioredoxin system facilitates the import of mitochondrial small Tim proteins. *EMBO Rep,* 13**,** 916-22.

ECKERS, E., PETRUNGARO, C., GROSS, D., RIEMER, J., HELL, K. & DEPONTE, M. (2013) Divergent molecular evolution of the mitochondrial sulfhydryl:cytochrome C oxidoreductase Erv in opisthokonts and parasitic protists. *J Biol Chem,* 288**,** 2676-88.

ENDO, T., YAMANO, K. & KAWANO, S. (2010) Structural basis for the disulfide relay system in the mitochondrial intermembrane space. *Antioxid Redox Signal,* 13**,** 1359-73.

FARRELL, S. R. & THORPE, C. (2005) Augmenter of liver regeneration: a flavin-dependent sulfhydryl oxidase with cytochrome c reductase activity. *Biochemistry,* 44**,** 1532-41.

FASS, D. (2008) The Erv family of sulfhydryl oxidases. *Biochim Biophys Acta,* 1783**,** 557-66.

FISCHER, M., HORN, S., BELKACEMI, A., KOJER, K., PETRUNGARO, C., HABICH, M., ALI, M., KUTTNER, V., BIEN, M., KAUFF, F., DENGJEL, J., HERRMANN, J. M. & RIEMER, J. (2013) Protein import and oxidative

folding in the mitochondrial intermembrane space of intact mammalian cells. *Mol Biol Cell,* 24**,** 2160-2170.

FISCHER, M. & RIEMER, J. (2013) The Mitochondrial Disulfide Relay System: Roles in Oxidative Protein Folding and Beyond. *Int J Cell Biol,* 2013**,** 742923.

FREY, T. G. & MANNELLA, C. A. (2000) The internal structure of mitochondria. *Trends Biochem Sci,* 25**,** 319-24.

GEBERT, N., CHACINSKA, A., WAGNER, K., GUIARD, B., KOEHLER, C. M., REHLING, P., PFANNER, N. & WIEDEMANN, N. (2008) Assembly of the three small Tim proteins precedes docking to the mitochondrial carrier translocase. *EMBO Rep,* 9**,** 548-54.

GEBERT, N., GEBERT, M., OELJEKLAUS, S., VON DER MALSBURG, K., STROUD, D. A., KULAWIAK, B., WIRTH, C., ZAHEDI, R. P., DOLEZAL, P., WIESE, S., SIMON, O., SCHULZE-SPECKING, A., TRUSCOTT, K. N., SICKMANN, A., REHLING, P., GUIARD, B., HUNTE, C., WARSCHEID, B., VAN DER LAAN, M., PFANNER, N. & WIEDEMANN, N. (2011) Dual function of Sdh3 in the respiratory chain and TIM22 protein translocase of the mitochondrial inner membrane. *Mol Cell,* 44**,** 811-8.

GEVORKYAN-AIRAPETOV, L., ZOHARY, K., POPOV-CELEKETIC, D., MAPA, K., HELL, K., NEUPERT, W., AZEM, A. & MOKRANJAC, D. (2009) Interaction of Tim23 with Tim50 Is essential for protein translocation by the mitochondrial TIM23 complex. *J Biol Chem,* 284**,** 4865-72.

GOODSELL, D. S. & OLSON, A. J. (2000) Structural symmetry and protein function. *Annu Rev Biophys Biomol Struct,* 29**,** 105-53.

GROSS, E., SEVIER, C. S., VALA, A., KAISER, C. A. & FASS, D. (2002) A new FAD-binding fold and inter-subunit disulfide shuttle in the thiol oxidase Erv2p. *Nat Struct Biol,* 9**,** 61-7.

GRUMBT, B., STROOBANT, V., TERZIYSKA, N., ISRAEL, L. & HELL, K. (2007) Functional characterization of Mia40p, the central component of the disulfide relay system of the mitochondrial intermembrane space. *J Biol Chem,* 282**,** 37461-70.

GUO, P. C., MA, J. D., JIANG, Y. L., WANG, S. J., BAO, Z. Z., YU, X. J., CHEN, Y. & ZHOU, C. Z. (2012) Structure of yeast sulfhydryl oxidase erv1 reveals electron transfer of the disulfide relay system in the mitochondrial intermembrane space. *J Biol Chem,* 287**,** 34961-9.

HAKIM, M., MANDELBAUM, A. & FASS, D. (2011) Structure of a baculovirus sulfhydryl oxidase, a highly divergent member of the erv flavoenzyme family. *J Virol,* 85**,** 9406-13.

HECKLER, E. J., RANCY, P. C., KODALI, V. K. & THORPE, C. (2008) Generating disulfides with the Quiescin-sulfhydryl oxidases. *Biochim Biophys Acta,* 1783**,** 567-77.

HERRMANN, J. M. & RIEMER, J. (2012) Mitochondrial disulfide relay: redox-regulated protein import into the intermembrane space. *J Biol Chem,* 287**,** 4426-33.

HILL, K., MODEL, K., RYAN, M. T., DIETMEIER, K., MARTIN, F., WAGNER, R. & PFANNER, N. (1998) Tom40 forms the hydrophilic channel of the mitochondrial import pore for preproteins [see comment]. *Nature,* 395**,** 516-21.

HOFHAUS, G., LEE, J. E., TEWS, I., ROSENBERG, B. & LISOWSKY, T. (2003) The N-terminal cysteine pair of yeast sulfhydryl oxidase Erv1p is essential for in vivo activity and interacts with the primary redox centre. *Eur J Biochem,* 270**,** 1528-35.

HOFMANN, S., ROTHBAUER, U., MUHLENBEIN, N., BAIKER, K., HELL, K. & BAUER, M. F. (2005) Functional and mutational characterization of human MIA40 acting during import into the mitochondrial intermembrane space. *J Mol Biol,* 353**,** 517-28.

HOOBER, K. L., JONEJA, B., WHITE, H. B., 3RD & THORPE, C. (1996) A sulfhydryl oxidase from chicken egg white. *J Biol Chem,* 271**,** 30510-6.

HULETT, J. M., LUEDER, F., CHAN, N. C., PERRY, A. J., WOLYNEC, P., LIKIC, V. A., GOOLEY, P. R. & LITHGOW, T. (2008) The transmembrane segment of Tom20 is recognized by Mim1 for docking to the mitochondrial TOM complex. *J Mol Biol,* 376**,** 694-704.

INABA, K. (2010) Structural basis of protein disulfide bond generation in the cell. *Genes Cells,* 15**,** 935-43.

KAWANO, S., YAMANO, K., NAOE, M., MOMOSE, T., TERAO, K., NISHIKAWA, S., WATANABE, N. & ENDO, T. (2009) Structural basis of yeast Tim40/Mia40 as an oxidative translocator in the mitochondrial intermembrane space. *Proc Natl Acad Sci U S A,* 106**,** 14403-7.

KODALI, V. K. & THORPE, C. (2010) Oxidative protein folding and the Quiescin-sulfhydryl oxidase family of flavoproteins. *Antioxid Redox Signal,* 13**,** 1217-30.

KOJER, K., BIEN, M., GANGEL, H., MORGAN, B., DICK, T. P. & RIEMER, J. (2012) Glutathione redox potential in the mitochondrial intermembrane space is linked to the cytosol and impacts the Mia40 redox state. *EMBO J,* 31**,** 3169-82.

KOVERMANN, P., TRUSCOTT, K. N., GUIARD, B., REHLING, P., SEPURI, N. B., MULLER, H., JENSEN, R. E., WAGNER, R. & PFANNER, N. (2002) Tim22, the essential core of the mitochondrial protein insertion complex, forms a voltage-activated and signal-gated channel. *Mol Cell,* 9**,** 363-73.

KOZIOL, J. (1971) Fluoremetric analyses of riboflavin and its coenzymes. *Methods in Enzymology,* 18**,** 253-285.

KURZ, M., MARTIN, H., RASSOW, J., PFANNER, N. & RYAN, M. T. (1999) Biogenesis of Tim proteins of the mitochondrial carrier import pathway: differential targeting mechanisms and crossing over with the main import pathway. *Mol Biol Cell,* 10**,** 2461-74.

KUTIK, S., STOJANOVSKI, D., BECKER, L., BECKER, T., MEINECKE, M., KRUGER, V., PRINZ, C., MEISINGER, C., GUIARD, B., WAGNER, R., PFANNER, N. & WIEDEMANN, N. (2008) Dissecting membrane insertion of mitochondrial beta-barrel proteins. *Cell,* 132**,** 1011-24.

LANGE, H., LISOWSKY, T., GERBER, J., MUHLENHOFF, U., KISPAL, G. & LILL, R. (2001) An essential function of the mitochondrial sulfhydryl oxidase Erv1p/ALR in the maturation of cytosolic Fe/S proteins. *EMBO Rep,* 2**,** 715-20.

LEE, J., HOFHAUS, G. & LISOWSKY, T. (2000) Erv1p from Saccharomyces cerevisiae is a FAD-linked sulfhydryl oxidase. *FEBS Lett,* 477**,** 62-6.

LEVITAN, A., DANON, A. & LISOWSKY, T. (2004) Unique features of plant mitochondrial sulfhydryl oxidase. *J Biol Chem,* 279**,** 20002-8.

LINDSAY, H., BEAUMONT, E., RICHARDS, S. D., KELLY, S. M., SANDERSON, S. J., PRICE, N. C. & LINDSAY, J. G. (2000) FAD insertion is essential for attaining the assembly competence of the dihydrolipoamide dehydrogenase (E3) monomer from Escherichia coli. *J Biol Chem,* 275**,** 36665-70.

LISOWSKY, T. (1992) Dual function of a new nuclear gene for oxidative phosphorylation and vegetative growth in yeast. *Mol Gen Genet,* 232**,** 58-64.

LISOWSKY, T. (1994) ERV1 is involved in the cell-division cycle and the maintenance of mitochondrial genomes in Saccharomyces cerevisiae. *Curr Genet,* 26**,** 15-20.

LISOWSKY, T., LEE, J. E., POLIMENO, L., FRANCAVILLA, A. & HOFHAUS, G. (2001) Mammalian augmenter of liver regeneration protein is a sulfhydryl oxidase. *Dig Liver Dis,* 33**,** 173-80.

LONG, C. M., ROHRMANN, G. F. & MERRILL, G. F. (2009) The conserved baculovirus protein p33 (Ac92) is a flavin adenine dinucleotide-linked sulfhydryl oxidase. *Virology,* 388**,** 231-5.

LONGEN, S., BIEN, M., BIHLMAIER, K., KLOEPPEL, C., KAUFF, F., HAMMERMEISTER, M., WESTERMANN, B., HERRMANN, J. M. & RIEMER, J. (2009) Systematic analysis of the twin cx(9)c protein family. *J Mol Biol,* 393**,** 356-68.

LONGEN, S., WOELLHAF, M. W., PETRUNGARO, C., RIEMER, J. & HERRMANN, J. M. (2013) The Disulfide Relay of the Intermembrane Space Oxidizes the Ribosomal Subunit Mrp10 on Its Transit into the Mitochondrial Matrix. *Dev Cell*.

LU, H. & WOODBURN, J. (2005) Zinc binding stabilizes mitochondrial Tim10 in a reduced and import-competent state kinetically. *J Mol Biol,* 353**,** 897-910.

LUTZ, T., NEUPERT, W. & HERRMANN, J. M. (2003) Import of small Tim proteins into the mitochondrial intermembrane space. *EMBO J,* 22**,** 4400-8.

MANNELLA, C. A. (2006) The relevance of mitochondrial membrane topology to mitochondrial function. *Biochim Biophys Acta,* 1762**,** 140-7.

MARTIN, S. R. & SCHILSTRA, M. J. (2008) Circular dichroism and its application to the study of biomolecules. *Methods Cell Biol,* 84**,** 263-93.

MASSEY, V. (2000) The chemical and biological versatility of riboflavin. *Biochem Soc Trans,* 28**,** 283-96.

MASSEY, V. & PALMER, G. (1966) On the existence of spectrally distinct classes of flavoprotein semiquinones. A new method for the quantitative production of flavoprotein semiquinones. *Biochemistry,* 5**,** 3181-9.

MATTEVI, A. (2006) To be or not to be an oxidase: challenging the oxygen reactivity of flavoenzymes. *Trends Biochem Sci,* 31**,** 276-83.

MCBRIDE, H. M., NEUSPIEL, M. & WASIAK, S. (2006) Mitochondria: more than just a powerhouse. *Curr Biol,* 16**,** R551-60.

MESECKE, N., BIHLMAIER, K., GRUMBT, B., LONGEN, S., TERZIYSKA, N., HELL, K. & HERRMANN, J. M. (2008) The zinc-binding protein Hot13 promotes oxidation of the mitochondrial import receptor Mia40. *EMBO Rep,* 9**,** 1107-13.

MESECKE, N., TERZIYSKA, N., KOZANY, C., BAUMANN, F., NEUPERT, W., HELL, K. & HERRMANN, J. M. (2005) A disulfide relay system in the intermembrane space of mitochondria that mediates protein import. *Cell,* 121**,** 1059-69.

MILENKOVIC, D., GABRIEL, K., GUIARD, B., SCHULZE-SPECKING, A., PFANNER, N. & CHACINSKA, A. (2007) Biogenesis of the essential Tim9-Tim10 chaperone complex of mitochondria: site-specific recognition of cysteine residues by the intermembrane space receptor Mia40. *J Biol Chem,* 282**,** 22472-80.

MILENKOVIC, D., RAMMING, T., MULLER, J. M., WENZ, L. S., GEBERT, N., SCHULZE-SPECKING, A., STOJANOVSKI, D., ROSPERT, S. & CHACINSKA, A. (2009) Identification of the signal directing Tim9 and Tim10 into the intermembrane space of mitochondria. *Mol Biol Cell,* 20**,** 2530-9.

MODEL, K., MEISINGER, C., PRINZ, T., WIEDEMANN, N., TRUSCOTT, K. N., PFANNER, N. & RYAN, M. T. (2001) Multistep assembly of the protein import channel of the mitochondrial outer membrane. *Nat Struct Biol,* 8**,** 361-70.

MORGAN, B., ANG, S. K., YAN, G. & LU, H. (2009) Zinc can play chaperone-like and inhibitor roles during import of mitochondrial small Tim proteins. *J Biol Chem,* 284**,** 6818-25.

MORGAN, B. & LU, H. (2008) Oxidative folding competes with mitochondrial import of the small Tim proteins. *Biochem J,* 411**,** 115-22.

MUNRO, A. W. & NOBLE, M. A. (1999) Fluorescence analysis of flavoproteins. *Methods Mol Biol,* 131**,** 25-48.

NAOE, M., OHWA, Y., ISHIKAWA, D., OHSHIMA, C., NISHIKAWA, S., YAMAMOTO, H. & ENDO, T. (2004) Identification of Tim40 that mediates protein sorting to the mitochondrial intermembrane space. *J Biol Chem,* 279**,** 47815-21.

NEUPERT, W. & HERRMANN, J. M. (2007) Translocation of proteins into mitochondria. *Annu Rev Biochem,* 76**,** 723-49.

NOOREN, I. M. & THORNTON, J. M. (2003) Diversity of protein-protein interactions. *EMBO J,* 22**,** 3486-92.

OTERA, H., TAIRA, Y., HORIE, C., SUZUKI, Y., SUZUKI, H., SETOGUCHI, K., KATO, H., OKA, T. & MIHARA, K. (2007) A novel insertion pathway of mitochondrial outer membrane proteins with multiple transmembrane segments. *J Cell Biol,* 179**,** 1355-63.

PAPIC, D., KRUMPE, K., DUKANOVIC, J., DIMMER, K. S. & RAPAPORT, D. (2011) Multispan mitochondrial outer membrane protein Ugo1 follows a unique Mim1-dependent import pathway. *J Cell Biol,* 194**,** 397-405.

PASCHEN, S. A., NEUPERT, W. & RAPAPORT, D. (2005) Biogenesis of beta-barrel membrane proteins of mitochondria. *Trends Biochem Sci,* 30**,** 575-82.

POPOV-CELEKETIC, J., WAIZENEGGER, T. & RAPAPORT, D. (2008) Mim1 functions in an oligomeric form to facilitate the integration of Tom20 into the mitochondrial outer membrane. *J Mol Biol,* 376**,** 671-80.

RAJE, S. & THORPE, C. (2003) Inter-domain redox communication in flavoenzymes of the quiescin/sulfhydryl oxidase family: role of a thioredoxin domain in disulfide bond formation. *Biochemistry,* 42**,** 4560-8.

REHLING, P., MODEL, K., BRANDNER, K., KOVERMANN, P., SICKMANN, A., MEYER, H. E., KUHLBRANDT, W., WAGNER, R., TRUSCOTT, K. N. & PFANNER, N. (2003) Protein insertion into the mitochondrial inner membrane by a twin-pore translocase. *Science,* 299**,** 1747-51.

RIGBY, K., ZHANG, L., COBINE, P. A., GEORGE, G. N. & WINGE, D. R. (2007) characterization of the cytochrome c oxidase assembly factor Cox19 of Saccharomyces cerevisiae. *J Biol Chem,* 282**,** 10233-42.

SCHAEFER-RAMADAN, S., GANNON, S. A. & THORPE, C. (2013) Human augmenter of liver regeneration: probing the catalytic mechanism of a flavin-dependent sulfhydryl oxidase. *Biochemistry,* 52**,** 8323-32.

SEVIER, C. S. (2012) Erv2 and quiescin sulfhydryl oxidases: Erv-domain enzymes associated with the secretory pathway. *Antioxid Redox Signal,* 16**,** 800-8.

SEVIER, C. S., CUOZZO, J. W., VALA, A., ASLUND, F. & KAISER, C. A. (2001) A flavoprotein oxidase defines a new endoplasmic reticulum pathway for biosynthetic disulphide bond formation. *Nat Cell Biol,* 3**,** 874-82.

SEVIER, C. S. & KAISER, C. A. (2006) Conservation and diversity of the cellular disulfide bond formation pathways. *Antioxid Redox Signal,* 8**,** 797-811.

SHIOTA, T., MABUCHI, H., TANAKA-YAMANO, S., YAMANO, K. & ENDO, T. (2011) In vivo protein-interaction mapping of a mitochondrial translocator protein Tom22 at work. *Proc Natl Acad Sci U S A,* 108**,** 15179-83.

SIDERIS, D. P., PETRAKIS, N., KATRAKILI, N., MIKROPOULOU, D., GALLO, A., CIOFI-BAFFONI, S., BANCI, L., BERTINI, I. & TOKATLIDIS, K. (2009) A novel intermembrane space-targeting signal docks cysteines onto Mia40 during mitochondrial oxidative folding. *J Cell Biol,* 187**,** 1007-22.

SIDERIS, D. P. & TOKATLIDIS, K. (2007) Oxidative folding of small Tims is mediated by site-specific docking onto Mia40 in the mitochondrial intermembrane space. *Mol Microbiol,* 65**,** 1360-73.

SIRRENBERG, C., BAUER, M. F., GUIARD, B., NEUPERT, W. & BRUNNER, M. (1996) Import of carrier proteins into the mitochondrial inner membrane mediated by Tim22. *Nature,* 384**,** 582-5.

SPILLER, M. P., ANG, S. K., CEH-PAVIA, E., FISHER, K., WANG, Q., RIGBY, S. E. & LU, H. (2013) Identification and characterisation of mitochondrial Mia40 as an iron-sulphur protein. *Biochem J*.

STOJANOVSKI, D., BOHNERT, M., PFANNER, N. & VAN DER LAAN, M. (2012) Mechanisms of protein sorting in mitochondria. *Cold Spring Harb Perspect Biol,* 4.

STOJANOVSKI, D., MILENKOVIC, D., MULLER, J. M., GABRIEL, K., SCHULZE-SPECKING, A., BAKER, M. J., RYAN, M. T., GUIARD, B., PFANNER, N. & CHACINSKA, A. (2008) Mitochondrial protein import: precursor oxidation in a ternary complex with disulfide carrier and sulfhydryl oxidase. *J Cell Biol,* 183**,** 195-202.

SZTOLSZTENER, M. E., BREWINSKA, A., GUIARD, B. & CHACINSKA, A. (2013) Disulfide bond formation: sulfhydryl oxidase ALR controls mitochondrial biogenesis of human MIA40. *Traffic,* 14**,** 309-20.

TAHALLAH, N., VAN DEN HEUVEL, R. H., VAN DEN BERG, W. A., MAIER, C. S., VAN BERKEL, W. J. & HECK, A. J. (2002) Cofactor-dependent assembly of the flavoenzyme vanillyl-alcohol oxidase. *J Biol Chem,* 277**,** 36425-32.

TAMURA, Y., HARADA, Y., SHIOTA, T., YAMANO, K., WATANABE, K., YOKOTA, M., YAMAMOTO, H., SESAKI, H. & ENDO, T. (2009) Tim23-Tim50 pair coordinates functions of translocators and motor proteins in mitochondrial protein import. *J Cell Biol,* 184**,** 129-41.

TAYLOR, A. B., SMITH, B. S., KITADA, S., KOJIMA, K., MIYAURA, H., OTWINOWSKI, Z., ITO, A. & DEISENHOFER, J. (2001) Crystal structures of mitochondrial processing peptidase reveal the mode for specific cleavage of import signal sequences. *Structure,* 9**,** 615-25.

TERZIYSKA, N., GRUMBT, B., KOZANY, C. & HELL, K. (2009) Structural and functional roles of the conserved cysteine residues of the redox-regulated import receptor Mia40 in the intermembrane space of mitochondria. *J Biol Chem,* 284**,** 1353-63.

TERZIYSKA, N., LUTZ, T., KOZANY, C., MOKRANJAC, D., MESECKE, N., NEUPERT, W., HERRMANN, J. M. & HELL, K. (2005) Mia40, a novel factor for protein import into the intermembrane space of mitochondria is able to bind metal ions. *FEBS Lett,* 579**,** 179-84.

TIENSON, H. L., DABIR, D. V., NEAL, S. E., LOO, R., HASSON, S. A., BOONTHEUNG, P., KIM, S. K., LOO, J. A. & KOEHLER, C. M. (2009) Reconstitution of the mia40-erv1 oxidative folding pathway for the small tim proteins. *Mol Biol Cell,* 20**,** 3481-90.

VALA, A., SEVIER, C. S. & KAISER, C. A. (2005) Structural determinants of substrate access to the disulfide oxidase Erv2p. *J Mol Biol,* 354**,** 952-66.

VAN DER LAAN, M., MEINECKE, M., DUDEK, J., HUTU, D. P., LIND, M., PERSCHIL, I., GUIARD, B., WAGNER, R., PFANNER, N. & REHLING, P. (2007) Motor-free mitochondrial presequence translocase drives membrane integration of preproteins. *Nat Cell Biol,* 9**,** 1152-9.

VAN WILPE, S., RYAN, M. T., HILL, K., MAARSE, A. C., MEISINGER, C., BRIX, J., DEKKER, P. J., MOCZKO, M., WAGNER, R., MEIJER, M., GUIARD, B., HONLINGER, A. & PFANNER, N. (1999) Tom22 is a multifunctional organizer of the mitochondrial preprotein translocase. *Nature,* 401**,** 485-9.

VITU, E., BENTZUR, M., LISOWSKY, T., KAISER, C. A. & FASS, D. (2006) Gain of function in an ERV/ALR sulfhydryl oxidase by molecular engineering of the shuttle disulfide. *J Mol Biol,* 362**,** 89-101.

VORONOVA, A., MEYER-KLAUCKE, W., MEYER, T., ROMPEL, A., KREBS, B., KAZANTSEVA, J., SILLARD, R. & PALUMAA, P. (2007) Oxidative switches in functioning of mammalian copper chaperone Cox17. *Biochem J,* 408**,** 139-48.

WAGNER, K., GEBERT, N., GUIARD, B., BRANDNER, K., TRUSCOTT, K. N., WIEDEMANN, N., PFANNER, N. & REHLING, P. (2008) The assembly pathway of the mitochondrial carrier translocase involves four preprotein translocases. *Mol Cell Biol,* 28**,** 4251-60.

WALLACE, D. C. (2005) A mitochondrial paradigm of metabolic and degenerative diseases, aging, and cancer: a dawn for evolutionary medicine. *Annu Rev Genet,* 39**,** 359-407.

WANG, W., WINTHER, J. R. & THORPE, C. (2007) Erv2p: characterization of the redox behavior of a yeast sulfhydryl oxidase. *Biochemistry,* 46**,** 3246-54.

WEBB, C. T., GORMAN, M. A., LAZAROU, M., RYAN, M. T. & GULBIS, J. M. (2006) Crystal structure of the mitochondrial chaperone TIM9.10 reveals a six-bladed alpha-propeller. *Mol Cell,* 21**,** 123-33.

WECKBECKER, D., LONGEN, S., RIEMER, J. & HERRMANN, J. M. (2012) Atp23 biogenesis reveals a chaperone-like folding activity of Mia40 in the IMS of mitochondria. *EMBO J,* 31**,** 4348-58.

WIEDEMANN, N., PFANNER, N. & RYAN, M. T. (2001) The three modules of ADP/ATP carrier cooperate in receptor recruitment and translocation into mitochondria. *EMBO J,* 20**,** 951-60.

WIEDEMANN, N., TRUSCOTT, K. N., PFANNSCHMIDT, S., GUIARD, B., MEISINGER, C. & PFANNER, N. (2004) Biogenesis of the protein import channel Tom40 of the mitochondrial outer membrane: intermembrane space components are involved in an early stage of the assembly pathway. *J Biol Chem,* 279**,** 18188-94.

WOUTERS, M. A., FAN, S. W. & HAWORTH, N. L. (2010) Disulfides as redox switches: from molecular mechanisms to functional significance. *Antioxid Redox Signal,* 12**,** 53-91.

WROBEL, L., TROJANOWSKA, A., SZTOLSZTENER, M. E. & CHACINSKA, A. (2013) Mitochondrial protein import: Mia40 facilitates Tim22 translocation into the inner membrane of mitochondria. *Mol Biol Cell,* 24**,** 543-54.

WU, C. K., DAILEY, T. A., DAILEY, H. A., WANG, B. C. & ROSE, J. P. (2003) The crystal structure of augmenter of liver regeneration: A mammalian FAD-dependent sulfhydryl oxidase. *Protein Sci,* 12**,** 1109-18.

WU, Y. & SHA, B. (2006) Crystal structure of yeast mitochondrial outer membrane translocon member Tom70p. *Nat Struct Mol Biol,* 13**,** 589-93.

YOUNG, J. C., HOOGENRAAD, N. J. & HARTL, F. U. (2003) Molecular chaperones Hsp90 and Hsp70 deliver preproteins to the mitochondrial import receptor Tom70. *Cell,* 112**,** 41-50.

ZARA, V., FERRAMOSCA, A., CAPOBIANCO, L., BALTZ, K. M., RANDEL, O., RASSOW, J., PALMIERI, F. & PAPATHEODOROU, P. (2007) Biogenesis of yeast dicarboxylate carrier: the carrier signature facilitates translocation across the mitochondrial outer membrane. *J Cell Sci,* 120**,** 4099-106.

ZARA, V., FERRAMOSCA, A., ROBITAILLE-FOUCHER, P., PALMIERI, F. & YOUNG, J. C. (2009) Mitochondrial carrier protein biogenesis: role of the chaperones Hsc70 and Hsp90. *Biochem J,* 419**,** 369-75.

ZHANG, R. M. & SNYDER, G. H. (1989) Dependence of formation of small disulfide loops in two-cysteine peptides on the number and types of intervening amino acids. *J Biol Chem,* 264**,** 18472-9.

8. APPENDICES

Appendix 1: Determination of superoxide production by Erv1

Reduction of oxygen by flavoenzymes can yield water, superoxide (O_2^-) or hydrogen peroxide (H_2O_2) as the final product (Massey, 1995). Recently, studies using human ALR showed that its rate of oxygen consumption decreased in the presence of superoxide dismutase (SOD), an enzyme that scavenges O_2^- (Daithankar et al., 2012). Here, similar experiments using Erv1 also showed a decrease in the rate of oxygen consumption when 5 mM TCEP was used as electron donor (Figure 9.1). In the absence of SOD the rate of oxygen consumption was 380 μM/min, but when SOD was added (80 U/mL) the rate of oxygen consumption decreased to 132 μM/min.

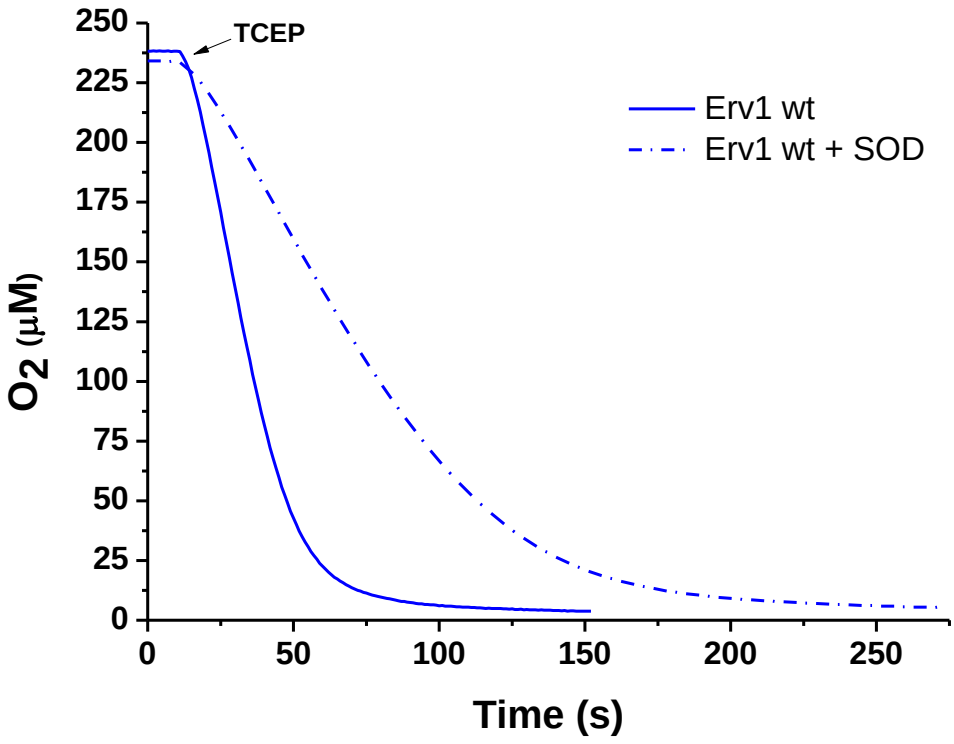

Figure 9.1 Formation of superoxide by Erv1

Oxygen consumption profile of Erv1 wt (3 μM) in the presence (—) or absence (-··-) of 80 U/mL of superoxide dismutase. Reactions were done at 25ºC in BAE with 5 mM TCEP as electron donor. The difference in the rate of reaction represents the superoxide/TCEP-mediated oxygen consumption.

This unexpected result is explained by an oxygen-phosphine radical chain reaction that consumes oxygen independently of ALR, and which was initiated by O_2^- (Figure 9.2). Thus, in the presence of SOD the side reaction was absent and the rate of oxygen consumption decreased (Daithankar et al., 2012). The percentage of oxygen consumed that is transformed into O_2^- can be calculated by taking advantage of this side reaction (Daithankar et al., 2012). In the absence of SOD the total turnover number ($TN_{No\,SOD}$) can be defined by the sum of three separate turnover numbers (equation 1): 1) production of water or H_2O_2 ($TN_{H_2O\,or\,H_2O_2}$), 2) production of O_2^- ($TN_{O_2^-}$), and 3) oxygen consumption propagated by a factor *F* from the interaction of O_2^- with TCEP ($F \times TN_{O_2^-}$). The total turnover number in the presence of SOD (TN_{SOD}) also includes the production of O_2^- and that of water or H_2O_2. However, in this case, and assuming O_2^- dismutates without reacting with TCEP, there is an extra oxygen molecule ($0.5TN_{O_2^-}$) formed by SOD (equation 2). Equations can then be obtained for $TN_{O_2^-}$ and $TN_{H_2O\,or\,H_2O_2}$ by subtracting these two total turnover numbers and rearranging the formulas (equation 3 and 4). Using the propagation factor for TCEP *F*=4.5 (Daithankar et al., 2012) a superoxide percentage of 38% was obtained (equation 5). This means about a third of the oxygen consumed is released as O_2^- when TCEP is used as electron donor of Erv1. The remaining 62% is released as either water or H_2O_2.

$$TN_{No\,SOD} = TN_{H_2O\,or\,H_2O_2} + TN_{O_2^-} + F \times TN_{O_2^-} \quad (1)$$

$$TN_{SOD} = TN_{H_2O\,or\,H_2O_2} + TN_{O_2^-} - 0.5 \times TN_{O_2^-} \quad (2)$$

$$TN_{O_2^-} = \frac{TN_{No\,SOD} - TN_{SOD}}{F - 0.5} = \frac{\Delta TN}{F - 0.5} \quad (3)$$

$$TN_{H_2O\,or\,H_2O_2} = TN_{Oxygen} - \frac{\Delta TN}{2F - 1} \quad (4)$$

$$Superoxide\ \% = 100 \times \left(\frac{TN_{O_2^-}}{TN_{O_2^-} + TN_{H_2O\,or\,H_2O_2}} \right) \quad (5)$$

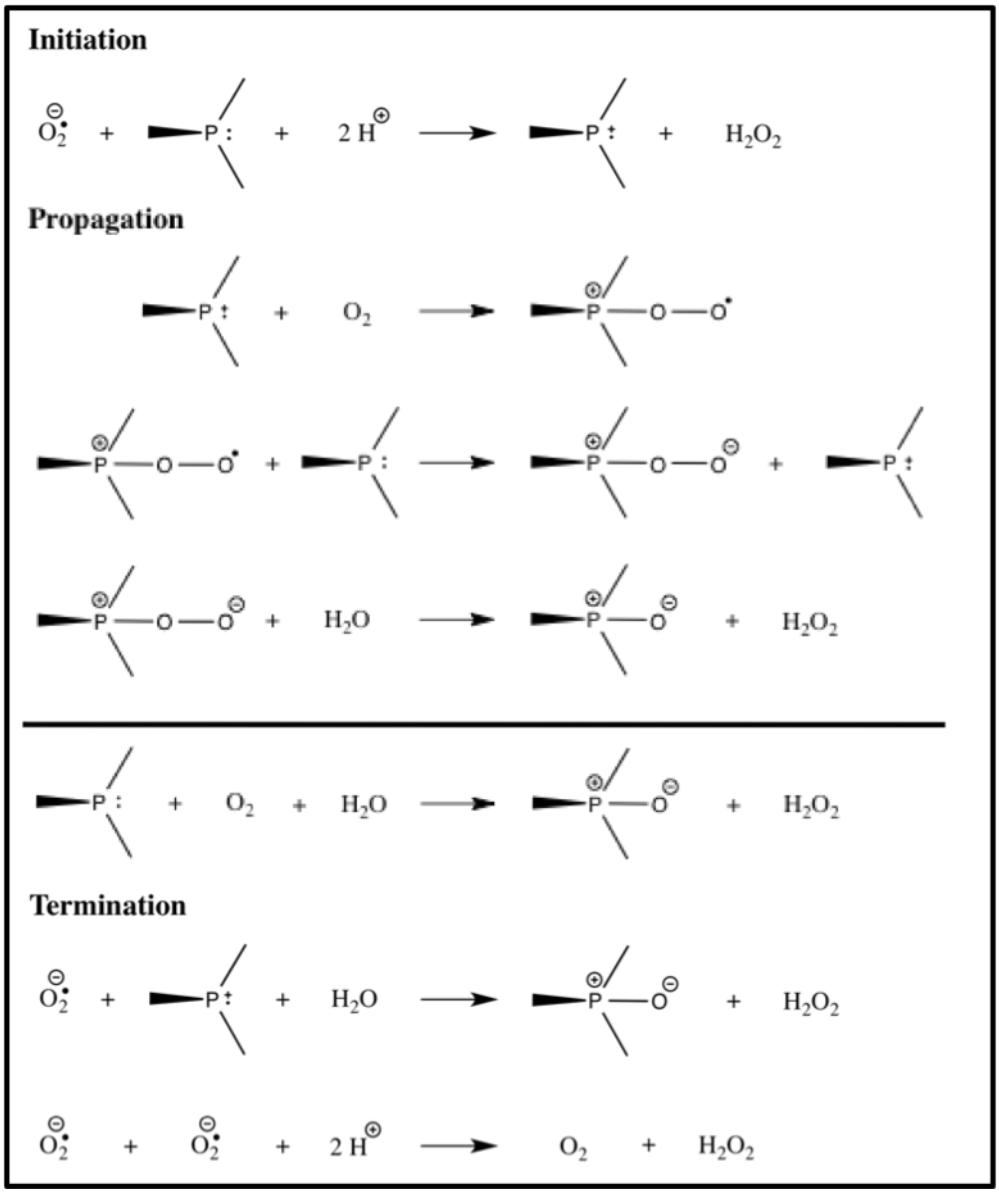

Figure 9.2 Proposed mechanism for the superoxide-catalysed oxygen consumption.

The chain reaction is initiated by superoxide reacting with phosphine (e.g. TCEP, THP) to form a phosphinium radical cation and hydrogen peroxide. Propagation steps include various phosphinium radical species with the overall consumption of oxygen and phosphine. Termination can occur by superoxide dismutation or the reaction of superoxide with a phosphinium radical cation.

DAITHANKAR, V. N., WANG, W., TRUJILLO, J. R. & THORPE, C. (2012) Flavin-linked Erv-family sulfhydryl oxidases release superoxide anion during catalytic turnover. *Biochemistry,* 51, 265-72.

MASSEY, V. (1995) Introduction: flavoprotein structure and mechanism. *FASEB J,* 9, 473-5.

Appendix 2: Effect of other mutations on Erv1

Chapter 5 showed the enzymatic activity of Erv1 fails in the Erv1 R182H mutant. Protein break down is due to a weaker FAD binding that causes FAD to be released during a reaction. And yet, the actual link between the defect and the R182H mutation is still missing. Why is FAD more weakly bound in the mutant? One possibility is that the hydrogen bond between R182 and the 2'-OH of the ribose moiety of FAD (Figure 9.3 A) (Guo et al., 2012) is disrupted in the Erv1 R182H mutant. To test the importance of hydrogen bonding in the stability of FAD binding other Erv1 mutants were tested for their oxidase activity (Figure 9.3 B). Initially, the tryptophan to phenylalanine mutant Erv1 W183F was checked for its oxygen consumption using 5 mM TCEP at 37°C. This mutant was selected because it has completely lost the hydrogen bond between W183 and FAD, and is close to R182. The mutant also forms a dimer so is structurally similar to Erv1 R182H. The data shows a much stronger oxidase activity defect for the Erv1 W183F mutant. At concentrations of 1 μM Erv1 R182H consumed ~60 μM of oxygen but Erv1 W183F only consumed ~12 μM of oxygen. This result implies the complete removal of a hydrogen bond that links the protein to FAD, in the region near R182, causes a strong defect on the oxidase activity of Erv1.

Next, when the arginine at position 182 was mutated into alanine (Erv1 R182A), the results obtained were quite puzzling. The Erv1 R182A mutant complete lacks the ability to make a hydrogen bond with FAD at position 182, and yet, its oxidase activity was somewhere between that of Erv1 wt and Erv1 R182H (Figure 9.3 B). Its final oxygen consumption was ~130 μM. Thus, the extent to which the hydrogen bond between R182 and FAD is important remains unclear.

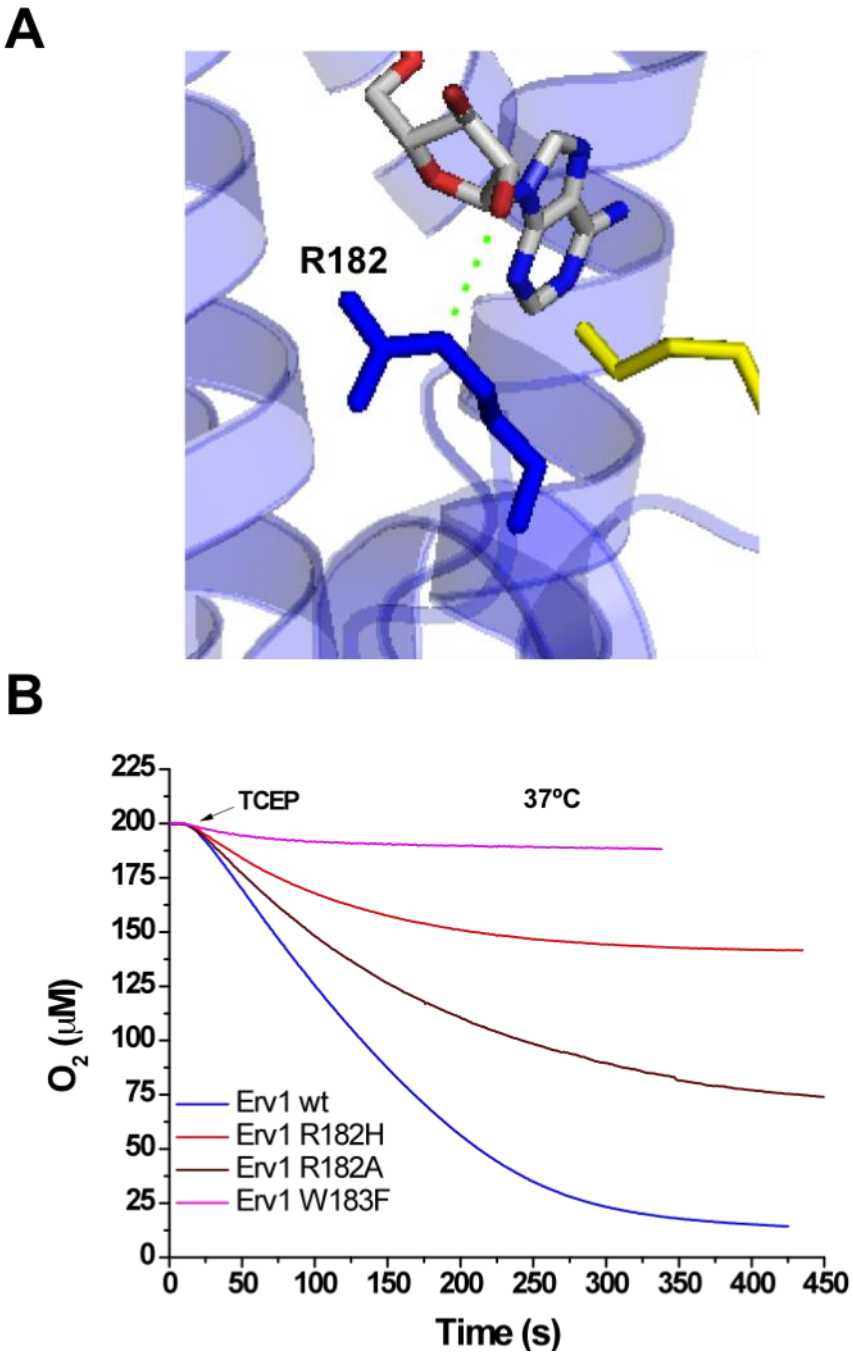

Figure 9.3 A Weaker hydrogen bond linked to the Erv1 R182H defect

A) Crystal structure of *Sc*Erv1 showing the hydrogen bond (dotted green) between arginine at position 182 and the 2'-OH of the ribose moiety of FAD. PDB: 4E0H.

B) Oxygen consumption profile of Erv1 wt (blue, 1 μM), Erv1 R182H (red, 1 μM), Erv1 R182A (dark red, 1 μM) and Erv1 W183F (magenta, 1 μM) using 5 mM TCEP as electron donor. Reactions were done at 37ºC in BAE buffer in the presence of 80 U/mL of superoxide dismutase.

GUO, P. C., MA, J. D., JIANG, Y. L., WANG, S. J., BAO, Z. Z., YU, X. J., CHEN, Y. & ZHOU, C. Z. (2012) Structure of yeast sulfhydryl oxidase erv1 reveals electron transfer of the disulfide relay system in the mitochondrial intermembrane space. *J Biol Chem,* 287**,** 34961-9.

Appendix 3: Publications

Publication 1

CEH-PAVIA, E., SPILLER, M. P. & LU, H. (2013) Folding and biogenesis of mitochondria small Tim proteins. *Int J Mol Sci,* 14**,** 16685-705.

Int. J. Mol. Sci. **2013**, *14*, 16685-16705; doi:10.3390/ijms140816685

OPEN ACCESS
International Journal of
Molecular Sciences
ISSN 1422-0067
www.mdpi.com/journal/ijms

Review

Folding and Biogenesis of Mitochondrial Small Tim Proteins

Efrain Ceh-Pavia †, Michael P. Spiller † and Hui Lu *

Manchester Institute of Biotechnology, Faculty of Life Sciences,
University of Manchester, 131 Princess Street, Manchester M1 7DN, UK;
E-Mails: efrain.cehpavia@postgrad.manchester.ac.uk (E.C.-P.);
michael.spiller@manchester.ac.uk (M.P.S.)

† These authors contributed equally to this work.

* Author to whom correspondence should be addressed; E-Mail: hui.lu@manchester.ac.uk;
Tel.: +44-161-275-1553; Fax: +44-161-306-5201.

*Received: 28 June 2013; in revised form: 1 August 2013 / Accepted: 7 August 2013 /
Published: 13 August 2013*

Abstract: Correct and timely folding is critical to the function of all proteins. The importance of this is illustrated in the biogenesis of the mitochondrial intermembrane space (IMS) "small Tim" proteins. Biogenesis of the small Tim proteins is regulated by dedicated systems or pathways, beginning with synthesis in the cytosol and ending with assembly of individually folded proteins into functional complexes in the mitochondrial IMS. The process is mostly centered on regulating the redox states of the conserved cysteine residues: oxidative folding is crucial for protein function in the IMS, but oxidized (disulfide bonded) proteins cannot be imported into mitochondria. How the redox-sensitive small Tim precursor proteins are maintained in a reduced, import-competent form in the cytosol is not well understood. Recent studies suggest that zinc and the cytosolic thioredoxin system play a role in the biogenesis of these proteins. In the IMS, the mitochondrial import and assembly (MIA) pathway catalyzes both import into the IMS and oxidative folding of the small Tim proteins. Finally, assembly of the small Tim complexes is a multistep process driven by electrostatic and hydrophobic interactions; however, the chaperone function of the complex might require destabilization of these interactions to accommodate the substrate. Here, we review how folding of the small Tim proteins is regulated during their biogenesis, from maintenance of the unfolded precursors in the cytosol, to their import, oxidative folding, complex assembly and function in the IMS.

Keywords: oxidative protein folding; small Tim; protein import; mitochondrial intermembrane space; AAC

1. Introduction

Mitochondria are essential eukaryotic organelles harboring 1000–2000 different proteins. Approximately 99% of the total mitochondrial proteins are encoded by nuclear DNA, synthesized as precursors in the cytosol, and imported into mitochondria via elaborate transport machineries. The small Tim (translocases of the inner membrane) proteins are a group of small intermembrane space (IMS) proteins with a strictly conserved "twin CX_3C" zinc-finger motif [1]. Members of the small Tim family are conserved and have been found in mammals, yeast and plants. *Saccharomyces cerevisiae*, for example, has five known small Tim proteins: Tim8, Tim9, Tim10, Tim12 and Tim13; of which Tim9, Tim10 and Tim12 are essential for cell viability [1–5]. The small Tim proteins play an essential chaperone-like role during the import of mitochondrial membrane proteins. They are in charge of chaperoning these hydrophobic membrane proteins through the aqueous mitochondrial IMS, transporting them from the translocase of the outer membrane (TOM) complex towards either the inner membrane (IM) or the outer membrane (OM) of mitochondria [6]. Their importance is illustrated by the fact that defects in human Tim8 lead to deafness dystonia syndrome [7,8]. For their function, the small Tim proteins assemble into at least two hexameric complexes, Tim9-Tim10 and Tim8-Tim13, where each complex includes three molecules of each subunit bound in an alternating form [9,10].

All mitochondrial IMS proteins are synthesized in the cytosol and have to be imported into mitochondria for their function. A unique feature for most of the IMS proteins is that their post-translational import is regulated by their cysteine redox state [11,12]. The biogenesis of the small Tim proteins is tightly coupled with their oxidative protein folding, which can be divided into four sequential steps: (i) In the cytosol the precursor proteins are kept in a reduced and unfolded form by cytosolic factors [13,14]; (ii) mitochondrial import of the reduced precursor proteins through the TOM complex [15]; (iii) oxidative protein folding in the IMS regulated by the mitochondrial import and assembly (MIA) pathway [16–18]; (iv) assembly of the oxidized, partially folded proteins into hexameric small Tim complexes [19,20]. All of these steps depend on the redox state of the conserved cysteine residues—while only reduced unfolded proteins can be imported into mitochondria, protein folding and complex formation requires disulfide bond formation. Here, we review the current knowledge regarding each step of the biogenesis and folding of the mitochondrial small Tim proteins with focus on Tim9 and Tim10. We will also discuss how the small Tim hexameric complex is assembled, and the mechanism by which this complex might perform its chaperone function.

2. Keeping the Precursor Protein Reduced and Unfolded in the Cytosol

Tim9 and Tim10 are two of the most important and best-characterized small Tim proteins. Circular dichroism and thiol-modification analyses showed that in the absence of a reducing agent the proteins are folded in an α-helical conformation stabilized by two pairs of intramolecular disulfide bonds [19,21,22]. The proteins become unfolded upon addition of a disulfide reducing agent (e.g.,

DTT, TCEP) even in the absence of a protein denaturant. Mitochondrial import analyses showed that the Cys-reduced states can be imported into mitochondria, whereas when oxidized the proteins are folded and import-incompetent [15,19,22] (Figure 1).

Figure 1. Only the Cys-reduced small Tim precursor proteins are import-competent. The small Tim proteins have to be kept in their reduced conformation while in the cytosol. Neither the fully nor the partially oxidized proteins can be imported into mitochondria. Oxidation could be brought about by GSSG, oxygen or reactive oxygen species (ROS). Partially oxidized proteins can be reduced by the cytosolic Thioredoxin system. Additionally, the reduced proteins could be stabilized by zinc binding, although it is uncertain whether the zinc-bound form can be imported directly.

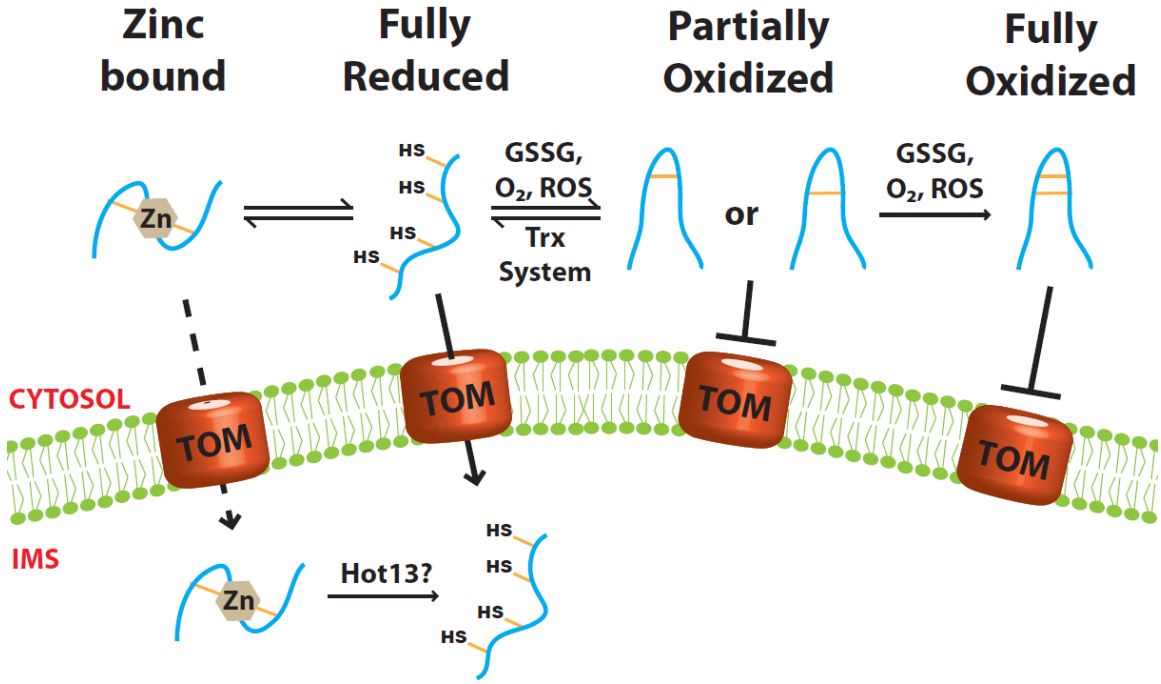

Glutathione, present in its reduced (GSH) and oxidized (GSSG) forms, is considered to be the major thiol-disulfide redox buffer of the cell. The total glutathione concentration in the cell is typically between 5 and 10 mM, and is mainly found in the reduced form in the cytosol and mitochondria [23]. *In vitro* studies have shown that GSSG at low micromolar concentrations is sufficient to oxidize the small Tim proteins and hinder their mitochondrial import [19,22]. Furthermore, once oxidized even 10 mM GSH is not sufficient to reduce the proteins [21,22]. The standard redox potentials for several small Tim proteins were determined [21,22] and showed similar values in the range of −0.31 to −0.33 V. Such low redox potentials are consistent with the oxidized proteins being stable in the mitochondrial IMS. However, because the IMS has a similar reducing environment to that of the cytosol [24], it suggests that precursor proteins could potentially be oxidized before they are imported. A few MIA pathway substrate proteins were recently shown to remain in the cytosol for several minutes before their import [25], which further reinforces the danger for precursor protein oxidation while in the cytosol. Therefore, after the precursor proteins are synthesized, a mechanism must exist to maintain them in a Cys-reduced and import-competent conformation, as well as to protect them from

oxidative folding, aggregation and subsequent degradation in the cytosol. A recent study suggested that degradation of non-imported IMS precursor proteins is accomplished by the ubiquitin proteasome [26].

Chaperones are important players in the biogenesis of mitochondrial proteins [27–30]. In mammalian cells, Hsp70 and a mitochondrial import stimulation factor (MSF) were shown to target presequence-containing matrix precursors to mitochondria [30]. Furthermore, the Hsp70 and Hsp90 chaperones were identified to target IM carrier precursor proteins to mitochondria. In yeast, Hsp70 was shown to facilitate the import of both matrix and IM proteins [27–30]. However, so far no studies have been reported as to whether the cytosolic chaperones are involved in the import of mitochondrial IMS proteins. In the absence of evidence for the role of chaperones, two models have been proposed to keep the small Tim proteins in their Cys-reduced, import-competent conformation in the cytosol: zinc binding and the cytosolic thioredoxin (Trx) system.

2.1. Role of Zinc Ions

All the small Tim proteins contain a strictly conserved "twin CX3C" zinc-finger motif. *In vitro* experiments have shown that both Tim9 and Tim10 can bind Zn^{2+} in their reduced form, at a molar ratio of 1:1, with K_d values between 8.0×10^{-8} and 8.0×10^{-10} M^{-1} determined using different methods [2,31,32]. Upon binding, the proteins undergo a small yet detectable conformational change that can be seen by both far UV circular dichroism and fluorescence. Removal of any of the cysteines in Tim9 or Tim10 abolishes zinc binding, indicating that all four cysteines are involved in zinc coordination [13,21,32]. In the presence of zinc ions the rate of oxidative folding of Tim9 by GSSG is about 14-fold slower than that of the apo-proteins (no zinc). Thus, zinc-binding can stabilize the reduced form and keep it from oxidation [21,22]. However, though the total cellular zinc concentration is estimated to be somewhere between 0.1 and 0.5 mM [33], the free zinc concentration in the cells is believed to be very low (~10^{-12} M) [34–37]. Furthermore, experimental results showed that zinc is a strong inhibitor of the sulfhydryl oxidase Erv1, a component of the MIA pathway used for the import of the small Tim proteins. Consequently, at the zinc concentration that most of the small Tim proteins can bind zinc, their mitochondrial import is inhibited [13]. Therefore, if zinc does work as a chaperone in the cytosol, it may work in cooperation with another unknown factor and must be removed at some point during protein import. To this end, the IMS protein Hot13 (Helper of Tim) has been suggested to act as a zinc-chelator protein that is involved in assembly or recycling of the small Tim proteins, and helps maintain the MIA components in a zinc-free state [38,39].

2.2. Role of the Cytosolic Redoxin Systems

A second model is based on our recent finding that the cytosolic Trx system facilitates the import of mitochondrial small Tim proteins [14]. Thioredoxins and glutaredoxins (Grx) are ubiquitous oxidoreductases in charge of thiol regulation and oxidative stress defense. Their main function is to reduce disulfide bonds found in proteins [40]. In the yeast *S. cerevisiae*, the Trx system comprises Trx1, Trx2, Trx reductase and NADPH. Trx1 and Trx2 act on substrate proteins while Trx reductase takes electrons from NADPH and transfers them to Trx1 and Trx2. Durigon *et al*. [14] recently showed that a Δ*trx1trx2* double deletion mutant has a strong growth defect under respiratory conditions. The mutant strain also has lower mitochondrial levels of the small Tim proteins. Importantly, mitochondrial

import studies confirmed that the import levels of both Tim9 and Tim10 increased significantly in the presence of the Trx1 system. A similar result was also obtained for Cox19, a CX_9C motif-containing substrate of the MIA pathway. Furthermore, an efficient disulfide bond transfer reaction was reconstituted using purified Tim10 and the Trx1 system. *In vitro* assays have also shown that Trx1 is capable of reducing the partially oxidized, one-disulfide-bonded intermediates of Tim10, while the fully oxidized protein was Trx-resistant [14]. These results suggest that the Trx system counterbalances the oxidative folding in the cytosol by reducing any early folding intermediates, which were shown to be import-incompetent as well [22].

A very recent study based on *in vivo* NMR analysis showed that overexpressed human Mia40 (a twin CX_9C motif-containing protein) was oxidatively folded in the cytosol of human embryonic kidney cells, and its folding state depended on the cytosolic Grx1 system and to a lesser extent on the Trx1 system [41]. Interestingly, while overexpressed human Mia40 is largely trapped in the cytosol, it has been shown that overexpressed yeast Mia40 is successfully imported into yeast mitochondria [42]. This difference may be because human Mia40 does not have an *N*-terminal mitochondria-targeting signal and is imported through the MIA pathway, while yeast Mia40 does have an *N*-terminal targeting signal and is imported via the translocase of the inner membrane 23 (TIM23) pathway [43–46]. However, purified human Grx1 cannot reduce human Mia40 *in vitro*, thereby implying an indirect link to the redox state of Mia40 [41].

In summary, both zinc-binding and the cytosolic Trx system can maintain the small Tim proteins in Cys-reduced forms. Due to its inhibitory activity, zinc alone is unlikely to be the major player in maintaining the precursors in their import-competent form in the cytosol. The Trx system not only facilitates the import of the small Tim proteins, but also of non-zinc binding proteins such as Cox19. Indeed, both the Trx system and the human Grx system are able to keep the CX_9C motif precursors proteins in their reduced form by preventing their oxidative folding at an early stage, and can thus facilitate the import of mitochondrial IMS proteins. Therefore, these systems appear to be an important primary factor in mediating the biogenesis of the redox-sensitive IMS proteins by reductively unfolding the proteins. Whether the cytosolic Grx system, particularly the yeast mitochondrial OM-anchored Grx2 [47], also plays a role in the import of the small Tim proteins is unknown. More studies are still required to understand the detailed molecular mechanisms of protein folding/unfolding in the cytosol.

3. Import, Folding and Oxidation

The small Tim proteins are found in their oxidized states in purified mitochondria and *in vivo* [19]. The identification of a disulfide relay system (Mia40-Erv1 system) in the mitochondrial IMS indicated that oxidative protein folding occurs in the IMS and completely changed the view of how IMS proteins fold and get imported [11,12]. For a long time it was believed that the IMS, like the cytosol, has a reduced environment and thus would not support protein disulfide bond formation. Conversely, oxidative protein folding has now been suggested as the reason many IMS proteins, including the small Tim proteins, are trapped inside the IMS [15,16]. In contrast to the less studied and ill-defined mechanism in the cytosol, many studies have been carried out in understanding the Mia40-Erv1 system (MIA pathway) and the molecular mechanism of oxidative protein folding in the mitochondrial IMS.

There are many excellent reviews about this disulfide relay system [11,12,48,49] and it will, therefore, only be explained briefly in this review. We will instead focus on the import and folding of the small Tim proteins, which are proven substrates of the MIA pathway.

3.1. Disulfide Relay System of the IMS

The MIA machinery localized inside the mitochondrial IMS was found to be required for import of many cysteine-rich IMS proteins, including the small Tim proteins [44,45,50]. The system includes two essential proteins: the disulfide carrier Mia40 that recognizes and transfers disulfides to newly imported substrate proteins, and the sulfhydryl oxidase Erv1 that reoxidizes reduced Mia40. Lastly, both oxygen and cytochrome *c* can act as the electron acceptors of Erv1 [11].

Figure 2. Proposed model for oxidative folding of the small Tim proteins. (1) Nucleophilic attack of the C_1 cysteine from the small Tim proteins; (2) Mia40-dependent folding initiated by hydrophobic interactions at the MISS/ITS segment, and stabilized by formation of an intermolecular disulfide bond; (3) Nucleophilic attack of the C_4 cysteine from the small Tim proteins; (4) Mia40-independent folding. The second helix is formed using the first helix as scaffold, and stabilized by formation of the first intramolecular disulfide bond in the small Tim proteins (C_1–C_4); (5) The second disulfide bond could be formed by either oxygen, GSSG or Mia40.

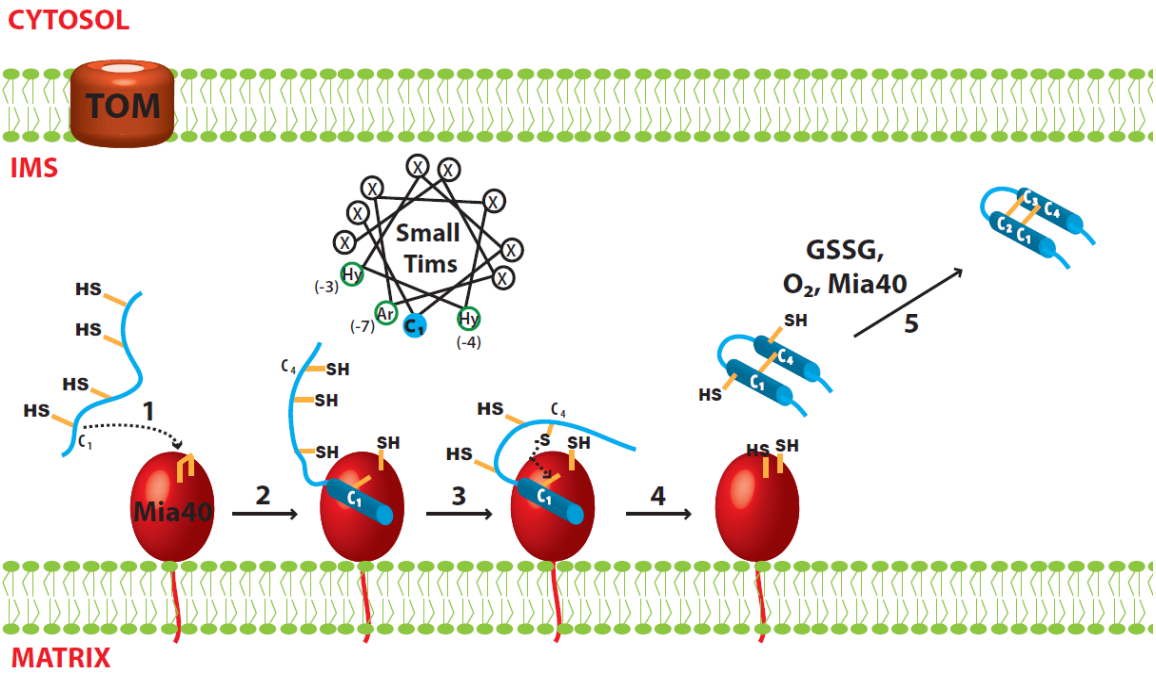

3.2. Import of the Small Tim Proteins

The small Tim proteins, like other mitochondrial proteins, reach the IMS by passing through the TOM complex in the OM. All small Tim proteins have an internal targeting signal called MISS (mitochondrial IMS sorting signal), or ITS (IMS-targeting signal). Inside the IMS, Mia40 functions both as an import receptor and a disulfide carrier. The MISS/ITS includes a cysteine residue that is important for mitochondrial import and docking to Mia40 (as a receptor) [51,52]. Systematic

mutagenesis studies showed that, for Tim9 and Tim10, the MISS/ITS consists of 9 amino acids upstream of the first (*N*-terminal) cysteine (C_1). Apart from the docking cysteine, hydrophobic residues at positions −3, −4, as well as an aromatic residue at position −7 from the cysteine are important; the consensus sequence is thus X[Ar]XX[Hy][Hy]XXC (Ar: aromatic residue; Hy: hydrophobic residue). These residues are arranged such that they point towards the same side of the α-helix (Figure 2). Indeed, an upstream or downstream shift of the docking C_1 cysteine in Tim9, where upon the distance from the hydrophobic residues to the cysteine is changed by a full helix turn, strongly impairs binding of the protein to Mia40 and its mitochondrial import [52]. This is because the hydrophobic residues are no longer in contact with the cleft in Mia40. On the other hand, swapping the MISS/ITS from the *N*-terminal to the *C*-terminal end of Tim10 does not affect its import, indicating its mitochondrial import occurs post-translationally. Furthermore, the MISS/ITS peptide is also sufficient for targeting non-mitochondrial proteins to the mitochondrial IMS [51,52].

3.3. Oxidative Folding of the Small Tim Proteins

Upon interaction with Mia40, the MISS/ITS becomes folded and forms an amphipathic helix that has the crucial hydrophobic and aromatic residues on one side and the non-essential residues on the other side. The hydrophobic side of the helix fits well into the hydrophobic cleft of Mia40. The folding of the small Tim MISS/ITS is induced by Mia40 via these hydrophobic interactions, and is further stabilized by formation of an intermolecular disulfide bond between the docking cysteine (C_1) of small Tims and a redox active cysteine of Mia40 [16–18,53]. Thus, these hydrophobic residues are crucial for the initial folding as they are precisely positioned to interact with Mia40 [18,51,52]. However, how the small Tim proteins become fully folded and oxidized after their initial interaction with Mia40 is still unclear.

The sequence of events after substrate recognition by Mia40 is better understood when looking at the folding steps of another MIA pathway substrate, human Cox17 (hCox17). hCox17 is part of a group of IMS proteins with a conserved twin CX_9C motif. A study by Banci *et al*. [18] showed that oxidation and folding are coordinated events in the hCox17 protein. The MISS/ITS segment of the protein is downstream of the docking cysteine Cys45 (C_3) and initially binds the hydrophobic cleft of Mia40, forming an intermolecular disulfide bond. Upon binding, the MISS/ITS segment folds into an α-helix spanning 15 residues downstream of the docking cysteine, while the rest of the protein remains unfolded [18]. In the absence of the docking cysteine the protein can still bind Mia40, albeit with a weaker affinity. Moreover, without the formation of the intermolecular disulfide bond the MISS/ITS segment remains unfolded [18]. Therefore, a disulfide bond is required to stabilize the initial folding of hCox17. The second step involves the nucleophilic attack of Cys36 (C_2) to break the intermolecular disulfide bond. The reaction creates the internal C_2–C_3 disulfide in hCox17 while, simultaneously, the second α-helix is formed. Interestingly this step is independent of Mia40-hCox17 uses the hydrophobic side of its first helix as a scaffold for the formation of the second helix [18]. Here, again, disulfide bond formation (oxidation) is coordinated with protein folding. After these two folding steps hCox17 has acquired the same secondary structure as the fully mature protein, but is still lacking one disulfide bond. This agrees with another finding showing that the outer disulfide bond (C_1–C_4) of yeast Cox19 (another CX_9C protein) cannot be formed in the absence of the inner disulfide (C_2–C_3) [54]. The outer

disulfide bond can be formed by different components depending on the surrounding conditions. Under aerobic conditions oxygen can easily oxidize the cysteines to form the second disulfide on an already-folded protein [55], whereas Mia40 can also completely oxidize the protein when found in vast excess [54]. Alternatively, *in vivo* assays have also suggested that Erv1 forms a tertiary complex with Mia40 and the small Tim proteins under certain conditions [56], thus creating the opportunity for Erv1 to insert the second disulfide.

The folding of small Tim proteins is less understood, mainly because the reduced proteins at high concentration tend to degrade and render any NMR analysis difficult [18]. Unlike hCox17, the small Tim proteins have a twin CX_3C motif, their docking cysteine is C_1 and the MISS/ITS segment is upstream of C_1. This means the outer disulfide is likely formed before the inner disulfide, contrary to what is seen for hCox17. Indeed, a double mutation of the outer disulfide cysteines (C1,4S) strongly inhibits the Tim9 interaction with Mia40 [16]. Additionally, a peptide corresponding to the MISS/ITS segment of Tim9 including the C_1 cysteine (RLYSNLVERC) was shown to bind Mia40 through an intermolecular disulfide bond [18,52]. Upon binding Mia40, the previously unfolded peptide was able to adopt a stable α-helix conformation [18]. Thus, the Mia40-induced folding of the MISS/ITS segment appears to be general for proteins with either a twin CX_3C or CX_9C motif (Figure 2). How the second disulfide bond is formed is an important controversial question and more experiments are needed to address it.

3.4. Oxidized Tim9 and Tim10

The fully oxidized small Tim proteins have a helix-loop-helix structure where the two helices are linked and stabilized by two intramolecular disulfide bonds, C_1–C_4 and C_2–C_3 [9,10,57]. The disulfide bonds are required to maintain the secondary structure of the proteins and also render them more resistant to trypsin digestion [19,31]. Sedimentation equilibrium studies showed that in a condition mimicking the physiological environment (Tris-HCl, pH 7.4, 150 mM NaCl) Tim9 forms a dimer and Tim10 a monomer [20,58]. No information is known regarding the oligomerization state of other small Tim proteins. So far no crystal structure of the individual small Tim proteins has been published. However, NMR studies have shown that both the N- and C-terminus of Tim10 are unstructured, whereas only the C-terminus of Tim9 is flexible [31]. Overall, both Tim9 and Tim10 exist in a molten-globule state in which secondary structures are formed, but the proteins do not pack together in a unique way [31]. Far UV circular dichroism studies showed that the individual oxidized small Tim proteins have similar secondary structure to that of the proteins in the hexameric complex [31].

4. Complex Assembly

4.1. Assembly Process of the Tim9-Tim10 Complex

Formation of the hexameric Tim9-Tim10 complex from the individual subunits can be divided into four kinetic steps (Figure 3). Stopped-flow experiments coupled with mutagenesis showed clear salt concentration dependence in the rate of assembly in the first two steps, but not in the last two steps. Furthermore, the overall rate of assembly depends on the pH in a bell-shaped profile, with two pKa values similar to the isoelectric points of Tim9 and Tim10.

Figure 3. Tim9-Tim10 hexameric complex assembly. The process can be separated into four kinetic steps: formation of a heterodimer (i), a tetramer (ii), a hexamer (iii) and a final hydrophobic rearrangement (iv). The two initial fast steps are controlled mainly by electrostatic interactions, whereas the final two slow steps are driven by hydrophobic interactions.

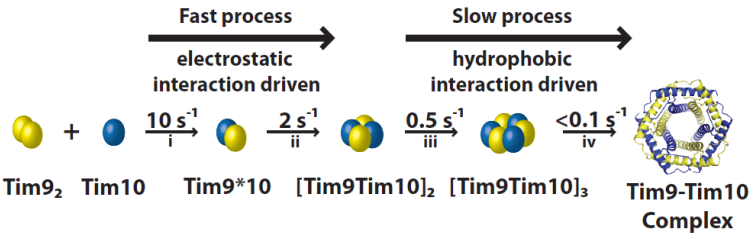

The initial step consists in the formation of a Tim9*10 heterodimer. Monomeric Tim10 binds allosterically to dimer Tim9, substituting one of the Tim9 subunits [20]. Two factors could favor heterodimerisation: (i) the central loop structures of Tim9 and Tim10 complement each other better than if they were to form an homodimer; (ii) Aryl groups in Tim9 and methionine residues in Tim10 interlace in the intersubunit surface, and this arrangement appears to improve the fit of the heterodimer [10]. These interactions with Tim9 also cause the flexible Tim10 structure to become more defined [31]. Once formed, the dimers quickly associate to form a tetramer further stabilized by electrostatic interactions. This is consistent with the presence of important intersubunit salt bridges formed between both sides of the Tim9/10 interfaces [59]. The third step includes the slow incorporation of another Tim9*10 dimer to form a hexameric complex. Lastly, hydrophobic-driven rearrangements produce the final complex [20,60]. As this multistep process occurs efficiently *in vitro*, there is not thought to be any cofactor assisting it. Interestingly, the major hydrophobic areas located between the *N*- and *C*-terminal helices may be less protected in the later hexameric assembly intermediates, suggesting that these complexes could play a role in substrate binding.

4.2. Structure of the Tim9-Tim10 Complex

Oxidative folding in the IMS allows the arrangement of the small Tim proteins into hexameric complexes. The crystal structures of the human and yeast Tim9-Tim10 complex have been solved, as well as that of the yeast Tim8-Tim13 complex [9,10,59]. All three complex structures are similar, adopting a donut-shaped configuration with an outer diameter of 50–60 Å, and an inner pore of 10–15 Å (Figure 4A). The structures resemble those of the prefoldin and Skp chaperones in terms of overall architecture [61–63]. The Tim9-Tim10 hexamer consists of three molecules of each subunit, arranged in a circle, with an inner, downward-pointing circle made from the subunits N-termini (often referred to as "tentacles" as in prefoldin and Skp), and an outer, outward-pointing circle ("α-propellers") made from the *C*-termini tilted outwards at 60° [10]. The steric bulk of the disulfide bonds in the individual subunits generate the characteristic structure of the complex, by causing the helices to splay outwards [10,59] (Figure 4B). Intermolecular salt-bridges between lysine and glutamate residues are critical to complex stability, while hydrophobic residues in the core are sequestered by junctions formed between inner and outer helices with the intermolecular contacts generally occurring in the *N*-terminal regions of the inner helices, and in the core regions of the outer

helices (Figure 4C,D). Additionally, hydrophobic residues form clusters in which two residues from one subunit (e.g., Tim9 V70 and F74) are surrounded by several hydrophobic residues from the neighboring subunit [64]. There is not an obvious hydrophobic pocket for substrate binding, suggesting that a conformational change is required for the chaperone function of the Tim9-Tim10 complex.

Figure 4. Tim9-Tim10 hexameric complex. (**A**) Crystal structure of yeast Tim9-Tim10 complex, top (**left**) and side (**right**) view respectively (PDB: 3DXR). Tim9 (yellow) and Tim10 (blue). The outer layer is formed by the six *C*-terminal helices (α-propellers) and the inner layer by the six *N*-terminal helices (tentacles); (**B**) Structure of Tim9 and Tim10 showing the two helices linked by intramolecular disulfide bonds (orange) (PDB: 3DXR); (**C**) Conserved salt bridge between a glutamate residue in the loop of Tim10 and a lysine residue in the outer helix of Tim9; (**D**) Alignment of Tim9 and Tim10 amino acid sequences. Fully conserved residues are marked with asterisks (*). Helical regions and the central loop are marked in blue and yellow respectively. Conserved cysteine residues are highlighted in green. Key charged residues are highlighted in pink (positively charged) and light blue (negatively charged), and salt bridges between them are marked with a dotted line. Central residues of hydrophobic clusters are highlighted in orange. *Sc*: *Saccharomyces cerevisiae*, *Sp*: *Schizosaccharomyces pombe*, *Nc*: *Neurospora crassa*, *Hs*: *Homo sapiens*, *Xl*: *Xenopus laevis*, *Gg*: *Gallus gallus*, *Dm*: *Drosophila melanogaster*, *Ce*: *Caenorhabditis elegans*.

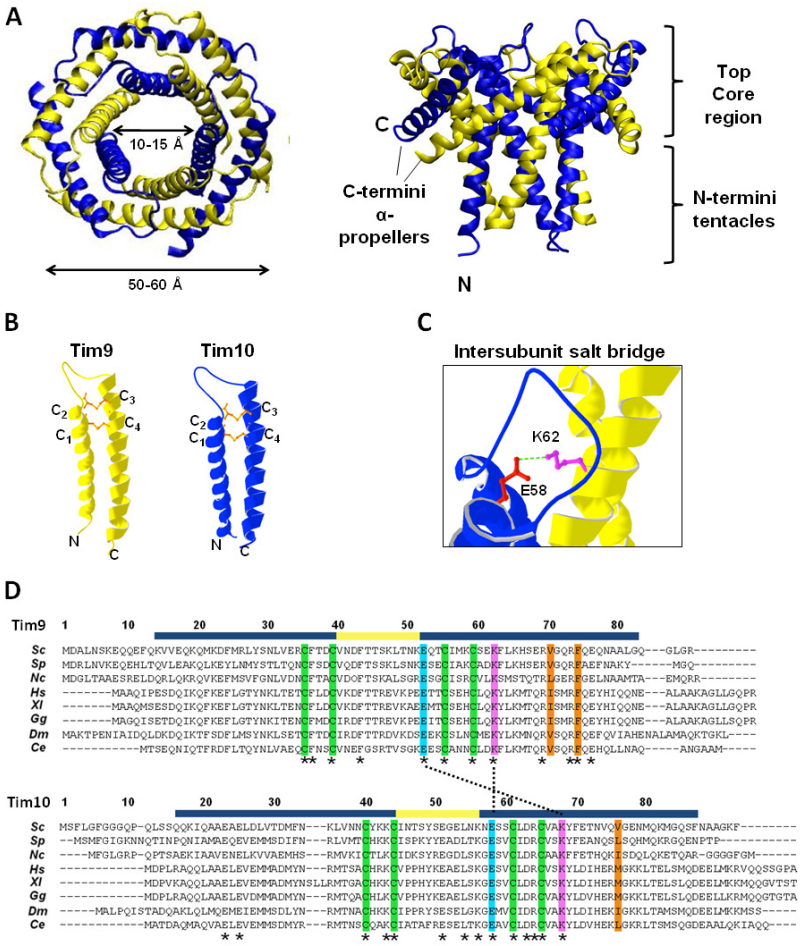

4.3. Stability of the Tim9-Tim10 Complex

Various parts of Tim9 and Tim10 have been studied for their role in complex formation and stability using purified proteins, *in organelle* analysis, and *in vivo* approaches. The importance of the N- and C-terminus of Tim9 and Tim10 in complex stability has been studied both *in vitro* and *in vivo*. Deletion of the C-terminus of Tim10 inhibits its interaction with Tim9 and, therefore, stops complex assembly. Similarly, a deletion of the C-terminus of Tim9 destabilized the complex. In contrast, mutation of the N-terminus of either Tim10 or Tim9 showed no considerable effect on complex formation [65]. Together, these data suggest that the C-termini ("propeller blades") of Tim9 and Tim10 are significantly more important for hexameric complex formation/stability than the N-termini ("tentacles").

The roles of specific amino acids of Tim9 and Tim10 in complex stability have also been investigated. The four conserved cysteine residues in the proteins form two pairs of intramolecular disulfide bonds while in the complex. They are required for complex formation and constricting the neck of the fixed-angle helical hairpin [59]. Their importance is highlighted by the human Tim8 cysteine mutation, C66W, found to cause deafness dystonia syndrome [7,8]. *In vitro* studies showed that reduced proteins in the presence or absence of zinc, or after blocking of the cysteines, are prevented from forming the hexameric complex [7,19,31,66]. Incorporation into the complex shields the disulfide bonds, making them resistant to DTT [19], whereas the individual subunits can be reduced [1,22]. A recent study showed that loss of any disulfide bond results in greatly reduced complex formation *in vivo* and instability of both proteins, but surprisingly has little effect on cell growth [67].

Other important stabilizing interactions are the intersubunit salt-bridges buried at the Tim9 and Tim10 interface [59]. Particularly important to these interactions are the glutamate residues Tim9E52 and Tim10E58 (*N*-terminal to the third cysteine in both Tim9 and Tim 10), and the nearby lysine residues Tim9K51 and Tim10K56 [59,68]. Stability of the Tim9-Tim10 complex in mitochondria is heavily disrupted by mutation of any of these residues [42,46,47]. These charged residues are highly conserved and located in the core region of the complex. The key intersubunit interactions are formed by the Tim9E52-Tim10K68 and the Tim9K62-Tim10E58 salt-bridges. However, as with the conserved cysteine residues, mutation of these charged residues, while significantly affecting detection of the Tim9-Tim10 complex, did not necessarily result in cell death. For example, the *tim9-19* mutant (a Tim9E52G mutation) does not form detectable levels of Tim9-10 complex, but still supports slow cell growth [69].

In contrast to the role of the cysteines and the salt-bridge interactions, the hydrophobic interactions between adjacent subunits are potentially more dynamic [59,64]. *In vitro* experimental studies and computational simulations suggested that dynamics of the hydrophobic interactions play a subtle and yet important role in stabilizing and regulating the function of the Tim9-Tim10 complex. Two hydrophobic clusters (A and B) were identified, each centered on key residues (Figure 3D, Val70 and Phe74 of Tim9 for cluster A, Val76 of Tim10 for cluster B) from one subunit that are surrounded by several hydrophobic residues from the other subunit [64]. Interestingly, at increased temperatures the stabilizing effect of these hydrophobic interactions is predicted to become destabilizing, which is in agreement with experimental results of a decreased rate of late-stage complex assembly at elevated

temperatures [64]. However, more experiments are required to know whether mutations of these hydrophobic residues disrupt complex formation or simply disturb its function in import of its substrate proteins.

Tim9 and Tim10 have also been shown to form a ternary hexameric complex with Tim12. Tim12 is an essential IMS protein in yeast associated peripherally with the translocase of the inner membrane 22 (TIM22) complex of the IM [70]. Tim12 is believed to link the Tim9-Tim10 complex with the TIM22 translocase during import of Tim9-Tim10 substrates. Although the Tim9-Tim10-Tim12 complex is less studied, it appears to consist of three Tim9, one Tim10, and two Tim12 [71]. Whether the complex forms through displacement of Tim10 molecules by Tim12 or through *de novo* interaction with free Tim9 and Tim10 subunits is not currently known.

5. Functional Mechanism of the Small Tim Proteins

The biological function of the small Tim proteins is to assist in the import of hydrophobic proteins into the mitochondrial inner and outer membranes [2–4,6,72]. The exact mechanism of substrate interaction and release from the small Tim proteins is not yet known. It is also not clear which form of the proteins, Tim9, Tim10 or the Tim9-Tim10 complex acts as the functional chaperone during the import of their substrate proteins; while it is generally believed that the hexameric complexes are essential for the chaperone function, some studies suggest that complex formation might not necessarily be required. Moreover, there is some level of substrate specificity between the two homologous small Tim complexes: the Tim8-Tim13 complex has been linked to Tim23 insertion [73], while Tim9-Tim10 is involved in the insertion of a wide range of OM and IM proteins, in particular the carrier proteins of the IM [2,3]. Here, we summarize the experimental results and proposed models that are based on the most studied model substrate of Tim9-Tim10: the ATP/ADP Carrier (AAC) protein.

5.1. Import of AAC

AAC, a mitochondrial IM protein, is one of the best-studied proteins in terms of its import and interaction with the small Tim proteins [2–4]. It belongs to a large family of IM carrier proteins that contain non-cleavable targeting sequences. AAC spans the IM six times comprised of three modular repeats of paired transmembrane domains. In contrast to the small Tims and many other mitochondrial proteins, AAC and carrier proteins are not necessarily imported into mitochondria as a linear polypeptide chain, and proper import appears to be dependent on the full intact protein [74,75]. Import of AAC can be divided into five stages [76–78]. The initial interaction with cytosolic chaperones (stage 1) is followed by association with the TOM complex (stage 2) in an ATP-dependent manner. Then the precursor passes through the IMS chaperoned by the small Tim proteins (Stage 3), followed by a membrane potential-dependent IM insertion by the TIM22 complex (Stage 4). Finally, the AAC is released and assembled into its functional form in the IM (Stage 5) (Figure 5A).

Figure 5. Small Tim function in carrier protein biogenesis. (**A**) Biogenesis of AAC. Stage I, precursor in the cytosol is bound by chaperones. Stage II, precursor engages the TOM complex at the mitochondrial OM. Stage III, precursor is bound by the small Tim proteins and chaperoned through the IMS. Stage IV, precursor interacts with Tim12 (in purple) and reaches the TIM22 complex. Stage V, the carrier protein is fully inserted in the IM and dimerizes into its functional form; (**B**) Model for small Tim proteins interaction with the AAC substrate. AAC binding is initiated through the N-termini of the small Tim subunits. AAC could either substitute a Tim9 subunit (competitive displacement) or cut across some of the complex subunits (bisecting dimerization). The two models are not mutually exclusive and at least one Tim9 subunit remains in close proximity to the substrate.

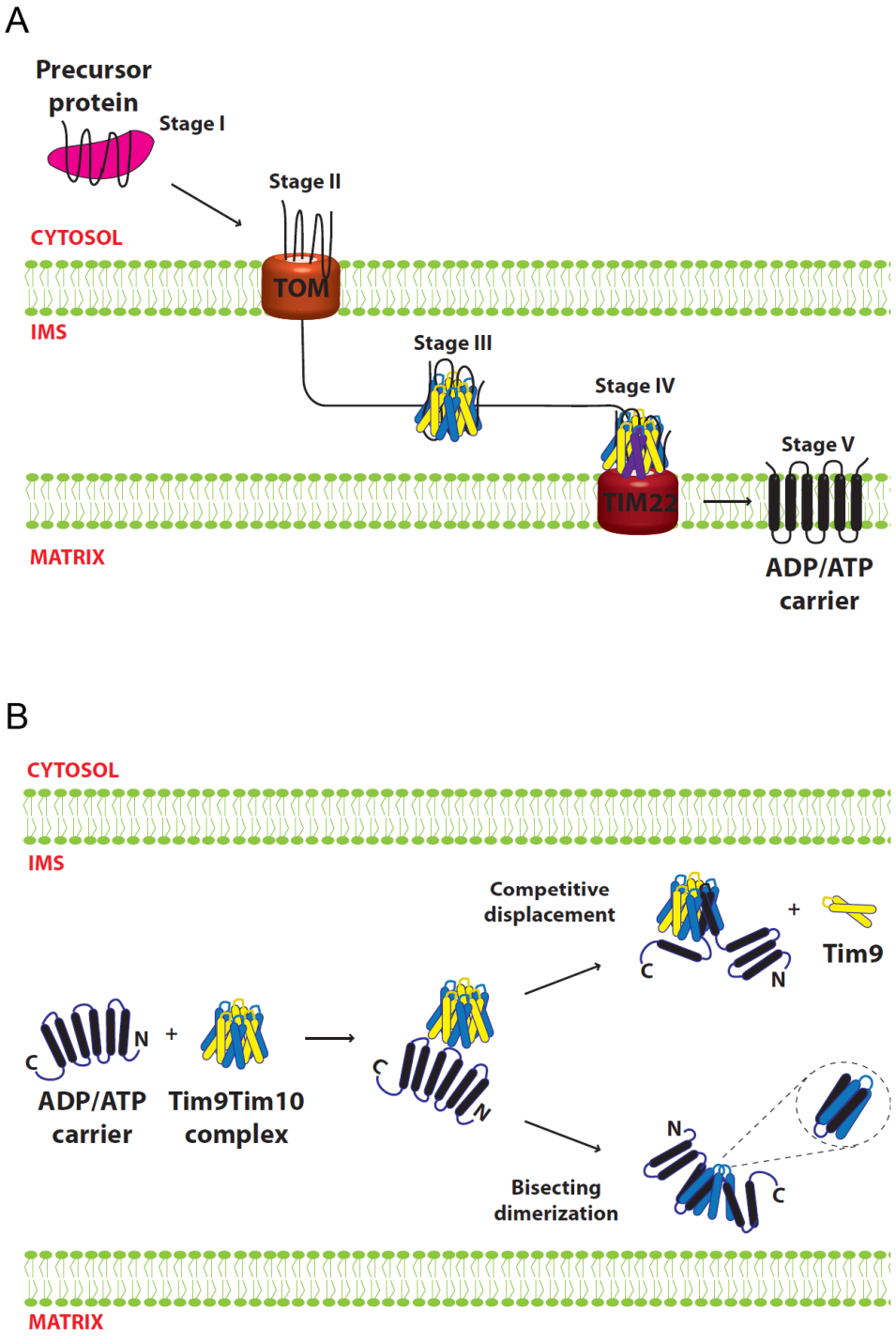

5.2. Models for Tim9-Tim10 Chaperone Function

The chaperone function of the small Tim proteins can be conceived as a multi-step process. It requires a mechanism that can both recognize and bind the substrate, and then release it. The first model for small Tim function proposed that the substrate binding is provided by individual Tim10 molecules, with the role of Tim9 being to stabilize Tim10 when it is not interacting with substrate. This model was proposed mainly based on studies showing that Tim10 can interact with AAC, whereas no stable interactions between Tim9 and AAC were detected using the same approaches (NMR, protein cross-linking and peptide spot assay) [2,4,10,75]. Furthermore, the Tim10-AAC interactions were severely disrupted by deletion of 30 amino acids at the Tim10 *N*-terminus [65], indicating a critical role for the *N*-terminal of Tim10 in substrate interaction. It was suggested that the loop regions of Tim10 line up in anti-parallel with AAC matrix loops ("carrier signatures"), with hydrophobic and complementary charged residues making contact [2]. However, Tim9 does not contain these complementary sequences and would therefore be unable to interact with AAC [4]. Instead, Tim9 function might be explained by the observation that mutations of *tim9* that result in low protein levels correlate with a reduction in Tim10 protein [4,67], suggesting that Tim10 is only stable in the presence of Tim9. As such, the interaction with Tim9 serves only to protect Tim10 from Yme1-mediated degradation. A simple model generated from these data is that Tim10 interacts and chaperones precursor AAC, while Tim9 acts to maintain an available pool of Tim10 in the absence of substrate.

The crystal structure of the mammalian Tim9-Tim10 complex supported the idea that Tim10 is the primary protein involved in substrate binding [10]. In contrast to the homologous Tim8-Tim13 complex, which can be modeled to encompass its relatively small substrate Tim23 in its central cavity [9], the structure of the Tim9-Tim10 hexameric complex does not appear to accommodate the AAC molecule, and the hydrophobic residues predicted to interact with the substrate are buried in intersubunit interactions [8,42]. Thus, substrate binding most likely takes place through conformational changes and/or subunit rearrangements that expose the binding surfaces of Tim10. Two models were proposed for how the substrate-binding regions might transition from being buried in the Tim9-Tim10 hexamer to binding AAC. In each case, one subunit is displaced and replaced by two helices of AAC. In the bisecting dimerization model, two transmembrane helices of AAC cut across the tentacles of a subunit in a tail-to-tail orientation. In the competitive displacement model, transmembrane helices four and five (H4, H5) of AAC displace a Tim9 subunit, with the H4-H5 loop of AAC positioned similarly to the loop regions of the small Tim proteins (Figure 5B). This model could explain why the AAC H4-H5 segment showed strongest binding to Tim10 in peptide spot assays [79,80]. The two models are not mutually exclusive but explain available experimental results from different angles, and they could work in combination allowing the rest of the substrate to fit within the complex [8]. In support of these models, the presence of a low-populated excited state of Tim9-Tim10 complex with disrupted intersubunit hydrophobic interactions would allow the complex to "breathe", thus providing an explanation for the initial substrate interaction with Tim10 [64]. In this scenario, some complexes will be more thermodynamically stable ("closed") and some will be more energetic ("open"). In the open phase some hydrophobic residues are exposed allowing Tim10 to interact with incoming precursors.

As discussed in Section 4.3, no consistent picture appears connecting the status of the Tim9-Tim10 complex, its interaction with substrate and cell viability. Interestingly, some mutations lack detectable Tim9-Tim10 hexameric complex on blue-native gels, but still can import AAC [42,45,46,57], suggesting the complex is not required for AAC import. However, several lines of evidence support the involvement of both Tim9 and Tim10 in substrate interaction. For example, Tim9 can co-immuno-precipitate AAC [80], and crosslinks between AAC and Tim9 are detectable under certain conditions [3,81]. Introduction of a fifth cysteine residue into Tim9 allowed clear crosslinking of Tim9 to AAC [56,57], strongly suggesting that these proteins are in close proximity. Furthermore, a Tim9 *N*-terminal deletion mutant, Tim9ΔN10, in which Tim10 remains stable, does not properly import AAC *in vitro* [59]. Thus, overall it seems that both Tim9 and Tim10 are in proximity to the substrate, and the presence of both proteins is required for normal substrate interaction. While Tim10 might provide the majority of the binding surfaces for AAC, it is more useful to view both Tim9 and Tim10 acting in concert to chaperone substrates through the IMS.

Taken together, the available data supports a model (Figure 5B), in which Tim9-Tim10 complex recognizes incoming substrate through the *N*-terminal tentacle regions of Tim9 and Tim10. This recognition triggers opening of the complex by promoting destabilization of the hydrophobic interactions between subunits, enabling helices of AAC to be incorporated into the complex and displacing a Tim9 subunit in the process via the "competitive displacement" mechanism. It is likely that, while Tim10 provides most of the substrate-binding capacity, at least one Tim9 subunit remains in close proximity to AAC during its transit through the IMS. It must be stated, however, that the models proposed remain speculative. Structural information on the conformation of the small Tim proteins while engaged in binding to substrate is required to fully understand the functional mechanism of the small Tim chaperones.

6. Conclusions

The biogenesis and function of the mitochondrial small Tim proteins is a process requiring correct protein folding at both a spatial and temporal level. Much of this process is centered on the four strictly conserved cysteine residues in each protein. The cysteines must remain reduced for the proteins to be imported into mitochondria. As a result, oxidative folding regulates the import of individual proteins, their stability, and their final assembly into a functional complex. The function of the small Tim proteins in chaperoning mitochondrial membrane precursors might, on the other hand, depend on more complicated, dynamic hydrophobic interactions. Despite the knowledge gained thus far, much remains to be investigated. For example, how the redoxin systems, metal ions, cytosolic chaperones and the proteasome all interact in the maintenance and degradation of the small Tim proteins while in the cytosol. Additionally, the detailed oxidative folding pathway of the small Tim proteins in the IMS remains a speculative model, with the proposed steps and order of disulfide bond formation still requiring experimental backup. Lastly, deciphering how the small Tim complexes remodel to incorporate both different subunit compositions, as well as incoming substrates, should help clarify the functional molecular mechanism of these chaperone proteins. Answering these and other questions will provide a clearer picture of oxidative protein folding in the IMS and the essential roles the small Tim proteins play in mitochondrial protein biogenesis.

Acknowledgments

E.C.-P. is funded by a PhD studentship from the Mexican National Council for Science and Technology (CONACyT). M.P.S. is a postdoctoral researcher funded by the Leverhulme Trust (to H.L.). Research in the group of H.L. has been funded by the Biotechnology and Biological Sciences Research Council, Leverhulme Trust, and the Royal Society.

Conflicts of Interest

The authors declare no conflict of interest.

References

1. Koehler, C.M. The small Tim proteins and the twin Cx3C motif. *Trends Biochem. Sci*. **2004**, *29*, 1–4.
2. Sirrenberg, C.; Endres, M.; Folsch, H.; Stuart, R.A.; Neupert, W.; Brunner, M. Carrier protein import into mitochondria mediated by the intermembrane proteins Tim10/Mrs11 and Tim12/Mrs5. *Nature* **1998**, *391*, 912–915.
3. Koehler, C.M.; Merchant, S.; Oppliger, W.; Schmid, K.; Jarosch, E.; Dolfini, L.; Junne, T.; Schatz, G.; Tokatlidis, K. Tim9p, an essential partner subunit of Tim10p for the import of mitochondrial carrier proteins. *EMBO J.* **1998**, *17*, 6477–6486.
4. Adam, A.; Endres, M.; Sirrenberg, C.; Lottspeich, F.; Neupert, W.; Brunner, M. Tim9, a new component of the TIM22.54 translocase in mitochondria. *EMBO J.* **1999**, *18*, 313–319.
5. Gentle, I.E.; Perry, A.J.; Alcock, F.H.; Likic, V.A.; Dolezal, P.; Ng, E.T.; Purcell, A.W.; McConnville, M.; Naderer, T.; Chanez, A.L.; *et al*. Conserved motifs reveal details of ancestry and structure in the small TIM chaperones of the mitochondrial intermembrane space. *Mol. Biol. Evol.* **2007**, *24*, 1149–1160.
6. Wiedemann, N.; Pfanner, N.; Chacinska, A. Chaperoning through the mitochondrial intermembrane space. *Mol. Cell* **2006**, *21*, 145–148.
7. Hofmann, S.; Rothbauer, U.; Muhlenbein, N.; Neupert, W.; Gerbitz, K.D.; Brunner, M.; Bauer, M.F. The C66W mutation in the deafness dystonia peptide 1 (DDP1) affects the formation of functional DDP1.TIM13 complexes in the mitochondrial intermembrane space. *J. Biol. Chem.* **2002**, *277*, 23287–23293.
8. Rothbauer, U.; Hofmann, S.; Muhlenbein, N.; Paschen, S.A.; Gerbitz, K.D.; Neupert, W.; Brunner, M.; Bauer, M.F. Role of the deafness dystonia peptide 1 (DDP1) in import of human Tim23 into the inner membrane of mitochondria. *J. Biol. Chem.* **2001**, *276*, 37327–37334.
9. Beverly, K.N.; Sawaya, M.R.; Schmid, E.; Koehler, C.M. The Tim8-Tim13 complex has multiple substrate binding sites and binds cooperatively to Tim23. *J. Mol. Biol.* **2008**, *382*, 1144–1156.
10. Webb, C.T.; Gorman, M.A.; Lazarou, M.; Ryan, M.T.; Gulbis, J.M. Crystal structure of the mitochondrial chaperone TIM9.10 reveals a six-bladed alpha-propeller. *Mol. Cell* **2006**, *21*, 123–133.
11. Herrmann, J.M.; Riemer, J. Mitochondrial disulfide relay: Redox-regulated protein import into the intermembrane space. *J. Biol. Chem.* **2012**, *287*, 4426–4433.

12. Sideris, D.P.; Tokatlidis, K. Oxidative protein folding in the mitochondrial intermembrane space. *Antioxid. Redox Signal*. **2010**, *13*, 1189–1204.
13. Morgan, B.; Ang, S.K.; Yan, G.; Lu, H. Zinc can play chaperone-like and inhibitor roles during import of mitochondrial small Tim proteins. *J. Biol. Chem.* **2009**, *284*, 6818–6825.
14. Durigon, R.; Wang, Q.; Ceh Pavia, E.; Grant, C.M.; Lu, H. Cytosolic thioredoxin system facilitates the import of mitochondrial small Tim proteins. *EMBO Rep.* **2012**, *13*, 916–922.
15. Lutz, T.; Neupert, W.; Herrmann, J.M. Import of small Tim proteins into the mitochondrial intermembrane space. *EMBO J.* **2003**, *22*, 4400–4408.
16. Milenkovic, D.; Gabriel, K.; Guiard, B.; Schulze-Specking, A.; Pfanner, N.; Chacinska, A. Biogenesis of the essential Tim9-Tim10 chaperone complex of mitochondria: Site-specific recognition of cysteine residues by the intermembrane space receptor Mia40. *J. Biol. Chem.* **2007**, *282*, 22472–22480.
17. Sideris, D.P.; Tokatlidis, K. Oxidative folding of small Tims is mediated by site-specific docking onto Mia40 in the mitochondrial intermembrane space. *Mol. Microbiol.* **2007**, *65*, 1360–1373.
18. Banci, L.; Bertini, I.; Cefaro, C.; Cenacchi, L.; Ciofi-Baffoni, S.; Felli, I.C.; Gallo, A.; Gonnelli, L.; Luchinat, E.; Sideris, D.; Tokatlidis, K. Molecular chaperone function of Mia40 triggers consecutive induced folding steps of the substrate in mitochondrial protein import. *Proc. Natl. Acad. Sci. USA* **2010**, *107*, 20190–20195.
19. Lu, H.; Allen, S.; Wardleworth, L.; Savory, P.; Tokatlidis, K. Functional TIM10 chaperone assembly is redox-regulated *in vivo*. *J. Biol. Chem.* **2004**, *279*, 18952–18958.
20. Ivanova, E.; Jowitt, T.A.; Lu, H. Assembly of the mitochondrial Tim9-Tim10 complex: A multi-step reaction with novel intermediates. *J. Mol. Biol.* **2008**, *375*, 229–239.
21. Lu, H.; Woodburn, J. Zinc binding stabilizes mitochondrial Tim10 in a reduced and import-competent state kinetically. *J. Mol. Biol.* **2005**, *353*, 897–910.
22. Morgan, B.; Lu, H. Oxidative folding competes with mitochondrial import of the small Tim proteins. *Biochem. J*. **2008**, *411*, 115–122.
23. Morgan, B.; Ezerina, D.; Amoako, T.N.; Riemer, J.; Seedorf, M.; Dick, T.P. Multiple glutathione disulfide removal pathways mediate cytosolic redox homeostasis. *Nat. Chem. Biol.* **2013**, *9*, 119–125.
24. Kojer, K.; Bien, M.; Gangel, H.; Morgan, B.; Dick, T.P.; Riemer, J. Glutathione redox potential in the mitochondrial intermembrane space is linked to the cytosol and impacts the Mia40 redox state. *EMBO J*. **2012**, *31*, 3169–3182.
25. Fischer, M.; Horn, S.; Belkacemi, A.; Kojer, K.; Petrungaro, C.; Habich, M.; Ali, M.; Kuttner, V.; Bien, M.; Kauff, F.; *et al*. Protein import and oxidative folding in the mitochondrial intermembrane space of intact mammalian cells. *Mol. Biol. Cell* **2013**, *24*, 2160–2170.
26. Bragoszewski, P.; Gornicka, A.; Sztolsztener, M.E.; Chacinska, A. The ubiquitin-proteasome system regulates mitochondrial intermembrane space proteins. *Mol. Cell Biol.* **2013**, *33*, 2136–2148.
27. Deshaies, R.J.; Koch, B.D.; Werner-Washburne, M.; Craig, E.A.; Schekman, R. A subfamily of stress proteins facilitates translocation of secretory and mitochondrial precursor polypeptides. *Nature* **1988**, *332*, 800–805.
28. Murakami, H.; Pain, D.; Blobel, G. 70-kD heat shock-related protein is one of at least two distinct cytosolic factors stimulating protein import into mitochondria. *J. Cell Biol.* **1988**, *107*, 2051–2057.

29. Becker, J.; Walter, W.; Yan, W.; Craig, E.A. Functional interaction of cytosolic hsp70 and a DnaJ-related protein, Ydj1p, in protein translocation *in vivo*. *Mol. Cell Biol.* **1996**, *16*, 4378–4386.
30. Young, J.C.; Hoogenraad, N.J.; Hartl, F.U. Molecular chaperones Hsp90 and Hsp70 deliver preproteins to the mitochondrial import receptor Tom70. *Cell* **2003**, *112*, 41–50.
31. Lu, H.; Golovanov, A.P.; Alcock, F.; Grossmann, J.G.; Allen, S.; Lian, L.Y.; Tokatlidis, K. The structural basis of the TIM10 chaperone assembly. *J. Biol. Chem.* **2004**, *279*, 18959–18966.
32. Ivanova, E.; Ball, M.; Lu, H. Zinc binding of Tim10: Evidence for existence of an unstructured binding intermediate for a zinc finger protein. *Proteins* **2008**, *71*, 467–475.
33. Frausto, J.J.R.; Williams, R.J.P. *The Biological Chemistry of the Elements*; Oxford University Press: Oxford, UK, 2001.
34. Sensi, S.L.; Canzoniero, L.M.; Yu, S.P.; Ying, H.S.; Koh, J.Y.; Kerchner, G.A.; Choi, D.W. Measurement of intracellular free zinc in living cortical neurons: Routes of entry. *J. Neurosci.* **1997**, *17*, 9554–9564.
35. Sensi, S.L.; Ton-That, D.; Sullivan, P.G.; Jonas, E.A.; Gee, K.R.; Kaczmarek, L.K.; Weiss, J.H. Modulation of mitochondrial function by endogenous Zn^{2+} pools. *Proc. Natl. Acad. Sci. USA* **2003**, *100*, 6157–6162.
36. Eide, D.J. Zinc transporters and the cellular trafficking of zinc. *Biochim. Biophys. Acta* **2006**, 1763, 711–722.
37. Haase, H.; Mocchegiani, E.; Rink, L. Correlation between zinc status and immune function in the elderly. *Biogerontology* **2006**, *7*, 421–428.
38. Mesecke, N.; Bihlmaier, K.; Grumbt, B.; Longen, S.; Terziyska, N.; Hell, K.; Herrmann, J.M. The zinc-binding protein Hot13 promotes oxidation of the mitochondrial import receptor Mia40. *EMBO Rep*. **2008**, *9*, 1107–1113.
39. Curran, S.P.; Leuenberger, D.; Leverich, E.P.; Hwang, D.K.; Beverly, K.N.; Koehler, C.M. The role of Hot13p and redox chemistry in the mitochondrial TIM22 import pathway. *J. Biol. Chem.* **2004**, *279*, 43744–43751.
40. Berndt, C.; Lillig, C.H.; Holmgren, A. Thioredoxins and glutaredoxins as facilitators of protein folding. *Biochim. Biophys. Acta* **2008**, *1783*, 641–650.
41. Banci, L.; Barbieri, L.; Luchinat, E.; Secci, E. Visualization of redox-controlled protein fold in living cells. *Chem. Biol.* **2013**, *20*, 747–752.
42. Spiller, M.P.; Ang, S.K.; Ceh-Pavia, E.; Fisher, K.; Wang, Q.; Rigby, S.E.; Lu, H. Identification and characterisation of mitochondrial Mia40 as an iron-sulphur protein. *Biochem. J.* **2013**, doi:10.1042/BJ20130442.
43. Chacinska, A.; Guiard, B.; Muller, J.M.; Schulze-Specking, A.; Gabriel, K.; Kutik, S.; Pfanner, N. Mitochondrial biogenesis, switching the sorting pathway of the intermembrane space receptor Mia40. *J. Biol. Chem.* **2008**, *283*, 29723–29729.
44. Chacinska, A.; Pfannschmidt, S.; Wiedemann, N.; Kozjak, V.; Sanjuan Szklarz, L.K.; Schulze-Specking, A.; Truscott, K.N.; Guiard, B.; Meisinger, C.; Pfanner, N. Essential role of Mia40 in import and assembly of mitochondrial intermembrane space proteins. *EMBO J.* **2004**, *23*, 3735–3746.

45. Naoe, M.; Ohwa, Y.; Ishikawa, D.; Ohshima, C.; Nishikawa, S.; Yamamoto, H.; Endo, T. Identification of Tim40 that mediates protein sorting to the mitochondrial intermembrane space. *J. Biol. Chem.* **2004**, *279*, 47815–47821.
46. Hofmann, S.; Rothbauer, U.; Muhlenbein, N.; Baiker, K.; Hell, K.; Bauer, M.F. Functional and mutational characterization of human MIA40 acting during import into the mitochondrial intermembrane space. *J. Mol. Biol.* **2005**, *353*, 517–528.
47. Porras, P.; Padilla, C.A.; Krayl, M.; Voos, W.; Barcena, J.A. One single in-frame AUG codon is responsible for a diversity of subcellular localizations of glutaredoxin 2 in Saccharomyces cerevisiae. *J. Biol. Chem.* **2006**, *281*, 16551–16562.
48. Koehler, C.M.; Tienson, H.L. Redox regulation of protein folding in the mitochondrial intermembrane space. *Biochim. Biophys. Acta* **2009**, *1793*, 139–145.
49. Endo, T.; Yamano, K.; Kawano, S. Structural basis for the disulfide relay system in the mitochondrial intermembrane space. *Antioxid. Redox Signal.* **2010**, *13*, 1359–1373.
50. Mesecke, N.; Terziyska, N.; Kozany, C.; Baumann, F.; Neupert, W.; Hell, K.; Herrmann, J.M. A disulfide relay system in the intermembrane space of mitochondria that mediates protein import. *Cell* **2005**, *121*, 1059–1069.
51. Milenkovic, D.; Ramming, T.; Muller, J.M.; Wenz, L.S.; Gebert, N.; Schulze-Specking, A.; Stojanovski, D.; Rospert, S.; Chacinska, A. Identification of the signal directing Tim9 and Tim10 into the intermembrane space of mitochondria. *Mol. Biol. Cell* **2009**, *20*, 2530–2539.
52. Sideris, D.P.; Petrakis, N.; Katrakili, N.; Mikropoulou, D.; Gallo, A.; Ciofi-Baffoni, S.; Banci, L.; Bertini, I.; Tokatlidis, K. A novel intermembrane space-targeting signal docks cysteines onto Mia40 during mitochondrial oxidative folding. *J. Cell Biol.* **2009**, *187*, 1007–1022.
53. Grumbt, B.; Stroobant, V.; Terziyska, N.; Israel, L.; Hell, K. Functional characterization of Mia40p, the central component of the disulfide relay system of the mitochondrial intermembrane space. *J. Biol. Chem.* **2007**, *282*, 37461–37470.
54. Bien, M.; Longen, S.; Wagener, N.; Chwalla, I.; Herrmann, J.M.; Riemer, J. Mitochondrial disulfide bond formation is driven by intersubunit electron transfer in Erv1 and proofread by glutathione. *Mol. Cell* **2010**, *37*, 516–528.
55. Banci, L.; Bertini, I.; Cefaro, C.; Ciofi-Baffoni, S.; Gallo, A.; Martinelli, M.; Sideris, D.P.; Katrakili, N.; Tokatlidis, K. MIA40 is an oxidoreductase that catalyzes oxidative protein folding in mitochondria. *Nat. Struct. Mol. Biol.* **2009**, *16*, 198–206.
56. Stojanovski, D.; Milenkovic, D.; Muller, J.M.; Gabriel, K.; Schulze-Specking, A.; Baker, M.J.; Ryan, M.T.; Guiard, B.; Pfanner, N.; Chacinska, A. Mitochondrial protein import: Precursor oxidation in a ternary complex with disulfide carrier and sulfhydryl oxidase. *J. Cell Biol.* **2008**, *183*, 195–202.
57. Allen, S.; Lu, H.; Thornton, D.; Tokatlidis, K. Juxtaposition of the two distal CX3C motifs via intrachain disulfide bonding is essential for the folding of Tim10. *J. Biol. Chem.* **2003**, *278*, 38505–38513.
58. Vial, S.; Lu, H.; Allen, S.; Savory, P.; Thornton, D.; Sheehan, J.; Tokatlidis, K. Assembly of Tim9 and Tim10 into a functional chaperone. *J. Biol. Chem.* **2002**, *277*, 36100–36108.

59. Baker, M.J.; Webb, C.T.; Stroud, D.A.; Palmer, C.S.; Frazier, A.E.; Guiard, B.; Chacinska, A.; Gulbis, J.M.; Ryan, M.T. Structural and functional requirements for activity of the Tim9-Tim10 complex in mitochondrial protein import. *Mol. Biol. Cell* **2009**, *20*, 769–779.
60. Ivanova, E.; Lu, H. Allosteric and electrostatic protein-protein interactions regulate the assembly of the heterohexameric Tim9-Tim10 complex. *J. Mol. Biol.* **2008**, *379*, 609–616.
61. Walton, T.A.; Sousa, M.C. Crystal structure of Skp, a prefoldin-like chaperone that protects soluble and membrane proteins from aggregation. *Mol. Cell* **2004**, *15*, 367–374.
62. Siegert, R.; Leroux, M.R.; Scheufler, C.; Hartl, F.U.; Moarefi, I. Structure of the molecular chaperone prefoldin: Unique interaction of multiple coiled coil tentacles with unfolded proteins. *Cell* **2000**, *103*, 621–632.
63. Korndorfer, I.P.; Dommel, M.K.; Skerra, A. Structure of the periplasmic chaperone Skp suggests functional similarity with cytosolic chaperones despite differing architecture. *Nat. Struct. Mol. Biol.* **2004**, *11*, 1015–1020.
64. Ivanova, E.; Pang, J.; Jowitt, T.A.; Yan, G.; Warwicker, J.; Sutcliffe, M.J.; Lu, H. Temperature-dependent study reveals that dynamics of hydrophobic residues plays an important functional role in the mitochondrial Tim9-Tim10 complex. *Proteins* **2011**, doi:10.1002/prot.23224.
65. Vergnolle, M.A.; Baud, C.; Golovanov, A.P.; Alcock, F.; Luciano, P.; Lian, L.Y.; Tokatlidis, K. Distinct domains of small Tims involved in subunit interaction and substrate recognition. *J. Mol. Biol.* **2005**, *351*, 839–849.
66. Roesch, K.; Curran, S.P.; Tranebjaerg, L.; Koehler, C.M. Human deafness dystonia syndrome is caused by a defect in assembly of the DDP1/TIMM8a-TIMM13 complex. *Hum. Mol. Genet.* **2002**, *11*, 477–486.
67. Baker, M.J.; Mooga, V.P.; Guiard, B.; Langer, T.; Ryan, M.T.; Stojanovski, D. Impaired folding of the mitochondrial small TIM chaperones induces clearance by the i-AAA protease. *J. Mol. Biol.* **2012**, *424*, 227–239.
68. Vergnolle, M.A.; Alcock, F.H.; Petrakis, N.; Tokatlidis, K. Mutation of conserved charged residues in mitochondrial TIM10 subunits precludes TIM10 complex assembly, but does not abolish growth of yeast cells. *J. Mol. Biol.* **2007**, *371*, 1315–1324.
69. Leuenberger, D.; Curran, S.P.; Wong, D.; Koehler, C.M. The role of Tim9p in the assembly of the TIM22 import complexes. *Traffic* **2003**, *4*, 144–152.
70. Jarosch, E.; Tuller, G.; Daum, G.; Waldherr, M.; Voskova, A.; Schweyen, R.J. Mrs5p, an essential protein of the mitochondrial intermembrane space, affects protein import into yeast mitochondria. *J. Biol. Chem.* **1996**, *271*, 17219–17225.
71. Gebert, N.; Chacinska, A.; Wagner, K.; Guiard, B.; Koehler, C.M.; Rehling, P.; Pfanner, N.; Wiedemann, N. Assembly of the three small Tim proteins precedes docking to the mitochondrial carrier translocase. *EMBO Rep*. **2008**, *9*, 548–554.
72. Truscott, K.N.; Wiedemann, N.; Rehling, P.; Muller, H.; Meisinger, C.; Pfanner, N.; Guiard, B. Mitochondrial import of the ADP/ATP carrier: The essential TIM complex of the intermembrane space is required for precursor release from the TOM complex. *Mol. Cell Biol.* **2002**, *22*, 7780–7789.
73. Leuenberger, D.; Bally, N.A.; Schatz, G.; Koehler, C.M. Different import pathways through the mitochondrial intermembrane space for inner membrane proteins. *EMBO J*. **1999**, *18*, 4816–4822.

74. Vergnolle, M.A.; Sawney, H.; Junne, T.; Dolfini, L.; Tokatlidis, K. A cryptic matrix targeting signal of the yeast ADP/ATP carrier normally inserted by the TIM22 complex is recognized by the TIM23 machinery. *Biochem. J.* **2005**, *385*, 173–180.
75. Endres, M.; Neupert, W.; Brunner, M. Transport of the ADP/ATP carrier of mitochondria from the TOM complex to the TIM22.54 complex. *EMBO J.* **1999**, *18*, 3214–3221.
76. Pfanner, N.; Hoeben, P.; Tropschug, M.; Neupert, W. The carboxyl-terminal two-thirds of the ADP/ATP carrier polypeptide contains sufficient information to direct translocation into mitochondria. *J. Biol. Chem.* **1987**, *262*, 14851–14854.
77. Ryan, M.T.; Muller, H.; Pfanner, N. Functional staging of ADP/ATP carrier translocation across the outer mitochondrial membrane. *J. Biol. Chem.* **1999**, *274*, 20619–20627.
78. Rehling, P.; Model, K.; Brandner, K.; Kovermann, P.; Sickmann, A.; Meyer, H.E.; Kuhlbrandt, W.; Wagner, R.; Truscott, K.N.; Pfanner, N. Protein insertion into the mitochondrial inner membrane by a twin-pore translocase. *Science* **2003**, *299*, 1747–1751.
79. Curran, S.P.; Leuenberger, D.; Oppliger, W.; Koehler, C.M. The Tim9p-Tim10p complex binds to the transmembrane domains of the ADP/ATP carrier. *EMBO J.* **2002**, *21*, 942–953.
80. Vasiljev, A.; Ahting, U.; Nargang, F.E.; Go, N.E.; Habib, S.J.; Kozany, C.; Panneels, V.; Sinning, I.; Prokisch, H.; Neupert, W.; *et al*. Reconstituted TOM core complex and Tim9/Tim10 complex of mitochondria are sufficient for translocation of the ADP/ATP carrier across membranes. *Mol. Biol. Cell* **2004**, *15*, 1445–1458.
81. Wiedemann, N.; Pfanner, N.; Ryan, M.T. The three modules of ADP/ATP carrier cooperate in receptor recruitment and translocation into mitochondria. *EMBO J.* **2001**, *20*, 951–960.

Publication 2

DURIGON, R., WANG, Q., CEH PAVIA, E., GRANT, C. M. & LU, H. (2012) Cytosolic thioredoxin system facilitates the import of mitochondrial small Tim proteins. EMBO Rep, 13, 916-22.

EMBO reports

scientific report

Cytosolic thioredoxin system facilitates the import of mitochondrial small Tim proteins

Romina Durigon[1], Qi Wang[1], Efrain Ceh Pavia[1], Chris M. Grant[2] & Hui Lu[1+]

[1]Manchester Institute of Biotechnology, Faculty of Life Sciences, and [2]Faculty of Life Sciences, University of Manchester, Manchester, UK

Thiol-disulphide redox regulation has a key role during the biogenesis of mitochondrial intermembrane space (IMS) proteins. Only the Cys-reduced form of precursor proteins can be imported into mitochondria, which is followed by disulphide bond formation in the mitochondrial IMS. In contrast to the wealth of knowledge on the oxidation process inside mitochondria, little is known about how precursors are maintained in an import-competent form in the cytosol. Here we provide the first evidence that the cytosolic thioredoxin system is required to maintain the IMS small Tim proteins in reduced forms and facilitate their mitochondrial import during respiratory growth.

Keywords: redox regulation; mitochondrial import; thioredoxin; oxidoreductase; folding

EMBO *reports* (2012) **13,** 916–922. doi:10.1038/embor.2012.116

INTRODUCTION

Mitochondria has important roles in various regulatory processes ranging from ATP generation to cell growth and apoptosis. Not surprisingly, therefore, mitochondrial dysfunction leads to life-threatening diseases, including diabetes, stroke, Alzheimer, and cancer. Protein import is essential for the biogenesis of mitochondria, as the majority (99%) of mitochondrial proteins are synthesized in the cytosol on cytosolic ribosomes, and thus have to be imported into mitochondria for their function. How precursor proteins are imported into mitochondria is a subject of intensive study and at least four main import pathways have now been characterized [1,2]. In contrast, little is known about how mitochondrial precursors are maintained in an import-competent form in the cytosol.

The import of many essential mitochondrial intermembrane space (IMS) proteins is regulated by their thiol-disulphide redox state [3–6]. Although disulphide bond formation is crucial for the function of these proteins inside mitochondria, oxidized precursor proteins cannot be imported into mitochondria and only Cys-reduced forms are import-competent [5,7,8]. Many IMS proteins, such as members of the 'small Tim' (e.g., Tim9, Tim10) and Cox17 (e.g., Cox17, Cox19) families, contain conserved Cys residues. Import of these proteins depends on the redox-sensitive mitochondrial import and assembly (MIA) pathway. Mia40 and Erv1 are the central components of the MIA pathway; they form a disulphide relay system in the IMS mediating the import and oxidative folding of these Cys-containing proteins [2,9].

Using the small Tim proteins as models, it has been shown that the oxidized proteins are thermodynamically stable under cellular glutathione redox conditions [7,10,11]. These proteins have a standard redox potential of -0.31 V to -0.33 V, which is more negative than that of the glutathione redox conditions in both the cytosol and mitochondrial IMS [7,10,12,13]. Such a redox stability of the small Tim proteins is consistent with their oxidized (disulphide bonded) state in the IMS, but not their reduced (thiol) states in the cytosol. Furthermore, studies showed that the precursors become oxidized during mitochondrial import and that this oxidation kinetically competes with their import [7]. Cytosolic factors are required to maintain these redox-sensitive precursors in a Cys-reduced, import-competent form in the cytosol before their import into mitochondria. Although zinc-binding can stabilize the small Tim proteins in their reduced forms *in vitro*, their relatively low-binding affinities (submicromolar to nanomolar) suggest that zinc-binding might not be the only or an important stabilizing factor during normal cell growth conditions [14,15]. How these redox-sensitive IMS precursors are maintained in an import-competent form in the cytosol is unknown.

The thioredoxin (Trx) and glutaredoxin (Grx) systems are ubiquitous oxidoreductases required for cellular thiol regulation and oxidative stress defence [16,17]. In the yeast *Saccharomyces cerevisiae*, there are two cytosolic Trx homologues (Trx1, 2) and two classical dithiol Grx homologues (Grx1, 2) located in the cytosol. A main function of these enzymes is to reduce disulphide bonds in their substrate proteins using electrons donated by nicotinamide adenine dinucleotide phosphate (NADPH). Oxidized Trx is reduced directly by NADPH and thioredoxin reductase (Trr), whereas Grx is reduced by glutathione using electrons donated by

[1]Manchester Institute of Biotechnology, Faculty of Life Sciences, University of Manchester 131 Princess Street, Manchester M1 7DN,
[2]Faculty of Life Sciences, University of Manchester, Oxford Road, Manchester M13 9PT, UK
[+]Corresponding author. Tel: +44 161 2751553; Fax: +44 161 3065201;
E-mail: hui.lu@manchester.ac.uk

Received 28 January 2012; revised 5 July 2012; accepted 13 July 2012; published online 10 August 2012

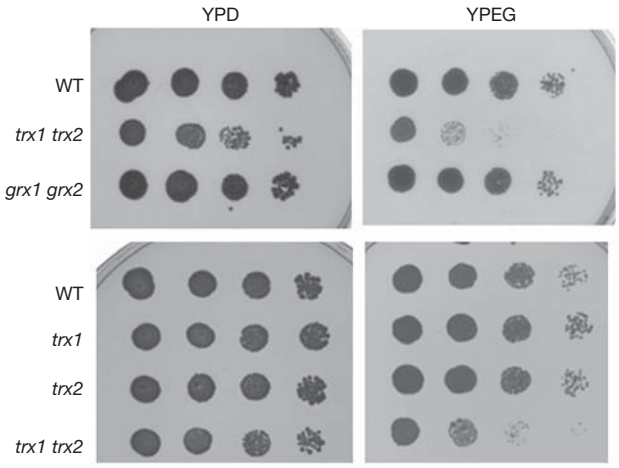

Fig 1 | The cytosolic Trx system is required for mitochondrial function. (**A**) Spot testing of cell growth with the wild-type (WT) and mutant yeast strains. The WT, *trx1 trx2* and *grx1 grx2* double or *trx1* and *trx2* single-deletion strains were spotted on YPD (left column) and YPEG (right column) plates at a series of 10-fold dilutions, followed by incubation at 30 °C for 2 days. grx, glutaredoxin; Trx, thioredoxin.

NADPH through glutathione reductase (Glr). In this present study we show that the cytosolic Trx system is required for yeast growth under respiratory condition and facilitates the import of mitochondrial MIA substrates by maintaining the precursors in a reduced form. An efficient disulphide bond transfer reaction was reconstituted using purified proteins, and we show that the Trx system preferentially catalyses the reduction of folding intermediates, rather than the fully oxidized protein.

RESULTS AND DISCUSSION

The Trx system is required for respiratory growth

To determine whether the cytosolic Trx and Grx systems are required for mitochondrial function, the wild-type (WT), *trx* and *grx* mutant strains were spotted onto fermentative and respiratory growth media (Fig 1). Although a double *TRX* deletion mutant (*trx1 trx2*) grows somewhat slower than the WT strain during fermentative growth (YPD), it is particularly inhibited for growth under respiratory conditions (YPEG). In contrast, the double *GRX* deletion mutant (*grx1 grx2*) grew comparably to the WT under both conditions. These results indicate that the Trx system might have an important role during the biogenesis of mitochondria. Growth of both the *trx1* and *trx2* single mutants was unaffected under respiratory conditions, consistent with an overlapping role for the two Trx proteins. This indicates that the respiratory growth defect of *TRX* deletion mutant (*trx1 trx2*) is not simply because of respiratory reactive oxygen species (ROS) production, as *trx2* mutants are hypersensitive to ROS, in contrast to *trx1* mutants that have WT levels of resistance [18]. Taken together, these results indicate that the cytosolic Trx system is required for maintaining mitochondrial function and probably facilitating the biogenesis of mitochondria. However, we cannot rule out that the defects seen in the *trx1 trx2* mutant strain is also contributed by other effects, as Trx proteins participate in various processes and have many client proteins.

To assess the function of Trx in biogenesis of mitochondrial proteins, protein expression was examined. While antibodies against Trx and Grx confirmed the deletion of these proteins, there were no obvious differences in the levels of the mitochondrial proteins (Mia 40 and MtHsp 70), although Tim9 and Tim10 seem to be slightly decreased in the *trx1 trx2* mutant (Fig 2A). To check this, mitochondria were isolated from the WT and mutant cells grown in YPEG, and protein concentrations determined. The steady-state levels of mitochondrial proteins from all four subcompartments are similar (not shown). This was not surprising, as the mutant was not unviable but grows slowly, and a small intensity difference will not be detectable by western blot. A similar result was shown for a *TOM5* (a non-essential component of the mitochondrial TOM translocase complex) deletion mutant [19]. Thus, the levels of the mitochondrial proteins under more stressful conditions were analysed. Cells were grown in fermentative YPD followed by a medium shift to respiratory YPEG for 6 h before mitochondria were isolated. The results clearly showed that the levels of the small Tim proteins (Tim9, Tim10 and Tim13) were decreased in the mitochondria of the *trx1 trx2* mutant strain, while no obvious decrease was observed for the other control proteins (Fig 2B). The same mitochondrial isolation and western blotting experiment were performed three times, and the levels of the small Tim proteins of the mutant strain were statistically lower than that of the WT strain ($P<0.05$, Fig 2C). These results provide *in vivo* evidence that the cytosolic Trx system is involved in facilitating biogenesis of the mitochondrial small Tim proteins.

The Trx system facilitates the import of IMS proteins *in vitro*

To verify whether the Trx system has an effect on the import of mitochondrial proteins, mitochondrial import was examined using radiolabelled Tim9 and Tim10, synthesized in rabbit reticulocyte lysates, in the presence or absence of purified Trx1, Trr1 and/or NADPH. To eliminate the effect of metal ions such as Zn^{2+}, all import experiments were carried out in the presence of 2 mM EDTA. After import for 30 min, reactions were treated with trypsin to remove un-imported materials, and mitochondrial import was analysed using SDS–PAGE (Fig 3A), revealing that in the presence of the Trx1 system (lane 2) the import level was increased compared with the control (lane 1; Fig 3A). A partial Trx system (without Trx1 or Trr1) slightly enhanced the import level, but not as efficiently as the full system. It should be noted that small amounts of the Trx and/or Grx system components might be present in reticulocyte lysates; however, the addition of the purified yeast system clearly increased import (lane 1 versus lane 2) confirming that the Trx system facilitates import of the small Tim proteins. The same effect was observed when Cox19, a CX_9C motif containing substrate of the MIA pathway (Fig 3A), was used as an import substrate. In contrast, no obvious effect was observed on the import of the matrix marker proteins F_1-ATPase subunit-β ($F_1β$) and mtHsp60, the inner membrane (IM) protein AAC, or the outer membrane porin. A time-course experiment confirmed that the Trx system increases the import of the small Tim proteins (Fig 3B). While the import seems to reach a stationary level after 5 min in the absence of Trx system, it was continuously increased with the presence of the Trx system over the whole time course. Furthermore, an 4-acetamido-4′-maleimidylstilbene-2,2′-disulfonic acid (AMS) assay showed that the redox state of mitochondrial Mia 40 was not

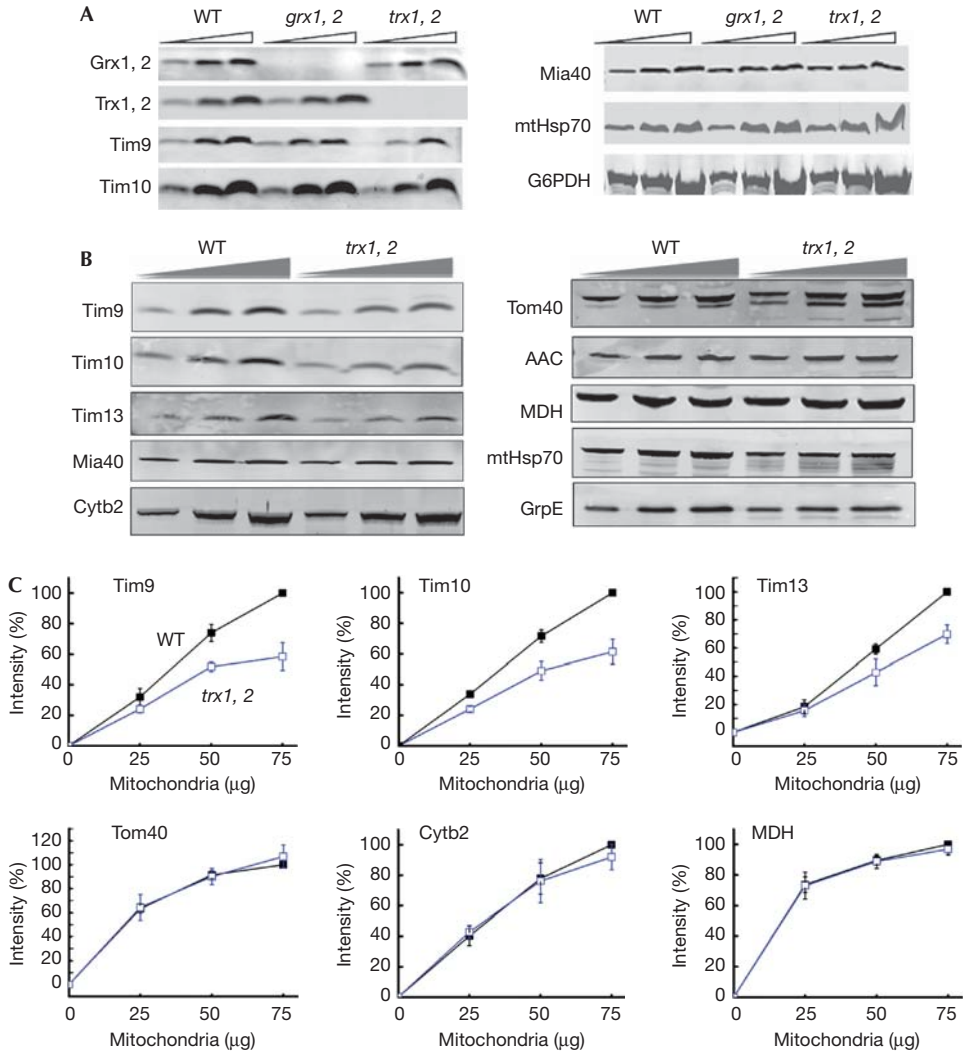

Fig 2 | Effects of the Trx system on protein expression level. (**A**) Western blots of cellular extracts from the wild-type (WT) and mutant cells. Yeasts were grown to exponential phase in YPEG medium, then lysed and analysed using antibodies against the indicated proteins. Cytosolic protein G6PDH was used as a loading control. (**B**) Western blots with mitochondria isolated from the WT and mutant cells. The WT and *trx1 trx2* yeast cells were grown in YPD to OD_{600} of 10 and shifted to YPEG for 6 h. Then mitochondria were isolated and analysed using antibodies against the indicated proteins. 25, 50 and 75 μg mitochondria were loaded. The IMS proteins (Tim9, Tim10, Tim13 and Cytb2); Mia40: IMS/IM anchored; the outer membrane Tom40; IM AAC; and matrix protein malate dehydrogenase (MDH), mtHsp70 and co-chaperone GrpE were analysed. (**C**) Quantification of proteins in the mitochondria isolated from the WT (black solid squares) and *trx1 trx2* (blue open squares) cells as described in **B**. The levels of the small Tim proteins were significantly different (by Student's *t*-test: Tim10 $P<0.05$ at all points, Tim9 and Tim13 $P<0.05$ at 50 and 75 μg), and not significantly different for the marker proteins. Error bars represent s.e. ($n=3$). grx, glutaredoxin; IM, inner membrane; IMS, intermembrane space; Trx, thioredoxin.

affected by the addition of the components of Trx system in the reactions (Fig 3C), and Mia 40 was mainly in the oxidized state as shown previously [20]. Taken together, these results indicate that (i) the Trx system selectively facilitates the import of the redox-sensitive precursors of mitochondrial IMS proteins, and (ii) the general mitochondrial import machineries are not affected by the presence of the Trx system.

The Trx system keeps small Tims in reduced forms

We anticipated that the mechanism of enhanced import of the small Tim proteins was that the Trx system can maintain the precursors in a reduced form. To confirm this idea, following the import assay described above, the redox state of the remaining un-imported proteins was analysed using the AMS thiol-modification assay (Fig 4A). The results indicate that while all the un-imported proteins were oxidized in the control (lane 1), the Trx1 system can maintain a large fraction of the proteins in a reduced form (lane 2). A small fraction of reduced proteins also existed in the reaction containing Trx1 (lane 4), but not Trr1 alone (lane 3). The same result was obtained for both Tim9 and Tim10.

Our results indicate that the presence of the Trx system causes an increased level of reduced precursors, and improved import of

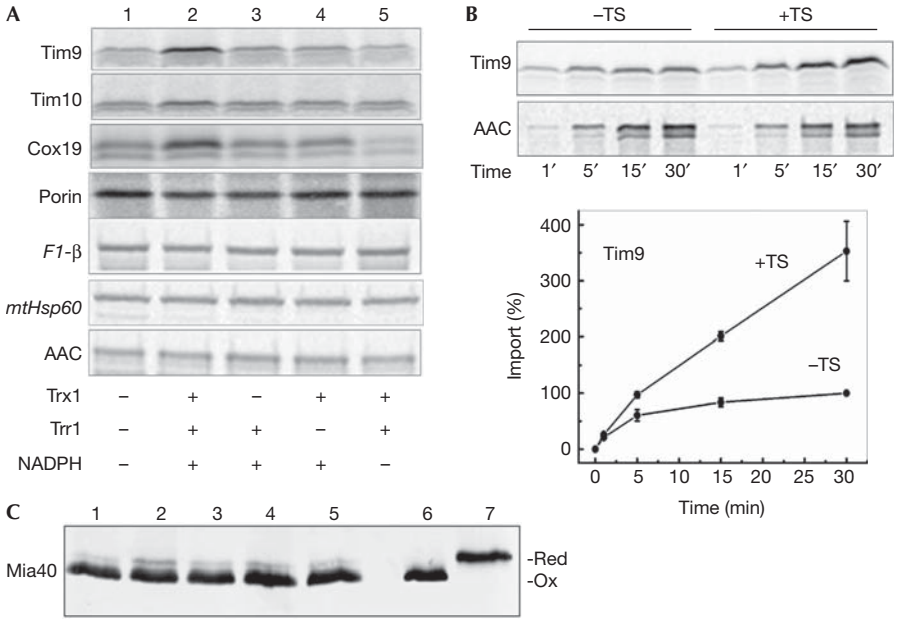

Fig 3 | The Trx system facilitates the import of MIA substrates. (**A**). Effects of Trx system on the mitochondrial import. *In vitro* translated radioactive precursor proteins as indicated were incubated with isolated mitochondria in the presence or absence of the purified Trx system at 25 °C for 30 min, followed by trypsin treatment to remove un-imported proteins. Then, all mitochondrial imports were analysed by SDS–PAGE and autoradiography. (**B**) Time course of Tim9 and AAC import in the presence (+TS) or absence (−TS) of the Trx system, and the qualification for Tim9 (bottom, −TS, 30 min as 100%). Error bars represent s.e. ($n >= 3$). (**C**) Western blot of 4-acetamido-4′-maleimidylstilbene-2,2′-disulfonic acid assay of Mia40 after incubating with components of Trx system at 25 °C for 20 min. Lanes 1–5 as in **A**, lanes 6 and 7 were oxidized (Ox) and reduced (Red) controls. MIA, mitochondrial import and assembly; NADPH, nicotinamide adenine dinucleotide phosphate; TS, Trx system; Trr, thioredoxin reductase; Trx, thioredoxin.

these precursors. However, as the mitochondrial import system contains many components, it remained possible that our results could be because of an indirect effect of the Trx system on some of these components. To address this, we asked whether the Trx system can directly reduce disulphide bonds of the small Tim proteins. Purified oxidized Tim10 was incubated with purified Trx1 in the presence and absence of purified Trr1 for 10 min, followed by the AMS assay. The results showed that a fraction of Tim10 was reduced by the presence of the Trx1 system (Fig 4B, lane 3), suggesting that Tim10 is a substrate of the Trx1 system. Consistently, the small Tim proteins cannot be reduced by Trx1 or Trr1 alone (lanes 2 and 4; note that in the absence of Trr1, Trx1 was in the oxidized inactive form). Thus the small Tim proteins can be reduced by the Trx system directly. However, only a fraction of the protein was reduced under these experimental conditions, indicating that the fully oxidized proteins might not be very good substrates of the Trx1 system.

Small Tims proteins are good substrates of Trx system

There are two intramolecular disulphide bonds in Tim9 and Tim10 formed between the Cys residues of the twin CX3C motif in juxtaposition (C1–C4, and C2–C3). Previous work showed that oxidative folding of the small Tim proteins occurs through formation of single disulphide–bonded intermediates and that these intermediates are also import-incompetent [7]. Thus, we asked whether the Trx system can reduce these folding intermediates more efficiently. For this, double Cys mutants with each disulphide bond mutated to Ser (C1,4S and C2,3S) were used. As shown in Fig 4C, all the Cys mutants can be fully reduced by the Trx1 system, and a time-course analysis confirmed that reduction of the mutants was very rapid. While only about 10% of native Tim10 was reduced after 10 min, all of the single disulphide–bonded mutants were reduced within 1 min (Fig 4D). Thus, reduction of the single-disulphide intermediates by the Trx1 system is at least 100-fold faster than that of the fully oxidized proteins.

To obtain more quantitative results, the reactions were measured by following absorption changes at 340 nm because of NADPH oxidation (Fig 5A), and the results were analysed using the Michaelis–Menten equation (Fig 5B). The catalytic constant k_{cat} and Michaelis constant K_m were determined to be 23 min^{-1} and 6.0 μM for Tim10C1,4S, and 29.0 min^{-1} and 5.3 μM for Tim10C2,3S, respectively, and the substrate efficiency (k_{cat}/K_m) was 3.8×10^6 M^{-1} min^{-1} for Tim10C1,4S, and 5.5×10^6 M^{-1} min^{-1} for Tim10C2,3S. This substrate efficiency is similar to that of the well-characterized substrates of Trx, such as ribonucleotide reductase, arsenate reductase and insulin [21–23]. This result confirms that both single-disulphide intermediates are excellent substrates of the Trx system, supporting our conclusion that the Trx system maintains the small Tim proteins in a reduced form in the cytosol and thus facilitates their mitochondrial import.

To understand why the Cys mutants, but not the WT proteins, are excellent substrates of the Trx system, overall folding of

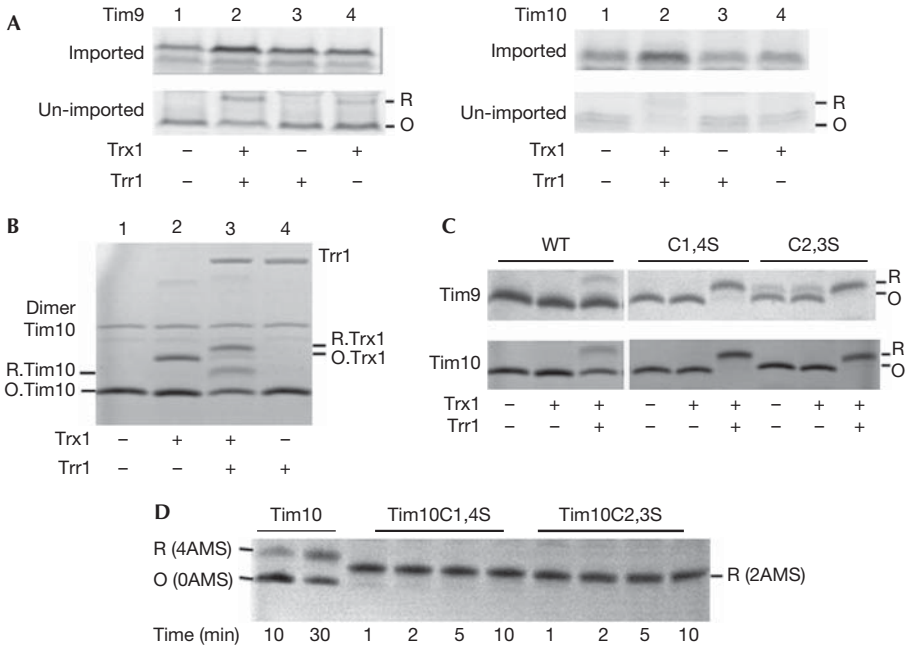

Fig 4 | Effects of Trx system on the redox state of Tim9 and Tim10. (**A**) Import and the redox state of un-imported small Tim proteins. The proteins were imported in the presence or absence of Trx system (TS: 1.5 μM Trx1, 0.5 μM Trr1 and 0.6 mM NADPH) at 25 °C for 30 min, and then each reaction was divided into two. One treated with trypsin for import analysis (top panels), the other was centrifuged and the supernatant was treated with AMS (bottom panels). (**B**) The Trx system reduces disulphide bonds of purified Tim10. Tim10 (10 μM) was incubated with 0.6 mM NADPH in the presence and absence of Trx1 (1.5 μM) and/or Trr1 (0.5 μM) at 25 °C for 10 min. Then the redox state was analysed by AMS assay. (**C**) AMS assay of the WT and double Cys mutant of Tim9 and Tim10 as described in **B**. (**D**) Time course of the reduction of WT and mutant Tim10 by the Trx system. (**B–D**), SDS–PAGE with Coomassie staining. The reduced (R) and oxidized (O) states are indicated. AMS, 4-acetamido-4′-maleimidylstilbene-2,2′-disulfonic acid; NADPH, nicotinamide adenine dinucleotide phosphate; Trr, thioredoxin reductase; Trx, thioredoxin; WT, wild-type.

these proteins was studied using far-ultraviolet circular dichroism (CD; Fig 5C). As shown previously, the WT proteins are folded with α-helical structure, which becomes unfolded on addition of a reducing agent, Tris(2-carboxyethyl)phosphine (TCEP). Clearly, both double Cys mutants of Tim10 display significantly lower CD signals than the oxidized WT protein (Fig 5C curves a, b and c). Oxidized Tim10C1,4S seems to be as unfolded as the reduced protein, and there is no obvious spectrum change on addition of TCEP (curves b and e). In comparison to the WT protein, Tim10C2,3S is partially folded and becomes unfolded on addition of TECP (curves c and f). Thus, together with the above enzyme kinetic study, our results revealed that the Trx enzymes preferably react with Tim10 in an unfolded or partially folded state. In other words, the Trx enzymes react with the folding intermediates preferably and effectively rather than the folded small Tim proteins, indicating a stereoselective control mechanism. This result is consistent with the fact that all the well-known substrate proteins of the Trx enzymes have a solvent-exposed disulphide bond. Such a stereoselective mechanism will not only allow the enzyme to recognize a wide range of substrates, but also to reduce disulphide bonds effectively at an early stage of protein folding. We presume that apart from the small Tim proteins, many more redox-sensitive proteins can be maintained in a reduced state through the redoxin system by preventing the formation of early folding intermediates.

CONCLUSION

In summary, whereas the MIA pathway is used for import and oxidative folding of many Cys-containing IMS proteins inside mitochondria, here we provide the first evidence that the cytosolic Trx system is required to keep the precursors in a reduced form in the cytosol and thus to facilitate their mitochondrial import. The Trx system specifically facilitates the import of redox-sensitive IMS proteins without affecting matrix and membrane proteins, through an efficient disulphide bond transfer reaction that could be reconstituted using purified proteins. Further, we show that single-disulphide folding intermediates of the small Tim proteins are excellent substrates of the Trx system. The Trx enzyme preferentially recognizes unfolded or partially folded Tim10, and thus catalyses the reduction of the folding intermediates rather than the fully oxidized small Tim proteins. Our findings provide important insight into the initial steps of mitochondrial protein biogenesis, specifically how mitochondrial precursors are maintained in an import-competent form in the cytosol.

METHODS

Materials. 4-Acetamido-4′-maleimidylstilbene-2,2′-disulfonic acid were obtained from Invitrogen Molecular Probes. EDTA was from BDH Co, and all other chemicals were obtained from the Sigma at the highest grade. The *yeast* strains used in this study were the isogenic derivatives of W303 as described previously [18].

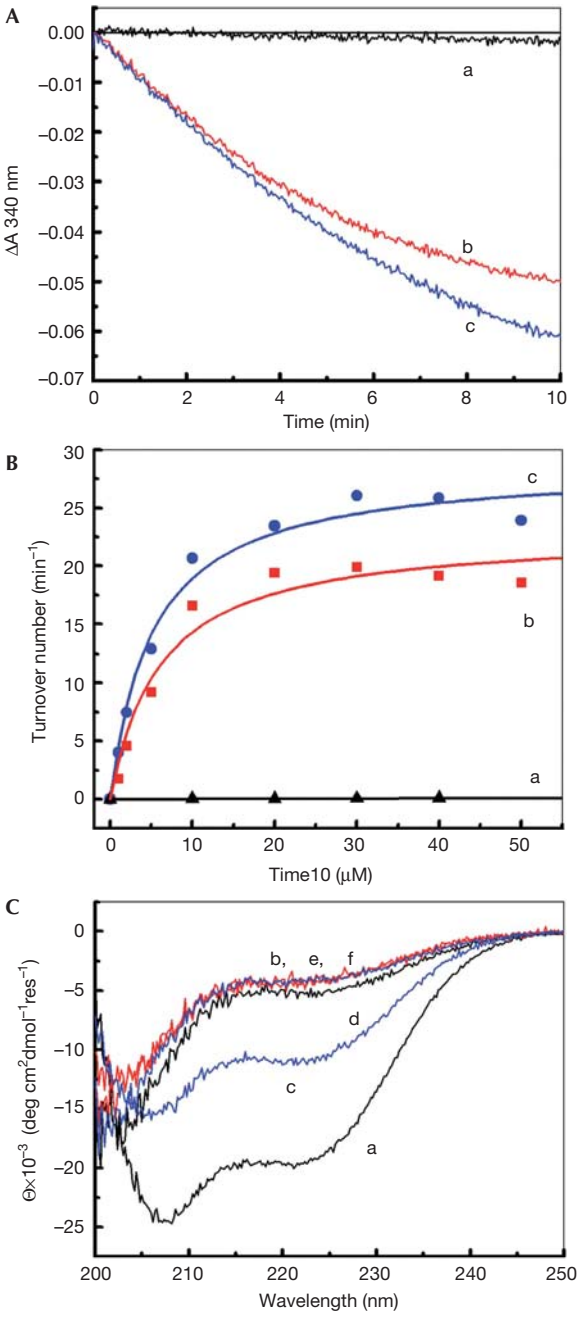

Fig 5 | Kinetic and structural analysis of the WT and mutant Tim10. (**A**) Time course of absorption change at 340 nm for 10 μM Tim10 WT (a), Tim10C1,4S (b) or Tim10C2,3S (c) in the presence of 0.1 μM Trx, 0.1 μM Trr1 and 140 μM NADPH, after subtraction of blank reaction in the absence of Tim10. (**B**) Michaelis–Menten plots of the WT (a), Tim10C1,4S (b) and Tim10C2,3S (c) as studied in **A**. The k_{cat} and K_m were determined to be 23 min^{-1}, 6.0 μM for Tim10C1,4S, and 29.0 min^{-1}, 5.3 μM for Tim10C2,3S, respectively. (**C**) Far-ultraviolet circular dichroism spectra of the WT Tim10 (a, d), Tim10C1,4S (b, e) and Tim10C2,3S (c, f), in the absence (a–c) or presence (d–f) of 1 mM TCEP at 25 °C for 1 h. NADPH, nicotinamide adenine dinucleotide phosphate; Trr, thioredoxin reductase; Trx, thioredoxin; WT, wild-type.

Protein preparations. Oxidized WT and mutant Tim10 were purified as described previously in buffer AE (50 mM Tris, pH 7.4, 150 mM NaCl, 1 mM EDTA) [10,24]. Trx1 and Trr1 were purified as described previously [25], and followed by gel filtration (Superde × 200 column). Flavin adenine dinucleotide was added to Trr1 before gel filtration. Trx1 concentration was determined using extinction coefficient of 10,095 $M^{-1} cm^{-1}$ at 280 nm, and Trr1 concentration was determined based on extinction coefficient of 11,300 $M^{-1} cm^{-1}$ for flavin adenine dinucleotide at 450 nm.

Miscellaneous. All experiments were carried out at 25 °C in buffer AE unless stated. AMS assay was performed as described in [7]. CD spectra were recorded as described in [14]. Mitochondria isolation and protein import analysis were performed as described previously [26,27]. All import reactions were performed in the presence of 2 mM EDTA. For steady-state levels of mitochondrial protein analyses, the WT and *trx1 trx2* yeast cells were first grown in YPD until OD_{600} of 10 and then, cells were isolated by centrifugation, washed twice with autoclaved milli-Q water, then shifted to grow in YPEG for 6 h before the mitochondria were isolated. For the Trx enzyme kinetic analysis, WT or mutant Tim10 (1–50 μM) was mixed with 0.1 μM Trx and 140 μM NADPH, and the reaction was initiated by adding 0.1 μM Trr1. The oxidation of NADPH was followed at 340 nm using a Cary300 spectrophotometer (Varian Ltd).

ACKNOWLEDGEMENTS

We thank to N. Pfanner, K. Hell and M. Pool for protein constructs; to M. Spiller for reading manuscript and helpful comments. H.L.'s research is supported by the Royal Society, Biotechnology and Biological Sciences Research Council and Leverhulme Trust.

Author contributions: H.L. designed the study. R.D., Q.W., E.C.P., C.M.G. and H.L. all designed and performed experiments. R.D., E.C.P. and H.L. analysed the experimental results. H.L. wrote the manuscript with input from C.M.G.

REFERENCES

1. Schmidt O, Pfanner N, Meisinger C (2010) Mitochondrial protein import: from proteomics to functional mechanisms. *Nat Rev Mol Cell Biol* **11:** 655–667
2. Chacinska A, Koehler CM, Milenkovic D, Lithgow T, Pfanner N (2009) Importing mitochondrial proteins: machineries and mechanisms. *Cell* **138:** 628–644
3. Herrmann JM, Hell K (2005) Chopped, trapped or tacked—protein translocation into the IMS of mitochondria. *Trends Biochem Sci* **30:** 205–211
4. Herrmann JM, Kauff F, Neuhaus HE (2009) Thiol oxidation in bacteria, mitochondria and chloroplasts: common principles but three unrelated machineries? *Biochim Biophys Acta* **1793:** 71–77
5. Lu H, Allen S, Wardleworth L, Savory P, Tokatlidis K (2004) Functional TIM10 chaperone assembly is redox-regulated *in vivo*. *J Biol Chem* **279:** 18952–18958
6. Mesecke N, Terziyska N, Kozany C, Baumann F, Neupert W, Hell K, Herrmann JM (2005) A disulfide relay system in the intermembrane space of mitochondria that mediates protein import. *Cell* **121:** 1059–1069
7. Morgan B, Lu H (2008) Oxidative folding competes with mitochondrial import of the small Tim proteins. *Biochem J* **411:** 115–122
8. Tokatlidis K (2005) A disulfide relay system in mitochondria. *Cell* **121:** 965–967
9. Hell K (2008) The Erv1-Mia40 disulfide relay system in the intermembrane space of mitochondria. *Biochim Biophys Acta* **1783:** 601–609
10. Lu H, Woodburn J (2005) Zinc binding stabilizes mitochondrial Tim10 in a reduced and import-competent state kinetically. *J Mol Biol* **353:** 897–910

11. Tienson HL, Dabir DV, Neal SE, Loo R, Hasson SA, Boontheung P, Kim SK, Loo JA, Koehler CM (2009) Reconstitution of the mia40-erv1 oxidative folding pathway for the small tim proteins. *Mol Biol Cell* **20:** 3481–3490
12. Hu J, Dong L, Outten CE (2008) The redox environment in the mitochondrial intermembrane space is maintained separately from the cytosol and matrix. *J Biol Chem* **283:** 29126–29134
13. Ostergaard H, Tachibana C, Winther JR (2004) Monitoring disulfide bond formation in the eukaryotic cytosol. *J Cell Biol* **166:** 337–345
14. Ivanova E, Ball M, Lu H (2008) Zinc binding of Tim10: Evidence for existence of an unstructured binding intermediate for a zinc finger protein. *PROTEINS: Struct Func Bioinf* **71:** 467–475
15. Lu H, Golovanov AP, Alcock F, Grossmann JG, Allen S, Lian LY, Tokatlidis K (2004) The structural basis of the TIM10 chaperone assembly. *J Biol Chem* **279:** 18959–18966
16. Holmgren A (1989) Thioredoxin and glutaredoxin systems. *J Biol Chem* **264:** 13963–13966
17. Meyer Y, Buchanan BB, Vignols F, Reichheld JP (2009) Thioredoxins and glutaredoxins: unifying elements in redox biology. *Annu Rev Genet* **43:** 335–367
18. Garrido EO, Grant CM (2002) Role of thioredoxins in the response of *Saccharomyces cerevisiae* to oxidative stress induced by hydroperoxides. *Mol Microbiol* **43:** 993–1003
19. Dietmeier K, Honlinger A, Bomer U, Dekker PJ, Eckerskorn C, Lottspeich F, Kubrich M, Pfanner N (1997) Tom5 functionally links mitochondrial preprotein receptors to the general import pore. *Nature* **388:** 195–200
20. Terziyska N, Grumbt B, Kozany C, Hell K (2009) Structural and functional roles of the conserved cysteine residues of the redox-regulated import receptor Mia40 in the intermembrane space of mitochondria. *J Biol Chem* **284:** 1353–1363
21. Zahedi Avval F, Holmgren A (2009) Molecular mechanisms of thioredoxin and glutaredoxin as hydrogen donors for Mammalian s phase ribonucleotide reductase. *J Biol Chem* **284:** 8233–8240
22. Messens J, Van Molle I, Vanhaesebrouck P, Limbourg M, Van Belle K, Wahni K, Martins JC, Loris R, Wyns L (2004) How thioredoxin can reduce a buried disulphide bond. *J Mol Biol* **339:** 527–537
23. Holmgren A (1979) Thioredoxin catalyzes the reduction of insulin disulfides by dithiothreitol and dihydrolipoamide. *J Biol Chem* **254:** 9627–9632
24. Ivanova E, Jowitt TA, Lu H (2008) Assembly of the mitochondrial Tim9-Tim10 complex: a multi-step reaction with novel intermediates. *J Mol Biol* **375:** 229–239
25. Mukhopadhyay R, Shi J, Rosen BP (2000) Purification and characterization of ACR2p, the *Saccharomyces cerevisiae* arsenate reductase. *J Biol Chem* **275:** 21149–21157
26. Meisinger C, Pfanner N, Truscott KN (2006) Isolation of yeast mitochondria. *Methods Mol Biol* **313:** 33–39
27. Morgan B, Ang SK, Yan G, Lu H (2009) Zinc can play chaperone-like and inhibitor roles during import of mitochondrial small Tim proteins. *J Biol Chem* **284:** 6818–6825

Publication 3

SPILLER, M. P., ANG, S. K., CEH-PAVIA, E., FISHER, K., WANG, Q., RIGBY, S. E. & LU, H. (2013) Identification and characterisation of mitochondrial Mia40 as an iron-sulphur protein. *Biochem J*. 455(1):27-35

Biochem. J. (2013) **455**, 27–35 (Printed in Great Britain) doi:10.1042/BJ20130442

Identification and characterization of mitochondrial Mia40 as an iron–sulfur protein

Michael P. SPILLER*, Swee Kim ANG*, Efrain CEH-PAVIA*, Karl FISHER*, Qi WANG*, Stephen E. J. RIGBY* and Hui LU*[1]

*Manchester Institute of Biotechnology, Faculty of Life Sciences, University of Manchester, 131 Princess Street, Manchester M1 7DN, U.K.

Mia40 is a highly conserved mitochondrial protein that plays an essential role in the import and oxidative folding of many proteins of the mitochondrial intermembrane space. Mia40 uses its redox active CPC motif to shuttle disulfides between its client proteins (newly imported proteins) and the thiol oxidase Erv1. As a thiol oxidoreductase, no cofactor was found in Mia40, nor is a cofactor required for this function. In the present study we, for the first time based on both *in vitro* and *in vivo* studies, show that yeast Mia40 can exist as an Fe–S (iron–sulfur) protein as well. We show that Mia40 binds a [2Fe–2S] cluster in a dimer form with the cluster co-ordinated by the cysteine residues of the CPC motifs. The biological relevance of the cofactor binding was confirmed *in vivo* by cysteine redox state and iron uptake analyses, which showed that a significant amount of cellular Mia40 binds iron *in vivo*. Furthermore, our oxygen consumption results suggested that the Fe–S-containing Mia40 is not an electron donor for Erv1. Thus we conclude that Mia40 is a novel Fe–S protein with a new cluster-binding motif (CPC), and apart from the thiol oxidoreductase activity, Mia40 may have another important, as yet undefined, function in cells.

Key words: CXC motif, cysteine redox state, iron–sulfur cluster, metal binding, mitochondrion.

INTRODUCTION

The mitochondrion is a vitally important organelle that performs essential functions in many biological processes from ATP generation and Fe–S (iron–sulfur) cluster biogenesis to signalling and cell death (apoptosis) [1–3]. Mia40 is an evolutionarily conserved protein located in the mitochondrial IMS (intermembrane space) of eukaryotic cells and in some organisms is tethered to the mitochondrial inner membrane. Although Mia40 of *S. cerevisiae* is anchored to the inner membrane through its N-terminal hydrophobic segment, the essential function of Mia40 relies on the conserved IMS-located C-terminal domain [4,5]. A well-characterized function of Mia40 is that it acts as an oxidative translocator or thiol oxidoreductase in the redox-regulated MIA (mitochondrial intermembrane space assembly) pathway [6–9].

Protein import is essential for the biogenesis of mitochondria, because approximately 99 % of mitochondrial proteins are synthesized in the cytosol and thus have to be imported into mitochondria for their function. The mitochondrial IMS harbours many proteins that contain conserved cysteine residues, such as members of the 'small Tim' (e.g. Tim9 and Tim10) and Cox17 families. Import of these proteins is regulated by their thiol-disulfide redox state [10,11]. Although disulfide bond formation is crucial for the function of these proteins inside mitochondria, only cysteine-reduced, and thus unfolded proteins, are import-competent [10,12]. Oxidative folding (disulfide bond formation) of the newly imported proteins occurs in the mitochondrial IMS and it depends on the thiol oxidoreductase function of Mia40.

Mia40 (also called Tim40) and Erv1, a FAD-dependent thiol oxidase, form a thiol oxidoreductase system in the IMS, catalysing the import and oxidative folding of their substrate proteins [6,13]. Mia40 contains six conserved cysteine residues (C1–C6) in its C-terminal domain, which are arranged in one CPC and two CX_9C (where X is any amino acid) motifs. Three intra-molecular disulfide bonds are formed between cysteine residues within the CPC (C1–C2) and juxtaposed between the two CX_9C motifs (C3–C6 and C4–C5) in the oxidized state (Figure 1A). Although CPC is redox-sensitive and acts as the redox active-site of Mia40, the CX_9C disulfide bonds are stable and play a structural role [14–16]. The structure of both the human and the yeast Mia40 C-terminal core domains showed that it is folded in an α-helical hairpin core (helix–loop–helix) stabilized by the two intra-molecular disulfides formed between the two CX_9C motifs and that it has a rigid long N-terminal loop with the CPC motif at the tip [14,16]. The thiol oxidoreductase mechanism involves this CPC cycling between reduced and oxidized states as it transfers electrons from substrate proteins to Erv1 [17,18].

Fe–S proteins play many essential roles in biology. They are involved in catalysis and electron transfer, as well as many regulatory processes through their sensing of changes in environmental conditions (e.g. gene expression and apoptosis) [3,19,20]. Despite the simple structure and composition of the ISCs (Fe–S clusters), their synthesis and assembly into apo-proteins is a highly complex and catalysed process as both elements are toxic to living cells in their free state [3,21]. Mitochondria play a central task in the biogenesis of all cellular Fe–S proteins, and this biogenesis is an essential function of mitochondria. Biogenesis of Fe–S proteins begins in the mitochondrial matrix through the ISC assembly system. Some Fe–S proteins remain in the mitochondria, but others are located in the nucleus or cytoplasm and require the ISC export machinery, which is located in the mitochondrial inner membrane and the IMS [3]. Thus all cytosolic and nuclear Fe–S proteins depend strictly on the function of both the mitochondrial ISC assembly and export machineries. However, little is known about how 'Fe/S' (as elements or as a compound) is exported from the mitochondrial matrix across the IMS to the cytosol. Experimental evidence suggests that yeast Erv1, the essential partner of Mia40 in the MIA pathway, is involved in export of

Abbreviations used: AMS, 4-acetamido-4′-maleimidylstilbene-2,2′-disulfonic acid; Fe–S, iron–sulfur; ICP-AES, inductively coupled plasma atomic emission spectroscopy; ISC, Fe–S cluster; IMS, intermembrane space; IP, immunoprecipitation; MIA, mitochondrial intermembrane space assembly; Mia40c, the C-terminal domain of Mia40; mtHsp70, mitochondrial heat-shock protein of 70 kDa; PI, pre-immune; SD, synthetic defined; TCEP, tris(2-carboxyethyl)phosphine; Tom40, 40 kDa translocase of the mitochondrial outer membrane.

[1] To whom correspondence should be addressed (email hui.lu@manchester.ac.uk).

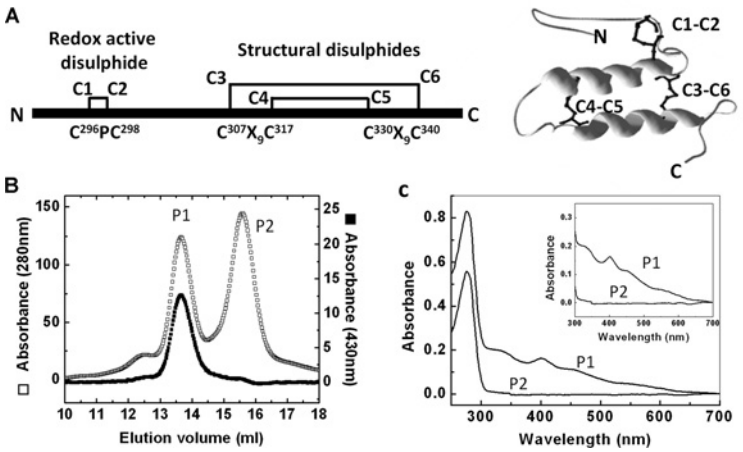

Figure 1 Structure, cofactor and dimerization of Mia40

(**A**) Schematic of the primary structure of C-terminal Mia40 with three disulfide bonds formed by the conserved cysteine motifs (left-hand panel) and the X-ray structure (right-hand panel) of the yeast *S. cerevisiae* Mia40 core domain (residues 284–365, PDB code 2ZXT) [15]. The structure was generated using the Swiss-PDBViewer 4.0.4 software. (**B**) Gel filtration profile (Superdex 200) of Mia40c monitored at 280 nm (○) and 430 nm (●). (**C**) UV–visible spectra of the gel-filtration purified Mia40c corresponding to the two elution peaks (P1 and P2) respectively.

the undefined 'Fe/S' from mitochondria to the cytosol [22], but its specific function is not known.

Connected to this potential role for Erv1 in ISC biogenesis, a previous study had suggested that recombinant human Mia40 might bind iron or an ISC when it was purified under reducing conditions [23], but no further studies were reported. In the present study, based on *in vitro* and *in vivo* results, we show that yeast Mia40 can exist as a Fe–S protein. It contains a [2Fe–2S] cluster in a dimer form with the cluster co-ordinated by cysteine residues of Mia40 CPC. The biological relevance of iron binding was confirmed by cysteine-redox state analysis and iron uptake assays using ^{55}Fe labelling *in vivo*. Treatment of the ISC bound form Mia40 (Fe–S–Mia40) with various redox reagents showed that it was stable at normal physiological levels of hydrogen peroxide, but at raised levels representative of oxidative stress the cluster dissociated. Furthermore, oxygen consumption analysis showed that Fe–S–Mia40 is probably not an electron donor for Erv1. Taken together, our results suggest a novel form of Mia40 as a Fe–S protein, with a role independent of its thiol oxidoreductase activity.

EXPERIMENTAL

Materials

AMS (4-acetamido-4′-maleimidylstilbene-2,2′-disulfonic acid) and TCEP [tris(2-carboxyethyl)phosphine] were obtained from Molecular Probes (Invitrogen). EDTA was from BDH, and all other chemicals were obtained from Sigma at the highest purity. A peptide corresponding to the C-terminal residues of yeast Mia40 was used to raise antibodies in rabbit against Mia40 (Eurogentec). Yeast strains used in the present study were wild-type strain CY4 [24], CY4 + pMPS27 (pRS426-Mia40 made in the present study), CY4 + pMPS28 (pRS426-Mia40CPS made in the present study) and CY4 + pMPS36 + pMPS35 (pMPS35 is pYES2-Bio2 made in the present study).

Yeast strains and mitochondrial isolation

S. cerevisiae strains used in the present study were the wild-type strain CY4 [24] and the Mia40 overexpression strain CY4M (CY4 + pMPS27). The plasmid pMPS27 (pRS426-Mia40) was constructed by amplifying the *MIA40* gene from yeast genomic DNA using the oligonucleotides EcoMia40F (5′-GGCTAGAATTCTCCCTTGCTGCTGTCATTGG-3′) and SalMia40R (5′-CGAGTCGACTTGGAAGAATCAGGCAAACC-3′). The resulting PCR product was cloned into the yeast 2-μ vector pRS426. Plasmid pMPS28, for overexpression of the cysteine mutant Mia40CPS, was generated by site-directed mutagenesis of pMPS27 using primers containing the desired mutation point. Sequences of mutagenic oligonucleotides can be provided upon request. Plasmid pMPS36 was the *MIA40* gene from pMPS27 cloned into the *HIS3* plasmid pRS423. Plasmid pMPS35, for galactose-induced overexpression of Bio2, was constructed by amplifying the *BIO2* gene using oligonucleotides YesBio2F (5′-CGCGGATCCATGATGTCTACTATCTACCGTC-3′) and YesBio2R (5′-TCCGCTCGAGTCAAGATCTGTCGTACTTAAATGC-3′) and cloning this into pYES2 (Invitrogen). For mitochondrial isolation, CY4 or CY4M was grown in SD (synthetic defined) medium for 16 h at 30 °C, and then lactate medium for 16 h at 30 °C. Mitochondria were isolated from yeast cells as described previously [25,26]. Generation of mitoplasts was performed as described previously [27].

Protein purification and characterization

Mia40c (residues 284–403), the C-terminal domain of Mia40, was cloned into pGEX 4T-1 vector (GE Healthcare), expressed in the *Escherichia coli* BL21(DE3) (Stratagene) or Rosetta-gami™ 2 (Novagen) cells, and purified as described previously [14,28]. Briefly, the GST–Mia40c fusion protein was purified using GST-affinity beads, followed by removal of the GST tag by thrombin cleavage to elute Mia40c. The protein was further purified by FPLC gel filtration using Superdex-75 or Superdex-200 column chromatography at 4 °C in buffer BA (50 mM Tris/HCl and 150 mM NaCl, pH 7.5). Cysteine mutants were generated by PCR site-directed mutagenesis (Stratagene) using Mia40c plasmid construct as DNA template and primers containing the desired mutation point. The mutants were purified using the same method as for Mia40c.

Multi-angle laser light scattering analysis was carried out using purified protein applied to a Superdex 200 gel filtration column in buffer BAE (BA plus 1 mM EDTA). Samples eluting from

the column passed through an in-line DAWN HELEOS-II laser photometer ($\lambda = 658$ nm) and an Optilab rEX refractometer. Light scattering intensity and eluent refractive index were analysed using ASTRA v5.3.4.13 software to give a weight-averaged molecular mass.

Absorption spectra were recorded using a Cary 300 spectrophotometer and 1 cm quartz cuvette at 25 °C as described previously [28]. The concentration of Mia40c was determined using an molar absorption coefficient of 11 835 $M^{-1} \cdot cm^{-1}$ at 280 nm. CD analysis was performed using a JASCO J810 spectropolarimeter with a 1- or 2-mm pathlength quartz cuvette at 25 °C as described previously [29]. Each spectrum represents an average of four scans from 200 to 260 nm (far UV-CD) or from 300 to 700 nm (vis-CD) at 0.2 nm intervals with the spectrum for buffer alone subtracted. EPR samples were prepared inside a Belle Technology anaerobic glove box ($O_2 < 1$ p.p.m.), by the addition of a 10-fold molar excess of sodium dithionite and rapidly frozen (approximately 20 s) in solid CO_2/ethanol. EPR spectra were recorded at X-band frequency using a Bruker ELEXSYS E500 spectrometer equipped with an ESR900 cryostat (Oxford Instruments). The sample temperature was 15 K. Spectra were recorded at non-saturating microwave power (50 μW), using 100 KHz modulation frequency and 0.2 mT modulation amplitude. A total of 16 scans were coadded and an 'NMR gaussmeter' (teslameter) was used to determine the g values.

Oxygen consumption of Erv1 was measured using a Clark-type oxygen electrode (Hansatech Instrument) at 25 °C. The freshly prepared coloured dimer fraction and monomeric fraction of Mia40c were incubated with 1.5 mM TCEP for 30 min at room temperature (20–25 °C), followed by gel-filtration (Superdex 75) chromatography to remove TCEP. Mia40c was pre-equilibrated at 25 °C in BAE buffer, followed by the addition of 1 μM Erv1 to catalyse the reaction. For this analysis, Mia40c protein concentration was measured using both BCA and Ellman's Reagent (ThermoScientific) according to the manufacturer's protocol.

In vivo redox state analysis

Mia40 redox state was analysed by growing CY4 yeast cells in YPD [1 % (w/v) yeast extract/2 % (w/v) peptone/2 % (w/v) glucose] at 30 °C to exponential phase, followed by treatment either with or without 50 mM NEM. Spheroplasts were then generated by resuspending the cells in 150 μl of spheroplast buffer with the addition of 0.27 mg/ml freshly prepared zymolase at room temperature for 30 min. The spheroplast samples were analysed using non-reducing SDS/PAGE (10 % gels) coupled with Western blotting with anti-Mia40 antibody.

IP (immunoprecipitation) and ^{55}Fe assay

CY4 + pMPS27 cells were grown to $D_{600} = \sim 0.4$ in SD − Ura (SD without uracil) medium and labelled for 1 h with either 10 μCi $^{55}FeCl_3$ and 1 mM sodium ascorbate, or with 10 μCi [^{35}S]methionine. Cells were lysed in 0.2 M sorbitol and 20 mM Hepes, pH 7.4, using glass beads. Lysates were then treated with 1 % digitonin to solubilize mitochondria. IP was carried out using IP buffer (200 mM NaCl, 50 mM Tris/HCl, pH 8, and 1.25 % Triton X-100) using 0.5 μl of anti-Mia40 antibodies per 1 attenuance unit of cells. ^{55}Fe and ^{35}S was measured using a Wallac 1414 Scintillation Counter in 4 ml of scintillation fluid. For comparison of Bio2 and Mia40 iron binding, CY4 + pMPS35 + pMPS36 was grown in galactose to overexpress both Mia40 and Bio2. Cells were labelled with either [^{35}S]methionine or ^{55}Fe, IPs were carried out as above and ^{35}S and ^{55}Fe were measured by scintillation counting. For estimation of protein levels, ^{35}S counts were divided by the number of methionine residues in the respective mature proteins (16 in Bio2 and six in Mia40). Iron incorporation was then calculated by dividing ^{55}Fe counts by the methionine-adjusted ^{35}S counts.

RESULTS

Presence of a cofactor and dimerization state of Mia40

Mia40c was expressed and purified from *E. coli*, and displayed a brownish colour. When the affinity-purified proteins were applied to a FPLC gel filtration column, they separated into two major peaks (Figure 1B). Absorption measurements revealed that peak 1 (P1) had absorption at 430 nm, but not peak 2 (P2). In agreement with this, P1 displayed a brown colour, whereas P2 was colourless. Furthermore, light-scattering measurement revealed that the P1 contained proteins with molecular mass of 30 kDa, whereas P2 had a molecular mass of 14.5 kDa. Thus, although the colourless Mia40c is a monomer, the protein forms a dimer in the presence of the brown chromophore. The same results were observed for Mia40c purified from both BL21 and Rossetti Gami cells, although there was relatively more brown dimer from BL21(∼70 %) than from Rossetti Gami cells (∼50 %).

The UV–visible spectrum of the dimer protein showed peaks at 335, 400 and 460 nm, and a shoulder at approximately 600 nm (Figure 1C). The spectrum features are indicative of an ISC protein. The observed absorption features of the dimer form are not seen with the monomer form of the protein. Thus these results show that a chromophore exists in Mia40 and that cofactor binding requires dimerization of the protein.

Identification of the cofactor as a [2Fe–2S] cluster

To identify the chromophore, we first analysed the metal contents of the two gel-filtration peaks using ICP-AES (inductively coupled plasma atomic emission spectroscopy). Figure 2(A) showed that only iron was detected as being present at significant levels, and it was mainly present in the dimer fractions and to a much smaller extent in the monomer fraction. We reasoned that the latter was due to incomplete separation of the dimer from the monomer, as a high concentration of the protein was loaded on to a gel-filtration column to obtain the large amount of protein required for this assay. A small amount of copper and zinc were detected in both fractions, and no other metals were detectable. The molar ratio of iron to Mia40c (per subunit) is approximately 0.16, indicating that not all of the proteins contain iron.

Next, CD spectroscopy was used to investigate the metal-binding sites and secondary structure of monomeric and dimeric forms of Mia40c. The CD spectrum of the dimer showed an interesting spectrum rich in features, with positive elliptical peaks at approximately 350, 380 and 405 nm, and negative bands at 310, 450 and 500 nm (Figure 2B). This spectrum resembles that of ISC proteins [30]. As expected, such a CD signal was not observed for the colourless monomer. On the other hand, both the dimer and monomer proteins showed very similar far-UV CD spectra (Figure 2C), suggesting that both species have similar overall secondary structures and are dominated by α-helices.

To further analyse the chromophore cofactor, EPR (electron paramagnetic resonance) spectroscopy was performed. The brown dimer fraction of Mia40c was EPR silent in the $g = 2$ region as purified, but showed a strong EPR signal upon reduction with sodium dithionite under anaerobic conditions (Figure 2D). The

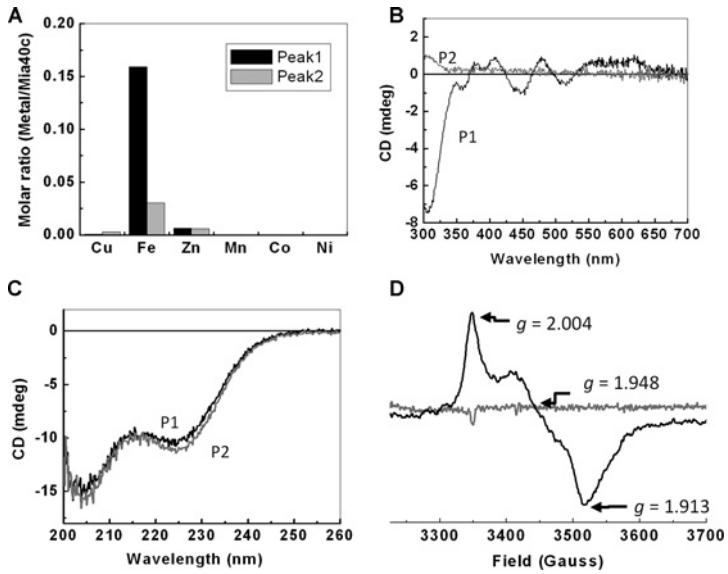

Figure 2 Identification of a ISC as the cofactor of Mia40

(**A**) ICP-AES analyses of the metal contents in the dimer (black bars) and monomer (grey bars) fractions of Mia40c. Mia40c was expressed as a subunit (monomer) in both cases. (**B**) UV–visible CD spectra of the dimer (black line) and monomer (grey line) Mia40c. (**C**) Far-UV CD spectra of the dimer (black line) and monomer (grey line) Mia40c. The same protein concentration (10 μM) of dimer and monomer were used. (**D**) The X-band EPR spectrum of the dimeric Mia40c with (black line) and without (grey line) addition of dithionite under anaerobic conditions. The dithionite-reduced protein (black line) exhibits a [2Fe–2S] cluster spectrum.

EPR spectrum exhibits features of a $[2Fe–2S]^+$ cluster of the 'thioredoxin-like' type (with g values typically 2.004, 1.950 and 1.922). Furthermore, this spectrum can be observed at 50 K, which together with the g values confirms the presence of a [2Fe–2S] cluster.

In summary, using ICP-AES and three spectroscopic methods (absorption, CD and EPR) we have shown that Mia40 can exist as an Fe–S-cluster-containing protein in which a [2Fe–2S] cluster is co-ordinated by two molecules of Mia40.

Biological relevance of the cofactor binding by Mia40 *in vivo*

Our *in vitro* studies showed that a proportion of bacterially expressed Mia40c is bound to iron in a [2Fe–2S] cluster, indicating that Mia40 is capable of binding iron in this fashion. We next asked whether the full-length mitochondrial Mia40 utilizes this capability by testing whether it binds iron *in vivo*. To determine whether this was the case, we used an iron-uptake assay in which radioactive iron (^{55}Fe) was used for detection as reported [22]. As described previously, detecting iron bound to mitochondrial Fe–S proteins Bio2 and Isu1 requires overexpression of these proteins [31,32]. This is probably due to a combination of the low activity of the ^{55}Fe isotope, inefficient IP and/or low levels of target protein. Thus to achieve sufficient levels of Mia40 to reliably detect iron-binding *in vivo* we overexpressed Mia40 using the multicopy plasmid pRS426. The protein levels in both whole-cell extracts and purified mitochondria were analysed by Western blotting (Figure 3A). Although the level of Mia40 increased significantly, the mitochondrial marker proteins [Tom40 (40 kDa translocase of the mitochondrial outer membrane) and mtHsp70 (mitochondrial heat-shock protein of 70 kDa)] were not affected (as expected). The similar increases for Mia40 in the whole-cell extract and isolated mitochondria suggested that overexpressed Mia40 was localized to mitochondria. Western blotting using antibodies against the cytosolic protein Zwf1 detected only trace amounts of this protein in mitochondrial preparations, indicating that mitochondria had been successfully isolated. To further verify that over-produced Mia40 was effectively localized into mitochondria and not retained in the cytosol, the cytosolic fraction following mitochondrial isolation was Western blotted for Mia40, mtHsp70 and the cytosolic protein Zwf1 (Figure 3B). No Mia40 was detected in the cytosol. Additionally, mitochondria from Mia40 overexpressing cells were subjected to swelling to generate mitoplasts, releasing IMS components and allowing accessibility to proteases. Unlike the matrix-localized mtHsp70 (which is only sensitive to protease following solubilization of mitochondria with Triton-X), overexpressed Mia40 in mitoplasts was sensitive to proteinase K (Figure 3C). This shows that the overexpressed Mia40 is correctly localized to the IMS, anchored to the inner membrane, and is not localized to the mitochondrial matrix.

To detect iron binding from the wild-type cells with and without overexpression of Mia40, cultures were labelled with ^{55}Fe for 1 h, lysed and treated with digitonin to solubilize mitochondrial membranes. Lysates were incubated with either anti-Mia40 antibody or with PI (pre-immune) serum. Subsequent analysis by scintillation counting showed that higher levels of ^{55}Fe were co-immunoprecipitated with anti-Mia40 antibody than PI serum in both cases (Figure 3D). Iron incorporation with Mia40 was highly specific, since only background levels of radioactivity were detected in both samples with PI serum, and a significant amount of ^{55}Fe was co-immunoprecipitated with anti-Mia40 antibody from cells overexpressing Mia40. These results demonstrate that Mia40 does indeed bind iron *in vivo*. Overall our results confirm that the ISC binding by Mia40 identified *in vitro* is biologically relevant.

Next, to detemine whether the co-immunoprecipitated ^{55}Fe levels are meaningful and to estimate the relative amount of Mia40 involved in iron binding, we attempted to compare the proportion of Mia40 that is iron-bound to the well-known mitochondrial FeS protein Bio2. By labelling cells with either [^{35}S]methionine, to monitor total protein, or with ^{55}Fe, we could gain an approximation of the amount of ^{55}Fe co-precipitated with either Bio2 or Mia40. Relative levels of protein were estimated

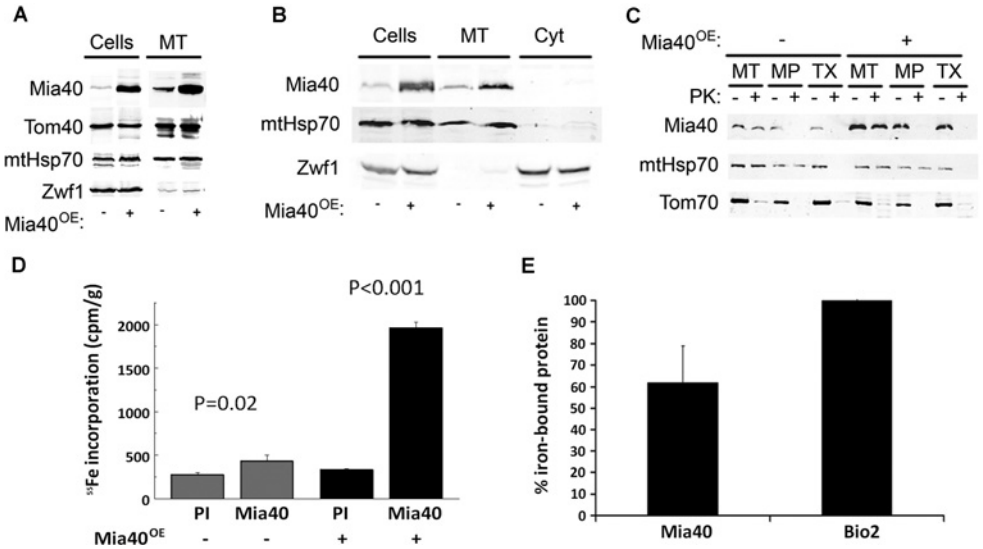

Figure 3 Mia40 binds iron *in vivo*

(**A**) Western blot analysis showing that overexpressed Mia40 accumulates in mitochondria. CY4 yeast without (−) or with (+) the Mia40 overexpression (Mia40^{OE}) plasmid was extracted for either total protein extracts (Cells) or mitochondrial protein (MT). Samples were separated by reducing SDS/PAGE (9% gels) and Western blotted using antibodies against Mia40, the mitochondrial proteins Tom40 and mHsp70, or the cytosolic protein Zwf1. (**B**) Overexpressed Mia40 does not accumulate in the cytosol. (−) or (+) Mia40 mitochondria were prepared as in (**A**), and the cytosolic fraction was saved. Total cell protein extracts (Cells), mitochondrial protein (MT) and cytosolic proteins (Cyt) were separated by SDS/PAGE (9% gels) and Western blotted with antibodies against Mia40, the mitochondrial matrix protein mtHsp70 and the cytosolic protein Zwf1. (**C**) Overexpressed Mia40 is localized to the IMS/inner membrane. (−) and (+) Mia40 mitochondria (MT) from (**A**) were swollen to produce mitoplasts (MP) or solubilized with Triton X-100 (TX) and incubated with (+) or without (−) 2 μg/ml proteinase K (PK). Samples were Western blotted for Mia40, mtHsp70 or the outer membrane protein Tom70. (**D**) Mia40 binds iron *in vivo*. CY4 yeast cells without (−) or with (+) Mia40 overexpression plasmid were grown to a D_{600} of 0.4, followed by labelling with ^{55}Fe. Cells were then lysed and mitochondria were solubilized with digitonin followed by IP using either PI or anti-Mia40 antibody. ^{55}Fe-labelled material was detected by scintillation counting and expressed as c.p.m. per g of yeast. The levels between PI and anti-Mia40 antibody were significantly different (Student's *t* test $P < 0.05$). The error bars represent the means ± S.D. ($n = 3$). (**E**) Comparison of the levels of iron-binding for Mia40 and Bio2. Cells overexpressing Mia40 and Bio2 were labelled with either ^{55}Fe as in (**D**) or with [^{35}S]methionine. Mia40 or Bio2 were immunoprecipitated, and the levels of iron co-precipitated with Bio2 or Mia40 were compared with the levels of the respective proteins (see the Experimental section for details). Data were plotted relative to Bio2 as 100% iron-bound.

by dividing the ^{35}S signal for Bio2 or Mia40 by the number of methionine residues in the respective proteins. ^{55}Fe signals were then taken as a proportion of this estimated protein level, based on Bio2 co-ordinating one 2Fe–2S cluster per molecule while assuming two Mia40 molecules co-ordinate one cluster. Figure 3(E) shows that, in comparison with Bio2, approximately 60 ± 18% of Mia40 is involved in iron binding. Although this result is only an approximation as it is based on the assumption that all overexpressed Bio2 is iron bound and that both proteins and their ISCs are equally stable during the IP procedure, it does indicate that a significant proportion of cellular Mia40 is bound to iron under the experimental conditions.

Co-ordination of the ISC by Mia40

Four cysteine residues are used to co-ordinate the vast majority of [2Fe–2S] clusters. Mia40 contains six conserved cysteine residues arranged in one CPC and two CX_9C motifs. Although the CPC disulfide is redox active, the two disulfides formed between the two CX_9C motifs are structurally important and very stable [33]. The fact that only the dimer fractions contain [2Fe–2S] clusters suggests that two reduced cysteine residues (thiols) from each subunit participate in the cluster binding. We reasoned that the cysteine residues of CPC are involved in the [2Fe–2S] cluster binding, so, for confirmation, we generated two single (SPC and CPS) cysteine mutants of Mia40c. Mutation of either the first or second cysteine residue of the CPC motif resulted in loss of the brownish colour and no absorption at wavelengths over 300–700 nm (Figure 4A). Therefore we conclude that one [2Fe–2S] cluster is probably co-ordinated by two Mia40 molecules via the four cysteine residues (thiols) of the CPC motifs. Next, we tested this conclusion *in vivo* by generating a Mia40CPS overexpression strain for ^{55}Fe uptake analysis. This Mia40CPS overexpression strain showed the same protein expression level as the Mia40WT overexpression strain (Figure 4B, inset), and the ^{55}Fe uptake assay showed clearly that Mia40CPS lost its ability to bind iron (Figure 4B), a result that is consistent with our *in vitro* finding. We also attempted to generate a plasmid for overexpression of Mia40SPC but were not successful.

Stability of Fe–S–Mia40

We observed that the brown colour of the protein was lost gradually under aerobic conditions (approximately 1 day at room temperature and few days at 4 °C), and, on the basis of SDS/PAGE, the colour change was not coupled with degradation of the protein. Thus the effects of redox reagents on the stability of the cluster binding were investigated by following the absorption change over time at 400 nm. Although the reducing agents DTT, GSH and GSSG showed little to no effect on the stability of the chromophore, H_2O_2 had a clear destabilizing effect on cluster binding (Figure 5A). Absorbance at 400 nm fell significantly within approximately 20 min upon addition of 1 mM H_2O_2 and the sample gradually became fully colourless, suggesting that the cluster was disassembled, while the protein was not degraded by H_2O_2 treatments based on SDS/PAGE analysis (Figure 6B).

Next, concentration-dependence of H_2O_2 on stability of the cluster-binding was investigated using the same method. The initial rates of the absorbance change (400 nm) were plotted against H_2O_2 concentration (Figure 5B). They showed that there

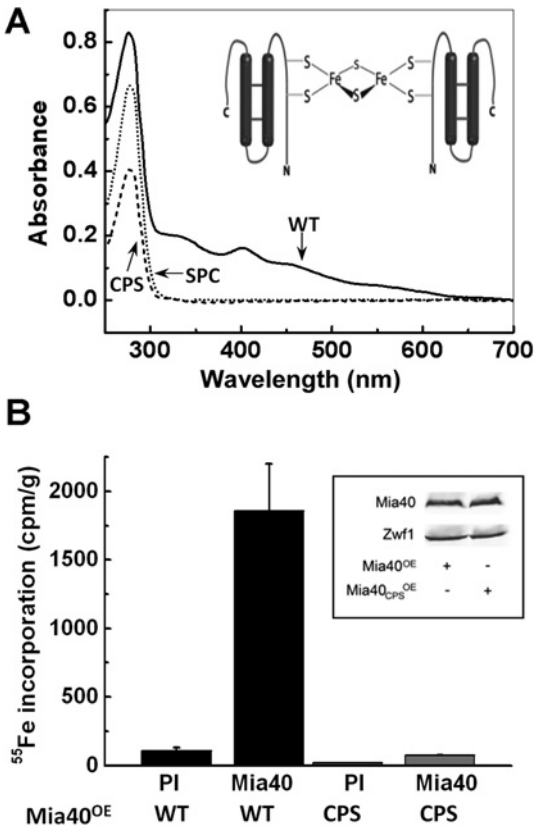

Figure 4 The ISC is co-ordinated by Mia40 CPC

(**A**) UV–visible spectra of the WT (69 μM), SPC (56 μM) and CPS (34 μM) mutants of Mia40c. Inset: schematic drawing of the cluster binding by Mia40. (**B**) ^{55}Fe uptake analysis with CY4 yeast cells containing Mia40WT (Mia40^{OE}) or Mia40CPS (Mia40$_{CPS}^{OE}$) overexpression plasmids as described in Figure 3(B). IP used either PI or anti-Mia40 antibody. The results are the means $\pm$ S.D. ($n = 3$). Inset: Western blotting analysis with Mia40 and Zwf1 (loading control) antibodies showing the same level of Mia40 overexpression.

was no obvious difference in the rate of absorbance change at H_2O_2 concentrations of up to approximately 25 μM; however, above 50 μM H_2O_2 the rate increased with H_2O_2 concentration linearly. Thus the cluster binding was stable under normal cellular conditions, but might be sensitive to elevated levels of chemicals produced by oxidative stress.

Redox state of CPC and oxidoreductase function of Fe–S–Mia40

The most obvious reason for the destabilization of Fe–S–Mia40 by hydrogen peroxide is that the CPC motif, which co-ordinates the [2Fe–2S] cluster, becomes oxidized. To test this, the redox state of the Mia40 CPC motif was analysed by AMS thiol-modification assay as described previously [28,34]. It showed that, although the P2 (monomer Mia40c) of the gel-filtration fraction was oxidized, the P1 (dimer Mia40c) fraction contained both reduced and oxidized proteins, as well as Mia40 dimer linked through intermolecular disulfide bonds (Figure 5A). This is consistent with the ICP-AES result that only a fraction of the Mia40c dimer contains iron. We reasoned that the ISC is co-ordinated by Mia40 in its CPC reduced form, and the oxidized forms with both inter- and intra-molecular disulfides cannot bind the cluster. Next, the effect of H_2O_2 on the redox state of Mia40 was analysed by AMS assay (Figure 5B). The result showed that the initially reduced protein became AMS-resistant on a timescale similar to that of the absorption decrease (Figure 5A, curve v), indicating that the reduced Mia40 became oxidized by addition of H_2O_2 and oxidation of Mia40 was coupled with the disassembly of the ISC rather than protein degradation (Figure 6B).

Furthermore, we confirmed that both reduced and oxidized states of Mia40 exist *in vivo*, by using a NEM thiol-modification assay. Yeast was grown in YPD to exponential phase followed by NEM thiol-alkylation and Western blotting with antibodies against Mia40 to detect the NEM-dependent size shift [11]. Western blot analysis revealed that Mia40 was split approximately 50/50 between the cysteine-reduced and oxidized forms under these conditions *in vivo* (Figure 6C).

It has been shown that the colourless monomeric Mia40c acts with Erv1 as a thiol oxidoreductase system in the mitochondrial IMS catalysing oxidative folding of newly imported proteins [6–9]. After transfer of the CPC disulfide to substrate proteins, reduced Mia40 is oxidized by Erv1, and reduced Erv1 can be reoxidized by cytochrome *c* or molecular oxygen *in vitro*. Thus oxygen consumption analysis was used to test whether Fe–S–Mia40 can be oxidized by Erv1 (Figure 6D) [26,28]. The result showed that the Fe–S–Mia40 is not an electron donor

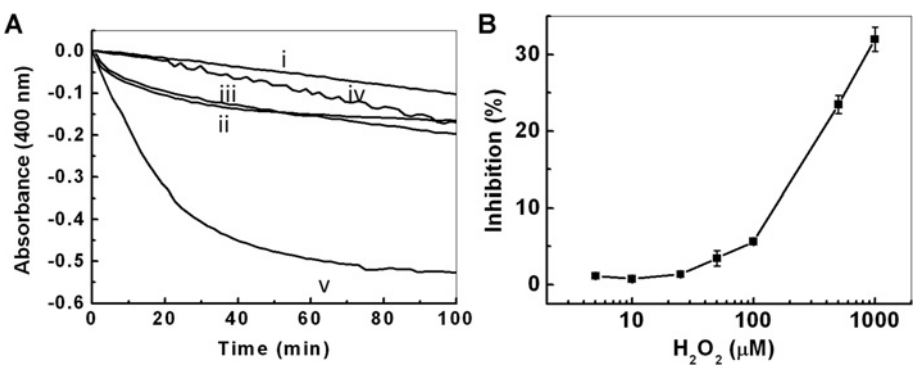

Figure 5 Stability characterization of Fe–S–Mia40

(**A**) Effects of redox reagents on the stability of Fe–S–Mia40 followed by absorption decrease at 400 nm. Time courses of the intensity changes in the absence (i) and presence of 5 mM DTT (ii), 5 mM GSH (iii), 1 mM GSSG (iv) or 1 mM H_2O_2 (v) were recorded. (**B**) H_2O_2 concentration dependence of the initial rate of the intensity decrease at 400 nm, based on the same measurements as described above.

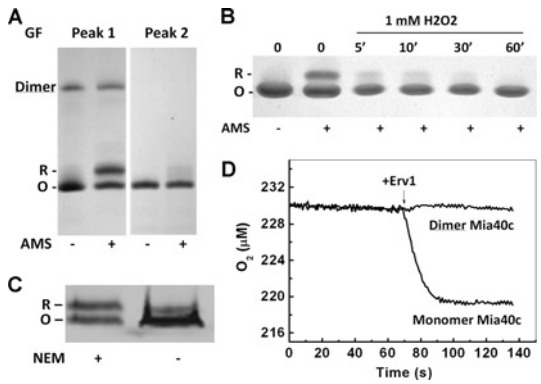

Figure 6 Redox state and functional characterization of Fe–S–Mia40

(**A**) Cysteine redox state of Mia40 was analysed using AMS thiol-modification assay. The reduced (R) and oxidized (O) states are indicated. (**B**) AMS assay of the redox state change during the time course of Mia40 incubation with 1 mM H_2O_2. (**C**) Analysis of Mia40 redox state *in vivo*. Yeast cells were grown to exponential phase followed by with (+) or without (−) NEM treatment, followed by preparation of spheroplasts and protein analysis using non-reducing SDS/PAGE (10 % gels) coupled with Western blotting using anti-Mia40 antibody. The reduced (R) and oxidized (O) states are indicated. (**D**) Time courses of oxygen consumption catalysed by Erv1 in the presence of the iron-containing dimer Mia40c and colourless reduced monomer Mia40c respectively. Mia40c was pre-equilibrated at 25 °C in BAE buffer, followed by the addition of 1 μM Erv1 at the time indicated.

for Erv1, although the cysteine residues of CPC were in the reduced form. Thus the Fe–S–Mia40 does not appear to be a thiol oxidoreductase, suggesting it has a separate function to the monomeric non-iron-cluster-containing form.

DISCUSSION

Mia40 is a novel ISC containing protein

On the basis of the absorption spectrum, it was suggested that human Mia40 may bind iron or a ISC *in vitro* [23]. The present study has established that the mitochondrial oxidoreductase Mia40 is an Fe–S protein. It can bind a ISC stably in a dimer form, and we have shown that a [2Fe–2S] cluster is co-ordinated by two molecules of Mia40 through its CPC motifs, since cysteine mutants of this motif lost their ability to bind the cluster based on absorption spectral analysis. This conclusion is also supported by two separate observations: (i) when CPC is oxidized, Mia40 is colourless; and (ii) both the apo and Fe–S-containing Mia40 display very similar far-UV CD spectra, indicating that the cluster-binding groups are located in a structurally unfolded range of the protein. It is consistent with the fact that the N-terminus of Mia40c (including the CPC motif) is flexible, whereas the CX_9C motifs are structurally important and form stable disulfide bonds. Thus we conclude that no obvious/significant secondary structure change was induced in the correctly folded C-terminal domain while the cysteine of the flexible CPC motif participated in ISC binding and dimerization of Mia40.

Previously, the cysteine redox state of Mia40 was mainly studied in organelles, using isolated mitochondria. In the present study, the redox state of Mia40 *in vivo* was analysed. In contrast with the organelle studies that showed that the majority of Mia40 was oxidized with only approximately 10 % of the protein having a reduced CPC motif [11,29], the results from the present study showed that approximately 50 % of Mia40 CPC was reduced *in vivo*, which is in agreement with the fact that a significant amount, approximately 60 %, of Mia40 was involved in the cofactor binding. Our result from the present study is broadly consistent with a recent study by Kojer et al. [35] in which they also showed that Mia40 exists in a mixture of oxidized (∼70 %) and reduced (∼30 %) forms *in vivo*. We hypothesize that the reduced Mia40 contains a ISC *in vivo*, and that the cofactor-containing Mia40 may not function as a disulfide carrier in the well-characterized MIA pathway. Our hypothesis is also consistent with the observation that the levels of reduced Mia40 did not decrease upon overexpression of Erv1 *in vivo*, whereas Mia40 was almost completely reduced in cells with lower levels of Erv1 [35]. The presence of separate populations of iron-bound and oxidized (non-iron-bound apo form) Mia40 *in vivo* raises the question of whether the relative proportions of these populations can change, perhaps in response to external stimuli. Our finding that iron-bound Mia40 can be converted to the apo form by high concentrations of H_2O_2, together with the observation that different levels of reduced and oxidized protein forms were detected under different conditions as discussed above, suggests that the amount of iron-bound Mia40 *in vivo* might depend on the cellular environment. An ability to modulate the relative proportions of iron-bound and apo-Mia40 would then allow the cell to regulate the thiol oxidase activity of Mia40.

Furthermore, our results suggest that purified Mia40c may bind the [2Fe–2S] cluster in its oxidized form $[2Fe–2S]^{2+}$, and it can be reduced to $[2Fe–2S]^{1+}$ upon addition of sodium dithionite. EPR spectroscopy confirmed that the purified Fe–S–Mia40 contains a $[2Fe–2S]^{1+}$ cluster of the 'thioredoxin-like' class (also once known as 'Meyer type') of ferredoxins when it is reduced using sodium dithionite [36,37].

Typically, [2Fe–2S] clusters are co-ordinated by CXXC motifs as shown for many proteins [38]. The cluster co-ordination by CPC and the induction of dimerization of a protein is novel and (to the best of our knowledge) has not been shown for a naturally existing protein before. A similar [2Fe–2S] cluster binding by CXC motifs was shown for mutants of bacterial TrxA in an engineered pathway [39]. By imposing evolutionary pressure, mutation of the TrxA CXXC motif to CXCC changed TrxA from a monomeric disulfide reductase into a [2Fe–2S] cluster bridged dimer and thiol oxidase, and similarly it was the first two cysteine residues (CXC) of CXCC involved in the cluster binding [39]. Thus the cluster of Mia40 probably represents a new form of ISC protein, and there may be more proteins with CPC or CXC motif(s) that are naturally Fe–S proteins.

Functional implication

Disulfide bond formation is crucial in the folding and function of many proteins. It requires dedicated oxidoreductase systems to ensure that the right disulfide bond is formed in the right place at the right time. Since its identification 8 years ago [4,5,27], extensive research has shown that Mia40 acts as a disulfide carrier, forming a thiol oxidoreductase system with Erv1 for import and oxidative folding of many mitochondrial IMS proteins. Compared with other disulfide carriers, e.g. PDI (protein disulfide-isomerase) of the ER (endoplasmic reticulum) lumen or DsbA of the periplasmic space of prokaryotic cells [40–42], Mia40 is unique. All other disulfide carriers (functional equivalent oxidoreductases) are members of the thioredoxin superfamily containing at least one thioredoxin active site with a CXXC motif, whereas Mia40 has a CPC redox active site. As a disulfide carrier, Mia40 is a monomer containing no cofactor. The Fe–S–Mia40 is a dimer bridged by a [2Fe–2S] cluster that is co-ordinated by four cysteine residues of the CPC motifs. One possible role for the formation of the ISC in Mia40 may represent a mechanism for regulating the thiol oxidoreductase activity of Mia40 and hence

mitochondrial protein import efficiency, perhaps in relation to oxidative stress.

A recent study showed that Mia40 can promote import of Atp23 (a protease that cleaves the presequence of ATP synthase subunit 6) in a cysteine-independent manner [43]. That study showed that a non-cysteine mutant of the IMS protein Atp23 is still imported in a Mia40-dependent manner, suggesting that Mia40, but not its thiol oxidoreductase activity, is important for import of Atp23. Although the cysteine residues of Fe–S–Mia40 CPC are reduced, oxygen consumption analysis suggested that the protein cannot transfer electrons to Erv1, indicating Fe–S–Mia40 may have a different function.

ISCs represent one of the most ancient and ubiquitous cofactors, being found in proteins involved in many vital and diverse biological processes, from electron transfer and iron homoeostasis to gene regulation and apoptosis. Though at present there is no proof for a physiologically relevant binding of ISCs to Mia40 *in vivo*, our *in vitro* results suggest that such a role of Mia40 is in principle conceivable. The biological function of the Fe–S–Mia40 is currently unknown, but it may be involved in, for example, regulating Mia40 thiol oxidoreductase activity, biogenesis of other Fe–S proteins, in the mitochondrial Fe/S export machinery, or in a currently unknown pathway. In the light of its IMS location and the fact that Erv1 plays an important role in the biogenesis of the cytosolic Fe–S proteins [22], it will be interesting to investigate whether Mia40 plays a role in the biogenesis of other Fe–S proteins.

AUTHOR CONTRIBUTION

Michael Spiller performed the *in vivo* yeast genetic experiments and analysed the results. Swee Kim Ang, Efrain Ceh-Pavia and Hui Lu performed the *in vitro* experiments and data analyses. Karl Fisher and Stephen Rigby performed the EPR experiments and analysed the data. Qi Wang and Hui Lu performed the cysteine redox state analysis. Michael Spiller and Swee Kim Ang generated the yeast strains and plasmids detailed in the study. Hui Lu was the principal contributor to the design of the experiments. Hui Lu and Michael Spiller wrote the paper, and all authors provided feedback and suggested revisions.

ACKNOWLEDGEMENTS

We thank Marjorie Howard and Thomas Jowitt of the faculty biomolecular analysis core facility for help with light scattering measurement; Paul Lythgon for ICP-AES analysis; and Roland Lill (Institut für Zytobiologie, Philipps-Universität Marburg, Marburg, Germany) for the anti-Bio2 antibody.

FUNDING

Research by H.L.'s group is supported by the Biotechnology and Biological Sciences Research Council [grant number BB/H017208] and the Leverhulme Trust [grant number F/00120/CB]. E.C.P. is supported by a Ph.D. studentship from the Mexican National Council for Science and Technology (CONACyT).

REFERENCES

1 Sickmann, A., Reinders, J., Wagner, Y., Joppich, C., Zahedi, R., Meyer, H. E., Schonfisch, B., Perschil, I., Chacinska, A., Guiard, B. et al. (2003) The proteome of *Saccharomyces cerevisiae* mitochondria. Proc. Natl. Acad. Sci. U.S.A. **100**, 13207–13212
2 Schmidt, O., Pfanner, N. and Meisinger, C. (2010) Mitochondrial protein import: from proteomics to functional mechanisms. Nat. Rev. Mol. Cell Biol. **11**, 655–667
3 Lill, R. (2009) Function and biogenesis of iron-sulphur proteins. Nature **460**, 831–838
4 Naoe, M., Ohwa, Y., Ishikawa, D., Ohshima, C., Nishikawa, S., Yamamoto, H. and Endo, T. (2004) Identification of Tim40 that mediates protein sorting to the mitochondrial intermembrane space. J. Biol. Chem. **279**, 47815–47821
5 Terziyska, N., Lutz, T., Kozany, C., Mokranjac, D., Mesecke, N., Neupert, W., Herrmann, J. M. and Hell, K. (2005) Mia40, a novel factor for protein import into the intermembrane space of mitochondria is able to bind metal ions. FEBS Lett. **579**, 179–184
6 Chacinska, A., Koehler, C. M., Milenkovic, D., Lithgow, T. and Pfanner, N. (2009) Importing mitochondrial proteins: machineries and mechanisms. Cell **138**, 628–644
7 Herrmann, J. M. and Riemer, J. (2010) Oxidation and reduction of cysteines in the intermembrane space of mitochondria: multiple facets of redox control. Antioxid. Redox Signal. **13**, 1323–1326
8 Banci, L., Bertini, I., Calderone, V., Cefaro, C., Ciofi-Baffoni, S., Gallo, A., Kallergi, E., Lionaki, E., Pozidis, C. and Tokatlidis, K. (2011) Molecular recognition and substrate mimicry drive the electron-transfer process between MIA40 and ALR. Proc. Natl. Acad. Sci. U.S.A. **108**, 4811–4816
9 Stojanovski, D., Bragoszewski, P. and Chacinska, A. (2012) The MIA pathway: a tight bond between protein transport and oxidative folding in mitochondria. Biochim. Biophys. Acta **1823**, 1142–1150
10 Lu, H., Allen, S., Wardleworth, L., Savory, P. and Tokatlidis, K. (2004) Functional TIM10 chaperone assembly is redox-regulated *in vivo*. J. Biol. Chem. **279**, 18952–18958
11 Mesecke, N., Terziyska, N., Kozany, C., Baumann, F., Neupert, W., Hell, K. and Herrmann, J. M. (2005) A disulfide relay system in the intermembrane space of mitochondria that mediates protein import. Cell **121**, 1059–1069
12 Morgan, B. and Lu, H. (2008) Oxidative folding competes with mitochondrial import of the small Tim proteins. Biochem. J. **411**, 115–122
13 Hell, K. (2008) The Erv1-Mia40 disulfide relay system in the intermembrane space of mitochondria. Biochim. Biophys. Acta **1783**, 601–609
14 Grumbt, B., Stroobant, V., Terziyska, N., Israel, L. and Hell, K. (2007) Functional characterisation of Mia40p, the central component of the disulfide relay system of the mitochondrial intermembrane space. J. Biol. Chem. **282**, 37461–37470
15 Kawano, S., Yamano, K., Naoe, M., Momose, T., Terao, K., Nishikawa, S., Watanabe, N. and Endo, T. (2009) Structural basis of yeast Tim40/Mia40 as an oxidative translocator in the mitochondrial intermembrane space. Proc. Natl. Acad. Sci. U.S.A. **106**, 14403–14407
16 Banci, L., Bertini, I., Cefaro, C., Ciofi-Baffoni, S., Gallo, A., Martinelli, M., Sideris, D. P., Katrakili, N. and Tokatlidis, K. (2009) MIA40 is an oxidoreductase that catalyzes oxidative protein folding in mitochondria. Nat. Struct. Mol. Biol. **16**, 198–206
17 Dabir, D. V., Leverich, E. P., Kim, S. K., Tsai, F. D., Hirasawa, M., Knaff, D. B. and Koehler, C. M. (2007) A role for cytochrome *c* and cytochrome *c* peroxidase in electron shuttling from Erv1. EMBO J. **26**, 4801–4811
18 Farrell, S. R. and Thorpe, C. (2005) Augmenter of liver regeneration: a flavin-dependent sulfhydryl oxidase with cytochrome *c* reductase activity. Biochemistry **44**, 1532–1541
19 Meyer, J. (2008) Iron-sulphur protein folds, iron-sulphur chemistry, and evolution. J. Biol. Inorg. Chem. **13**, 157–170
20 Sheftel, A., Stehling, O. and Lill, R. (2010) Iron-sulphur proteins in health and disease. Trends Endocrinol. Metab. **21**, 302–314
21 Balk, J. and Lobreaux, S. (2005) Biogenesis of iron-sulphur proteins in plants. Trends Plant Sci. **10**, 324–331
22 Lange, H., Lisowsky, T., Gerber, J., Muhlenhoff, U., Kispal, G. and Lill, R. (2001) An essential function of the mitochondrial sulfhydryl oxidase Erv1p/ALR in the maturation of cytosolic Fe/S proteins. EMBO Rep. **2**, 715–720
23 Daithankar, V. N., Farrell, S. R. and Thorpe, C. (2009) Augmenter of liver regeneration: substrate specificity of a flavin-dependent oxidoreductase from the mitochondrial intermembrane space. Biochemistry **48**, 4828–4837
24 Grant, C. M., MacIver, F. H. and Dawes, I. W. (1996) Glutathione is an essential metabolite required for resistance to oxidative stress in the yeast *Saccharomyces cerevisiae*. Curr. Genet. **29**, 511–515
25 Meisinger, C., Pfanner, N. and Truscott, K. N. (2006) Isolation of yeast mitochondria. Methods Mol. Biol. **313**, 33–39
26 Morgan, B., Ang, S. K., Yan, G. and Lu, H. (2009) Zinc can play chaperone-like and inhibitor roles during import of mitochondrial small Tim proteins. J. Biol. Chem. **284**, 6818–6825
27 Chacinska, A., Pfannschmidt, S., Wiedemann, N., Kozjak, V., Sanjuan Szklarz, L. K., Schulze-Specking, A., Truscott, K. N., Guiard, B., Meisinger, C. and Pfanner, N. (2004) Essential role of Mia40 in import and assembly of mitochondrial intermembrane space proteins. EMBO J. **23**, 3735–3746
28 Ang, S. K. and Lu, H. (2009) Deciphering structural and functional roles of individual disulfide bonds of the mitochondrial sulfhydryl oxidase Erv1p. J. Biol. Chem. **284**, 28754–28761
29 Durigon, R., Wang, Q., Ceh Pavia, E., Grant, C. M. and Lu, H. (2012) Cytosolic thioredoxin system facilitates the import of mitochondrial small Tim proteins. EMBO Rep. **13**, 916–922
30 Li, H., Mapolelo, D. T., Dingra, N. N., Naik, S. G., Lees, N. S., Hoffman, B. M., Riggs-Gelasco, P. J., Huynh, B. H., Johnson, M. K. and Outten, C. E. (2009) The yeast iron regulatory proteins Grx3/4 and Fra2 form heterodimeric complexes containing a [2Fe-2S] cluster with cysteinyl and histidyl ligation. Biochemistry **48**, 9569–9581
31 Molik, S., Lill, R. and Muhlenhoff, U. (2007) Methods for studying iron metabolism in yeast mitochondria. Methods Cell Biol. **80**, 261–280
32 Muhlenhoff, U., Gerber, J., Richhardt, N. and Lill, R. (2003) Components involved in assembly and dislocation of iron-sulphur clusters on the scaffold protein Isu1p. EMBO J. **22**, 4815–4825

33 Terziyska, N., Grumbt, B., Kozany, C. and Hell, K. (2009) Structural and functional roles of the conserved cysteine residues of the redox-regulated import receptor Mia40 in the intermembrane space of mitochondria. J. Biol. Chem. **284**, 1353–1363
34 Lu, H. and Woodburn, J. (2005) Zinc binding stabilizes mitochondrial Tim10 in a reduced and import-competent state kinetically. J. Mol. Biol. **353**, 897–910
35 Kojer, K., Bien, M., Gangel, H., Morgan, B., Dick, T. P. and Riemer, J. (2012) Glutathione redox potential in the mitochondrial intermembrane space is linked to the cytosol and impacts the Mia40 redox state. EMBO J. **31**, 3169–3182
36 Cardenas, J., Mortenson, L. E. and Yoch, D. C. (1976) Purification and properties of paramagnetic protein from *Clostridium pasteurianum* W5. Biochim. Biophys. Acta **434**, 244–257
37 Meyer, J., Bruschi, M. H., Bonicel, J. J. and Bovier-Lapierre, G. E. (1986) Amino acid sequence of [2Fe-2S] ferredoxin from *Clostridium pasteurianum*. Biochemistry **25**, 6054–6061
38 Beinert, H., Meyer, J. and Lill, R. (2004) Iron-sulphur proteins. Academic Press, San Diego
39 Masip, L., Pan, J. L., Haldar, S., Penner-Hahn, J. E., DeLisa, M. P., Georgiou, G., Bardwell, J. C. and Collet, J. F. (2004) An engineered pathway for the formation of protein disulfide bonds. Science **303**, 1185–1189
40 Collet, J. F. and Bardwell, J. C. (2002) Oxidative protein folding in bacteria. Mol. Microbiol. **44**, 1–8
41 Freedman, R. B. (1995) The formation of protein disulphide bonds. Curr. Opin. Struct. Biol. **5**, 85–91
42 Sevier, C. S. and Kaiser, C. A. (2006) Conservation and diversity of the cellular disulfide bond formation pathways. Antioxid. Redox Signal. **8**, 797–811
43 Weckbecker, D., Longen, S., Riemer, J. and Herrmann, J. M. (2012) Atp23 biogenesis reveals a chaperone-like folding activity of Mia40 in the IMS of mitochondria. EMBO J. **31**, 4348–4358

Received 27 March 2013/8 July 2013; accepted 8 July 2013
Published as BJ Immediate Publication 8 July 2013, doi:10.1042/BJ20130442